A search for low surface brightness dwarf galaxies in different environments.

by

Sarah Roberts

A thesis submitted to

Cardiff University

for the degree of

Doctor of Philosophy

2005

ProQuest LLC
789 East Eisenhower Parkway
P.O. Box 1346
Ann Arbor, MI 48106-1346

ACKNOWLEDGEMENTS

There are lots of people I have to thank in this thesis, both for their academic and thier personal support. My biggest thanks goes to Dr. Jon Davies, my PhD supervisor. He has helped, encouraged,advised, pushed and prodded me throughout my PhD, and I owe him quite a few beers for it! He was the best supervisor a student could ask for, and I really do count myself lucky to have been his student - Diolch yn fawr Jon!

Next I'd like to thank my officemates for making coming into Uni so enjoyable! Thanks Simon for your mischevious sense of humour, knowledge of all things astronomical, and endless supply of chewing gum! Thanks Robbie for your words of HI wisdom, for reading through my thesis and helping make it so much better, and also for the relaxing games of Keyball! Rory - thanks for making our observing trip much more entertaining with your musical and table-tennis talents! Also, not forgetting my old office mate and friend, Sabina, who, when I first started my PhD, was always there to help me out with whatever problems or questions I had, no matter how busy she was at the time. Grazie Sabina!

I also have to thank the gang from the Terminal room - Kris and Tim for their help when I needed it, and Dave and Hannah for their help with all my computing questions. You have the patience of Saints! (Thanks also for the duelling pistols!!) Also, thanks to Gustav for helping me out with all my statistics and programming problems - tack så mycket för alltig Gustav! And Haley, thank you so much for reading through my thesis at the end - I'm sure you had better things to do with your time! You're a seren!

A big thanks also to Paul Roche for giving me a job whilst I was writing up, which meant that I could afford to buy food and pay my rent! And thanks to Edward, Fraser and Dave for keeping me amused and unstressed towards the end of my thesis writing - you're great workmates to be sure!

To Wing I'd like to say a massive 'xie xie' for all your support and encouragement whilst I was finishing this thesis. You really did help me through it. Wo ai ni.

Finally, I'd like to thank my brothers, Huw and Gwyn, and my parents for all their encouragement throughout my PhD. To mum and dad especially - thank you for everything. I can finally do what you keep telling me to do and relax!

To mum and dad

ABSTRACT

Current theories of large scale structure and galaxy formation predict the existence of numerous low mass dark matter haloes in the Universe today. If these haloes contain sufficient stars they should be detectable as low luminosity stellar systems or dwarf galaxies.

We have searched for these objects in four regions of increasing density - the general field, the area around a giant spiral galaxy, the low density Ursa Major cluster, and the high density Virgo cluster. Using identical deep optical data covering a total of $60^{\circ 2}$ and probing fainter magnitudes than has been done previously, we used identical selection and detection methods to compare the dwarf galaxy populations in these different environments.

We found substantially more dwarfs per giant galaxy in the Virgo cluster (~20:1) compared to the field environment (6:1 max). A comparison of the HI properties and (B-I) colours for the objects for which we had additional data also showed that in general, the cluster objects are redder and gas poor compared to the objects in the field.

We discuss the possible mechanisms which may have resulted in creating a population of cluster dwarf galaxies, which would explain the high number density which we found in our data. It is likely that a combination of tidal interactions and transformation of infalling dIrrs into dEs will result in the large population of cluster dwarfs. Conclusive evidence regarding their formation must now be obtained by a more detailed investigation of their stellar populations.

The lack of dwarf galaxies in the field region is likely to be due to the effect of inefficient star formation in the field environment compared to the cluster. Thus the low mass dark matter haloes predicted by CDM models must still be 'dark' and can only be identified by further deep HI studies of the field environment, and future gravitational lensing studies of substructure.

Contents

List of Figures

List of Tables

Chapter 1

Introduction

1.1 The beginnings of Extra-galactic Astronomy

In the 17th century, Charles Messier, a French astronomer with a passion for comets, compiled one of the finest catalogues of galaxies and other deep sky objects which is still in use today. One night, whilst comet hunting he came across 3 comet-like objects which did not move across the sky. Fearing that these would cause confusion among other comet hunters, Messier began to compile a catalogue of such nebulous objects to prevent their false identification. The catalogue contained information on Messier's observations of nebulae, star clusters and spiral nebulae, the nature of which was unknown at the time, and provoked much discussion. It was not until early in the 20th century that the origin of these fuzzy spiral nebulae, discovered by Messier, was finally determined.

For more than 30 years the argument on the nature of spiral nebulae raged; the 'Great Debate' as it became to be known, reached its climax at a meeting

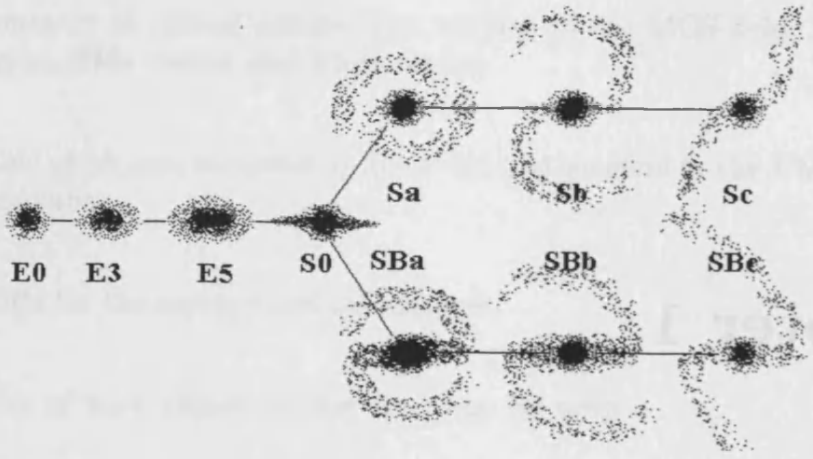

Figure 1.1: Hubble's 1936 classification of galaxies

for astronomers held in 1920. At this astronomical meeting, 2 astronomers with opposing views on the scale of the Universe, were invited to discuss the nature of the objects found in Messier's catalogue. Heber Curtis believed that these nebulae were 'island universes', that is, objects much like the Milky Way, but external to our Galaxy. He believed that the Universe contained many of these objects. Harlow Shapley on the other hand believed the spiral nebulae to be small gas clouds in our Galaxy, and believed that the Universe only consisted of one giant galaxy. The debate was finally resolved a few years later when Hubble determined the distance to the Andromeda nebulae using Cepheid variables, and thus proved Curtis correct in his assumption that these spiral nebulae, or galaxies, were in fact external to our own Galaxy. The field of extra-galactic astronomy was born.

Much work followed on the existence and classification of these galaxies. Hubble's famous tuning fork diagram (Fig. 1.1) illustrates the classes in which he put the galaxies based upon their morphology. He separated the objects into 3 main categories - ellipticals, normal spirals and barred spirals. Those galaxies which did not fit into any of these 3 classes were classified as Irregulars.

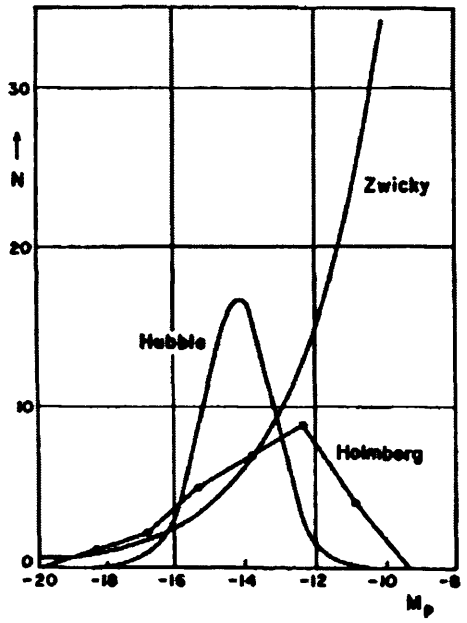

Figure 1.2: The LFs derived by Hubble, Holmberg and Zwicky.

Hubble mistakenly assumed that his classification scheme described also the evolutionary path of galaxies. We now know that this is not the case and that most galaxies do not change morphology during their lifetime unless they are part of a collision or merger with another galaxy. The evolution of galaxies and their formation can be investigated using an important tool known as the galaxy luminosity function.

1.2 The Galaxy Luminosity Function

The Luminosity Function (LF) of galaxies tells us about the relative number of bright and faint galaxies. It is defined as *'the number of galaxies per unit volume per interval of luminosity or magnitude'*. By looking at the spread in galaxy luminosities, their evolution can be studied and various cosmological models tested.

The first work to be carried out on the LF of galaxies was undertaken by Hubble in the 1930s (Hubble, 1936a,b,c). After a study of distant high surface brightness spiral and elliptical galaxies with known redshift, he claimed that the LF of galaxies was Gaussian in shape centered at $M_B \sim -18$ with σ=0.85mag. In 1950, Holmberg (1950) published a paper following his study of 28 galaxies in the Local Group and around M81 and M101. Included in his results were the known faint dwarfs of the LG. Thus his LF, although similar in shape to Hubble's, was skewed towards fainter galaxies. A maximum was also found by Abell (1960) in his LFs for 5 galaxy clusters. Zwicky (1957,1964) however, did not favour the LFs found by previous studies - he argued that there should not be a maximum in the LF; his study of 704 galaxy clusters gave a distribution with an exponentially increasing tail. The differing forms of the LF up to this point are illustrated in Fig. 1.2. The plot, taken from Zwicky's 1964 paper shows Hubble's original Gaussian LF, Holmberg's improved LF with its faint-end skew, and Zwicky's LF with the exponential tail as found from his large sample of galaxy clusters.

Further work on the galaxy luminosity function was carried out by Kiang (1961). His sample of 600 field galaxies resulted in a cubic law for the brighter galaxies and an exponential tail for the fainter objects. He stated that the discrepancy between Hubble and Zwicky's LFs was due to selection effects in their data. For the types of objects they included in their sample, both Hubble and Zwicky's LFs were correct. Hubble's galaxies were high surface brightness (HSB) objects, and his sample did not include any of low surface brightness (LSB), thus a Gaussian shape would be expected from his data. Zwicky's sample however contained nearly all LSB objects - thus his LF had an exponential tail. In 1976, Schechter proposed an analytical expression for a universal LF which had 3 free parameters obtainable from the data. The Schechter function, which is widely accepted and

used today is given in absolute magnitudes as:

$$\Phi(M)dM = \phi^* 10^{-0.4(\alpha+1)M} e^{-10^{0.4(M^*-M)}} dM \tag{1.1}$$

where:

- $\Phi(M)$ = density of galaxies within the range M→ M+dM
- ϕ^*= normalisation parameter
- M = absolute magnitude
- M^* = characteristic absolute magnitude (at knee of graph)
- α = gradient of slope of faint end

The function has two parts - a power law which dominates at low luminosities and an exponential cutoff which dominates at the high luminosities, giving the characteristic bell-shape for the brighter galaxies part of the LF. Schechter fitted this expression to data from de Vaucouleurs & de Vaucouleurs 1964 Reference Catalogue of Bright Galaxies to produce a general Luminosity function of bright, nearby galaxies (Fig 1.3), and to Oemler's 1974 data for a cluster luminosity function (Fig 1.4). As can be seen in the two figures, he found a good fit for both data sets using his expression.

The parameter, α, which represents the gradient of the faint end slope has been the focus of many a study into dwarf galaxy populations in different environments in the Universe, since a steep faint end slope (a more negative α) implies that there are numerous low luminosity dwarf galaxies, as is suggested by current models

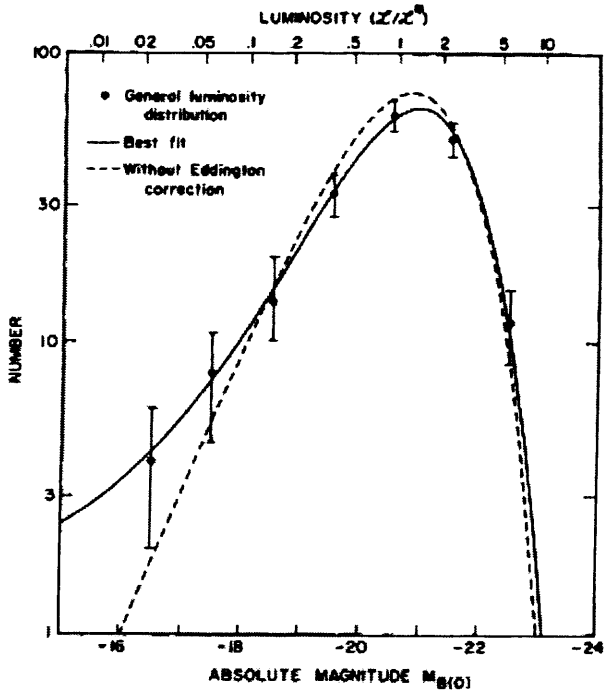

Figure 1.3: Schechter's LF plot for bright nearby galaxies. The solid line gives the best fit to the data, whereas the dashed line gives the fit when no correction is made for the uncertainty in absolute magnitudes.

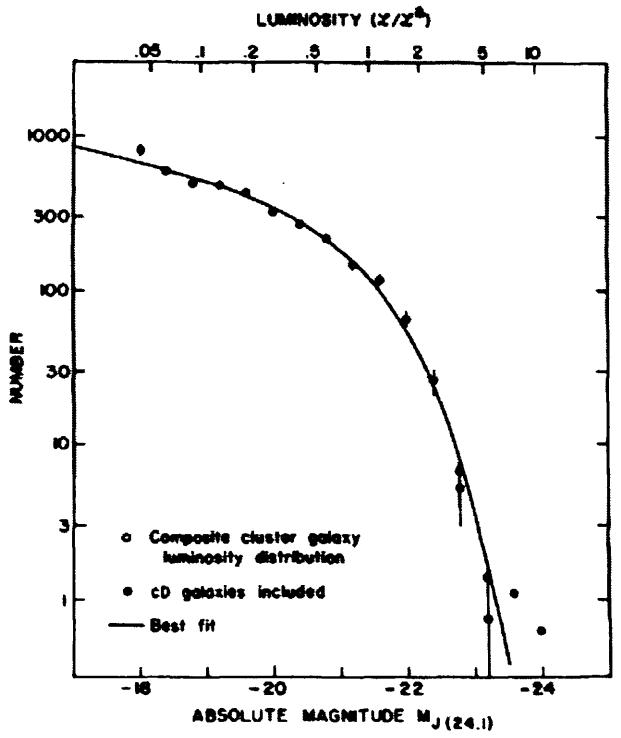

Figure 1.4: Schechter's LF plot for cluster galaxies taken from Oemler's (1974) data.

of hierarchical structure formation (described later). Data from the recent large redshift surveys carried out by SLOAN and 2dF have been used to define the global Luminosity Function of galaxies (Blanton et al. 2001, Norberg et al. 2002), with both surveys producing a consistent result for the faint-end slope, $\alpha \approx -1.2$. This value is somewhat flatter than typically predicted by most Cold Dark Matter (CDM) theoretical models of large scale structure and galaxy formation.

We discuss the predictions from CDM models for populations of low luminosity (dwarf) galaxies in the Universe in the next section, and detail the various mechanisms which are implemented within these models to bring the observations in line with the theoretical predictions.

1.3 Dwarf galaxy populations: Theory vs. Observations

1.3.1 Theory

Any models of galaxy formation must be able to explain both the small scale ripples in the cosmic microwave background and the large scale structure in the Universe.

Galaxies form in the Universe through the growth of density fluctuations produced after a period of inflation. Any tiny fluctuation in density in the Universe produces regions which are slightly overdense, and regions which are slightly underdense. Gravity acts in these regions so that in the overdense areas, the gravitational potential well deepens, and more matter is attracted here, away from the underdense regions. Eventually the matter in the potential wells collapses, and protogalaxies are formed, with further gravitational attraction causing larger scale structure to occur.

The type of dark matter (DM) present in the Universe at the time of collapse is very important as it determines the scale of objects which form first. If the DM is assumed to be Hot DM, it has a lot of energy and is therefore able to escape from the gravitational potential well in which it originates. Thus, fluctuations on small scales disappear and larger objects form first, eventually fragmenting to form the smaller sized objects which we see today. This is known as the 'top-down' scenario.

If the DM is assumed to be cold however, fluctuations on all scales can be found, and smaller objects collapse first to form protogalaxies, with merging forming the larger galaxy groups and clusters. This is known as the 'bottom-up' sce-

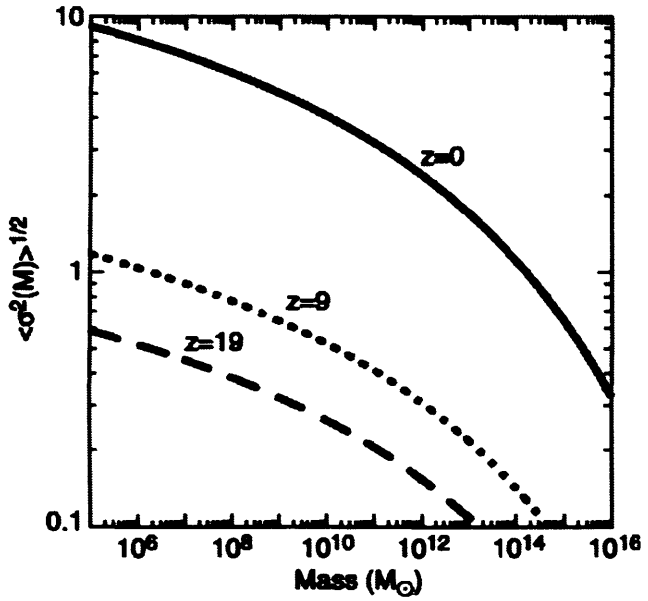

Figure 1.5: Scale sizes of objects collapsing at z=0 (solid line), z=9 (dotted line) and z=19 (dashed line).

nario. This is the model most commonly used in galaxy formation simulations (known as the concordance CDM model) and is the model we will be testing via the observations described in this thesis.

Objects of different masses form from the collapse of haloes when the primordial fluctuations reach an amplitude of ~1. At this point, the fluctuations enter the non-linear regime. Fig 1.5 (Miralda-Escudé, 2003) shows the scales which are collapsing at the present epoch, z=0 (solid line), when the Universe was ~500 million years old (z=9, dotted line) and when the Universe was ~200 million years old (z=19, dashed line) on a plot of rms mass fluctuation, δM/M vs. mass.

At z=0, fluctuations of the order of ~1 correspond to masses of $10^{14}M_\odot$, i.e. the size of galaxy clusters. These are the masses of haloes collapsing now. Compared to a redshift of 9, fluctuations of the same amplitude were collapsing on much smaller scales of $\sim 10^6 M_\odot$ (dwarf galaxy sized objects) at this epoch. However, this is not to say that dwarf galaxy sized objects only formed at z=9,

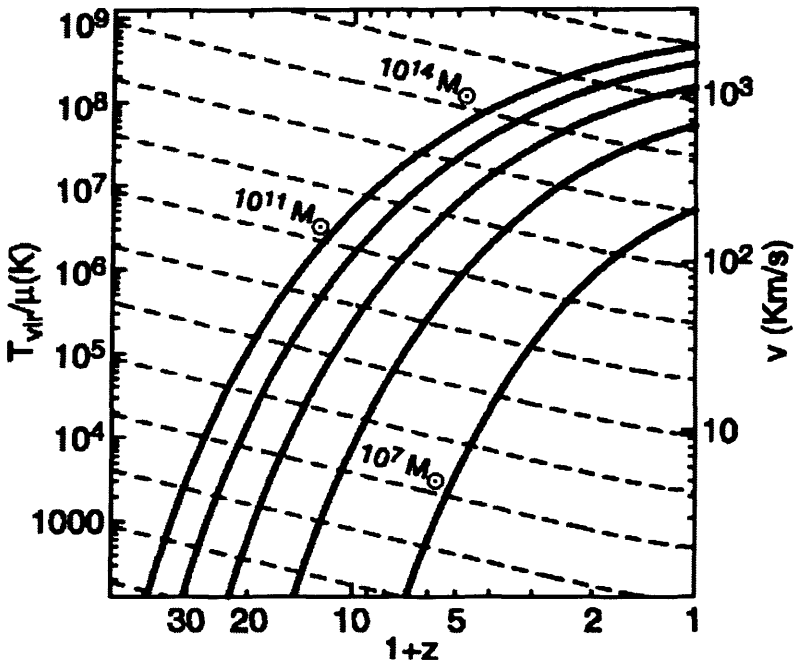

Figure 1.6: Plot illustrating collapse scales for fluctuations in range 1σ-5σ. Also plotted are the virialized temperature and velocity dispersion of the objects.

and galaxy groups are only forming now. The distribution of fluctuations in the Universe is Gaussian, thus although the likelihood for large objects to be collapsing at present is high, a small number could have formed at higher redshifts. The probability of objects of various masses collapsing at different redshifts is shown in Fig 1.6 (Miralda-Escude,2003). The lower solid line on the plot represents a 1σ fluctuation, with the increasingly higher lines showing 2,3,4 and 5σ fluctuations respectively. A typical dwarf galaxy forms from the collapse of a $\sim 10^6 M_\odot$ halo. On this scale, a 1σ fluctuation collapses around z$\sim$6, so the majority of dwarf-sized objects form at that time. However, this scale size also collapses from 3σ fluctuations at z$\sim$20, thus a small number of objects with masses $\sim 10^6 M_\odot$ will have formed at this time.

Fig 1.6 also shows the velocity dispersion of the objects, and virialized temperature of the gas in the halo. The timescale on which the gas cools to form

stars and make the halo visible is dependent upon this temperature. If the gas in the halo is above a threshold temperature, the gas pressure can support against collapse, thus preventing star formation (SF). Once the gas has cooled, it can condense until the density reaches a critical value after which star formation occurs. If for some reason however, the gas is inhibited from cooling, perhaps due to an external ionising background, it will not collapse to form stars, and the halo will not light up to be observable as a galaxy. Thus if comparisons are made between the number of haloes predicted to form via the CDM model with the observed number of galaxies, there will be a discrepancy. This, together with a description of how SF may be prevented in the haloes, is discussed further in the next section.

Models and simulations

The modelling of structure and galaxy formation is computationally difficult in a single simulation. On the one hand models are needed which show formation of the large scale structure, occurring on scales of tens of Mpcs. However, the formation of individual galaxies in the Universe and the processes occurring in these objects must also be modelled in detail and these occur on much smaller scales of parsecs or kiloparsecs. In order to simulate the formation of small galaxies over a large enough volume to study clusters, billions of particles are needed in the simulations, and this has not always been possible.

The first N-body simulations of structure formation using computers were carried out in the 1960s using only 100 particles; vast improvements since then have led to $\sim 10^{10}$ particles being used in such simulations, although even with this number of particles, the smallest scale that can be modelled is still only $\sim 10^6 M_{\odot}$. Processes occurring on smaller scales than this can still not be modelled in the

same simulation.

The first step in modelling structure and galaxy formation in the Universe is forming the large scale structure via DM halo simulations. The next step is forming galaxies in these haloes. Adding a baryonic component to N-body simulations makes it possible to look at galaxy formation, but it puts a huge demand on the computation. Since SF and feedback processes are the important physics ongoing in the DM haloes, they must be modelled to give an accurate picture of how the Universe as we see it, has formed. This is where semi-analytic models come in - such models include prescriptions for gas cooling, star formation and feedback mechanisms in the DM haloes. The equations used in these models primarily set criteria for:

- when the gas in the dark matter halo can cool and therefore collapse to form stars
- the rate at which stars form
- the rate at which supernova (SN) explosions occur
- how much gas is lost from the halo when SN do occur

Combining the results of N-body simulations with semi-analytic models enables both the larger and smaller scale structure to be studied.

N-body with Semi Analytic Models

Kauffmann et al. (1993) used a previously developed algorithm utilising Monte Carlo techniques, to follow the paths and merging histories of DM haloes from high redshift to the present time. With specific formulae governing baryonic processes

in the DM haloes, galaxies were formed in individual haloes, and their evolution followed as their DM haloes merged with other haloes. At the end of the run, Kauffmann et al. were able to look at the properties of each halo, and compare the numbers of each halo mass with observations of different mass galaxies in the Universe in order to predict the numbers of each galaxy mass that should be observable today.

The main steps in their models were as follows:

- At a given redshift, the gas in a DM halo cools and collapses to form stars at a predefined rate. The criteria for SN explosions and loss of gas into the ISM due to the injection of energy from the SN explosion, was predefined, thus once the criteria for feedback was fulfilled, gas was lost from the galaxy.
- At a later redshift, the halo merged with another DM halo which is already likely to have accreted other DM haloes.
- At this point, any gas in the accreted haloes which has not cooled to form stars, is shock heated.
- The shock heated gas eventually cools onto the central galaxy of the DM halo. The central galaxy is assumed to be the galaxy which was at the centre of the largest accreted DM halo. The galaxies at the centre of the other accreted DM haloes become satellites of the central galaxy.

In order to include merging in their model, Kauffmann et al. calculated a dynamical friction timescale for each satellite, dependent upon its initial orbital radius about the central galaxy, its baryonic mass and its circular velocity. The probability of the satellite merging at each time step of the model was calculated,

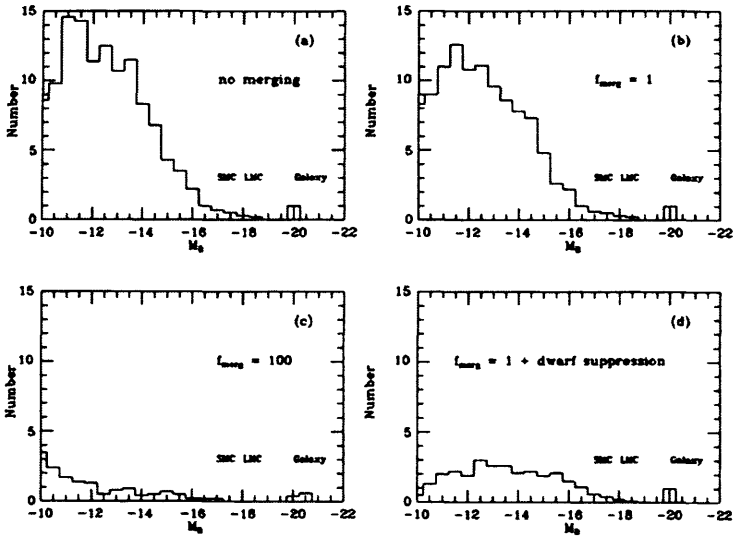

Figure 1.7: LF of MW sized DM halo with a) no merging or dwarf galaxy suppression (upper left); b) merging factor =1 (upper right); c) merging factor =100 (lower left); d) merging and dwarf galaxy suppression (lower right).

and the rate of merging adjusted by multiplying the merging probability by a free parameter, f_{merge}. One aspect of the model which was not particularly realistic however was that the satellites could not merge with each other - they could only merge with the central galaxy in their halo.

With their model, Kauffmann et al. first looked at how one of their DM haloes, with a circular velocity of 220km/s, compared with observations of the Milky Way (which has a similar circular velocity). In their model, they tuned the two free parameters determining the star formation and feedback efficiency so that the luminosity and cold gas content of the central galaxy in the DM halo agreed with the observed properties of the Milky Way. Their LF for the MW sized DM halo using the then favoured cosmological model (Ω_b=0.1, Ω_0=1, Λ=0) is shown in Fig. 1.7 (a). At the faint end, ($M_B \leq$-14) there are predicted to be over 100 galaxies. This is obviously more than the observed number of satellites around the MW (Mateo (1998) lists $\sim$ 11 dwarf companions). In an attempt to reduce this

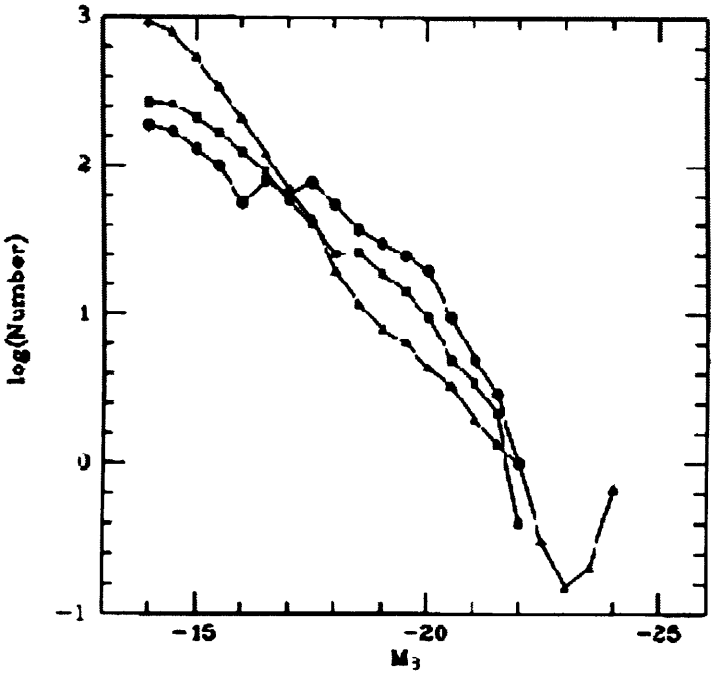

Figure 1.8: LFs of Virgo sized DM halo for model with no merging (triangles) and for model with merging, suppression of gas cooling for haloes with $v_{circ} \leq 150$km/s at redshifts between 1.5 and 5 and suppression of star formation in haloes with $v_{circ} \geq 500$km/s (squares). The observed Virgo cluster LF (Binggeli et al. 1985) with faint-end slope, α=-1.35, is given by the circles.

excess, Kauffmann et al. looked at the factors which could decrease the numbers of small mass haloes and therefore faint galaxies. Fig 1.7 (b) shows the LF after merging of the haloes is introduced. This clearly does not reduce the faint galaxies sufficiently to match observations. Increasing the merging rate by a factor of 100 (Fig 1.7 (c)) has the required effect on the numbers of faint galaxies, but results in a LF which now under-produces all galaxies with luminosities similar to the Large and Small Magellanic clouds. Fig 1.7 (d) shows the effect on the LF of merging, together with dwarf galaxy suppression. In this model, gas was not allowed to cool in haloes with $v_{circ} \leq 150$km/s at redshifts between 1.5 and 5. Although the LF is in much better agreement with the observations, Kauffmann et al. comment that the amount of suppression used is rather strong. Without this suppression however, they cannot convincingly produce similar LFs for their MW sized DM halo when compared with the observed numbers of the satellites of the MW.

With the free parameters set for the model of the MW, Kauffmann et al. then used these same values to investigate the observed properties of larger systems such as galaxy clusters. They chose to compare their model with the Virgo cluster ($V_{circ} \sim 1000$km/s), due to its wealth of observational data. Fig 1.8 shows the LF for the DM haloes with circular velocities similar to that of the Virgo cluster. The filled circles illustrate the LF found by Binggeli et al.(1985) from their photographic data covering 6° of the central region of the Virgo cluster. The LF from the model with no merging is plotted with triangles. Once again the faint end slope is steep compared with the observations. The observed LF of Binggeli et al. gives a faint end slope value of $\sim$ -1.35. However, since this result was published, deeper surveys of the Virgo cluster using CCD data have been conducted which have uncovered a population of fainter dwarf galaxies (Trentham & Hodgkin, 2002) than Binggeli found with his data. Thus, the observed faint end slope value has increased from

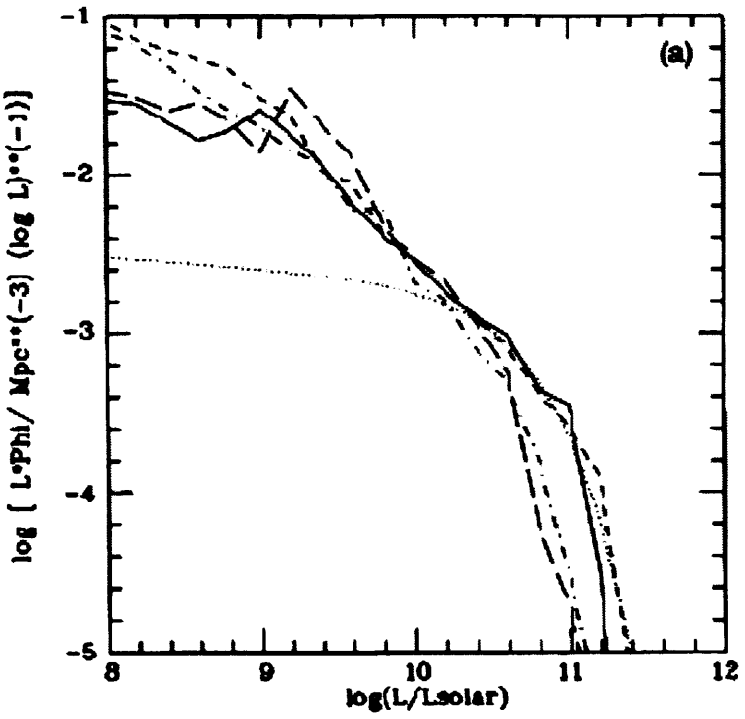

Figure 1.9: LFs of field DM haloes for model with no merging (short-dashed line, Ω_b=0.2) and for model with merging and suppression of gas cooling for haloes with $v_{circ} \leq 150$km/s at redshifts between 1.5 and 5 (solid line, Ω_b=0.2). The dot-dashed lines and long- dashed lines show the LFs for the 2 same models but with Ω_b=0.1. The observed field LF is given by the dotted line.

Binggeli's estimate to -1.6. This decreases the difference between the observed LF and the predicted LF for the model with no merging as seen in Fig 1.8, although the model with no merging still under-predicts the numbers of brighter galaxies slightly. The second LF produced by Kauffman et al. and plotted on Fig. 1.8 is for the model which includes merging and suppression of gas cooling in haloes with $v_{circ} \leq 150$km/s at redshifts between 1.5 and 5 to flatten the faint end, and suppression of star formation in haloes with $v_{circ} \geq 500$km/s to adjust the bright end. The resulting LF now appears to match up well with the observations from Binggeli et al's. galaxy catalogue.

Kauffmann et al. also produced LFs for haloes in the field and compared them

to the field galaxy LF derived from the CfA catalogue of Moore et al.(1993). This is plotted in Fig 1.9. The dotted line represents a Schechter fit to the observational field data, which gives a faint end slope of -1.07. Similar to the MW and Virgo models, Kauffmann et al. plot LFs for models with no merging (short-dashed line, Ω_b=0.2) and with merging and dwarf galaxy suppression (solid line, Ω_b=0.2). The dot-dashed lines and long- dashed lines show the LFs for the same two models but with Ω_b=0.1. It is clear from this plot that even when the gas cooling and therefore subsequent formation of dwarf galaxies is suppressed, and merging included, there are still far too many predicted faint galaxies compared with observations. Thus, the models of Kauffmann et al. show that even with such mechanisms, the predicted numbers of faint galaxies in the field and low density environments do not match up with the numbers found in observations, but there appears to be greater agreement in the higher density cluster environment. This result remains valid whether the standard cosmological model is used, or whether a model with non-zero cosmological constant is implemented.

N-body simulations

Moore et al. (1999) also investigated the substructure of galactic and cluster sized DM haloes compared with observations of the MW and its satellites and the Virgo cluster, using numerical simulations. To resolve the substructure of the DM haloes with a limited number of particles they used a scheme which allowed them to select interesting regions from a large cosmological simulation, and study it at a higher resolution in a subsequent simulation. They generated two sets of initial conditions to look over the cosmological volume with two resolutions. The first set contained $\sim 10^7$ particles in the whole volume, the second set had less than 10^6 in a specific cluster. They then looked at the substructure by the following method:

- The lower resolution simulation was run to a redshift of 0. At this epoch, they selected a virialized cluster which was considered interesting i.e. a Virgo sized cluster halo.
- They then flagged any particles located at distances up to twice the virial radius of the cluster, and traced them back to their initial conditions. The particles in this region were the ones which they wanted to study further with a higher resolution.
- Beyond this region of interest, a lower mass and force resolution was used with increasing distance by combining particles at their centre of mass.
- The simulation was then run again to z=0, using a higher resolution.

This method was used to pick out haloes both similar to the Virgo cluster, and with similar circular velocities and isolation as the MW, from a simulated volume of 10^6 Mpc^3. The results of these simulations were then compared with observations. Fig 1.10 shows the mass distributions of these simulated haloes, with the cluster halo in the upper figure and the galactic halo in the lower figure. The mass distribution of both haloes appear strikingly similar with a large amount of substructure in both, even though the cluster halo formed 5 Gyrs after the galactic halo, and has a mass of $5\times10^{14}M_{\odot}$ compared with the galactic halo's mass of $2\times10^{12}M_{\odot}$.

Using the bound particles in these haloes, Moore et al. measured the halo masses, circular velocities, radii and orbits in order to compare them directly with observations. The results of these comparisons are shown in Fig.1.11. Plotted here are the abundance of haloes as a function of their circular velocities, normalised to the circular velocity of the parent halo in which they are situated. The solid

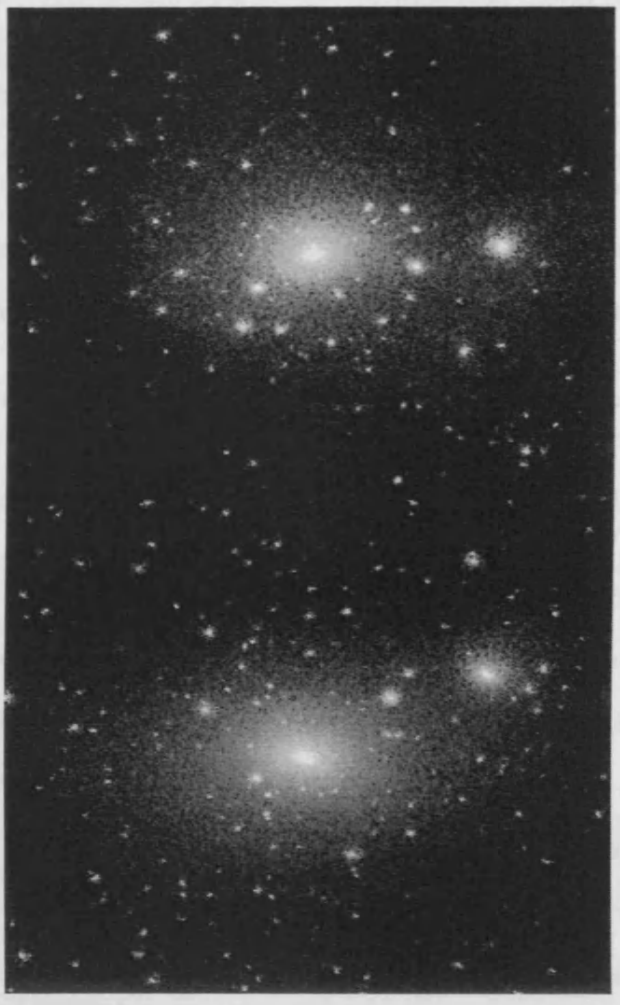

Figure 1.10: Mass distribution for simulated cluster (upper figure) and galactic halo (lower figure)

line shows the data for the simulated cluster with the observational Virgo cluster catalogue of Binggeli et al. (VCC, 1985), plotted with circles and Poissonian error bars. The two distributions seem to be in relatively good agreement. The dashed lines represent the simulated galactic halo, both for z=0 and 4 billion years ago. The two appear quite similar suggesting that the evolution of the halo has not significantly altered its substructure. A comparison of these simulated data to the distribution of satellites around the MW (dotted line) however shows a huge discrepancy. The models predict ~50 times more satellites around the MW sized halo than are observed for dwarf galaxies more massive than the MW dSphs. A point to consider here however is that Moore et al. calculate the circular velocities of the haloes using their bound mass which consists of a DM component as well as a luminous part within the bound radius. *Observed* circular velocities are based upon the luminous component of the galaxy within the luminous radius of the galaxy only. Thus there might be a slight difference in the circular velocities obtained with simulations and those calculated from observations. However, even accounting for this does not improve the fit between the simulated galactic halo and the observed number of MW satellites dramatically.

Klypin et al. (1999) also show evidence of a dwarf galaxy deficiency in their study of the Local Group dwarfs. Using published data to compile a list of Local Group satellites with circular velocities greater than 10 km/s, they ran simulations of two cosmologies, ΛCDM ($\Omega_0 = 0.3, \Omega_\Lambda = 0.7$, h=0.7) and SCDM($\Omega_0 = 1.0$, h=0.5), to see how many satellites would be predicted by the hierarchical theory. They then compared the observations with their results, as shown in Fig. 1.12. The open circles and solid line in the graph illustrate their SCDM and ΛCDM predictions respectively, whereas the triangles show the observational results. Although at $V_{circ} > 50 km/s$ their simulations appear to agree well with the simulations, in

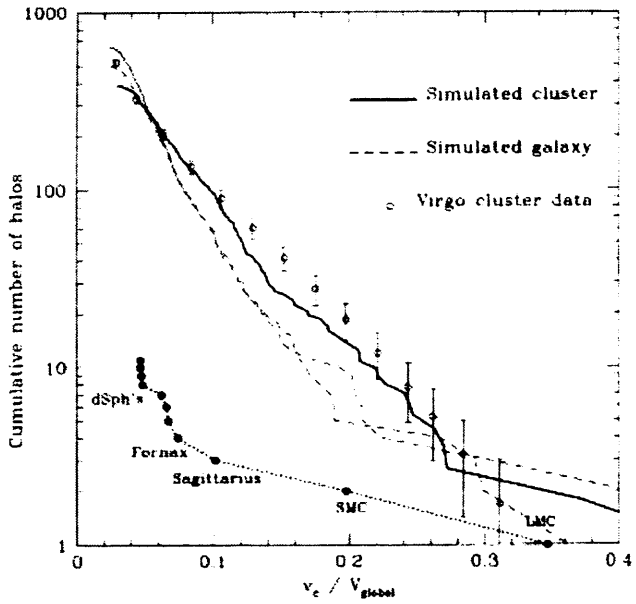

Figure 1.11: Abundance of haloes as a function of their circular velocity (Moore et al., 1999). The solid line represents the simulated cluster halo, the dashed line the MW sized halo both now and 4 billion years ago, and the observational cluster data is plotted with open circles. Data for the satellites of the MW are shown by the dotted line.

the circular velocity range 10-30km/s, the ΛCDM model overpredicts the number of dwarfs in the LG by about a factor of 5. Klypin et al. attempt to explain this discrepancy by suggesting that either the missing satellites are High Velocity Clouds (clouds of neutral hydrogen with large dispersions from the Galactic circular velocity, and no detectable stars) which have been observed in the LG or that there are a large number of DM satellites in the LG that cannot be detected as they are not luminous enough. This low luminosity may result from early feedback by supernovae (SN) expelling gas from the galaxy, or by the presence of a photoionizing background which suppresses star formation in the haloes. These and other mechanisms invoked to explain the discrepancy between predictions of low mass DM haloes and observations of low mass galaxies will be discussed later.

It is clear that while the simulations of a CDM dominated universe appear to agree quite well with observations of low mass galaxies in the higher density envi-

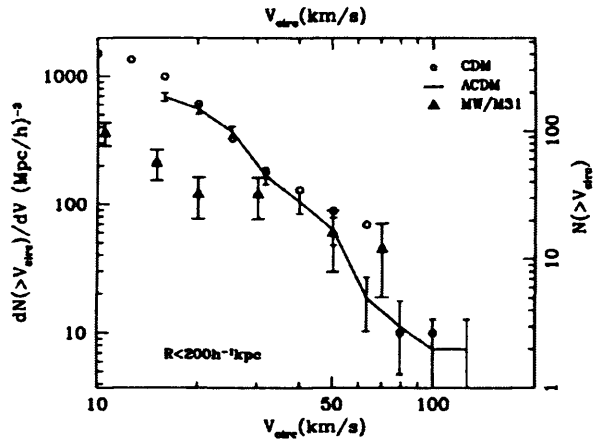

Figure 1.12: Comparison of haloes with measured circular velocities from CDM predictions and observational data for the Local Group (Klypin et al. (1999).

ronments, such as clusters, there is a problem in the lower density environments, such as in groups and around individual galaxies. Whilst these types of galaxies are low luminosity and low surface brightness, and therefore difficult to detect, advances in technology mean that present day searches for these galaxies using CCD data rather than photographic plates, should turn up such objects if they actually do exist. This 'substructure' problem as it is known has led many groups to carry out surveys to quantify the population of dwarf galaxies in different environments by finding the faint end slope of the LF (described by a Schechter function).

1.3.2 Observations

The Virgo cluster, being one of the closest galaxy clusters to us, has been the subject of many a study into its dwarf galaxy population. Reaves (1956) was the first to investigate these galaxies in Virgo. Using photographic plates taken with the Lick 20-inch Carnegie astrograph, Reaves studied the cluster, looking at the low surface brightness nebulae which had been previously identified as possible Virgo dwarf galaxy members during a Supernova program. He split the nebulae

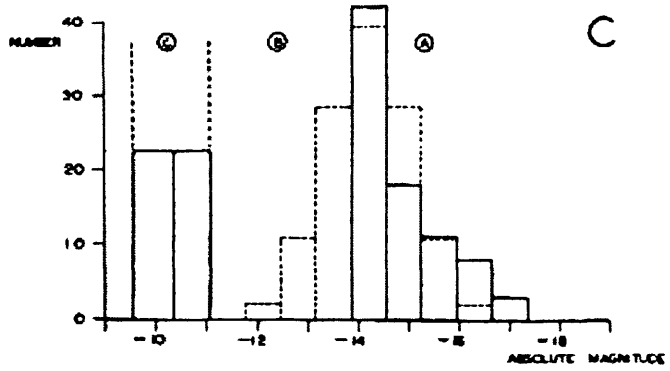

Figure 1.13: Distribution of luminosities of galaxies in the Virgo cluster. The distribution of brighter galaxies is shown by the solid line in part A, with the predicted fit of Hubble's LF plotted as the dotted line in sections A and B. The distribution of IC-3475 type objects is plotted with a solid line in section C.

into 5 categories - dEs, dIrrs, dSpirals, Sculptor-type objects, and IC-3475-type objects. These latter galaxies were found to be extremely low surface brightness with no spiral features or centrally concentrated nuclei, and with nothing similar in the Local Group. Reaves found approximately 1000 of these objects, 48 of which he deemed as highly probable or certain dwarf galaxies in the Virgo cluster. It was these dwarfs that Reaves chose to use to study the distribution and effect on the cluster LF. These objects were both numerous and unlikely to be confused with background galaxies, and thus he considered them more suitable to use than the other dwarf galaxy types he detected in the cluster. Reaves' LF for Virgo, including these objects is shown in Fig. 1.13. Note the magnitude scale is not accurate since Reaves used a distance to Virgo of 2.2 Mpc, which is much smaller than the recently determined distance of 16 Mpc (Jerjen et al. 2004). His calculated values for the absolute magnitudes of the galaxies will therefore be a factor of $\sim$ 4 fainter than the actual values, shifting his faintest (M$\sim$-10) galaxies to M$\sim$-14.

When compared with the luminosity distribution of the Local Group (Fig.

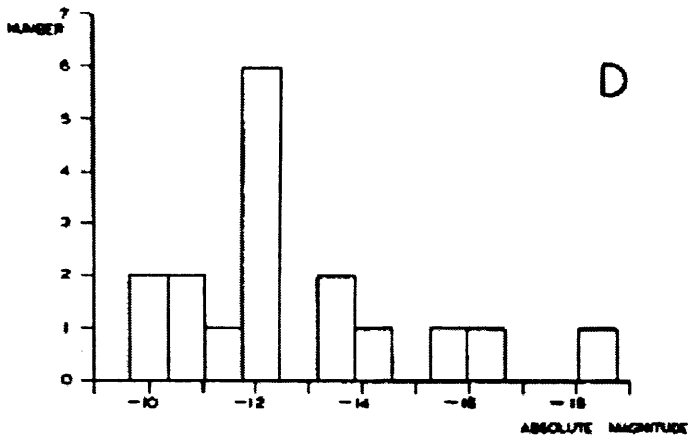

Figure 1.14: Distribution of luminosities of galaxies in the Local Group (Reaves, 1956).

1.14), Reaves concluded that there must be many more Virgo members with -10$\geq M_B \geq$-14 which had been missed by his survey. The fainter population of the Virgo Cluster was investigated by Binggeli et al. (1985) who surveyed $\sim 140^{o^2}$ of the Virgo cluster and produced a catalogue of members and possible members (the VCC) of the cluster based on morphological grounds. This will be discussed in much more detail in Chapter 2. A fitted Schechter function over all galaxy types in the VCC data with B$\leq$20 (M_B $\sim$-11.7 or -11.02 using the more recently determined distance modulus of 31.02) produced a faint-end slope value of -1.30 (Sandage et al. 1985). Further study of the Virgo cluster LF using photographic data was carried out by Phillipps et al. (1998). They found a very steep value of $\alpha \sim$-2.2 in the R-band, using a very different method to identify cluster galaxies. They subtracted galaxy counts obtained from fields outside of the cluster away from those inside the cluster to be left with the residual (small) cluster contribution. These methods however have consistently led to luminosity functions much steeper than those derived by other methods. Trentham & Hodgkin (2002) found the B-band faint-end slope of the LF of the Virgo cluster to be $\approx$ -1.4 for galaxies with absolute magnitudes in the range -18$\leq M_B \leq$-11. Sabatini et al. (2003)

found a faint-end slope value of -1.6 using the same optical data set as Trentham & Hodgkin, but using selection criteria derived from simulations. This criteria maximised cluster object detections, and minimised background contamination (this thesis is a continuation of that work, so the method and results from that survey will be described in more detail later). All these surveys of the Virgo cluster prove the existence of a large population of dwarf galaxies. Another elliptical dominated cluster, richer than Virgo which has been studied extensively is the Coma cluster. Situated $\sim$ 85 Mpc away (Jensen et al. 1999), Coma was surveyed by Karachentsev et al. (1995) with the aim of finding a population of LSB dwarf galaxies. Down to a limiting absolute magnitude M_R $\sim$-10, they found an excess of faint galaxies in the cluster centre, and calculate that there should be $\sim$ 4000 of these objects in the cluster. They found the ratio of dwarf (galaxies fainter than $M_R\sim$-18) to giant galaxies (M_R <-18) in the cluster, (DGR) of 20:1, implying a large population of cluster dwarfs. Milne & Pritchet (2002) also found a large number of dwarf galaxies in the Coma cluster. Using optical images from the HST, reaching the faintest magnitudes sampled as yet, $M_V \sim -7.5$, they found a faint-end slope, α $\sim$-1.75. Mobasher et al. (2003) however, in their spectroscopic survey of the Coma cluster, found a faint-end slope of only $\sim$-1.18. Their LF was however, only measured to M_R $\sim$-16, thus they missed the very faint dwarf galaxy population in their study.

Since the Coma cluster is dominated by elliptical galaxies, and the core of the Virgo cluster contains a larger fraction of giant ellipticals than spirals, and the core is where the dwarf galaxies are concentrated, one might conclude that elliptical-dominated clusters contain large populations of dwarf galaxies. Trentham (1997) found steep faint-end slope values for 3 spiral-rich clusters (Abell 262, NGC 507 and Abell 194) within z=0.016. For magnitudes between -14< M_R <-10, Trentham derived the faint-end slopes, α to be in the range, -1.8< α <-1.6. The

dwarf galaxy population of the diffuse, spiral-rich Ursa Major cluster was also studied by Trentham et al. (2001). They surveyed ~18 sq. degrees of the Ursa Major cluster to a magnitude limit of R=21.5, and found a flat slope of α=-1.1 for galaxies within -17<M_R<-11. Similar faint end slopes have been found for the field from large redshift survey estimates, such as Sloan and 2dF. Data from these recent surveys have been used to define the global (averaged over all environments) Luminosity Function (LF) of galaxies (Blanton et al. 2001, Norberg et al. 2002). These two surveys produce a consistent result for the faint-end slope of the LF, $\alpha \approx -1.2$. However, it is important to note that these redshift surveys have only accurately measured the LF for $M_B < -17$ (Driver & de Propis, 2003). It is not at all clear whether the extrapolation of the LF to fainter magnitudes is valid. The only low density environment where the LF appears to be well measured fainter than $M_B = -17$ is the Local Group (Mateo, 1998, Pritchet & van der Bergh, 1999) and this gives a flat faint-end slope ($\alpha = -1.1$) down to faint magnitudes of $\sim$ $M_B = -10$.

The discrepancy between number of low mass halos produced in numerical and semi-analytic models, and the number of dwarf galaxies observed in low density environments is obvious. However, care must be taken with this comparison -in the main the simulations are of dark matter haloes and it is these that are overproduced in the simulations. To relate dark matter haloes to observations of luminous galaxies requires some modelling of the way in which baryonic material falls into the dark halo and how it is subsequently converted into stars. These physical processes are not straightforward to model. As mentioned earlier in this chapter, the formation of stars from gas in a DM halo occurs once the gas has cooled sufficiently in the halo. The numbers of observable galaxies is then determined by the gas density, temperature etc and by feedback mechanisms such as SN explosions.

If SN explosions do occur, part of their energy is injected into the gas, expelling all or a fraction of it. If all the gas is expelled, there will be none available for further star formation and the halo will gradually fade and become invisible to observers. The idea of SN expelled gas is one of many which are used in theoretical models of galaxy formation to help match up the results with observations.

Prior to discussing the physical mechanisms which are invoked in theoretical models to help match the observed properties of galaxies with predictions, we shall describe briefly the observed properties of dwarf galaxies, and how they are generally morphologically classified.

Dwarf galaxies are generally split into 3 families according to their morphology, magnitude and gas content. The families are dwarf ellipticals (dE), dwarf spheroidals (dSph) and dwarf irregulars (dIrr), although there does not seem to be a clear distinction between dEs and dSphs. Mayer et al. (2001) describe dEs as ellipsoids with absolute magnitudes in the range -17<M_B<-15 and surface brightness, $\mu_B \leq$ 21 mag/sq. arcsec. Their definition for dSphs differs slightly in that they have $M_B \sim$ -9 and $\mu_B \geq$ 24 mag/sq. arcsec. Grebel et al. consider dSph galaxies to be less massive than dEs, but structurally similar, although others consider them to be the same objects - e.g. van Zee (2004), Ferguson & Binggeli (1994). A number of reviews on the properties of dwarf galaxies (Ferguson & Binggeli, 1994; Mateo, 1998), do not give a clear distinction between the two types of objects, if in fact they are separate classes of galaxies. It is generally accepted that dE galaxies are the types of ellipsoidal dwarf galaxies found in the Virgo cluster with $\gtrsim$-11, whereas dSphs describe the fainter dwarfs found in the Local Group with absolute magnitudes in the approximate range -7$\geq M_B \geq$-10. The common feature that dE/dSphs have is that they are generally found to be gas-poor and do not appear to have ongoing SF. dIrr galaxies, which are more commonly found in the field and

lower density environments on the other hand, are gas-rich and usually have HII regions associated with them and so have a much more irregular appearance. Finally there are blue compact dwarfs (BCDs) which have bright central HII regions and lots of HI gas, but are rather elliptical in shape and ultra compact dwarfs (UCDs), a relatively new class of dwarf galaxies. These objects are thought to be the stripped remnants of nucleated dwarf ellipticals, so contain little or no HI gas.

In this thesis, we describe the search for low surface brightness ($\mu_B \geq 23$ mag/sq. arcsec), dwarf galaxies with absolute magnitudes, -14$\leq M_B \leq$-10 at the distance of the Virgo cluster. Since we sample the absolute magnitude range where the separation of dEs and dSphs is unclear, for the objects we detect which are elliptical in shape, and whose properties obey our absolute magnitude and surface brightness criteria (as explained in more detail in chapter 4) we use the terms dE and dSphs to mean the same types of objects.

1.3.3 Feedback mechanisms

As discussed earlier, CDM predicts far more low mass haloes in regions of low density than observations of dwarf galaxies have found. The various theories put forward to reconcile the predictions with observations can be split into two main categories - one which suggests dwarf galaxies can be formed by other means than from small-scale fluctuations in regions where a large population of dwarfs are found, and one which suggests that the formation of dwarfs can be suppressed in regions where there seems to be a lack of dwarfs.

- **Suppression of dwarf galaxies** - There could be some sort of feedback mechanism which suppresses the formation of dwarf galaxies in different en-

vironments, preventing them from forming in large numbers in lower density environments such as the field, but allowing them to form in the higher density regions.

- **Creation of dwarf galaxies** - It could be that the dwarf galaxies found in clusters of galaxies are not wholly those primordial objects predicted to form via CDM structure formation theory, but are a separate cluster population formed by mechanisms which are at play in the dense environment but not in the field.

These two possibilities are discussed in more detail below.

Suppressing star formation in dwarf galaxies

Photoionization

One of the first to suggest the role of a photoionizing background in the suppression of dwarf galaxy formation was Efstathiou (1992). He suggested that in haloes of low circular velocities, a photoionizing background from nuclear activity or star formation would increase the cooling times of the gas in the haloes, therefore suppressing the formation of stars in the halo, and subsequently suppressing the formation of dwarf galaxies themselves. Thoul & Weinberg (1996) investigated this possibility by the use of high resolution hydrodynamical simulations of gas collapse in haloes. They found that the presence of a photoionizing UV background heats the gas in haloes, and thus for haloes with $V_{circ} \leq$30km/s (corresponding to M$\leq 1\times10^9 M_\odot$), the gas is totally prevented from collapsing, whereas for haloes with $V_{circ} \geq$75km/s (corresponding to M$\geq 2\times10^{10} M_\odot$), it has little effect on the gas collapse. This UV background therefore prevents small galaxies from forming, but

does not affect the formation of larger ones. This idea was further studied by Tully et al. (2002) who introduced the idea of photoionization 'squelching'. Using semi-analytical models of galaxy formation to look at gas collapse in haloes, again with an external photoionizing background, they found that dwarf sized haloes which collapsed before the reionization epoch which they assume to be at a redshift, z, of ~6, were able to retain their gas and form stars. Similar sized haloes which formed after reionization however could not form stars as the gas was too hot to collapse into the halo. Thus the formation of dwarf galaxies was inhibited after the epoch of reionization. Tully et al. used the densities of the Virgo and UMa clusters to infer the cluster collapse times to show that dwarf sized haloes will preferentially collapse earlier (i.e. before reionization) in regions of higher density and later (after reionization) in lower density areas, thus explaining the large numbers of dwarfs found in Virgo compared to Ursa Major.

A requirement of Tully's model is that potential cluster dwarf galaxy sized objects form before reionization. However, recent results from WMAP (Spergel, 2003) puts the epoch of reionization at a high redshift of ~20, which is a time when mass fluctuations of this size in CDM models are extremely rare. At this redshift the fluctuations which collapse to form $10^6 M_\odot$ sized objects are 3σ fluctuations. They are 1σ fluctuations, and therefore much more common at a redshift ~ 6 (Miralda-Escude, 2003). Thus this model needs to be reconsidered in the light of the WMAP result.

There have been other studies which investigate how reionization may affect the formation of dwarf galaxies. Susa & Umemura (2004), in their 3D hydrodynamical simulations, found that early reionization was highly destructive for galaxies with masses $\leq 10^8 M_\odot$ and circular velocities $\leq 20 \mathrm{km} s^{-1}$ - almost all of the gas in these sized haloes was photo-evaporated, effectively preventing star formation.

In haloes which are more massive and have greater velocities however practically all the gas was transformed into stars even after the epoch of reionization at ~17. Kravtsov et al. (2004) carried out high resolution numerical simulations to follow the evolution of DM haloes in a CDM cosmology. Their results suggest that in the denser environments, a larger fraction of sub-haloes were more massive in the past than in less dense environments, thus they were able to accrete gas and form stars before tidal stripping led to dramatic mass loss and a decrease in their circular velocities. Today they would be seen as faint, LSB dwarf galaxies in groups and clusters, but not in the field. Combining the results of Susa & Umemura and Kravtsov et al. raises the possibility that some present day low mass galaxies could have been part of larger mass haloes in the past. The gas in these large haloes would not have been affected by reionization and would therefore be able to form stars before being tidally stripped and evolving into the low mass galaxies which we see today.

Gas expulsion via supernovae winds

The expulsion of gas from the low mass DM haloes by the injection of energy from the first population of SN (Dekel & Silk, 1986) is the general feedback mechanism treated analytically in models when attempting to reconcile the observed number of dwarf galaxies in the Universe with the number of DM haloes predicted from CDM. Once the gas is expelled from the halo, it is no longer available for star formation, thus the halo remains dark and undetectable. For this expulsion to occur, the gas must have enough energy injected into it that it can escape from the halo. Dekel & Silk show that a protogalaxy with virial velocity V $> V_{critical}$(~100km/s) will not expel its gas from its halo, and will form a 'normal' galaxy. Those protogalaxies with V$< V_{critical}$ however will lose their halo gas after the SN injected energy, and will either form a diffuse dwarf galaxy, or, in the case

of total mass loss, the halo will remain invisible. However, the results of the models of Mac-Low & Ferrara (1999) show that the effect of SN explosions in dwarf galaxies is inefficient at removing gas from the halo. This is clearly a mechanism which needs further investigation.

Pressure Confinement

The mechanism described above of losing gas due to SN winds does not explain the *environmental* dependence of the dwarf galaxy population - if only this feedback mechanism was at play in the halo, star formation should be suppressed equally in all environments. Babul & Rees (1992) suggest that the quantity of gas lost from these low mass haloes via SN driven winds depends upon the external pressure exerted onto the halo by the intergalactic medium. In a low density medium where the external pressure is low ($nT \leq 1cm^{-3}K$), the first SN would expel all the gas from the halo, preventing stars from forming, so no galaxy would be visible. In a high density medium, such as in a cluster, where $nT \geq 10^4 cm^{-3}K$, the SN winds would blow out the gas but it would not reach beyond the galaxy's halo. After some time the gas would fall back onto the galaxy centre, resulting in bursts of star formation. In environments where $nT \geq 10^5 cm^{-3}K$, i.e. at the very centre of clusters, the expelled gas would not go beyond the starburst region and observations would show either one prolonged star burst or very shortly separated bursts of star formation in the galaxy. This, suggests Babul & Rees, may explain the nucleated dwarf ellipticals which have been observed.

Creating dwarf galaxies

Morphological Transformation

There are 3 main processes which are prevalent in galaxy clusters but rarely occur in the field. These are ram pressure stripping, tidal interactions and pressure confinement of expelled halo gas. The process of pressure confinement has been discussed in the previous section as it becomes important when gas is expelled from a halo by SN winds. Here we describe in more detail ram pressure stripping and tidal forces. These 2 processes allow morphological transformation of a galaxy to occur. Moore et al. (1999) suggest that such 'galaxy harassment' could be responsible for the excess dwarf galaxy population in the Virgo cluster. In this scenario, dwarf elliptical galaxies are formed when infalling LSB spiral galaxies are 'harassed' in the cluster by the giant galaxies and stirred up by tidal forces, subsequently losing their gas, resulting in a change into a dwarf elliptical (dE). Evidence to support this theory comes from a study of Virgo cluster dwarfs, conducted by Conselice et al. (2001). They show that the dwarf ellipticals found in Virgo have a cluster velocity distribution closer to that of the spirals than that of the earlier type galaxies. The dwarf velocity distribution is quite wide, and is non-Gaussian with a total velocity dispersion of 726km s^{-1}, similar to that of the spirals, which is 776km s^{-1}. The dwarf galaxies appear not to be relaxed and are less dynamically evolved than the Virgo cluster core elliptical population, indicating that they are a population of recently formed objects, possibly as a result of accretion into the cluster.

However, other studies have proposed that it is in fact dIrrs which are transformed into dE galaxies in the cluster environment. Sabatini et al. (2005) show that the dwarf galaxies detected in the Virgo cluster are too small to be the result of the harassment process proposed by Moore et al. (1999). They propose that the dE galaxies are the result of an earlier infalling dIrr galaxy population which may be associated with the faint blue galaxies seen at higher redshift ($0.5 < z < 1.5$).

They suggest that the star formation of these small infalling haloes is enhanced by the weak tidal interactions with the cluster potential and other cluster galaxies - these types of interactions are not available to galaxies in lower density environments like the field so these haloes have their evolution advanced by the cluster environment and they are changed into dE type objects.

Grebel et al (2003) investigated the possibility that dIrrs may be the progenitors of dSph galaxies by studying the metallicities and HI gas content of 40 early-type and late-type dwarf galaxies in the Local Group and field. They show that for a given luminosity, the dIrrs are more metal-poor than the dSphs. Since it is the older stellar populations of these objects which are being studied, one would assume that if they started out as similar objects but took different evolutionary paths to separately become dIrrs and dSphs, then their early star formation rates would be similar, and thus their metallicities would also be comparable. The result found by Grebel et al. of differing metallicities therefore puts doubt on the idea that dIrrs have evolved to become dSphs. Another point to consider is that dSphs have no detectable HI gas, and, according to Grebel et al., do not rotate. Thus, dIrrs, which are both HI rich and supported by rotation, would have to lose their angular momentum and all their gas if they are to form into the gas poor, non-rotating dSphs which we see today. Grebel et al. say that it is possible that tidal interactions could remove the gas from the dIrrs, but this would not explain how there are isolated dSphs. They do not agree that dIrrs are the progenitors of dSphs. Instead, they consider 'transition-type dwarf galaxies' to be likely candidates for the evolution into dSphs. These types of objects have properties of both dIrrs and dSphs - they are low luminosity and contain old stars, as do dSphs, but they are also rich in HI gas, as are dIrrs. Their place on the luminosity-metallicity diagram overlap with that of the dSphs, unlike the dIrrs, which are offset from the

dSphs on such a plot. Their star formation rates are low, so it is not likely that they will lose their gas very soon. Grebel et al. therefore conclude that in order to transform them into dSphs, a gas-cleaning mechanism has to be invoked - ram pressure stripping is their favoured method in this case.

However, van Zee et al. (2004) present observations of 16 dwarf ellipticals in the Virgo cluster which show that at least 7 of them have a significant rotational component, contrary to what other studies have previously shown (Bender et al. 1991; Ferguson & Binggeli 1994) and posing a problem for the reasoning of Grebel et al. as to why dIrrs could not evolve to become dSphs. Although Mayer et al (2001) suggest 'tidal stirring' as a mechanism to enable angular momentum loss, Grebel et al. comment that this would not explain the existence of isolated dSphs where they cannot have experienced repeated tidal shocks to evolve into dSphs. The results of van Zee et al. (2004) show that there is a possibility that *some* dIrrs may evolve to become what we see as dEs/dSphs today, although the matter of what happens to the gas in the dIrr is still under question. van Zee et al. suggest that stripping of infalling dIrrs into clusters such as Virgo can account for at least some of the dEs in the cluster. They argue that since it is likely to be Local Group analogs which are falling into the cluster, there must be a large population of dIrr type galaxies falling in (since these types of objects are more commonly found in lower density environments), and most will lose their gas via stripping mechanisms, therefore becoming dEs.

Tidal Interactions

Another type of dwarf galaxy formed by its environment is the tidal dwarf galaxy (TDG). These objects form in the tidal tails produced by the collision or merger of larger galaxies. During such interactions between two spiral galaxies, gas

and stars are pulled from the galaxies forming giant streams along which clumps of stars and gas form. Over time, the stream fades, but some of the clumps may stay together as a bound object known as a tidal dwarf galaxy. Okazaki & Taniguchi (2000) modelled the formation of such dwarfs from interactions between disk and S0 galaxies. For each galaxy interaction occurring in a hierarchically formed Universe, 1-2 TDGs are formed. However, their study was based on galaxy cluster collapse at high redshifts, and they comment that it is likely that some, if not most, of these newly formed TDGs would either merge together to form higher mass objects, or fall back onto the parent galaxy during subsequent evolution of the cluster. TDGs are not likely to constitute a large fraction of the cluster dwarf population, although their existence in clusters could be verified by investigating stellar populations and metallicities. Since they form out of pre-existing galaxies, they will have evidence of both young and old stellar populations, the old from the parent galaxy, and the new from later gas collapse onto the newly formed galaxy.

1.4 Summary

The hierarchical clustering theory of structure formation in the Universe says that small scale objects form first in the Universe, and subsequently merge together to form larger objects. There should however, according to this theory still be numerous small mass objects left in the Universe today. If these objects can form stars then they should be visible as dwarf galaxies. The galaxy LF is a measure of the relative numbers of bright and faint galaxies in the Universe. A steep faint-end slope of this function implies the existence of numerous dwarf galaxies. Steep slopes have been found in many cluster environments such as Virgo and Coma, but large redshift surveys of the field have produced LFs with flat faint-end slopes

- they have failed to find the numbers of dwarfs predicted by CDM. There are 2 possibilities -

- Dwarf galaxies could be created in the cluster environment through processes such as galaxy harassment and tidal interactions. This would increase the population of dwarfs in these regions.
- The formation of dwarf galaxies could be suppressed by feedback processes such as gas expulsion due to SN winds, or the presence of a photoionizing background. Any suppression mechanism however must be environment dependent to explain why there are fewer dwarfs in the field than in clusters.

Although there is a discrepancy between predicted numbers of dwarf galaxies and observed numbers, this issue is clouded by non-uniform datasets. Different surveys reach different magnitude and surface brightness limits with their data, and detection methods and selection criteria vary in the identification of dwarf galaxies. We aim to eliminate this source of confusion with our identical data sets in this thesis. Reaching fainter magnitudes than in previous surveys, we have over 60 sq. degrees of optical data in B and I, covering regions of varying density in the Universe. Using exactly the same detection algorithm and selection criteria for identifying dwarf galaxies, we search for LSB dwarfs in this data to firstly ensure that nothing has been missed by previous surveys, and secondly to compare the results with CDM predictions. The colour data, together with HI observations for a number of our detected galaxies, enables us to investigate the possible formation scenarios of the dwarf galaxies, and decide whether they are the primordial population as predicted by CDM, or if they have formed more recently from processes ongoing in their environment.

The thesis is set out as follows:

- Chapter 2 describes the environments that we have sampled with our data in this thesis, ranging from the high density Virgo cluster to the low density field.

- Chapter 3 describes the instruments used to obtain both the optical and HI data used in this thesis and discusses the limits of our data.

- Chapter 4 describes how LSB dwarf galaxies were detected and selected in our datasets. The detection algorithm which was specifically written to detect faint objects is described, together with an explanation of how the selection criteria was chosen from numerical simulations to preferentially select LSB dwarf galaxies and minimise background contamination.

- In Chapter 5, the optical results for the four data sets are presented, detailing the number density of LSB dwarf galaxies found, how they are clustered, what their colours are and how they differ for each environment.

- The HI results for both pointed observations of field galaxies and a search for HI in the UMa cluster are given in Chapter 6.

- Finally, in Chapter 7 we present our discussion and conclusions from our results.

Chapter 2

The Environments

As discussed in Chapter 1, there appears to be an environmental dependence of the observed dwarf galaxy population. We have sampled four very different environments in order to study the populations and properties of dwarf galaxies in each environment to investigate if they are the primordial objects predicted by CDM, or if they have formed more recently due to environment dependent processes. We present a discussion of these four environments in this chapter.

2.1 Virgo cluster

The Virgo cluster is an irregularly shaped, dense cluster of galaxies situated at a distance of approximately 16 Mpc (Jerjen et al. 2004) and covering an area of $\sim 100^{\circ^2}$ on the sky. It is currently forming from several infalling clouds and subclusters (the details of which shall be discussed later), which, as explained in Chapter 1, is expected from CDM theory. The cluster has a high velocity

dispersion of ~715 km/s, and crossing time of approximately a tenth of a Hubble time (Trentham & Tully, 2002). Compared to other galaxy clusters it also has a relatively high number density of galaxies - using our definition of a giant galaxy, $M_B \leq$ -19, we find 5 times as many giants in the Virgo cluster area than UMa, which has a crossing time approximately equal to a Hubble time. The probability of interactions between galaxies in Virgo is therefore likely to be high because of the higher density and shorter crossing time. As discussed in the previous chapter, such interactions may play an important role in the formation and evolution of dwarf galaxies in the cluster environment. Another factor which may affect the evolution of galaxies in the Virgo cluster is the presence of a hot intra-cluster X-ray gas. The existence of this gas in Virgo was first studied by Böhringer (1994) using the ROSAT observatory. He found X-ray emission extending across the whole 10° of the cluster, but centered upon the 3 giant Ellipticals, M87, M86 and M49. Such a medium is likely to affect the evolution of galaxies travelling through the cluster as it increases the amount of gas stripped from them due to ram pressure stripping.

The Virgo cluster contains a mix of galaxy types, the location of which confirm Dressler's (1980) morphology-density relation. The giant elliptical galaxies are found predominantly at the centre of the cluster, whilst the late-types, are found towards the outskirts. Of the approximately 1300 known members of the cluster found by Binggeli et al. (1985), ~6% were giant early-type galaxies, ~17% were giant late-types, and the remaining, most numerous galaxy types, were classified as dwarf galaxies.

As discussed in Chapter 1, Reaves (1956) was the first to conduct a detailed study of the dwarf galaxy population in Virgo. He found a number of objects which he concluded were certain or probable dwarfs in the cluster, and proposed that there were many more with absolute magnitudes in the range -10$\leq M_B \leq$-14

which his survey had missed. Deeper data would be needed to probe the fainter objects in the cluster.

The most comprehensive survey of the Virgo cluster was carried out by Binggeli et al. (1985) using the Las Campanas du Pont 2.5 metre telescope. This survey consisted of photographic data of 67 fields extending 6° from the cluster core (defined as M87), and a tip of the Southern Extension.

With a completeness limit of $B_T \leq 18$ for their data, Binggeli et al. were able to detect galaxies down to $M_B \sim -13.0$ (assuming our distance modulus of 31.02 and H_0=75kms^{-1}Mpc^{-1}) and effective surface brightness of 25.5 mag/arcsec^2. Their Virgo Cluster Catalogue (VCC) contained information on the 2096 galaxies detected in the region of their data fields, classified as members of the cluster or background galaxies, according to their morphologies and available redshift data. Of the 2096 galaxies found, 1277 were classified as members of the Virgo cluster, 574 were possible members, and 245 were found to be background. Through analysis of the members and possible members of the Virgo cluster, Binggeli et al. found the LF of all the cluster galaxies was well fitted by a Schechter function with faint end slope, α∼-1.25. When corrected for completeness, and extrapolating down to M_B ∼-11.0, this led to an increase in the faint-end slope, α, to ∼-1.30. The LF for Virgo is shown in Fig.2.1. The line labelled 'divergent' in the figure refers to a faint-end slope value of -2.

Binggeli et al. studied in detail the kinematics of the galaxies classified as members and possible members of the cluster. They found that the early and late type galaxies, although distributed differently in the cluster, with the early types concentrated around the centre, and the late-types at the edge of the cluster, had similar mean velocities (1062±68km^{-1} for late types; 1134±45 kms^{-1} for early

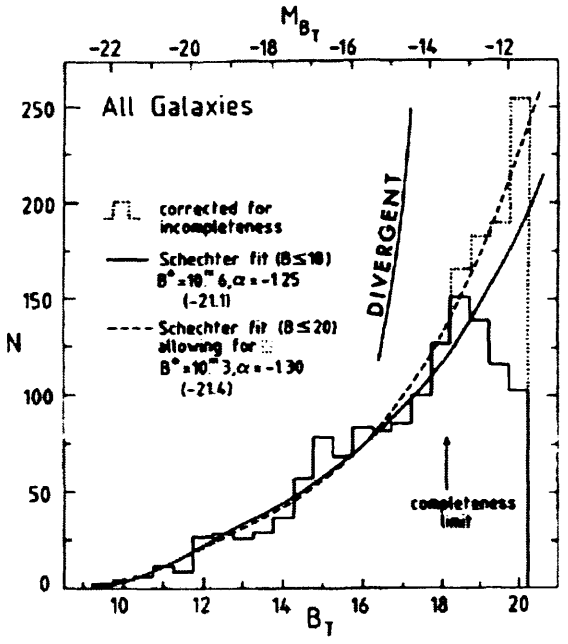

Figure 2.1: Luminosity Function of all Virgo Cluster galaxies (Binggeli et al. 1985). The 'divergent' line represents a faint-end slope of -2.

types). However, the velocity dispersions for these galaxy types *did* differ significantly. The early-type galaxies had a much lower velocity dispersion of 573kms^{-1} compared to 888kms^{-1} for the late-types, implying that the late-type galaxies are in fact infalling or have fallen recently, towards the cluster core.

In their survey, Binggeli et al.(1987) also found evidence that the Virgo cluster is made up of subclusters, centered upon M87 (Subcluster A) and M49 (Subcluster B). These subclusters can be seen in Figure 2.2 plotted over the positions of all cluster members. Subcluster A is a double structure containing 2 subclumps centered upon M87 and M86. The boundaries of subclusters A and B are defined in Binggeli et al. (1993) - *Small A* consists of an inner or core boundary enclosed by a radius of 2° centered upon M87. *Big A* is the irregularly shaped outer or halo boundary. Cluster B is defined by 3 circles centered upon M49 with increasing radii. *Small B* has a radius of 1.6°, *Intermediate B* has radius 2° and *Big*

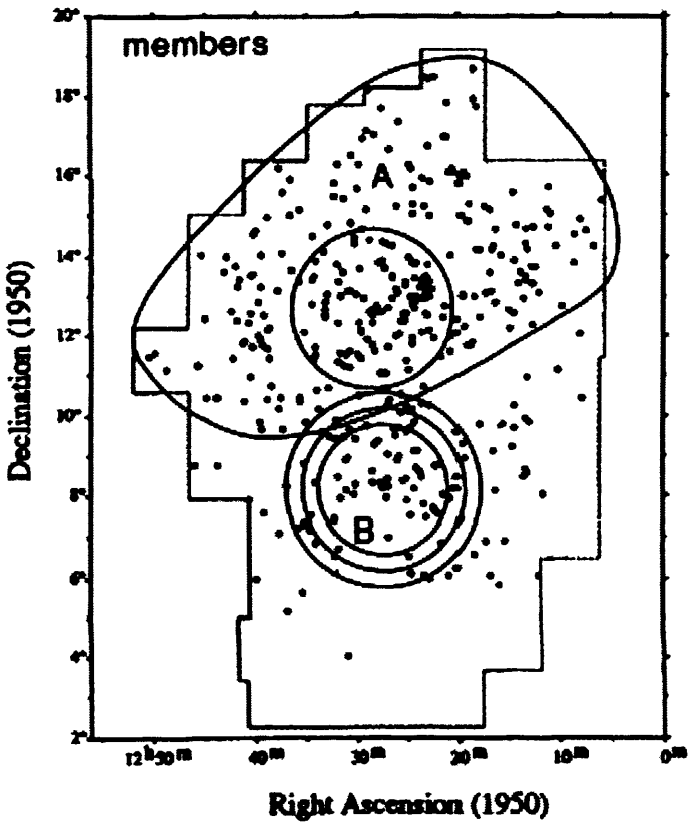

Figure 2.2: Positions of sub-clusters A and B in the Virgo cluster as described in Binggeli et al. (1993). *Small A* can be seen as the central circle, with *Big A*, the irregular shape surrounding it. The three radii for *Small B*, *Intermediate B* and *Big B* can be seen as the 3 circles underneath subcluster A.

B has radius 2.4°. As is obvious from Fig.2.2, subcluster A is more extended in space than B, but it is also more extended in velocity with a velocity dispersion of $\sim$750kms^{-1} compared to $\sim$400kms^{-1}. It contains mostly early-type galaxies whereas Subcluster B is dominated by late-types.

The kinematics of the dwarf galaxies in the M86 subclump of Subcluster A showed that this subclump is actually falling onto the M87 subclump from the back of the cluster (Binggeli et al. 1999). This was verified by Böhringer's (1994) study of the X-ray gas structure in the cluster, further emphasising the non-spherical

geometry of Virgo.

The distances to the sub-clumps in the Virgo cluster have been determined by Feldmeier et al.(2004). Using planetary nebulae data for the cluster, Feldmeier et al. estimated upper limits for the distances to subclusters A and B as 12.7±0.4Mpc and 14.1±0.8Mpc respectively. They also estimated the depth of the cluster - stating that it '*is more than 2.6 times as deep as it is wide*'. This depth, they say agrees well with results from other Virgo cluster studies, such as Yasuda, Fukugita & Okamura (1997) who used the B-band Tully Fisher relation to estimate the distances to spirals in the Virgo cluster. They found a large scatter in the distances, due, they claim, to the large depth of the cluster from 12 Mpc to 30Mpc. Jerjen, Binggeli & Barazza (2004) also used surface brightness fluctuations of a sample of dEs in the cluster to estimate a cluster depth of $\sim$ 6 Mpc.

Apart from the subclusters there are also smaller clouds present in the region (Binggeli et al., 1987), namely, the M cloud which is NW of M86, and the W cloud which is SW of the M87 sub-clump. These can be seen in Fig. 2.3 together with the positions of the two subclusters, *Small A* and *Big B*. Binggeli et al. (1993) used the velocity information and morphological criteria of galaxies to help distinguish between cluster galaxies and the nearby background objects i.e. those objects in the clouds. They found the mean velocity of the Virgo cluster to be 1050±35kms^{-1}, and the galaxies in the M and W clouds to have mean velocities of $\sim$ 2000kms^{-1}. Thus, they considered both clouds to be at twice the distance of the Virgo cluster. Ftaclas et al. (1984) also consider the M and W clouds to be further than Virgo due to their mean velocities; they estimate the cluster mean velocity to be 960-1000kms^{-1} with the M and W cloud mean velocities of 2179kms^{-1} and 2198kms^{-1} respectively. Ftaclas et al. also claim the existence of another cloud in the Virgo cluster region, the N cloud. With a mean velocity of 1500kms^{-1}, they also assume

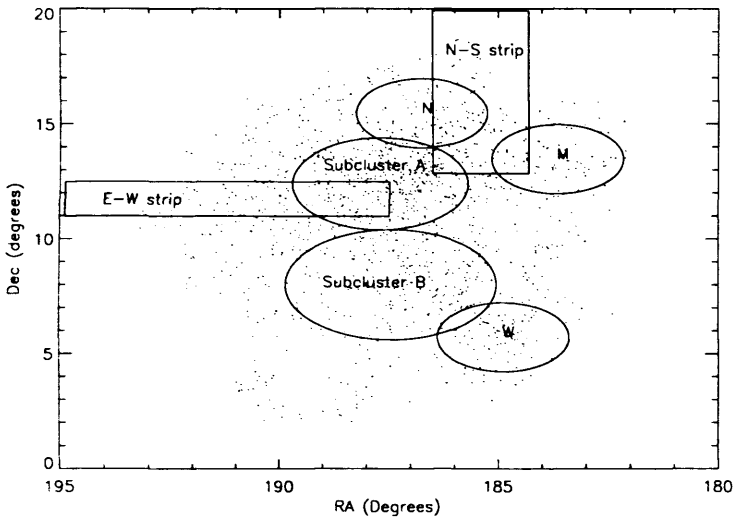

Figure 2.3: Positions of the 2 Virgo cluster data strips in relation to the sub-clusters and clouds in the cluster. The area enclosed by Subcluster A is *Small A*.

this cloud to be distant. Binggeli et al. (1987) however, consider it to be part of the Virgo cluster proper based on their velocity estimates and morphological criteria.

Area covered by our data

The detailed study of the Virgo Cluster, carried out by Binggeli et al., reached absolute magnitudes, $M_B \sim$-13.0, and isophotal surface brightness values of $\sim$25.5 Bmag/arcsec^2. Although a large population of dwarf galaxies was uncovered in this survey, deeper data are needed to probe the population to even fainter magnitudes. Our deep CCD data covering 15 sq. degrees of the Virgo cluster extending from the centre of the cluster (defined as M87) Northward reach central surface brightnesses of $\sim$26 Bmag/arcsec^2, and absolute magnitudes down to -10. This strip can be seen labelled as 'N-S strip', in Fig. 2.3. The East-West (E-W) strip also plotted in this figure was surveyed in a similar study by Sabatini et al. (2003, 2005). We

compare the results of the N-S strip with those of the E-W strip in Chapter 5 of this thesis. This will enable us to investigate the effect the different parts of the cluster may have on the population of cluster dwarf galaxies. The N-S strip overlaps partly with the N and M clouds and also over a small part of *small A* and most of *Big A*. The E-W strip samples Subcluster A only .

2.2 UMa cluster

The UMa cluster is situated at approximately the same distance (18.6 Mpc, Trentham & Tully, 2002) as the Virgo cluster. However, unlike Virgo, it is populated predominantly by late-type galaxies and there is no concentration towards a central cluster core. It also has a lower velocity dispersion than Virgo, of $\sim$ 150km/s compared to $\sim$ 700km/s. We calculate the number density of giant galaxies, using our definition of a giant as having $M_B \leq$-19, over the extent of the cluster ($\sim$7.5°) to be $\sim$1 giant per Mpc^2 - 5 times less than in Virgo. The crossing time for UMa is comparable to a Hubble time, thus one would expect few galaxy-galaxy interactions to have occurred in this cluster. The low density of the cluster has even led to comments (Zwaan et al. 1999) that when compared to other classical clusters, UMa is more like an overdensity of galaxies rather than a cluster. If this is true, then the processes described in Chapter 1 which are prevalent in the cluster region, such as ram pressure stripping and tidal interactions, are quite unlikely to have played a large role in the formation or evolution of galaxies in UMa. Neither has UMa any appreciable X-ray emission, so its galaxies, unlike in Virgo, will not be affected by the presence of a hot intra-cluster gas.

The UMa cluster is situated at a position in the Universe where other clouds

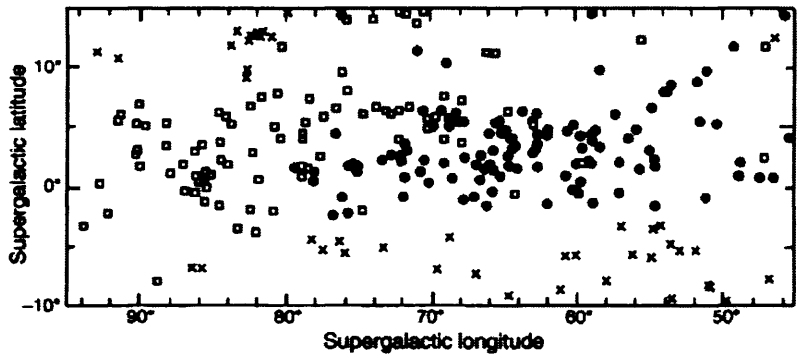

Figure 2.4: Projected plot of all galaxies in Tully's NBG catalogue obeying V_0<2000kms^{-1} and 45°<SGL<95°. The open squares represent galaxies from the Coma-Sculptor cloud, the solid circles are those in the UMa cloud (of which the UMa cluster is a part), and the crosses are those from other structures.

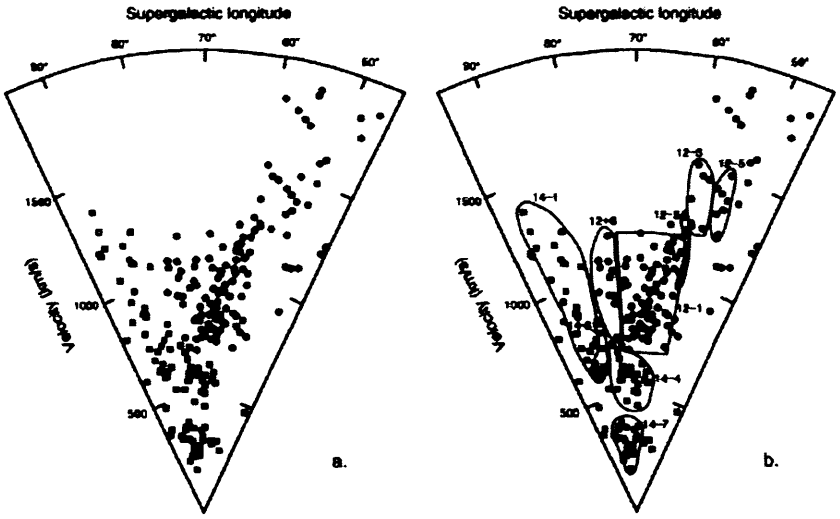

Figure 2.5: Redshift cone diagram of all galaxies obeying V_0<2000kms^{-1} and 45°<SGL<95°. The left figure shows the distribution of these galaxies. In the right hand figure, the galaxies have been grouped into separate clouds (as defined by Tully, 1987). The open squares at the left hand side and lower part of the cone represent those galaxies from the Coma-Sculptor cloud, the solid circles are those in the UMa cloud, which contains the UMa cluster. The UMa cluster as defined by Tully et al. is the rectangular shaped region labelled 12-1.

and filaments are located. This can therefore cause confusion in the classification of the cluster members. Tully et al. (1996) undertook an extensive study of the UMa region in order to define criteria for membership of the cluster so that further work could be carried out on the cluster galaxy populations. This task was helped by the limited velocity range of the galaxies attributed to the cluster. Fig 2.4 shows the position of all galaxies with velocities less than 2000km/s from Tully's Nearby Galaxies Catalogue (Tully, 1988). The open squares represent galaxies in the Coma Sculptor cloud, filled circles with the UMa cloud, which includes the UMa cluster, and crosses with other structures. Although this figure appears quite confused, an enhanced view can be seen in Fig 2.5, where a velocity axis is added to the data. The symbols in this plot are the same as for Fig. 2.4. With this information, Tully separated the galaxies into groups (defined by the calculated gravitational force between galaxies), which can be seen in the right hand plot of Fig 2.5). The extent of the UMa cluster is shown, labelled as Group 12-1. In terms of velocity and position, it is defined by:

- *Radial extent* - 7.5° radius centered upon α=$11^h56.9^m$, δ=49°22′ (B1950);
- *Velocity extent* - $700 < V_{helio}+30\sin l\cos b < 1210 kms^{-1}$.

With the UMa cluster separated from adjoining nearby galaxy groups and clouds, the populations of galaxies in the actual cluster could be studied in detail. The first such study of the dwarf galaxy population in the Ursa Major cluster was carried out by Trentham et al. (2001) using the UH8K and CFH12K mosaic CCD cameras on the Canada-France-Hawaii-Telescope (CFHT) during two observing runs in 1996 (Tully, 1996) and 1999. Their survey covered ~18 sq. degrees of the cluster in the R band down to a magnitude of 21.5 (corresponding to $M_R \sim -9.85$),

and surface brightness limit of 27 Rmag/arcsec^2. They then conducted follow-up B, R and I observations of candidate dwarf galaxies found in their surveyed area. Their criteria of membership or possible membership of the UMa cluster was decided by two parameters which measured the magnitude of the inner and outer parts of the galaxy. A condition for membership was then assigned to each galaxy where '0' implied that the galaxy was a definite cluster member, confirmed by HI data; '1' was a probable member but with no HI detection, '2' implied the galaxy was possibly a member but possibly background and a classification of '3' meant that the galaxy was probably a background galaxy, but could be a member.

The LFs for the UMa cluster obtained by Trentham et al. are shown in Fig 2.6. The histograms in both the upper and lower figure represent the LF of the bright galaxies found from their 1996 data. The dashed lines in the figures are the best-fitting power laws to the 1999 data for galaxies fainter than $M_R \sim$-18. The dot-dash line represents a Schechter fit to the combined 1996 and 1999 data, where the faint end slopes, α, were found to be -1.01 for all objects classified as '0' or '1', and -1.16 for objects classified '0-3'. Also plotted for comparison on the plots is the LF found by Phillipps et al. (1998) for their study of the Virgo cluster for which they found a much steeper faint-end slope, α, of -2.26$\pm$0.14 over -16$<M_R<$-11.5. Although the method they used to select cluster galaxies usually leads to steep values being found, as discussed in Chapter 1, Binggeli et al. also found a steeper faint-end slope for Virgo than Trentham et al. found in UMa. This apparent lack of dwarf galaxies in UMa compared to Virgo again highlights the differences between the two clusters.

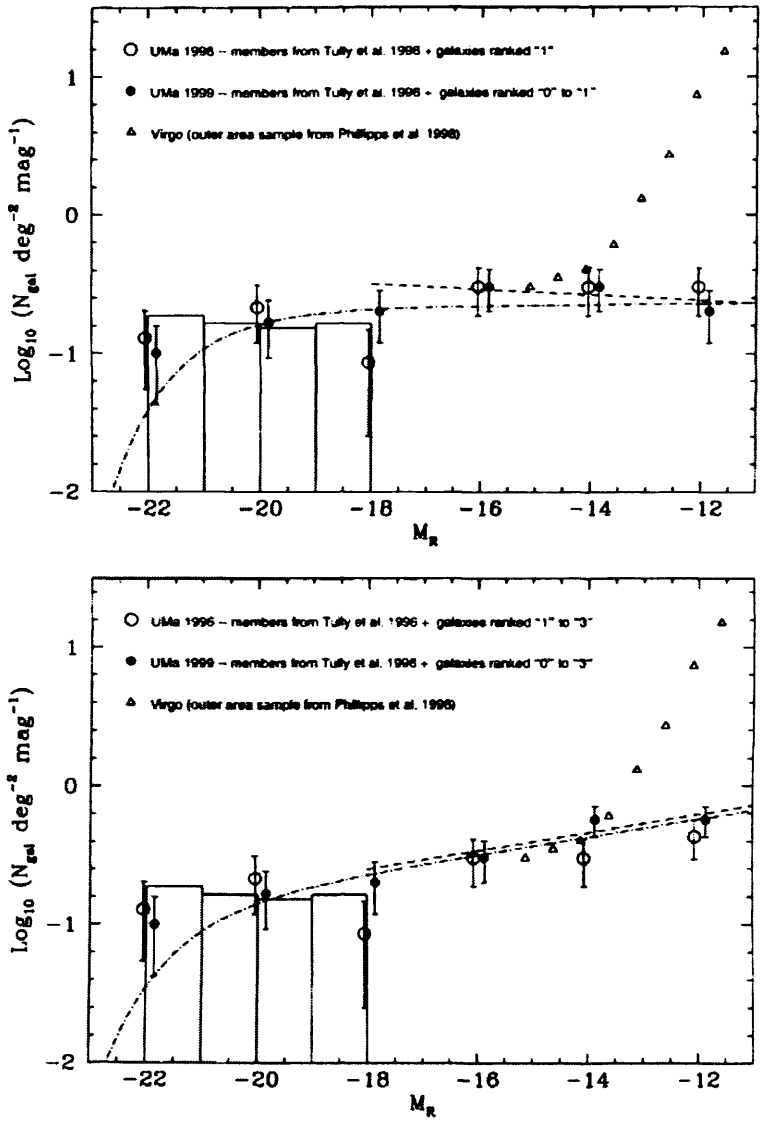

Figure 2.6: Luminosity functions for Trentham et al.'s. data of the UMa cluster. The upper figure presents the LF for galaxies classified as '0' or '1'. The lower figure represents the galaxies classified '0-3'. Phillipps et al.'s (1998) LF for the Virgo cluster is also plotted for comparison.

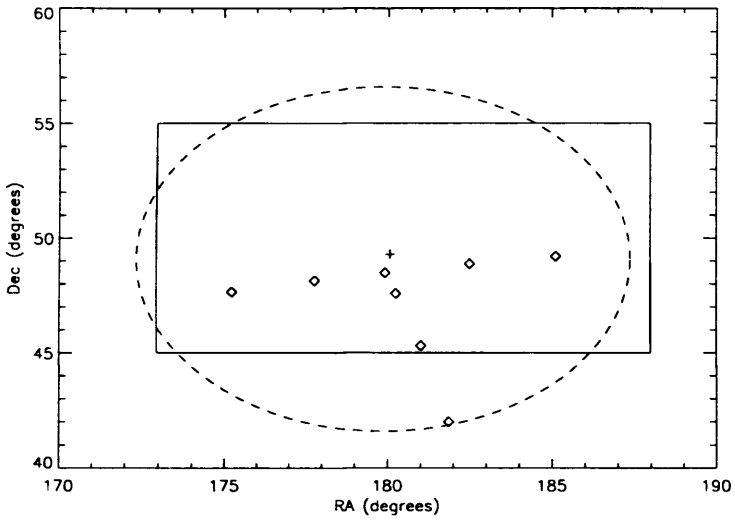

Figure 2.7: Positions of optical fields (plotted as diamonds) and extent of HI data cube (rectangular box) with respect to centre of UMa cluster ($11^h59^m28.3^s$; 49°05′18″) as marked by the cross. Also plotted is the extent of the cluster, defined by Tully (1996) as a radius of 7.5°, marked by the dashed ellipse.

Area covered by our data

Our optical data fields of the UMa cluster, obtained in Spring 2002 using the WFC on the INT, are shown as diamonds in Fig. 2.7. Reaching absolute magnitudes of ∼-10 and surface brightnesses of ∼26Bmag/arcsec^2, the data covers 8 fields totalling 1.68 deg^2. All fields corresponded to a number of fields studied by Trentham et al. (2001) in their more extensive R-band survey. Also plotted in Fig. 2.7 is the area covered by the HIJASS data cube used in our HI study of the cluster (see Chapter 6).

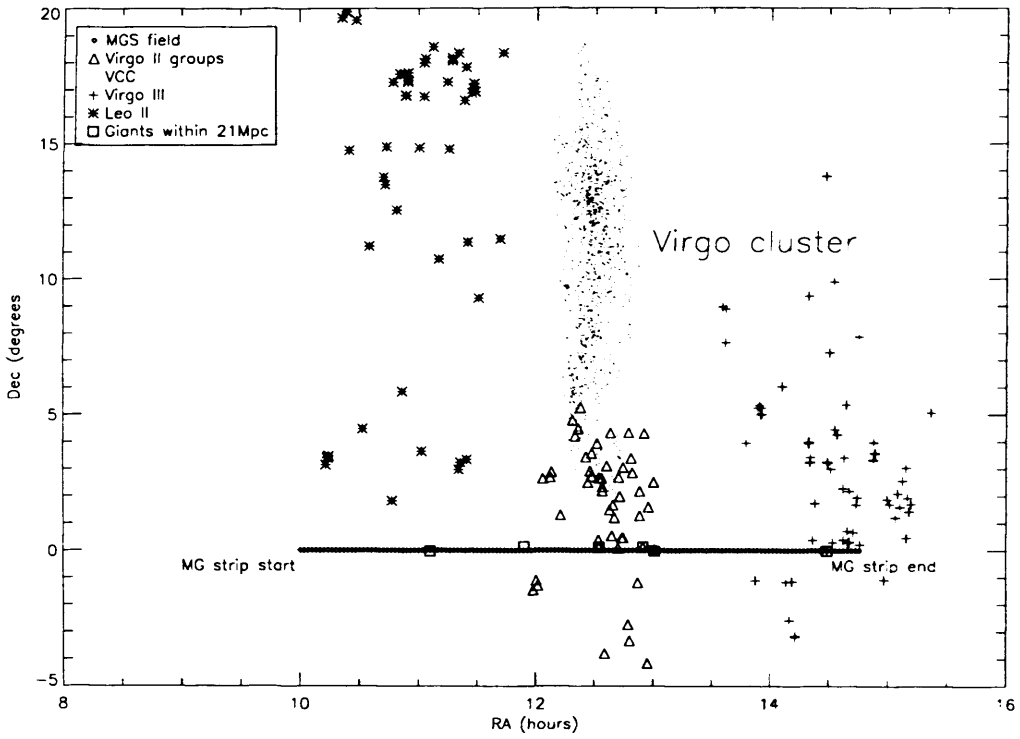

Figure 2.8: Positions of MGS in relation to the Virgo cluster, Virgo and Leo sub-groups and giant ($M_B \leq$-19) galaxies within 21 Mpc that lie along the strip.

2.3 Field - The Millennium Galaxy Strip

The field environment studied for this thesis was taken from a strip of 144 fields running along the celestial equator from RA 10hrs through to RA $\sim$ 15hrs (Liske et al. 2003). The path of the strip, (known as the Millennium Galaxy Strip - MGS) can be seen relative to nearby galaxies in Fig. 2.8.

Starting just South of the Leo group, the strip passes very close to two giant ($M_B \leq$-19) spiral galaxies within 21 Mpc (see Chapter 4 for an explanation of this distance limit), before passing through the Virgo Southern Extension, (plotted as triangles in the figure). Although named the Virgo Southern Extension, this region it is not actually part of the Virgo cluster itself. de Vaucouleurs (1961) stated that

'the southern Virgo cloud is closely similar to the Ursa Major cloud and probably no more directly related to the Virgo cluster proper, except in so far as both are galaxy clouds within the Local Supercluster' (and as shown in Chapter 5, our optical results confirm this statement). The galaxies in this region therefore are not likely to be as dense in number as those in the actual cluster. After passing through this extension, the strip then passes back into an apparently empty region Eastwards before ending in a filament of galaxies known as the Virgo III cloud. In this thesis, we assume a distance limit of 21 Mpc for detecting objects in the field data with the same range of magnitudes and surface brightnesses as that of the Virgo and UMa cluster surveys. This is explained in more detail in Chapter 4, but with this limit in mind, we can estimate the number density of giant galaxies (defined as those with $M_B \leq$ -19) in the area of this strip out to 21 Mpc, to be $\sim$ 1 per Mpc^2, which is comparable to the Ursa Major cluster number density, and much less than that of the Virgo cluster.

As mentioned in Chapter 1, the largest surveys conducted to find the LF of the field were the SDSS and 2dF redshift surveys (Blanton et al. 2001, Norberg et al. 2002). These surveys both found a faint-end slope of $\sim$-1.2 for the field but only for M_B <-17. Estimates of the faint-end slope of the general field for magnitudes fainter than this have only been carried out by Driver et al.(2005), who used the same MGS data as ourselves, to find a faint-end slope, $\alpha\sim$-1.13$\pm$0.02 over an approximate magnitude range of -22.6$\geq M_B \geq$-14.6. Thus in their study, Driver et al. looked at apparently faint galaxies whilst we are interested in intrinsically faint and LSB galaxies.

Area covered by our data

The Millennium Galaxy strip data was obtained during four observing runs in 1999 and 2000 using the WFC on the INT, and consists of 144 fields in B and I, running along the celestial equator (Liske et al. 2003). The first field was positioned at α (J2000)=$10^h00^m00^s$, δ (J2000)= 00°00′ 00″, with the following fields offset by 30 arcmins along the equator. The final field was therefore at α (J2000)=$14^h48^m00^s$, δ (J2000)= 00°00′ 00″. With these deep CCD data we can reach magnitudes down to m_B∼21 and central surface brightnesses of ∼26 mag/arcsec^2. The total area of the strip which we analysed for this thesis was 30 deg^2.

2.4 M101

This large, face-on spiral galaxy is situated at a distance of ∼6.6Mpc (Karachentsev 1996) and has an absolute magnitude, M_B ∼-21.5. It is the dominant galaxy of the M101 group, which, being nearby, has been the subject of a number of studies, the main aim of which was to distinguish between members of the group and nearby field galaxies.

Holmberg (1950) undertook the first study into possible members of the M101 group by looking at the redshifts, positions and resolvability of galaxies near M101 during a photometric study of nearby galaxies for Lund Observatory. He concluded that the M101 group consisted of M101, M51 and its companion NGC 5195, NGC 5204, NGC 5474 and NGC 5585. He also named 4 possible members for which there was no redshift data available, thus he could not confirm their membership in the group. In 1964, he revised his results for the M101 group; NGC 5195

and M51 he decided were further away than M101, the remaining members he considered to be at an intermediate distance, and M101 he concluded, was an isolated foreground galaxy. This uncertainty relating to the group members led Sandage & Tammann (1974) to study new redshifts of the possible M101 group members to verify if they were indeed part of the same group. They found that the majority of Holmberg's original group members from 1950 *were* part of the same group at the same distance, except for M51 and NGC 5195 which they stated to be at a further distance. Thus Sandage & Tammann's definition of the M101 group consisted of M101, NGC 5204, NGC 5474, NGC 5477, NGC 5585 and Ho IV (DDO185). Further work into the membership of the M101 group was carried out by Garcia (1993) who used data from LEDA [1] of 6392 nearby galaxies up to a limiting magnitude of B$\sim$14 to identify the groups with which they were associated. He identified the same galaxies as Sandage & Tammann as members of the M101 group, although he considered Ho IV only a possible, not definite member of the group. Karachentsev (1996) also undertook a search for companions around nearby (V_0<500km/s) massive (M> $3\times10^{11}M_{\odot}$) galaxies. Around M101, he found 8 possible members - those found by Sandage & Tammann, but also UGC 9405 and NGC 5238. The deepest and most recent study of M101 and its companions was undertaken by Bremnes et al. (1999) who carried out CCD photometry of the dwarf-type galaxies in and around the M101 group as part of their multi-colour survey of dwarf galaxies within the 10 Mpc volume. They found 13 members and possible members of the group as shown in Fig 2.9 (taken from their paper). The definite group members are represented by triangles, possible group members by inverted triangles, and field galaxies by squares. The position of M101 is marked by a the large cross at $\sim$14h, with M51, M63 and UGCA 342 (all considered non-M101 group galaxies) marked with smaller crosses. The filled triangle near M101

[1] Lyon Extragalactic Database

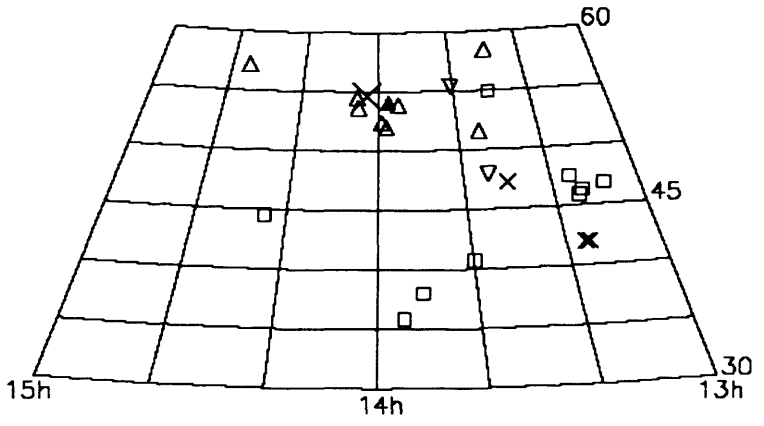

Figure 2.9: Positions of M101 group members (triangles), possible members (inverted triangles), field galaxies (squares), M101 (large cross) and M51, M63 and UGCA 342 (smaller crosses). The filled symbols indicate early-type galaxies; the unfilled symbols, late-types.

represents the sole early-type dwarf galaxy in the vicinity of M101 (UGC 0882)- the remaining dwarfs are all late types with absolute magnitudes in the range of $\sim$ -14 $\geq$ M_B $\geq$ -17. In comparison, the MW has 11 definite companions (Mateo, 1998), the faintest of which is Draco, a dSph with M_B $\sim$-7.6. Thus a deeper search may find similar diffuse dSph galaxies around M101 as are found around the MW.

2.4.1 Area covered by our data

Bremnes et al. comment that there does not seem to be a population of very faint and diffuse dwarfs in the region of M101; the faintest member has an absolute magnitude M_B $\sim$-14. Their attempt at finding new dwarf companions on POSS II Schmidt films added only 1 additional possible member to the list. A deeper CCD survey is clearly the next step forward in trying to find any fainter companions which may have been missed by the photographic plate inspection. We obtained the optical B band CCD data for fields surrounding M101 using the WFC on the INT in May 2004. This data reach absolute magnitudes down to $M_B$$\sim$-8 at the

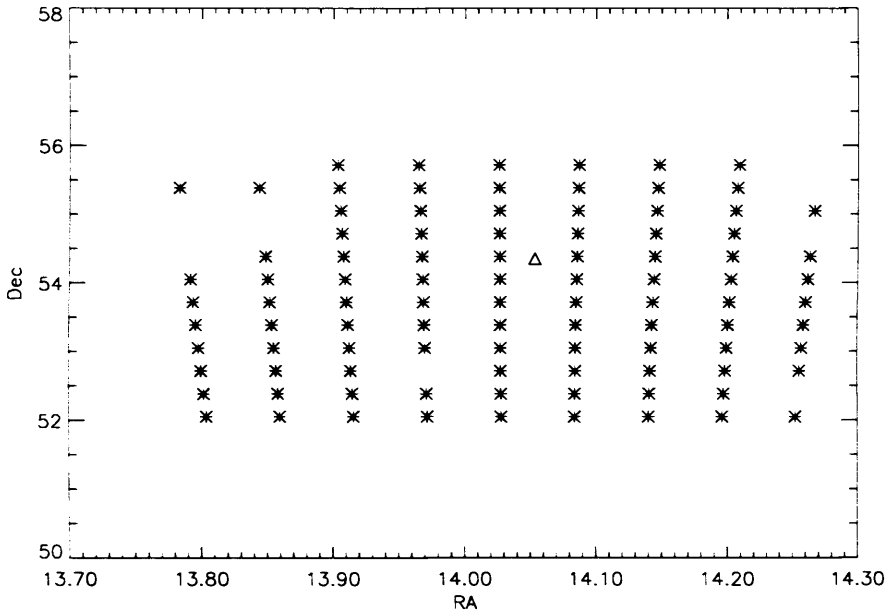

Figure 2.10: The positions of the data fields (star symbols) taken surrounding M101 (plotted as a triangle).

distance of M101 and surface brightnesses as low as 26Bmag/arcsec^2. Thus any faint objects which may have been missed by previous surveys around M101 should be detected in this deeper data set. The data fields' positions relative to M101 can be seen in Fig 2.10. Marked with a triangle is the position of M101. The field centres are plotted as stars. In total, 95 fields were observed, covering an area of $\sim$20 sq. degrees. Those with bad fringing were not used, reducing the effective area used, to $\sim$15.5 sq. degrees.

2.5 Summary

In this chapter we have discussed the 4 very different environments which we sampled for this thesis. Our aim was to search for and study the properties of, LSB dwarf galaxies in a range of environments, using identical data-sets and identical

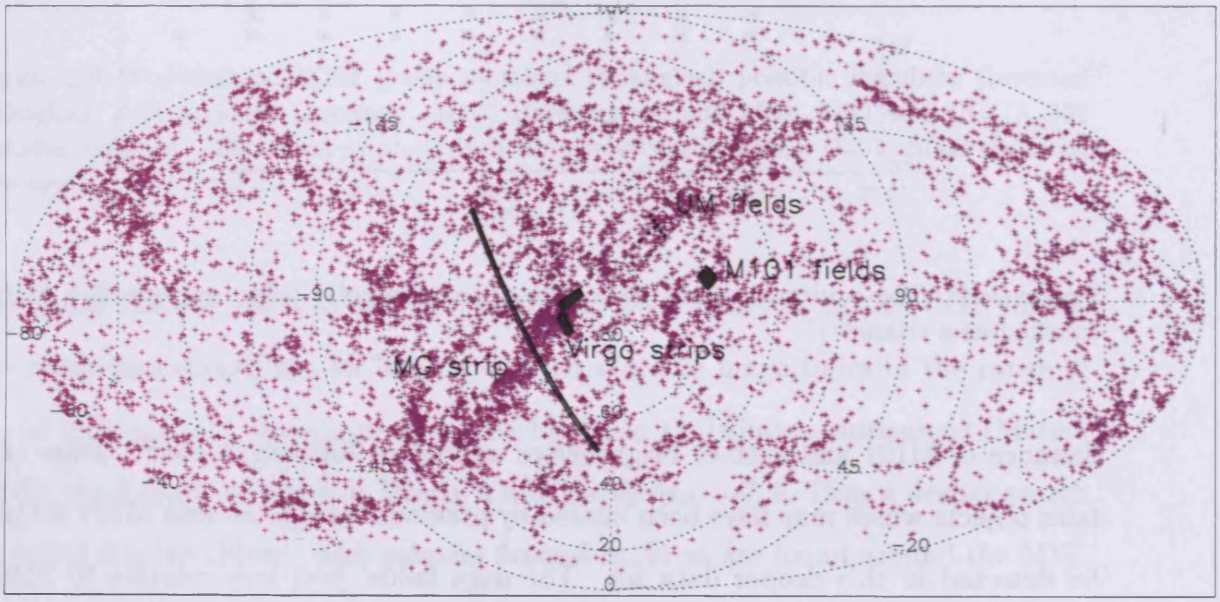

Figure 2.11: Positions of MGS, Virgo cluster data strips (both E-W and N-S),fields in Ursa Major and M101 fields viewed from the North galactic pole. The MGS is indicated by the long thin line, which passes through the Virgo Southern extension at approximately its midpoint. The two Virgo data strips are situated above the MGS, whilst the UMa fields can be seen plotted as filled circles. Just below the UMa fields are the fields taken around M101. Also plotted in this figure are all galaxies listed in NED with $v < 4500$ km^{-s}.

selection methods. All the optical data was obtained using the Wide Field Camera on the Isaac Newton Telescope, La Palma, the details of which shall be discussed in the next chapter. This deep CCD data will enable us to detect objects which may have been missed by previous searches down to M_B~-10 (at the distance of Virgo), and central surface brightness, μ_0~26 mag/arcsec^2. The regions covered by the datasets are shown in relation to each other in Fig. 2.11, together with all galaxies listed in NED with v $\leq$4500kms^{-1}. In summary the environments studied are:

- **Virgo cluster** - This dense (~5 giants/Mpc^2) cluster of galaxies is still in the process of forming from a collection of clouds and sub-clusters. The ellipticals in the cluster are concentrated towards the core of the cluster (defined by the region with the highest X-ray emission). The most numerous type of galaxy in the cluster, the dEs, also cluster around the core whereas the later-type galaxies are predominantly found towards the outskirts.

  We have surveyed $\sim$ 15 sq. degrees of this irregular cluster in the B band along a strip extending North to South (N-S strip) and sampling the sub-cluster environment of Virgo. We also have data for a strip extending East to West towards the cluster edge, with which we can compare the N-S strip results. We also have additional I band data for the majority of the Virgo cluster fields which we use to study the colours of the detected galaxies in the cluster.

- **Ursa Major cluster** - This cluster is much less dense than the Virgo cluster (~1 giant/Mpc^2) and its galaxies do not have any concentration around a cluster core. It is dominated by late-type galaxies, and previous CCD searches for dwarf galaxy cluster members have so far found very few (Trentham et al., 2001). We have surveyed $\sim$ 2 sq. degrees of this loose, low

density cluster in the optical B band. In HI, we have looked at an 8°×8° data cube covering the optical region and beyond.

- **Millennium Galaxy Strip** - Our field data was obtained from a 30 sq. degrees strip along the celestial equator. The density of giant galaxies along this strip (out to 21 Mpc) was approximately the same as that in UMa - 1 giant per Mpc^2. We surveyed this strip in the optical B and a smaller area in I. We have also carried out pointed HI observations of a sample of objects found in this strip using the Arecibo Radio Telescope.

- **M101** - Previous searches for dwarf companions around this giant spiral galaxy (Bremnes et al., 1999) using photographic plates failed to find any dwarfs fainter than M_B=-14. We have surveyed $\sim$ 15.5 sq. degrees around the region of M101 in the optical B band using deep CCD data. With a magnitude limit, $M_B\sim$-8, we can therefore probe further, the faint dwarf galaxy population in this region.

Chapter 3

Data

3.1 Introduction

Since ancient times, people have been curious about the heavens, and have carried out surveys mapping the positions of stars, planets and galaxies visible in the sky. The first star catalogue, containing 800 stars, was created as early as 350BC by the Chinese astronomer Shih Shen, and since then, many maps and catalogues of the Universe have been made by astronomers all over the world.

It was not until the 1800s however that astronomers could have a permanent image of the sky. The invention of photography and photographic plates allowed astronomers to finally record the large areas that they surveyed. The Palomar Observatory Sky Survey (POSS-I) carried out in the 1950s was the first (almost) all sky survey. Taking nearly a decade to complete, astronomers used the 48-inch Schmidt Telescope at the Palomar Observatory in California, to image the Northern sky in different colours. The data they obtained is still used today,

although advances in technology now mean that such large areas can be surveyed much more efficiently and to a greater depth than in the past.

The photographic plates used in the first large area surveys were not very efficient detectors - only ~5% of the incident light on the plate is successful in triggering a chemical reaction which produces an image on the plate; the remaining 95% is wasted. An improvement on these image detectors came in the form of charge-coupled devices or CCDs. These thin pieces of silicon containing arrays of pixels are now more than 90% efficient at detecting the light falling on them. Thus they are ideal detectors for faint, large area surveys of the night sky.

In this chapter we describe the instruments used to obtain the data for this thesis. As described previously, the data covers regions of the Virgo cluster, Ursa Major cluster, general field, and the area around the spiral galaxy, M101. We obtained optical data for all these environments in the B band, and for some fields, in the I band also. In order to make proper comparisons of the dwarf galaxy population in these four different environments, all variables (e.g. instrument, band exposure times, selection criteria) should ideally be identical. We have achieved this with our optical data, which was all obtained using the same instrument, technique (filter band, exposure time) and selection criteria. We can be confident therefore that we really are comparing 'like with like' in our environmental comparisons. To study the properties of the objects which we detect in our surveys, we also obtained HI data covering a region of $8° \times 8°$ in the Ursa Major cluster, and pointed HI observations for specific objects detected in the field.

3.2 Instruments - optical

3.2.1 Wide Field Survey

The main instrument used to obtain all the optical data for this thesis was the Wide Field Camera (WFC) on the 2.5m Isaac Newton Telescope (INT) in La Palma. The WFC is a mosaic of 4 thinned EEV 4096K×2048K CCDs with pixel size 0.33″ and total sky coverage of 0.29 sq. degrees. It is arranged on the sky as shown in Fig. 3.1. On this figure, the 4 CCDs are numbered 1-4, with the auto-guider marked with a 5. The dashed circle outlines the total area covered by the filters, whilst the solid circle defines the un-vignetted area. As can be seen in this figure, CCD 3 suffers from severe vignetting thus images on this CCD were not used. This reduced the total field of view to 0.21 sq. degrees.

The Virgo cluster and field data (named the 'Millennium galaxy Strip' or MGS) used in this thesis was taken as part of the Wide Field Survey (WFS), a multi-colour data survey covering over 200 sq. degrees of sky. The survey began in August 1998, and has covered a number of regions in the Northern hemisphere, including the Virgo cluster, Pleiades and a strip along the celestial equator (MGS). At the time that the WFS was commissioned, other large area surveys were being undertaken at different wavelengths (e.g. SDSS, 2MASS), thus one of the main aims of the WFS was to cover the same regions but to deeper magnitudes. A comparison of the limits of three wide field CCD surveys is shown in Table 3.1. The SDSS aims to map a quarter of the entire sky, imaging millions of galaxies in 5 filters (u,g,r,i, and z). The limiting magnitude of the survey in r is ∼23.1, thus the WFS as a whole reaches fainter magnitudes than this larger survey. The National Optical Astronomy Observatory's Deep Wide-field Survey (NOAO Deep

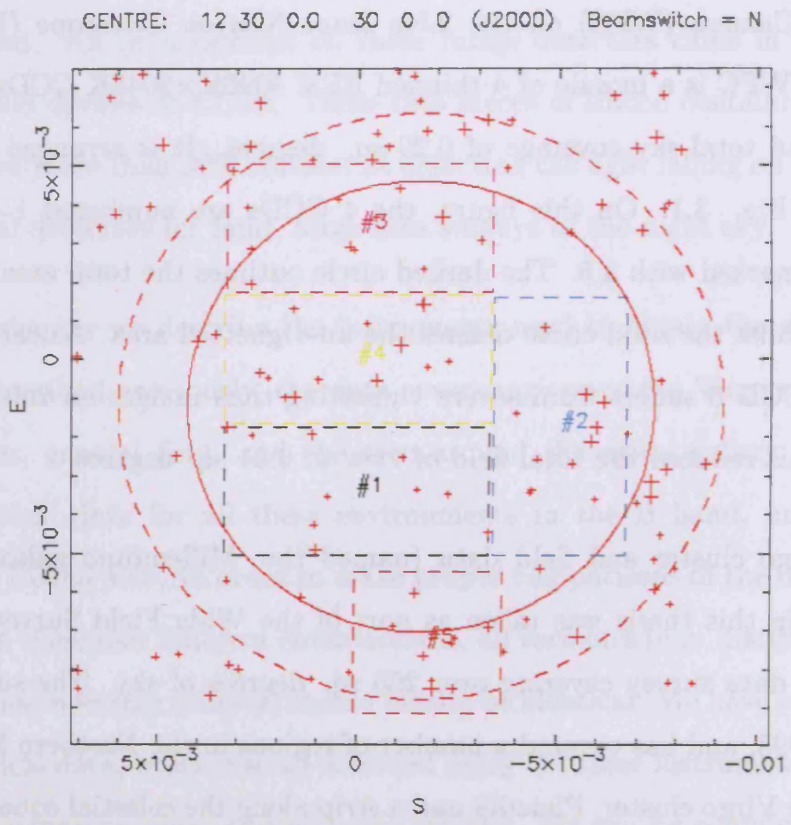

Figure 3.1: Arrangement of WFC CCDs on sky with East to the left, and South downwards. Each CCD is numbered, 1 to 4, whilst the auto-guider is numbered 5. The dashed circles encompasses the total area of the filters, whereas the solid circles define the area inside which vignetting does not occur.

WFS) is a deep optical and NIR survey designed to study large scale structures at z>1 by imaging a range of object types. This survey reaches r magnitudes ~25.8 but covers only a tenth of the area surveyed by the WFS.

Survey	*Area covered*	*r band mag limit*
WFS	200 sq. degrees	24.5
SDSS	10,000 sq. degrees	23.1
NOAO Deep WFS	18.6 sq. degrees	25.8

Table 3.1: A comparison of recent wide field CCD surveys

Observations

Observations of the 4 environments studied in this thesis were carried out using the WFC during runs from 1999 to 2004. The area covered in each region, and the band obtained are outlined in Table 3.2. The exposure times used were 750s in

Region	*Date observed*	*Area covered*	*Band obtained*
Virgo cluster	2001 (Sabatini et al.) 2002 (Roberts et al.)	~13°^{2}(E-W strip) ~15°^{2} (N-S strip)	B, I
Ursa Major cluster	2002 (Roberts et al.)	~1.7°^{2}	B
Field (MGS)	1999, 2000 (Liske et al.)	~37.5°^{2}	B, I
M101	2004 (Roberts et al.)	~15°^{2}	B

Table 3.2: Data obtained for each observing run

the Johnson B band, and 1000s in the I band. When possible, twilight flats were obtained in both the evening and morning of each night's observing, and Landolt standard star fields were observed at intervals throughout each night. The median measured seeing for all datasets is shown in Table 3.3. Poor seeing has the effect of smearing out objects on the CCD images, making them appear larger than their actual size. However, we can account for this by adjusting our selection criteria, as explained in Chapter 4.

Environment surveyed	*Median seeing (arcsec)*
Virgo cluster - NS strip	2.2
Virgo cluster - EW strip	1.9
UMa cluster	1.9
MGS (field)	1.3
M101	1.8

Table 3.3: Median seeing for each data set

Data Reduction

Once obtained, the data was reduced and calibrated using the Cambridge Astronomical Survey Unit pipeline (http://www.ast.cam.ac.uk/ wfcsur/index.php). This included the following steps:

- **De-biasing** - The noise on a CCD image originates from a number of sources. Two examples are the electronics and the amplifier (used to amplify the signal received by the telescope). The noise can vary with both position on the CCD and over time and must be removed from the CCD image. This is done by taking bias frames (zero second exposures with the telescope shutter closed). These frames give a measure of the noise on the CCD which is not due to external illuminating light sources, and the noise inherent to the instrument can then be removed.

- **Bad pixel replacement** - Some pixels in a CCD frame can be faulty and give false signal values. Due to the way that a CCD is read-out, this could in turn cause a column or row of inaccurate pixel values. Thus, any known bad pixels on the CCD image are flagged as part of the data reduction process, and their values replaced with estimates from interpolation of other pixel values.

- **Non-linearity correction** - On the WFC, none of the CCD responses are linear. This is corrected as part of the pipeline process.

- **Flat-fielding** - The sensitivity of each pixel to light on a CCD varies randomly. The sensitivities can be calibrated by obtaining an approximately evenly illuminated image and comparing the pixel values. This is done using a number of twilight sky flats which are combined to give a master sky flat.

- **De-fringing** - Fringing on the WFC occurs for wavelengths redder than R, and thus affects our I band data. It is reduced in the pipeline process by use of a fixed fringe pattern mask. This decreases the fringing on the image by approximately a factor of 10 or more.

- **Gain correction** This is carried out in order to ensure that the sky level in each CCD frame is approximately the same (to a 0.5% level).

Data Limits

The typical 1σ sky noise of the data from the WFC corresponds to $\sim$ 26 mag per sq. arcsec in the B band and $\sim$ 24 in the I. As shown in the discussion of the efficiency of the detection algorithm in Sabatini et al. (2003), this means that with this data we are capable of detecting objects with central surface brightnesses as low as 26 Bmag/arcsec^2. At a distance of 16 Mpc (our assumed distance of the Virgo cluster), and for objects with minimum scale-sizes of 3″ (justified in Chapter 4), with this data we can reach absolute magnitudes down to $M_B\sim$-10. Unlike previous, less deep surveys, we are therefore capable of detecting dwarf galaxies similar to those found in the Local Group at the distance of the Virgo cluster.

3.2.2 SDSS

One of the aims of this work was to investigate the colours of detected objects in the different environments. We had B and I band data for the Virgo cluster and for some fields of the MGS. However, there was no I band data available for the fields covering the objects we detected in the MGS, thus in order to calculate the colours of these objects, SDSS data was used. In order to be consistent with the magnitudes used to find (B-I), we used SDSS g and i data for the MGS objects, and converted them to B and I using the equations given on the WFC website and by Cross et al. (2004). This ensured that the data for the B-I colours of the MGS objects were consistent - the magnitudes were measured over the same apertures.

3.3 Instruments - HI

3.3.1 Arecibo

The 305m Arecibo telescope is the world's most sensitive radio telescope. With the spherical primary reflecting dish built into a natural crater in the ground, the telescope uses secondary and tertiary reflectors inside a Gregorian dome 137m above the main dish to focus the radiation to the horn antennae for measurement. This dome is positioned on an azimuth arm, and can move up to 20° from the vertical to point to and track an object. The telescope has a number of receivers which can be used by the observer, depending on the project being carried out.

Observations

In May 2003 a sample of 12 objects from our optical catalogue of candidate LSB dwarf galaxies found previously in the MGS data (see Chapter 5) was observed by Sabatini et al. using the Arecibo radio telescope. A further 46 were observed by Roberts et al. in January 2004. Data were taken in 2003 with the L-Band Narrow receiver (see Sabatini et al. 2003) and in 2004 with the L-Band Wide receiver, in both cases using 2048 channels. All observations were taken using the position-switching technique, with the blank sky (or OFF) observation taken for the same length of time, and over the same portion of the Arecibo dish as was used for the on-source (ON) observation. Each 5min+5min ON+OFF pair was followed by a 10s ON+OFF observation of a well-calibrated noise diode. The velocity search range was 100 to 9600 km s^{-1} and the velocity resolution 2.6 km s^{-1}. The instrument's half power beam width at 21 cm is 3.6′ and the pointing accuracy is about 5″. The pointing positions used were the optical centre positions of the target galaxies found in the MGS data.

Data reduction

Using standard IDL data reduction software available at Arecibo, corrections were applied for the variations in the gain and system temperature with zenith angle and azimuth, a baseline of order one to three was fitted to the data, excluding those velocity ranges with HI line emission or radio frequency interference (RFI), the velocities were corrected to the heliocentric system using the optical convention, and the polarisations were averaged. All data were boxcar smoothed to a velocity resolution of 12.9 km s^{-1} for further analysis.

Data Limits

The average rms noise on the data was ~0.6mJy. The HI mass limit of this data can be found by:

$$M_{HI} = 2.356 \times 10^5 d^2 \int S_v dv \tag{3.1}$$

where M_{HI} is the mass of HI in solar units, d is the distance to the galaxy in Mpc, S_v is the flux density, and the integral is over velocity. With this data, assuming a 4σ detection we would expect to detect a dwarf galaxy with velocity width of 50kms^{-1} at a distance of 21 Mpc if it had $M_{HI} > 1 \times 10^7 M_\odot$ (see Chapter 4 for explanation of MGS data distance limit).

3.3.2 HI Jodrell All Sky Survey (HIJASS)

HIJASS is a blind 21cm survey of the Northern sky conducted using the 76m Lovell Telescope at Jodrell Bank, Manchester (Lang et al. (2003)). Carried out between 2000 and 2002, it covers an area of ~1115°^{2} above a declination of ~22°, including the Ursa Major cluster, and Northern Celestial Cap. The velocity range of the survey was -3500 - 10,000kms^{-1}, although due to local interference effects, the useful velocity range is -1000 - 10,000kms^{-1}. There is also a region between 4500 and 7500 kms^{-1} which is affected by radio frequency (RF) interference. We have used an 8°×8° cube of data covering the UMa cluster region to complement our optical data. From Tully et al.'s. (1996) definition of the UMa cluster given in the previous chapter, we use a velocity range of 628 < V_{helio} <1138 kms^{-1} to define the extent of the cluster, centered upon ($11^h59^m28.3^s$;49°05′18″) (Trentham et al., 2001). The HIJASS data has a velocity resolution of 18.1kms^{-1} and an average rms noise of 13mJy beam^{-1}.

Data Reduction

The data reduction was carried out by members of the HIJASS team. The LIVEDATA software package (Barnes et al. 2001) was used for bandpass correlation and calibration of the data. The data was then split into cubes of 8°×8° by GRIDZILLA (Barnes et al. 2001), with pixel size 4′ ×4′. Finally, POLYCON (written by Zambonini & Minchin) was used to remove continuum emission from the baselines of the spectra.

Data Limits

The average rms noise of the HIJASS data cube is 13mJy beam^{-1}. For a 4.5σ detection we would expect to detect a dwarf galaxy with velocity width 50kms^{-1} and HI mass $\sim 2 \times 10^8 M_\odot$ at an Ursa Major distance of 18.2 Mpc.

3.4 Summary

3.4.1 Optical data

We have obtained deep CCD data using the WFC on the INT for the 4 regions surveyed in this thesis. We have B band data for all regions, with additional I band data for a number of fields in the Virgo cluster and MGS datasets. The 1σ sky noise of this data is $\sim$ 26 magnitudes per sq. arcsec in B and $\sim$ 24.5 in I. We can therefore detect objects with central surface brightnesses down to $\sim$26Bμ and absolute magnitudes, $M_B\sim$-10 (assuming a distance of 16 Mpc and minimum scale-size of 3″). We describe the results from the optical data in Chapter 5.

3.4.2 HI data

We have pointed HI observations from the Arecibo telescope for 68 objects found with our detection algorithm and selection criteria in the MGS data. The rms noise of this HI data is ~0.6mJy. Thus, assuming a 4σ detection we would expect to detect a dwarf galaxy with velocity width of 50kms^{-1} at a distance of 21 Mpc if they have M_{HI} of $> 1.2 \times 10^7 M_\odot$.

We have searched an $8° \times 8°$ cube of HIJASS data covering the UMa cluster and overlapping with the region containing our UMa optical data. For a 4.5σ detection in this data we would expect to detect a galaxy with velocity width 50kms^{-1} and HI mass $> 2 \times 10^8 M_\odot$ at a distance to UMa of 18.2 Mpc.

Chapter 4

Detection and Selection

As discussed in chapter 1, LSB dwarf galaxies are important probes of galaxy formation and evolution. Predictions of CDM indicate that there should be large numbers of these objects in the Universe today, but current observations have failed to find them in the numbers predicted. One reason for this could be due to the difficulty in detecting these types of objects. By definition, LSB objects have surface brightnesses which fall below the surface brightness level of the sky ($\approx 23B\mu$), thus previous searches for these objects could have missed them as they did not search to faint enough levels - this is especially true for searches on photographic plates. Recent CCD surveys have unearthed an increasing number of LSB galaxies, primarily due to deeper imaging, but also due to improved algorithms for the detection of these objects. Standard detection algorithms, for example Sextractor (Bertin & Arnouts, 1996), use the 'connected pixels' method to find objects; a group of connected pixels that are above a threshold value from the background is assumed to belong to an an object and is identified as a detection. However, as this only makes use of the connected pixels, the signal-to-noise ratio

for the detection needs to be quite high, thus low signal-to-noise LSB galaxies are selected against. The algorithm implemented in this thesis was developed with the specific aim of emphasising faint, diffuse objects on CCD frames i.e. to detect LSB objects. It was written by Sabatini et al. (1999, 2003), and we outline the main steps in the first section of this chapter.

Since we are investigating the population of LSB dwarf galaxies in different environments of the Universe, we need to be consistent in the types of objects which we select. This can be difficult however if the types of objects in different environments are themselves very different. Current wisdom would describe the cluster population as dominated by rather featureless dE galaxies and the field by irregular galaxies (dIrr). Even so, to try to be as consistent as possible we have used the same selection criteria for each environment observed (except for M101, as explained later). The selection criteria used for this purpose were originally chosen following simulations carried out by Sabatini et al. (2003), and were optimised for a cluster of galaxies at the distance of Virgo. However, the MGS data samples the field, and is not an overdensity of galaxies at one distance. Also, the M101 data was used to look at objects at the same distance as M101. Thus we have to ensure that the same selection criteria *can* be used for the different data sets. In the second section of this chapter, we discuss the original simulations as carried out by Sabatini et al., then we explain how this selection criteria is still valid for selecting field dwarf galaxies over a range of distances and how it can be modified to select companions around nearby galaxies.

As discussed in the previous chapter, for a sample of the objects detected in the MGS field data, we have pointed HI observations. We describe the detection method used for this data and the selection criteria used to determine if the optical detection was also a source of HI. As also discussed in the previous chapter, we

have HI data for a region covering the UMa cluster. The final part of this chapter explains how this data cube was searched twice by eye, and by the use of an automated procedure to detect possible HI sources in the cluster.

4.1 The Optical Detection Algorithm

The main steps in the optical detection algorithm used in this thesis to detect possible LSB dwarf galaxies on CCD frames are:

- Background fluctuation flattening
- Removal of other astronomical objects
- Convolution of images with filters
- Classification of candidates
- Application of selection criteria
- Eye-ball Confirmation

These steps are described in more detail below.

4.1.1 Background fluctuation flattening

In order to be able to detect LSB galaxies on CCD frames using a detection algorithm, the background must be as flat as possible. Although our CCD data is flat-fielded by the INT pipeline, it is also passed through an additional background flattening routine as the first part of the detection algorithm, prior to convolution

with the filters. This step is carried out by Sextractor to give a homogeneous flat image. The image is divided into a grid of sub-arrays and a value for the local sky from this grid estimated. We used grid sizes of 128 or 256 pixels, depending on the data fields being used, as explained below. If the grid size is too small, the background value estimate can be affected by random noise or objects in the frame, and there is a possibility that part of the flux from diffuse objects (such as LSBs) in the image may be absorbed into the background. However, the chosen grid size cannot be too large or it will not be able to reproduce the small scale variations in the background. For the Virgo, MGS and UMa data fields, the largest objects which we expected to detect (see below) were 9″ or 27 pixels, therefore a grid size of 128 pixels ($\sim$ 43″) ensures that such objects will be preserved. Objects which we expect to detect around M101 will be closer by a factor of $\sim$3 than objects in the other data sets, so the largest object we expect to find in the M101 data fields which are similar to those found in the Virgo, UMa and MGS data are $\sim$27″, corresponding to 81 pixels. Thus in this case, a grid size of 256 pixels ($\sim$ 84″) ensures these large objects will not be lost in the background fluctuation flattening procedure. The local sky estimate is then calculated from the mean values of the pixels in the grid. Although this process only reduces the noise on the CCD by about 6%, it improves the use of filters later on in the detection process.

4.1.2 Removal of other astronomical objects e.g. stars, bright galaxies, etc.

To minimise any contamination of the sample, for example by stellar haloes which when convolved with the filters could be mistaken for LSB objects, the possible contaminants must be masked on the CCDs prior to the convolution process. There

are two parts to this process - firstly, the big bright objects (saturated stars, bright galaxies) must be removed, followed by the small, sharp objects (bad pixels, cosmic rays). It would be possible to use Sextractor for this purpose but it is not very efficient and leaves stellar haloes in the final image which, if then convolved with a filter could be mistaken for a LSB galaxy due to their similar surface brightness. A separate program was written for the purpose of removing saturated and bright objects and then Sextractor used to mask the smaller stellar objects. For the first part of the masking procedure, Sextractor is used to detect all the objects in the images, and their isophotal area and weighted flux (surface flux weighted by their peak flux) examined. Fig 4.1, taken from Sabatini et al. (2003) shows a plot of the isophotal area vs. weighted flux for the Sextractor detections from a typical CCD image. On this figure, the saturated objects can be seen at the top, the stellar locus as the diagonal line extending across the central part of the figure, and the area where the diffuse objects, such as galaxies, are located, in the lower part of the figure. The objects to be masked can therefore be chosen from this plot - those objects which are in the saturated region must obviously be masked, together with those objects which lie along the stellar locus region. The objects which have areas of less than 90 pixels are left unmasked as they could be small galaxies.

The objects to be removed from the image are masked with the median sky value and Poissonian noise, with the area over which the mask is placed, determined from the size parameters given by Sextractor. This method however could result in galaxies being removed from the CCD image if their centres were on the border of the mask. Simulations showed that galaxies would be detected if they are at a minimum distance of 1 galaxy scale-length from the mask border; if they are any closer they will be missed.

Once the larger objects have been masked, Sextractor is then used to mask

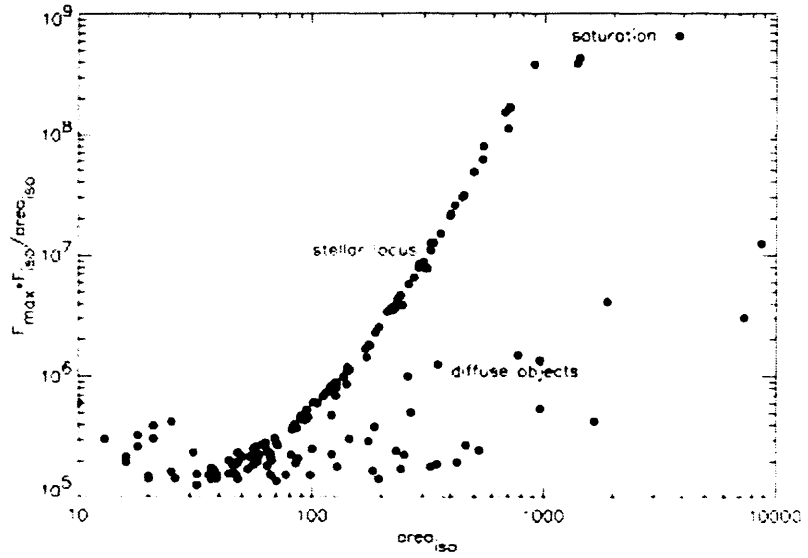

Figure 4.1: Sextractor detections of objects from a typical CCD image. The regions where diffuse galaxy type objects, stellar objects, and saturated objects are clearly labelled.

the smaller stellar objects, to produce a cleaned CCD image. Fig. 4.2 shows how a typical CCD image looks before and after this cleaning process.

4.1.3 Convolution of image with specifically designed filters

The first consideration when designing a filter is what size to choose for the detection of LSB galaxies. Galaxies have a range of sizes, therefore, the filters used should also range in size. However, this would result in having to use a very wide band-pass filter which would then give many unwanted objects. Using different filters of each size and looking at the results from each would take a long time. It was decided that the best option was to apply a combination of filters of different sizes which would give one final significance image with each object of different size being emphasised at the same time on this image. The filters were designed to detect exponential disk objects as this is the best function which would fit the

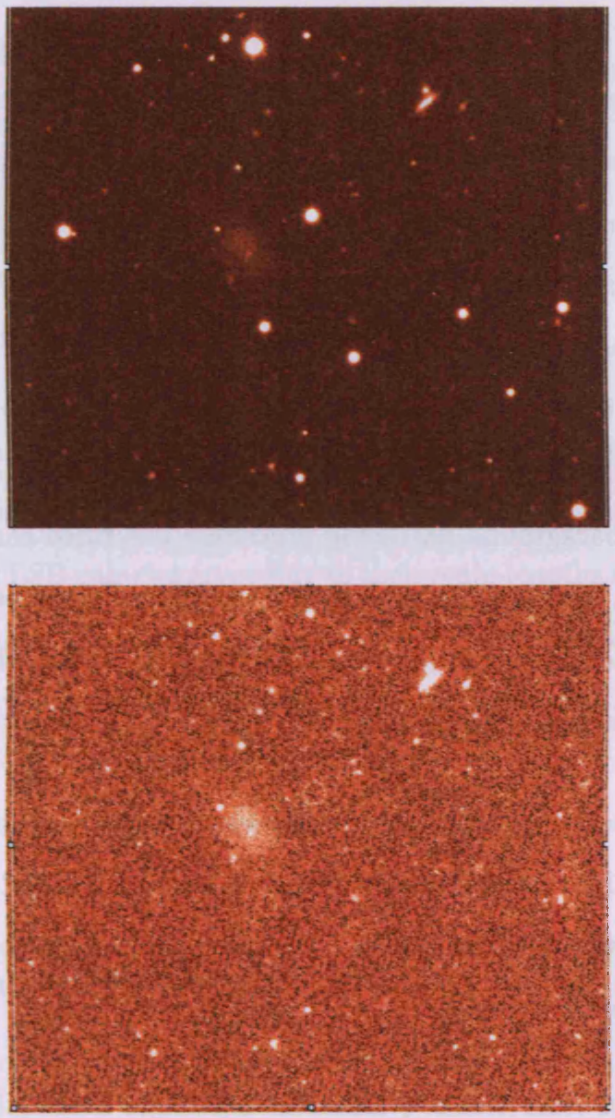

Figure 4.2: CCD image prior to masking procedure (top) and after cleaning (bottom). The stellar objects in the original image have been masked with the median sky value and Poissonian noise to produce the cleaned image. The LSB near the centre of the image, and the small galaxy towards the upper right part of the image remain unmasked and visible on the cleaned CCD image.

surface brightness profile of a dwarf galaxy. After the image is cleaned it is convolved with the filters, giving an output of convolved images on which objects of different sizes are enhanced depending on the filter size. A final image is then built up by combining these convolved images, with pixel values that are equal to the maximum value in the series of convolved images. Thus, in this single image, all the objects corresponding to the different sizes of filters are emphasised. It was decided that filters of scale-size 1, 2, 3, 4, 5, 6, 7,and 9 $''$ would be best to use for the Virgo, MGS and UMa datasets, to ensure that a range of dwarf galaxy sizes would be enhanced at these distances (the 1$''$ and 2$''$ filters were used to detect bad pixels and small background objects which were subsequently removed from the catalogue of possible dwarf galaxy detections. 9$''$ is the largest objects that should remain after the background flattening procedure described earlier). As discussed earlier, the M101 data is $\sim$3 times closer than the other datasets; since we want to detect the same types of objects in this dataset as in the other 3 areas, we had to change the filter sizes accordingly.

Thus for an approximate distance difference of 3, to detect the same types of objects in the M101 data as for the Virgo, UMa and MGS data, the filter sizes used in the detection algorithm were multiplied by 3. This gave filters of 3, 6, 9, 12, 15, 18, 21, and 27 $''$.

4.1.4 Classification of candidates

Possible dwarf and LSB galaxies are identified by selecting all peaks in the final significance image that are 3σ above the residual noise fluctuations. The scale-length of each object is assumed to be equal to the size of the filter which best fitted the object. The peak flux of the object is measured from this final image,

so that photometry can be obtained for the objects. Since the galaxy scale-length (α) is assumed to be equal to the filter size, the central flux of the galaxy can be measured and the central surface brightnesses (μ_0) calculated, together with the total apparent magnitude of the galaxy using:

$$m = \mu_0 - 5log\alpha - 2.0 \tag{4.1}$$

4.1.5 Application of selection criteria

Once the detection algorithm has produced an output catalogue of possible dwarf galaxies in the data, selection criteria are applied to the catalogue to preferentially pick out true dwarf LSB galaxies according to their scale-lengths and central surface brightness. The choice of selection criteria is described in the next section of this chapter, but application of this criteria leads to stars and small, faint background objects being removed from the object catalogue, leaving a catalogue of likely dwarf galaxy candidates to be inspected visually.

4.1.6 Eye-ball confirmation

Occasionally the detection algorithm identifies possible candidates which are obviously not dwarf or LSB galaxies i.e. the remaining halo surrounding a masked bright star, or the path of a satellite (Fig. 4.3). Applying the selection criteria for such objects does not automatically remove them from the catalogue since they still have scale-lengths and surface brightnesses which are within the selection criteria range. These detections are removed from the list of possible candidates once confirmed as contaminants by eye. This is the part of the detection procedure

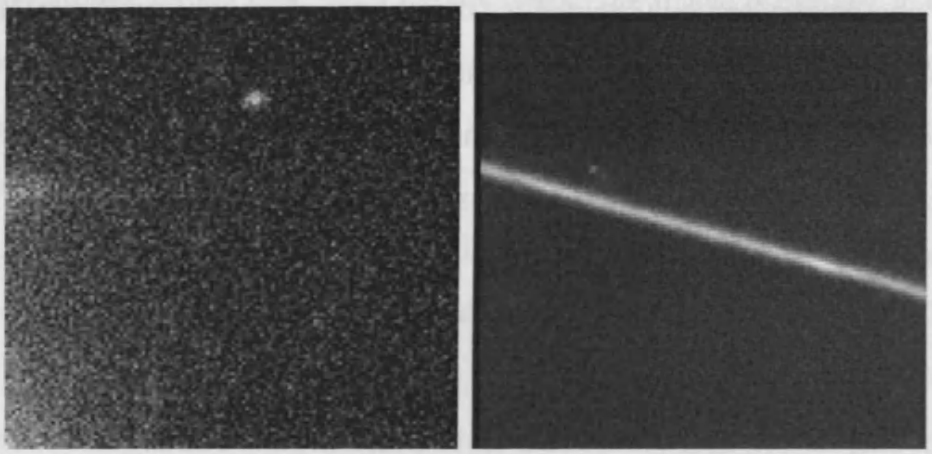

Figure 4.3: Examples of obvious non-galaxy objects detected by algorithm - here it has mistaken the halo of a masked star (left) and the trail of a satellite (right) as detections.

which takes up the most time, since it is not an automated method.

4.2 Optical Selection Criteria

4.2.1 Original simulation

The simulations originally carried out by Sabatini et al. (2003) to choose the selection criteria were based upon the following method - first, the 'background' Universe was simulated by randomly populating a conical volume of Universe (using: $\Omega_M = 0.3$, $\Omega_\Lambda = 0.7$, $h_{100} = 0.75$) according to a given Schechter LF and surface brightness-magnitude relation (Driver, 1999). Next, a cluster of galaxies was then simulated at the same distance as the Virgo cluster, but with the faint-end slope of the LF left as a free parameter so it could be varied in different runs. The conical volume was analysed from z=0.001 to z=1.5, and the output of the two simulations was a catalogue of galaxies for both the background and the cluster,

providing information on, among other parameters, the redshift, magnitude, scale-length and surface brightness of the 'background' and cluster galaxies. By applying different selection criteria to both the background and cluster galaxy samples, it was possible to determine the best criteria which would maximise the detection of cluster dwarfs and minimise the contamination by background galaxies. The criteria of central surface brightness, $\mu_0 \geq 23B\mu$, and scale-length, $\alpha \geq 3''$ was found to be the best for such a simulation. The method used to determine the background sky on the CCD frames also meant that there was an upper limit of $9''$ to the size of objects detected using this method. As discussed in Chapter 2, the 1σ surface brightness limit was approximately 26 $B\mu$. Thus these criteria lead to a detection parameter space of $23 \leq \mu_0 \leq 26$ $B\mu$ and $-10 \geq M_B \geq -14$ for the Virgo cluster data. However, some objects marginally fainter than $\mu_0 = 26$ were included in the lists of optical detections in the different environments as such an object in the Virgo cluster was demonstrated to be real via an HI detection (Sabatini et al. 2005). This was the selection criteria used for our Virgo N-S strip and UMa cluster data. We discuss the criteria for our field data in the next section.

MGS field selection criteria

The above selection criteria and simulations were optimised for a cluster of galaxies at approximately the distance of Virgo and was therefore also suitable for use on the UMa cluster data since this cluster is at approximately the same distance as Virgo. However, the MGS field data does not sample an overdensity of galaxies concentrated at one distance. but we want to be consistent with our detection and selection method. To ensure a proper comparison of the dwarf galaxies in each environment we want to detect the same sorts of objects in the field with the same intrinsic properties of magnitude and surface brightness as those detected in the

Virgo and UMa clusters using the selection criteria specified above. By considering the smallest, faintest galaxy detectable with this criteria in Virgo, we can estimate the distance over which we expect to be detecting similar objects in the MGS field data. The faintest galaxy ($M_B = -10$) will, according to the surface brightness magnitude relation of Driver (1999),

$$\mu_0 \approx (0.6 \pm 0.1)M_B + (32 \pm 1.3) \tag{4.2}$$

have a central surface brightness, $\mu_0 \sim 26\mathrm{B}\mu$. Assuming a scale-length, α of $3''$, its apparent magnitude, m, can be found by:

$$m = \mu_0 - 5log\alpha - 2.0 \tag{4.3}$$

Substituting this into the distance modulus equation:

$$m - M = 5logd - 5 \tag{4.4}$$

where M is its absolute magnitude and d its distance in parsecs, gives a distance of 21 Mpc. The Virgo cluster lies at a mean distance of about 16 Mpc but probably extends to 21 Mpc (Jerjen et al. 2004). Thus for the MGS field data, we are able to detect exactly the same types of objects (magnitudes and surface brightnesses) as we detected in our Virgo cluster survey using the same selection criteria if they lie within 21 Mpc. We can therefore make a direct comparison between the two very different environments.

Contamination

We now have a distance limit to which we can say that the objects we detect in the MGS field data have the same properties as those objects detected in the Virgo and UMa clusters. We now need to find out what the degree of contamination in this data might be - i.e. how many objects in the MGS field data will satisfy our selection criteria but will actually lie at a distance greater than 21 Mpc? There is also the possibility of there being nearby galaxies that are fainter than M_B=-10, but we assume that their surface brightness is less than 26Bμ (from the μ_0-mag relation) and they will therefore not be detected.

We have run the same 'background' simulation as Sabatini et al. (2003) to estimate this contamination. A cone of Universe was randomly populated with galaxies using various faint-end slopes of the LF (α=-1.0 to -2.0) but keeping ϕ (=0.0068 Mpc^{-3}) and M_B^* (=-20.3) constant (Norberg et al. 2002) and again using Driver's surface-brightness magnitude relation (Driver, 1999), given above. The simulation was run over a 300°×300° volume up to z$\sim$0.05. Such a large volume was sampled to ensure that the nearby volume was well represented. The simulations output a catalogue of objects in this volume, and the selection criteria ($23 \leq \mu_0 \leq 26$ $B\mu$ and $3'' \leq h \leq 9''$) were then applied to this catalogue. This enabled us to see the distances to which we detected objects, and what percentage of these objects also satisfied $-10 \geq M_B \geq -14$. Fig. 4.4 shows a plot of the distribution of numbers of selected objects ($23 \leq \mu_0 \leq 26$ $B\mu$ and $3'' \leq h \leq 9''$) with increasing distance and varying faint end LF slope. As can be seen, the numbers grow with distance until approximately 20 Mpc, so the selection criteria restricts the numbers of distant galaxies included in the sample, as required.

In Fig. 4.5 we show how the percentage of selected objects, which also satisfy

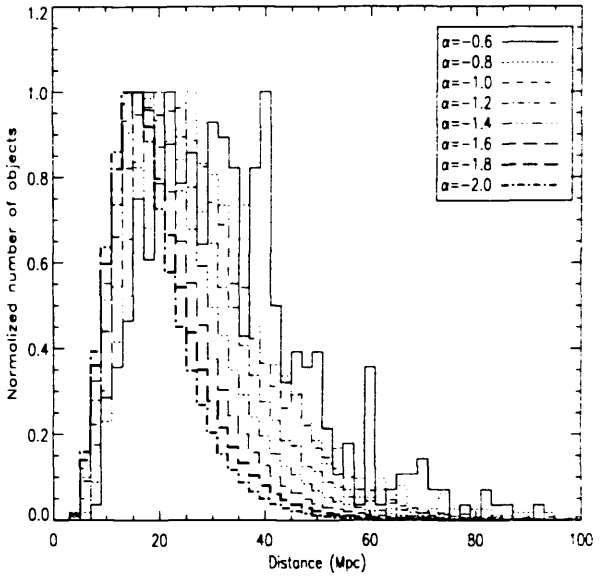

Figure 4.4: Distribution of distances for selected objects with properties in the range $23 \leq \mu_0 \leq 26$ $B\mu$ and $3'' \leq h \leq 9''$ at increasing distance for varying values of α.

the absolute magnitude criteria, changes for different LF faint-end slopes. For the MGS field data, the model predicts that within 21 Mpc, between 25% and 55% of the galaxies detected will have the same intrinsic properties as those detected in the Virgo cluster sample. We take this into account when calculating the dwarf to giant ratio and numbers of objects per sq. degree in this data set, as described in Chapter 5.

M101 selection criteria

The selection criteria used to pick out LSB dwarf galaxies was optimised for an overdensity of galaxies at the distance of Virgo, i.e. 16 Mpc. However, M101 is closer than the Virgo cluster but we want to detect the same types of objects around M101 which we detect in Virgo and the MGS and UMa data sets. Thus the scale-

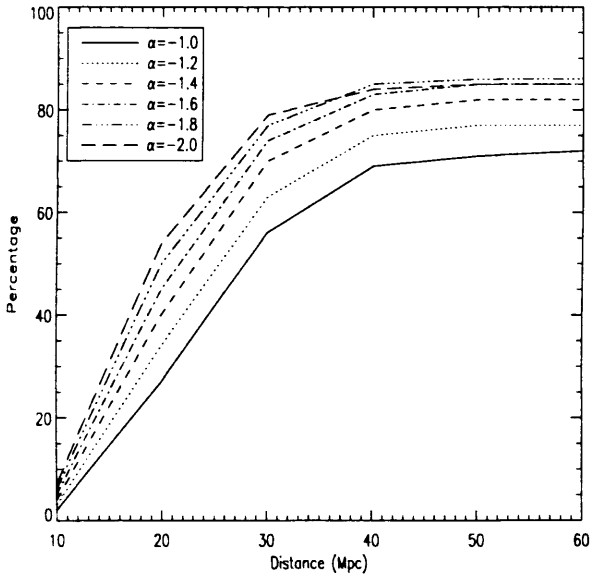

Figure 4.5: Percentage of selected galaxies having intrinsic properties in the range $23 \leq \mu_0 \leq 26$ $B\mu$ and $-10 \geq M_B \geq -14$ at increasing distance for varying values of α.

length criteria for detecting companions of M101 had to be altered accordingly. For the M101 data, in order to ensure we detect the same types of objects as those in the other 3 data sets, we used the criteria of $23 \leq \mu_0 \leq 26$ and $9'' \leq \alpha \leq 27''$ to find possible LSB dwarf companions around M101.

We show in Fig. 4.6 the percentage of objects selected with this new criteria, which are within the absolute magnitude range of $-10 \geq M_B \geq -14$ for varying faint-end slopes. Within a distance of ~6.9 Mpc, between 40-55% of galaxies will have properties similar to those dwarf galaxies found in Virgo and will lie at approximately the same distance as M101, thus are likely to be companions of this giant galaxy. We also used the original criteria of $23 \leq \mu_0 \leq 26$ $B\mu$ and $3'' \leq h \leq 9''$ in this data set to pick out possible LSB dwarf galaxies in the field covering the region around M101 (up to a distance of 21 Mpc), as described in the previous section. We will then compare the results for the MGS and M101 data since they

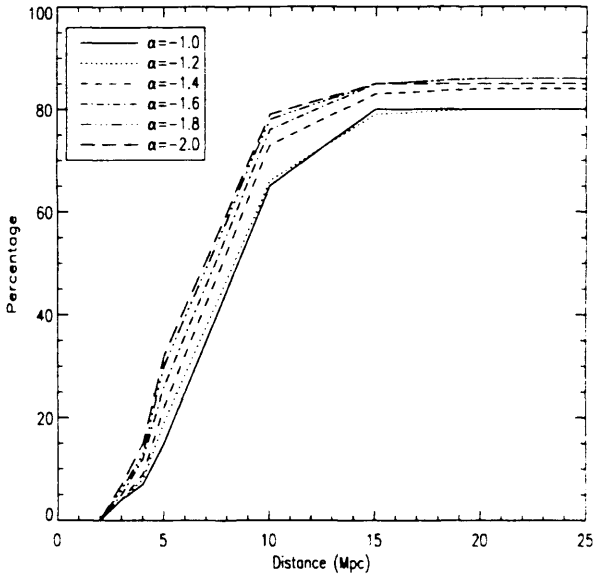

Figure 4.6: Percentage of galaxies selected with adjusted scale-length criteria having intrinsic properties in the range $23 \leq \mu_0 \leq 26\ B\mu$ and $-10 \geq M_B \geq -14$ at increasing distance for varying values of α.

both sample the field environment.

4.2.2 Influence of seeing

Although our chosen numerical simulation selection criteria for finding LSB dwarf galaxies in the Virgo, UMa and MGS field data was $23 \leq \mu_0 \leq 26\ B\mu$ and $3'' \leq h \leq 9''$, this was a rather idealised situation. In reality the frames are influenced by the seeing and in some cases this was quite bad. Fig. 4.7 illustrates the influence of the seeing on the number of detections made in the Ursa Major data. The number of detections increases rapidly as the seeing degrades above about $2.5''$ and stars are smeared out into diffuse objects. We considered the influence of the seeing on the measured scale-length of galaxies by convolving simulated galaxies of scale-

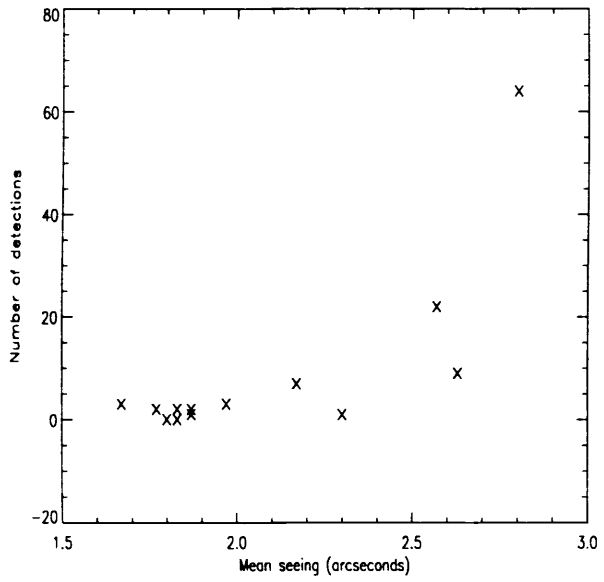

Figure 4.7: How seeing affected the number of detections

length 3″ with a 1.5-2.5″ Gaussian seeing function. The result was a measured scale-length of order 4″. Thus galaxies with intrinsic scale-lengths of 3″ will have *measured* scale-lengths of approximately 4″. Our final image selection criteria therefore was $23 \leq \mu_0 \leq 26$ Bμ, $4'' \leq \alpha \leq 9''$ for the Virgo, UMa ,MGS field and M101 region (up to 21 Mpc) environments, and $23 \leq \mu_0 \leq 26$, $9'' \leq \alpha \leq 27''$ for detecting companions around M101, up to ~6.9 Mpc.

4.3 HI Detection and Selection

4.3.1 MGS Field data

Pointed HI observations of 63 optical detections in the MGS field data found using the detection algorithm and selection criteria described above, were carried out

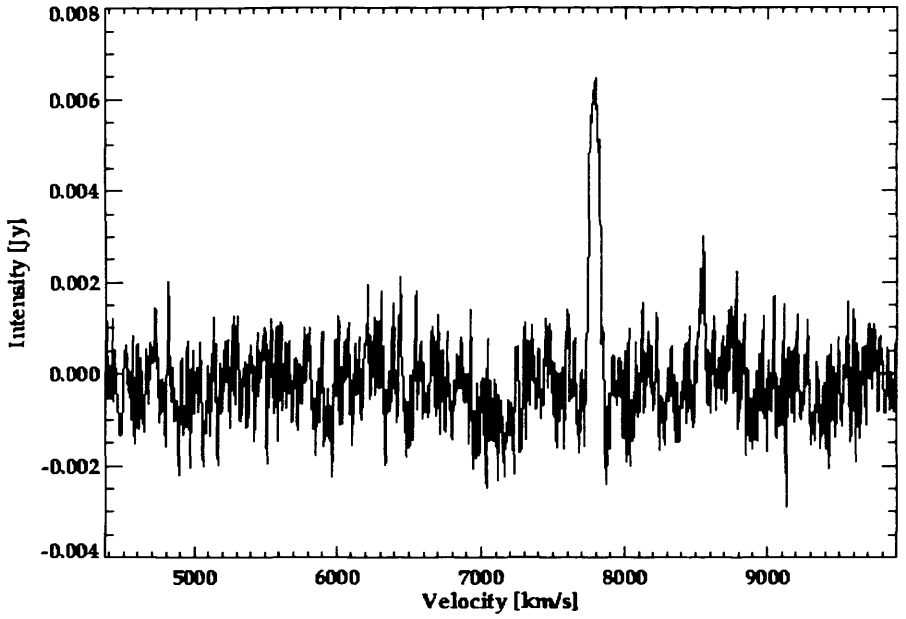

Figure 4.8: An example HI spectra from the MGS data. The detection can easily be seen as a 8.2σ peak at $\sim$7784 kms^{-1}

using the Arecibo radio telescope. Spectra of these optical detections were obtained and studied to see if the object was a source of HI. An example of a typical spectra for a HI detection is shown in Fig 4.8, where the peak at $\sim$7784kms^{-1} is an obvious detection of HI. An example of a non-detection is shown in Fig 4.9.

For all of the spectra, the rms noise level was determined, and for the detected peaks, the central velocity, velocity width at the 50% level of peak maximum, and the integrated flux were determined. From the spectra, any peaks which were above 4σ were classified as detections (private communication, Karen O'Neil) - those which had 4σ peaks were classed as possible HI detections. Those which had peaks lower than this were rejected. The HI mass of the identified sources were then calculated using Equation 3.1 (Chapter 3). In order to identify sources whose HI detections might have been confused by nearby galaxies, we queried the NED and HyperLeda databases and inspected DSS images over a region of 10′ radius

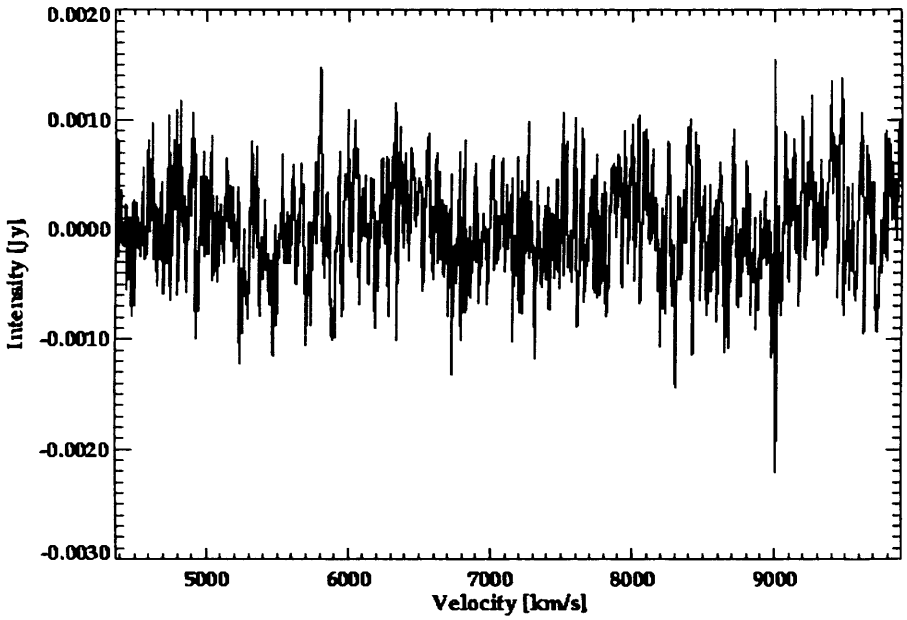

Figure 4.9: An example HI spectra from the MGS data in which there was no HI detection.

surrounding the centre position of each source. Experience from those who analyse HI data (Garcia, private communication), indicates that the HI source is invariably found within the central beam of the telescope. Thus a 10′ radius should account for all possible objects.

4.3.2 UMa data

As explained in Chapter 3, we had 21cm data from the HIJASS survey, covering an area of 8°×8° in the UMa cluster, and overlapping with our optical data fields. In order to identify possible galaxies in the HIJASS data cube, the cube was initially inspected by eye. For this purpose the karma package, *kvis* (Gooch, 1996) was used to visualise the data. The declination and velocity axes were studied whilst stepping through in right ascension. Possible galaxies were identified as bright

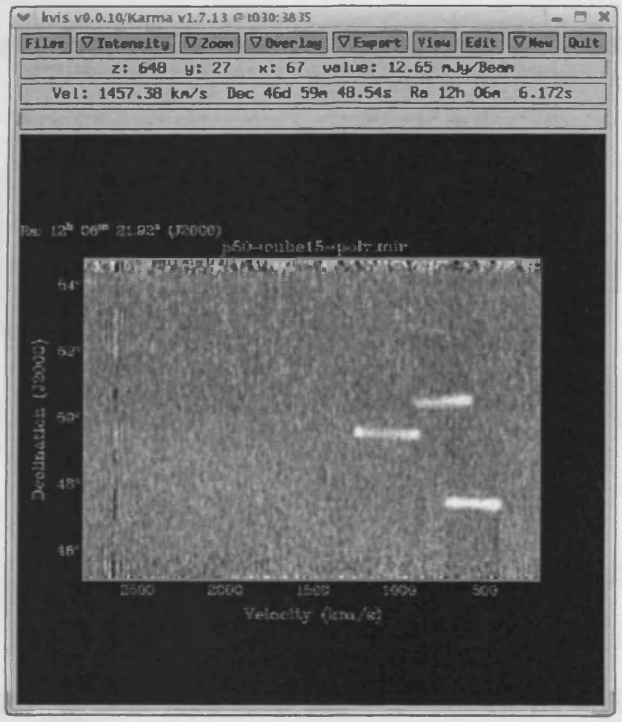

Figure 4.10: Snapshot of *kvis* screen. Here, the declination and velocity axes are studied whilst stepping through in right ascension. Three obvious HI detections can be seen as bright regions on the right side of the data screen.

spots which showed up during the stepping through procedure (an example can be be seen in Fig 4.10).

Once a galaxy was identified by this method, its parameters were then measured using the *miriad* routine, *mbspect*. Once the coordinates of the galaxy are inputted, along with an estimate of the width over which to fit the profile and baselines, the procedure then gives a fit of the spectrum of the detection, along with the peak and integrated flux measurements, line centre and velocity width for the 50% and 20% measurements and the rms noise and barycentric velocity.

Once all the possible detections were made by eye, an automated galaxy finder, *polyfind* (Davies et al. 2001), was then run on the data cube. *Polyfind* is an automated procedure designed to find candidate galaxies in HI data cubes by

the use of cross-correlation fitting of matched templates. The program searches for peaks in the HI data cube which are above 4σ of the measured noise in each channel (private communication, Robert Minchin). It then fits a series of Gaussian templates (with FWHM values ranging from 23 to 500km/s) to this peak, and finds the best fitting template and a value for the correlation coefficient which effectively says how good the fit is. If the fit is good enough (i.e. the correlation coefficient is above a predefined value of 0.75 - private communication, Robert Minchin), then this peak is highlighted as a possible HI source in the data. If the correlation coefficient is below the predefined value, the peak is rejected. *Polyfind* then outputs a list of peaks for which it has successfully fitted templates. However, in this list there are some multiple detections i.e. single objects with more than one fitted template. A second program, *Polypurge*, is run over the data to find the best fitting template for the multiple detections for peaks 4.5σ above the noise (private communication - Robert Minchin). The output is then a final list of possible HI sources in the data cube.

The HI data cube had previously been inspected by a second person, and a list made of the coordinates and velocities of the possible detections. Thus, the cube was searched independently three times in total, twice by humans and once by an automated finding procedure, so hopefully, all possible HI sources with masses $\geq$ $2 \times 10^8 M_{\odot}$, velocity width greater than 25kms^{-1} and peak SNR of $\geq 4.5\sigma$, present in the data, were identified.

For all the HI detections in the HIJASS cube, a search was made in NED to see if they had an optical counterpart. As defined by Lang et al. (2003), if the HI source position was within $6'$ (i.e. within the radius of the telescope beam, which has FWHM of $12'$) and 100kms^{-1} in velocity of an object in NED, then this was assumed to be the optical source of the HI galaxy.

4.4 Summary

4.4.1 Optical

The optical detection algorithm implemented in this thesis was developed with the specific aim of emphasising faint, diffuse objects on CCD frames i.e. to detect LSB objects. The method uses a Fourier convolution of the images with matched templates and is completely automated, so it can be run over large sets of CCD data. The algorithm makes use of *all* the flux in the object, not just the edge pixels, thus ensuring low SN objects can also be detected. By convolving the objects with filters of different scale-lengths, a final significance image can be produced from a combination of all the images. On this final image, objects of each scale-length are emphasised. Possible LSB dwarf galaxies are then identified if their peak fluxes are significantly above the noise fluctuations in the final image. Photometry is carried out on the objects to give a final object catalogue with details of the objects' parameters. Selection criteria is then applied to the catalogue to preferentially select LSB dwarf galaxies.

One of the most important factors in this investigation of LSB dwarf galaxy populations in different environments is the ability to detect the same types of objects in each environment. Selection criteria was originally chosen by Sabatini et al. (2003) to preferentially select LSB dwarf galaxies in the Virgo cluster, at a distance of 16 Mpc. The criteria maximised the detection of dwarf galaxies in the cluster, whilst minimising the contamination from background objects. The criteria chosen for this was $23 \leq \mu_0 \leq 26$ Bμ, $4'' \leq \alpha \leq 9''$. We used this criteria for both the Virgo and UMa cluster data-sets, as they are both at approximately the same distance. We also used this criteria for the MGS field data, and make a

statistical adjustment for the detected objects with no known redshifts, assuming they are within 21 Mpc (as explained in Chapter 5). This is the distance to which we can say that we are detecting the same types of objects in the field as found in Virgo and UMa. For the M101 data, we used this selection criteria to again search for objects within 21 Mpc, but also to find possible companions of this giant galaxy at a distance of ~6.9Mpc, the scale-length criteria was scaled accordingly.

4.4.2 HI

We had pointed HI observations for 63 of the objects detected in the MGS field data from the Arecibo radio telescope. Spectra for all these optical sources were studied using IDL software to verify if the object was a source of HI. For detected peaks of 4σ or above, the central velocity, velocity width at 50% level of the peak maximum, the integrated flux and the HI mass were determined.

We also analysed an $8° \times 8°$ cube of HIJASS data covering the UMa region. The cube was inspected twice by eye by using the *karma* software package, *kvis* to detect bright spots when stepping through the cube in right ascension, declination or velocity. The cube was also analysed using an automated HI galaxy finder, *polyfind* , which uses the method of cross-correlation fitting of matched templates. Thus, all HI sources satisfying the selection criteria of a 4.5σ detection, $M_{HI} \geq 2 \times 10^8 M_{\odot}$, and velocity width $V_{50} \geq$ 25kms^{-1}, should be found.

Chapter 5

Results - optical

As discussed in Chapter 1, the hierarchical clustering theory of structure formation in the Universe predicts numerous small mass haloes in the Universe today. If these objects form stars then we should be able to detect them as dwarf galaxies. However, searches for these objects have highlighted a discrepancy between the predicted numbers and observations.

We have surveyed over 60 sq. degrees of deep CCD data in 4 different regions of the Universe - the general field, a region around the spiral galaxy, M101, the Ursa Major cluster and the Virgo cluster. Our first aim with these data-sets was to search for LSB dwarf galaxies, initially to probe fainter magnitudes which had not previously been observed as a check to see if any had been missed by previous searches. Our second aim was to compare the numbers of dwarf galaxies in each environment with the predictions of CDM. We used the detection algorithm and selection criteria described in the previous chapter to find such objects in these environments. In this chapter we discuss the results from our optical search beginning in the least dense region, the field. The results from this data set (Roberts et

al. 2004) will show what can be expected when looking at a random part of the sky, and are important since, as we explain later, we can use the results from the field to define the background counts in the cluster data sets. We will then present the results of our search around M101 which can be compared with both the field results and observations of companions around the Milky Way. We then move onto the UMa cluster, a region where spiral galaxies similar to M101 are coming together to form a cluster, and finally we present our results for the Virgo cluster which is currently building itself out of Local Group and small group analogues.

5.1 The MGS

Our MGS field survey covered $\sim$ 30 sq. degrees of the region shown in Fig. 2.8 (Chapter 2). The main motivation for surveying the general field was to search for LSB dwarf galaxies which may have been missed by previous searches, as with our data we can reach magnitudes, $M_B\sim$ -10 at a distance of 16 Mpc. As we discussed in Chapter 1, previous searches did not find many LSB dwarf galaxies, thus with our deeper survey we would hope to uncover these types of objects if they exist.

We described in Chapter 4 that for each of the four environments surveyed in this thesis we used the same selection criteria to detect dwarf galaxies in the data. These selection criteria were chosen following simulations of a cluster of galaxies at 16 Mpc with a uniform background. To find the limit to which we could therefore detect dwarfs in the field, where there is no such overdensity of galaxies, we ran a simulation of just the background Universe. The distance limit to which we can assume that we are detecting dwarf galaxies in the general field which are similar to the types of dwarf galaxies in the Virgo cluster, is $\sim$ 21 Mpc. If we restrict our

analysis for the MGS to within 21 Mpc we can make a direct comparison between the two very different environments.

5.1.1 Numbers per sq. degree

In the 30 sq. degrees of the MGS survey we found 110 objects, each of which was confirmed by eye. In the main, the detected objects were very different to those detected in our Virgo cluster survey (Sabatini et al. 2003; this thesis). The Virgo cluster survey detections were predominately smooth diffuse objects (dE galaxies). In the field a large fraction of the detections are rather 'clumpy' objects making it much more difficult to distinguish whether they were groups of faint distant objects or nearby irregular galaxies. We therefore decided to divide our list of MGS field detections into two groups: those we are sure are individual galaxies (examples are shown in Fig.5.1) and those that we are less confident of (examples shown in Fig. 5.2). Their parameters are given in Tables 5.1 and 5.2 respectively. For the 'sure' objects we have 51 detections, corresponding to $\sim 2\pm1$ per sq. degree. By including the 59 'unsure' objects, the number density rises to $\sim 4\pm1$ per sq. degree (assuming Poisson errors).

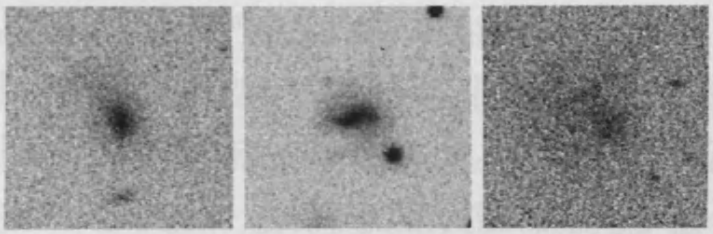

Figure 5.1: Examples of objects easily classified as 'sure' galaxies (from Table 5.1).

We can compare these results with our model predictions of the background number density for LFs with varying faint-end slopes. The model results are shown

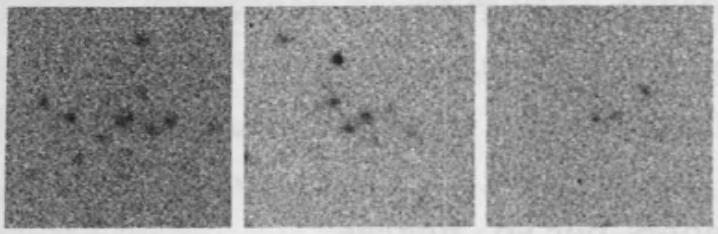

Figure 5.2: Examples of objects classified as 'unsure detections' (from Table 5.2). One object very similar to those shown above was confirmed via a HI detection as a Virgo cluster dIrr galaxy.

in Table 5.3.

For our observed number density of $\sim$ 2-4 objects per sq. degree we would expect the field LF to have a faint-end slope, $\alpha\sim$ -1.4 to -1.6. Since we are restricting our analysis to field objects within 21 Mpc, we can see from Fig. 4.5 that according to our model, $\sim$ 45% of our detections should have similar intrinsic properties to those detected in the Virgo cluster and lie within 21 Mpc. For our 'sure' list this gives a value of 23 $\pm$5 objects within 21 Mpc. We have velocity information for 34 objects in this list - 4 have velocities which place them within 21 Mpc, the remaining 30 are at further distances. If we assume that the 16 'sure' objects which have no HI or optical velocity information lie within 21 Mpc, then this gives a total of 20 objects which lie within 21 Mpc, which is excellent agreement with our model prediction. This shows that we should not be worried that a large number of the 'sure' detections are at distances greater than 21 Mpc - it may even be quite obvious why there are a large number of background 'sure' objects with velocity information - Fig. 5.3 shows the central surface brightness distributions for the 'sure' objects with redshifts (solid line) and those without redshifts (dashed line). It is clear from this plot that those objects with redshift information also have the highest surface brightness values. Redshifts are easier to obtain for higher surface brightness galaxies at further distances, and difficult to obtain for LSB galaxies,

even if they are nearby. Fig. 5.3 illustrates this bias clearly.

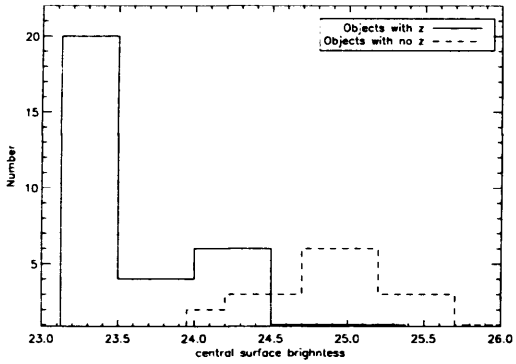

Figure 5.3: Distribution of blue central surface brightness for objects with (solid line) and without (dashed line) redshift information.

Comparing our model expectations with our observations when including the 'unsure' objects also, is not so easy to do since the majority of the 'unsure' objects (~92%) have no velocity information. Thus we cannot say for sure whether they are within or beyond 21 Mpc. Our model predicts 50±7 out of our 110 detections will lie within 21 Mpc, but without velocity information we cannot comment on how well the predictions and observations match up when we include the 'unsure' objects in our analysis.

One comparison which we *can* make however is between the predicted distance distribution of objects selected with our selection criteria (Fig. 4.4, Chapter 4) and the observed distance distribution for our objects with velocity information (Fig. 5.4). Although the predicted peak at about 21 Mpc can clearly be seen, there is also an excess of galaxies at distances greater than 70 Mpc. The model has been useful in that it enabled us to clearly specify the problem and to define the consequences of our selection criteria when looking in the field region, but now we have the distances to so many objects it now appears to be a poor representation of the data - the Universe is more complicated than our simple model.

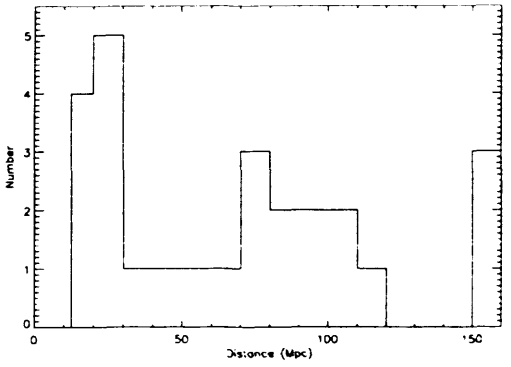

Figure 5.4: The distribution of measured distances for all objects with velocity information from the 'sure' and 'unsure' lists.

Background Objects

We commented earlier that one of the reasons why the field MGS data is important is because it can be used to define the background counts for use when we study the cluster datasets. From our MGS data we conclude that when looking at a random part of the sky, the expected number density of *all* objects will be $\sim$ 4 per sq. degree. Splitting the detections into 'sure' and 'unsure' we would expect to find $\sim$ 2 per sq. degree for each when looking in the general field. Thus, in our survey of the Virgo cluster, any number density of objects greater than these we would expect to be due to the cluster itself.

We said earlier that to compare the field dwarf galaxies to those detected in the Virgo cluster, and to ensure we are detecting similar objects, we should restrict our analysis of MGS field objects to those within 21 Mpc. For the MGS 'sure' objects, 67% of the objects have velocity and therefore distance, information so we can be sure for over two thirds of our objects that we are excluding those which lie further than 21 Mpc. With the 'unsure' objects this is difficult to do because only 8% have velocity information, so for the majority of these objects we do not know whether they are within 21 Mpc or further away. However, we can look at the likelihood

that these objects are within 21 Mpc based upon the velocity information that we do have for some of the objects, and their morphologies.

If we compare the morphologies of the 'unsure' MGS field objects to those of the 4 'sure' galaxies within 21 Mpc, it is clear that they are very different. The 'unsure' objects are very clumpy looking objects (Fig. 5.2). However, not even the 'sure' galaxy classified as dIrr (Fig. 6.1, Chapter 6) looks like any of the 'unsure' detections. So, based upon their morphology alone it seems highly unlikely that these 'unsure' detections are nearby dIrrs. They certainly appear more like distant groups of objects.

Another indication that these 'unsure' detections are more likely to be distant objects rather than nearby dIrrs is that 3 out of the 5 with velocity information (60%) have v>50,000kms^{-1}. From the 'sure' list only 1 object from the 34 with velocity information (3%) has v>50,000kms^{-1}, and this was regarded as a 'sure' detection due to its spheroidal morphology - we were confident that it was a true individual galaxy. The 'unsure' objects with high velocities are all very clumpy in nature - one is even classed as a galaxy cluster from the SDSS and two others are identified in NED as faint pairs of galaxies, so it seems plausible that the remaining faint clumpy objects in the 'unsure' list which appear morphologically very similar, are also background groups or pairs of objects. A final point to note is the HI detections of the 'unsure' objects. Although this is discussed in more detail in Chapter 6, we comment here that out of the 25 'unsure' objects observed at 21cm using the Arecibo radio telescope, there were only 2 detections, 1 of which is only a marginal detection and needs follow up observations. Thus 92% of the 'unsure' objects observed at 21 cm have no detectable HI, which further indicates that these objects are not likely to be nearby dIrrs, but are background groups of objects.

Based upon the above discussion, we conclude that the 'unsure' objects are predominantly faint groups of objects at large distances (>>21 Mpc) and not nearby dwarf galaxies. When we come to analyse the Virgo cluster data later in this Chapter we exclude the 'unsure' objects from the analysis and show that this gives a good result for the separation of cluster and background objects (henceforth, our definition of 'background' objects is that they are further than 21 Mpc).

5.1.2 Dwarf to Giant Ratio (DGR)

In our search for LSB dwarf galaxies in different environments we sample the luminosity function over a very limited range (-10 $\geq M_B \geq$ -14) thus to compare the results in different regions we use a Dwarf to Giant Ratio (DGR). We define the DGR as the number of dwarfs with -10$\geq M_B \geq$-14 divided by the number of galaxies with $M_B \leq$ -19. By comparing the DGRs for each environment from the field through to the dense Virgo cluster, we can gain information on how the environment may play a part in the formation of dwarf galaxies. We have used NED to find all catalogued galaxies within our survey area that lie within 21 Mpc and have $M_B \leq -19$. There are six galaxies that satisfy this criteria. Our simulation of a 'background' Universe, described in Chapter 4 predicts that there should be 0.3. Thus, as mentioned earlier, the volume sampled by the MGS to 21 Mpc is overdense in bright galaxies when compared to our simulation by about a factor of 20. This illustrates the difficulty of finding a 'typical' region of the Universe. Although the region sampled by the MGS is less dense than, for example, the Virgo cluster, it is more dense than that sampled by the large area redshift surveys which provided the data for our simulation. The main reason for this overdensity is that the MGS crosses the Virgo southern extension. Four of the

six bright galaxies reside in this region. Thus if all of our 110 detections were to lie within 21 Mpc we would have a DGR of 18. This would correspond to a LF faint-end slope of $\alpha \sim -1.2$. As we have shown, only a small fraction of our detected galaxies actually reside within 21 Mpc and so the LF of this particular region of the Universe has a very flat faint-end slope even when observed to the very low surface brightness limit of our survey. This was also the conclusion reached by Driver et al. (2005) who used the same data set to investigate the LF in the magnitude range -22.6$\geq M_B \geq$-14.6. They found a faint-end slope value of -1.13$\pm$0.02, thus our results indicate that there are no very LSB galaxies which were missed by Driver et al. With our survey we extend the search for LSB dwarf galaxies down to $M_B \sim$-10 (at a distance of 16 Mpc), thus ensuring that even the very faintest dwarf galaxies in the field should not be missed if they exist. It is extremely important to sample such faint magnitudes as the very faint objects may be those galaxies which help reconcile the apparent discrepancy between current observations of dwarf galaxies and predicted numbers of low mass DM haloes from CDM theory.

To be as fair as possible to the results of CDM theory, in our calculation of the DGR we would like to find the *maximum* possible DGR for the field which is consistent with our data. We have four dwarf galaxy (-14 $\leq M_B \leq$ -10) detections from our 'sure' list (Objects 12, 13, 31 and 33) which have measured velocities placing them within 21 Mpc. This gives a DGR of 0.7. Including the possible detection of Object 48 from Table 5.2 ('unsure' list) increases this to 0.8. To ensure we find the maximum possible DGR from our data we must allow for the possibility that some of the unobserved objects in the two lists lie within 21 Mpc. From the list of 'sure' objects, 4 out of the 34 objects with redshift information (i.e. 12%) lie within 21 Mpc. If we assume the same percentage of objects lie within 21 Mpc for *all* 51 objects in the 'sure' list, this would give 6 objects. Similarly, for

the 'unsure' objects, 5 had redshift information with only 1 being within 21 Mpc (i.e. 20%). Assuming the same percentage of all 59 'unsure' objects lie within 21 Mpc gives a total of 12 objects. Thus with 6 possible objects from the 'sure' list within 21 Mpc and 12 possible from the 'unsure' list, this increases the DGR to 3.

In Chapter 4 we said that we can detect all galaxies with $-14 \leq M_B \leq -10$ within 21 Mpc. This is actually only true if they follow the Driver (1999) surface brightness relation. At fainter magnitudes some galaxies of higher surface brightness will be missed because they are too small. The volumes over which dwarf galaxies can be detected compared to the volume out to 21 Mpc are listed in Table 5.4; this is the visibility function.[1]

As can be seen, for higher surface brightnesses and fainter magnitudes we do not sample the whole volume - the objects are too small at larger distances. So, our observations do not rule out a population of faint galaxies with higher surface brightness in the field, UMa or Virgo cluster. We must consider if there is any evidence of such a population. Given the sparse numbers of detections for those magnitudes and surface brightnesses for which we *do* have full volume coverage, the LF would have to do something very strange if the numbers predicted by CDM are to be accounted for. In the Local Group there are 10 galaxies that satisfy our magnitude and surface brightness selection criteria. Of these, half lie in the region where we do not have full volume coverage as indicated by Table 5.4. If the same was also true for the MGS region and we were missing half of our objects due to incomplete volume coverage then the DGR would double from 3 to 6. We conclude that there is no large population of higher surface brightness dwarf galaxies that have been missed in the MGS data and that, at most, the DGR is 6,

[1]Note that this does not affect our comparison with the other datasets because they are all observed over a similar depth.

which corresponds to a LF with faint-end slope, $\alpha\sim$-1.0.

5.1.3 Association with bright galaxies

The lower plot of Fig. 5.5 shows the total number of optical detections along the MGS as a function of their RA. The dotted histogram includes all the detections we found along the strip (i.e. all those listed in Tables 5.1 and 5.2); the solid histogram includes just those 'sure' objects which we list in Table 5.1. Shown in both the upper and lower plots of Fig.5.5 is the approximate position of the Virgo Southern Extension, plotted as a dashed line between RA of 180-200 and a distance of approximately 16Mpc. Interestingly, it appears to be situated just where there is a dip in the total number of detections. The total number of detections is higher at both ends of the survey, where the galactic latitude is between 40 and 52 degrees. Beyond $\sim$199°, towards the end of the strip, the extinction rises steeply from an approximately constant value of 0.21 mag to 0.3 mag. It is possible that some of the unsure detections may be groups of faint stars within our Galaxy. The upper plot of Fig. 5.5 shows the positions along the MGS of the 6 bright galaxies ($M_B \leq -19$) within 21 Mpc. We can also see if any of the detected galaxies are possible companions of the brighter galaxies. In the review of Mateo (1998) of the Local Group, the furthest dwarf galaxy companion of the Milky Way is at a distance of 250 kpc. For each bright galaxy we have indicated this distance on the upper plot of Fig. 5.5. Objects 12 and 13 are almost certainly companions of NGC3521. Object 31 lies in the Virgo Southern Extension but does not seem to be associated with any of the bright galaxies. Object 33 is at about the same velocity as NGC4517 though the projected separation is 1.2 Mpc so it is unlikely to be a companion of this galaxy.

The number of giant galaxy companions is lower than might have been expected when compared with the Milky Way. The MW has 11 definite companions (Mateo, 1998), 4 of which (Sculptor, Fornax, Carina and UMi) we would expect to detect with our selection criteria if they were within 21 Mpc. We explained in Chapter 4 that during the masking of bright galaxies on the CCD frames, any objects within 1 scale-length of the bright galaxy will also be masked by the procedure. We checked the surrounding areas of the bright galaxies in the MGS to see if any nearby companions had been masked during this automatic procedure, and found no masking of nearby galaxies had taken place. Thus either the bright galaxies in our survey region do not have dwarf companions like the Milky Way's or they are being hidden in some way, possibly due to projection effects i.e they are behind the galaxy disc. A similar result applies to the Virgo cluster dwarfs (Sabatini et al. 2003) - not all the dwarf galaxies found in Virgo appear to be preferentially associated with the bright cluster galaxies.

No.	RA (J2000)	Dec (J2000)	m_B	μ_0	Scale-length ('')	Comments	logM_{HI} ($M_\odot$)	W_{50} (km s^{-1})	Velocity (km s^{-1})
1	10 10 42.01	-0 07 39.6	17.7	23.2	5.0	Sp, NO	-	-	v_{opt} = 17,630
2	10 12 32.73	-0 09 45.3	18.1	23.1	4.0	Irr, NO	-	-	v_{opt} = 17,214
3	10 22 20.79	-0 15 51.3	20.0	25.0	4.0	Irr, ND	-	-	-
4	10 29 23.30	-0 16 05.0	19.4	24.9	5.0	?	8.9	44	v_{HI} = 7323
5	10 35 29.38	-0 00 54.7	17.1	23.3	7.0	Irr, NO	-	-	v_{opt} = 8400
6	10 40 14.92	-0 06 46.2	19.1	24.1	4.0	Irr	8.7	117	v_{HI} = 5642
7	10 39 34.40	-0 08 49.9	20.2	25.2	4.0	Sph, ND	-	-	-
8	10 39 23.75	-0 16 45.4	19.6	25.5	6.0	?, ND	-	-	
9	10 44 43.56	-0 11 39.6	16.9	23.1	7.0	Irr, NO	-	-	v_{opt} = 4479
10	10 52 40.55	-0 01 15.9	18.2	23.2	4.0	Irr	8.1	69	v_{HI} = 1772
11	10 52 39.61	-0 00 36.9	20.7	25.7	4.0	Sph	-	-	-
12	11 04 40.22	0 03 29.5	16.9	23.7	9.0	Sph	6.2	25	v_{HI} = 835
									v_{opt} = 801
13	11 04 38.6	0 04 53.8	20.2	25.2	4.0	Sph	-	-	-
14	11 04 20.55	0 01 18.4	19.6	24.6	4.0	Irr, ND	-	-	-
15	11 12 50.23	0 03 37.1	18.0	23.0	4.0	Sph, NO	-	-	v_{opt} = 28,636
16	11 15 26.76	-0 09 40.9	18.3	23.2	4.0	Sp, NO	-	-	v_{opt} = 22,800
17	11 20 52.62	-0 00 07.7	18.7	23.7	4.0	Sph, ND	-	-	-
18	11 39 57.79	-0 16 29.7	20.2	25.7	5.0	Sph, ND.	-	-	
19	11 41 07.52	-0 10 00.6	18.8	24.3	5.0	Sp	9.5	45	v_{HI} = 11,901
20	11 43 21.01	0 01 43.1	18.4	23.4	4.0	?, NO	-	-	v_{opt} = 5643
21	11 55 58.49	0 02 36.2	19.2	24.2	4.0	Irr	9.1	90	v_{HI} = 7791
22	12 00 47.67	-0 01 23.2	16.3	23.0	9.0	Sp, NO	-	-	v_{opt} = 1878
23	12 01 43.69	-0 11 03.6	17.1	23.3	6.0	?, NO	-	-	v_{opt} = 44,937
24	12 07 10.38	-0 15 34.1	18.1	23.6	5.0	Sp, NO	-	-	v_{opt} = 6735
25	12 19 30.21	-0 13 15.3	19.4	24.4	4.0	Sph, ND	-	-	-
26	12 21 02.48	0 00 22.4	19.1	24.1	4.0	Irr	8.6	83	v_{HI} = 6224
27	12 23 42.18	-0 15 25.8	17.4	23.7	7.0	Sp	9.0	117	v_{HI} = 7509
28	12 24 30.78	0 04 15.9	16.7	23.4	9.0	Irr	8.6	83	v_{HI} = 2062
									v_{opt} = 4642
29	12 39 47.62	0 02 28.8	18.1	24.9	9.0	Irr, ND	-	-	-
30	12 46 53.1	-0 09 15.2	19.6	24.6	4.0	Sph, ND	-	-	
31	12 50 04.79	-0 13 56.6	17.6	24.4	9.0	Sph	6.3	29	v_{HI} = 754
32	12 50 45.22	0 03 44.8	18.1	23.1	4.0	?, NO	-	-	v_{opt} = 14,400
33	12 52 34.05	-0 10 04.0	18.4	23.4	4.0	Irr	7.0	98	v_{HI} = 1018
									v_{opt} = 1077
34	13 18 49.53	0 04 07.6	21.0	26.0	4.0	?	6.9	24	v_{HI} = 2340
35	13 24 56.17	-0 08 02.0	18.0	23.0	4.0	Sp, NO	-	-	v_{opt} = 19,949
36	13 38 42.6	-0 15 11.7	17.5	23.4	6.0	?, NO	-	-	v_{opt} = 5940
37	13 45 56.03	-0 01 32.0	20.7	25.7	4.0	?, ND	-	-	-
38	13 50 00.79	0 03 43.8	20.0	25.0	4.0	Irr, ND	-	-	-
39	13 56 23.88	-0 07 50.3	19.6	25.1	5.0	Irr, ND	-	-	-
40	13 55 22.78	-0 00 02.7	20.9	26.0	4.0	?, ND	-	-	-
41	13 59 47.85	-0 01 53.9	18.5	24.0	5.0	Sp, ND	-	-	-
42	14 04 55.97	-0 08 17.2	20.5	25.5	4.0	Irr	8.1	148	v_{HI} = 3728
43	14 06 36.73	0 03 55.5	19.2	24.2	4.0	?	8.8	97	v_{HI} = 7335
44	14 07 44.70	0 04 16.0	19.2	24.2	4.0	Sph, NO	-	-	v_{opt} = 93,680
45	14 11 55.22	0 04 35.7	18.2	23.2	4.0	?, NO	-	-	v_{opt} = 11,670
46	14 14 16.57	-0 15 34.3	18.5	23.5	4.0	?, NO	-	-	v_{opt} = 11,610
47	14 20 33.93	-0 09 17.6	18.1	23.6	5.0	Sph	7.4	6.3	v_{HI} = 1610
									v_{opt} = 1574
48	14 24 03.96	0 03 58.5	18.2	23.2	4.0	Sp, NO	-	-	v_{opt} = 46,655
49	14 36 53.51	-0 14 54.3	18.4	23.4	4.0	?, NO	-	-	v_{opt} = 30,231
50	14 38 43.43	-0 04 48.4	19.2	24.9	4.0	Irr, ND	-	-	-
51	14 39 59.91	-0 11 10.2	17.6	23.4	6.0	Irr	8.4	244	v_{HI} = 1859

Table 5.1: Table of 'sure' optical detections in the MGS. In the comments column, NO and ND refer to 'Not Observed' and 'observed but Not Detected' at 21 cm respectively (the HI results will be discussed in more detail in the next Chapter). Note objects 10/11 and 12/13 lie in the same Arecibo beam, but are distinct in the optical image. Objects 34 and 42 are possible detections and will need confirming.

Index	*RA (J2000)*	*Dec (J2000)*	μ_0	*Scale-length* (arc sec)	*Comments*	$\log M_{HI}$ ($M_\odot$)	W_{50} (km s^{-1})	Veloci (km s^{-}
1	10 08 24.06	-0 08 13.7	25.5	7.0	clumpy, NO	-	-	-
2	10 08 24.33	-0 00 44.1	26.0	7.0	clumpy, NO	-	-	-
3	10 08 43.39	-0 03 15.0	25.7	5.0	clumpy, NO	-	-	-
4	10 08 07.72	0 00 14.2	26.0	5.0	clumpy, NO	-	-	-
5	10 10 05.13	0 01 54.2	26.2	6.0	v. faint looks like disc-shape, ND	-	-	-
6	10 12 42.23	-0 15 57.0	26.2	7.0	blank sky?, NO	-	-	-
7	10 24 25.28	-0 10 57.3	25.6	4.0	clumpy, NO	-	-	-
8	10 23 36.23	-0 15 40.1	25.8	5.0	clumpy, NO	-	-	-
9	10 29 22.06	-0 10 12.4	26.2	5.0	v. faint, NO	-	-	-
10	10 29 23.10	-0 12 22.0	25.9	4.0	v.faint but good profile, ND	-	-	-
11	10 38 23.67	0 01 47.2	26.5	6.0	clumpy, NO	-	-	-
12	10 44 26.21	0 02 25.1	26.1	6.0	clumpy, NO	-	-	-
13	10 44 43.43	-0 15 09.9	25.9	4.0	FPG?, NO	-	-	-
14	10 43 28.92	0 00 29.3	26.4	6.0	clumpy with cloud?, ND	-	-	-
15	10 50 52.50	0 04 56.9	25.9	4.0	clumpy, NO	-	-	-
16	11 00 40.76	-0 00 25.6	26.2	7.0	dot, NO	-	-	-
17	11 02 37.44	-0 15 45.0	26.0	4.0	clumpy, NO	-	-	-
18	11 04 31.47	-0 07 43.4	25.9	6.0	Unsure, ND	-	-	-
19	11 16 22.88	-0 02 12.6	25.4	9.0	Faint pair of galaxies within 0.2′ , NO	-	-	-
20	11 18 17.20	-0 01 23.1	26.0	4.0	v. faint, ND	-	-	-
21	11 02 37.41	-0 15 45.2	26.4	7.0	clumpy, NO	-	-	-
22	11 04 31.47	-0 07 43.0	25.9	4.0	clumpy, NO	-	-	-
23	11 18 44.61	-0 10 43.9	25.6	7.0	Faint pair of galaxies within 0.1′ , NO	-	-	-
24	11 23 48.90	-0 16 09.6	24.9	7.0	clumpy, NO	-	-	-
25	11 23 21.0	-0 03 19.7	26.3	6.0	faint but good profile, ND	-	-	-
26	11 28 29.10	-0 08 09.0	26.1	7.0	clumpy, NO	-	-	-
27	11 33 39.30	-0 15 27.6	26.3	6.0	dot, NO	-	-	-
28	11 37 16.75	0 02 36.6	26.1	5.0	dot, ND	-	-	-
29	11 38 47.57	-0 06 37.3	25.7	4.0	clumpy, ND	-	-	-
30	11 58 19.36	-0 01 39.5	25.5	4.0	clumpy, NO	-	-	-
31	12 19 42.74	0 05 09.6	25.8	5.0	clumpy, ND	-	-	-
32	12 34 13.75	-0 16 30.8	26.5	7.0	dot, ND	-	-	-
33	12 45 32.92	0 00 09.0	26.37	6.0	Unsure, ND	-	-	-
34	12 49 32.11	-0 02 00.5	26.3	4.0	v.faint clumpy, NO	-	-	-
35	12 54 35.98	-0 02 39.6	26.2	4.0	Unsure, ND	-	-	-
36	12 58 37.48	-0 10 08.7	26.1	5.0	clumpy, ND	-	-	-
37	13 03 22.26	-0 00 06.0	26.0	4.0	clumpy, NO	-	-	-
38	13 05 23.59	0 00 00.7	26.3	5.0	Sph, ND	-	-	-
39	13 09 51.20	-0 12 44.5	25.1	6.0	SDSS galaxy cluster, NO	-	-	v_{opt} = 9(
40	13 13 45.49	-0 04 32.4	26.2	6.0	clumpy, ND	-	-	-
41	13 30 24.09	-0 03 25.3	26.3	7.0	clumpy	8.4	164	v_{HI} = 5
42	13 38 05.01	-0 09 01.3	25.7	4.0	v.faint clumpy, NO	-	-	-
43	13 45 59.37	-0 04 47.2	26.3	5.0	v. faint clumpy, ND	-	-	-
44	13 45 53.75	-0 02 48.7	26.4	5.0	v. faint clumpy, NO	-	-	-
45	13 46 07.18	-0 16 54.8	23.1	4.0	SDSS galaxy, NO	-	-	v_{opt} = 5(
46	13 50 20.97	0 01 02.4	26.6	7.0	v.faint, ND	-	-	-
47	13 50 10.85	-0 02 28.8	26.2	4.0	v.faint clumpy, NO	-	-	-
48	14 05 38.08	-0 08 18.7	25.9	4.0	clumpy	6.4	28	v_{HI} =
49	14 06 14.44	0 02 39.8	25.8	4.0	v.faint dot, NO	-	-	-
50	14 05 41.01	0 02 13.0	26.1	5.0	clumpy, NO	-	-	-
51	14 15 16.70	-0 03 22.4	25.7	4.0	clumpy, ND	-	-	-
52	14 18 48.79	-0 02 46.4	25.9	9.0	clumpy, NO	-	-	-
53	14 20 57.95	0 04 46.0	26.0	4.0	clumpy, ND	-	-	-
54	14 20 42.42	-0 04 02.2	26.1	7.0	clumpy, ND	-	-	-
55	14 26 17.75	0 03 42.9	25.4	4.0	clumpy, NO	-	-	-
56	14 35 47.58	0 03 00.8	25.8	5.0	clumpy with cloud?, ND	-	-	-
57	14 37 23.96	0 01 05.4	26.0	5.0	dot v. good profile, ND	-	-	-
58	14 40 21.50	-0 03 51.2	25.7	5.0	clumpy, ND	-	-	-
59	14 46 10.43	0 02 47.4	24.6	4.0	SDSS galaxy, NO	-	-	v_{opt} = 8(

Table 5.2: Table of 'unsure' detections in the MGS. 'ND' in the comments column means observed but not detected at 21cm, 'NO' refers to the objects not observed at 21cm. Object 48 is a marginal detection that will need confirmation. Full details of the HI detections are given in the next Chapter.

α	*No. objects per* deg^2
-0.6	0.005
-0.8	0.02
-1.0	0.1
-1.2	0.2
-1.4	1
-1.6	5
-1.8	24
-2.0	127

Table 5.3: The predicted number of objects detected with $23 \leq \mu_0 \leq 26$ $B\mu$ and $3'' \leq h \leq 9''$ for each LF faint-end slope, α.

μ_0			M_B		
	-10	**-11**	**-12**	**-13**	**-14**
26	99	100	100	100	100
25	25	99	100	100	100
24	6	25	99	100	100
23	2	6	25	99	100

Table 5.4: Relative volumes, expressed as a percentage, that galaxies of different surface brightnesses (μ_0) and magnitudes (M_B) can be detected within - the visibility function.

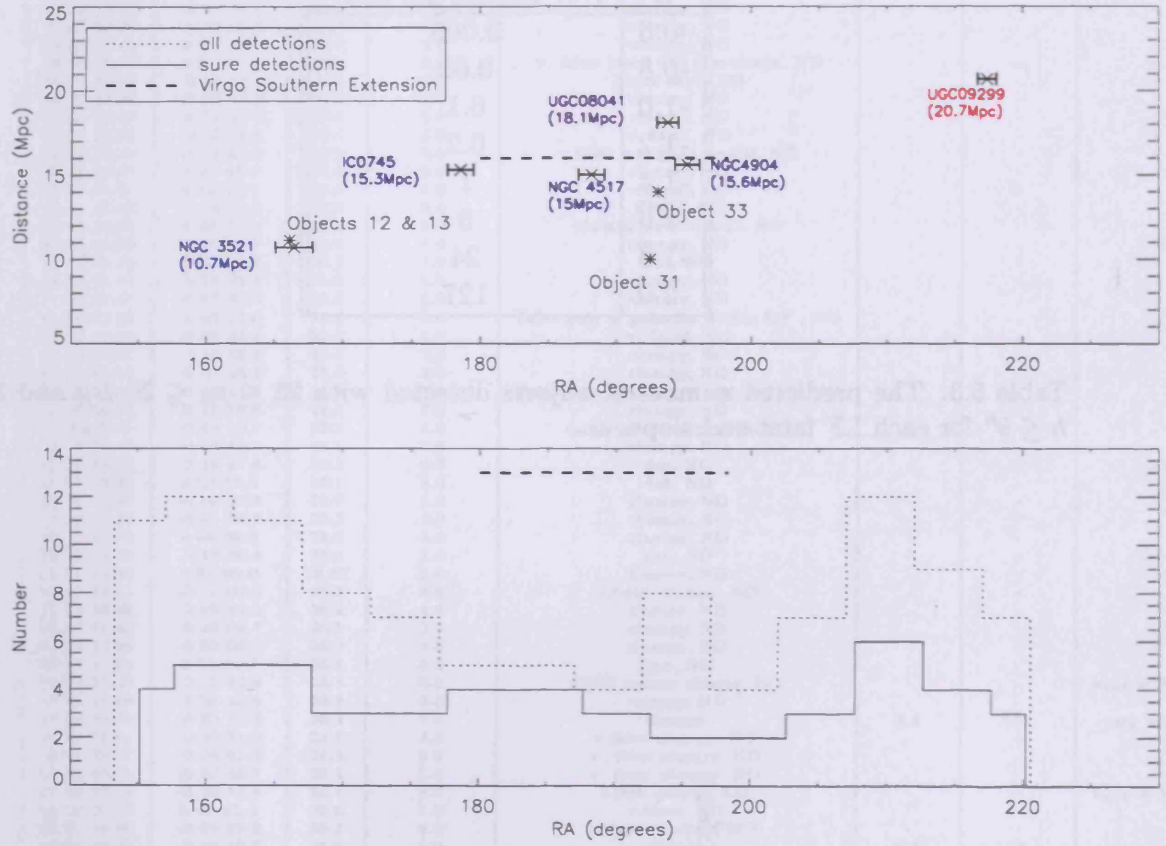

Figure 5.5: The upper figure illustrates the possible association of dwarf galaxies with giant galaxies. The giant galaxies (within 21 Mpc) are labelled on the plot, with the lower galaxies being those which are closer to us, as indicated by the distance scale on the y axis. The error bars on the giant galaxies indicate a projected distance of 500 kpc. The positions of dwarf galaxies with redshifts are also marked. In the lower plot the dashed histogram is the distribution of all the detections (Tables 5.1 and 5.2). The solid histogram shows the distribution of the 'sure' optical detections from Table 5.1. The approximate extent of the Virgo Southern Extension is shown on both plots as a bold dashed line.

5.1.4 Galaxy colours

The colours of the objects which we detect in the field can be compared with the colours of objects detected in the Virgo cluster to give us an idea of how the environment may affect the evolution of dwarf galaxies. We present and discuss our comparison for the (B-I) colours of the objects detected in these 2 environments in Section 5.4.4 of this Chapter. Here we give only the MGS field galaxy colours.

The (B-I) colours for the four 'sure' objects detected in the MGS with known velocities and within 21 Mpc are given in Table 5.5. Objects 12 and 13, both dSphs have similar (B-I) values within their errors, and are relatively blue objects compared to Object 31 which has the reddest colour of all. Object 33, a dIrr is also bluer than Object 31, but it is not the bluest object out of these 4, even though it is the only dIrr. As we mentioned in the previous section, Objects 12 and 13 are almost certainly companions of NGC 3521- perhaps the tidal influence of this giant galaxy on these 2 dwarf companions has recently triggered SF in these two objects. This might explain why their (B-I) colours are bluer than the 2 dwarf galaxies which do not appear bound to a giant.

Object number	*Type*	*B-I*
12	dSph	0.83 ± 0.05
13	dSph	1.00 ± 0.27
31	dSph	1.60 ± 0.09
33	dIrr	1.17 ± 0.09

Table 5.5: Table of colours for the 'sure' MGS objects within 21Mpc

The colour distributions of the 'sure' and 'unsure' objects separately are shown in Fig. 5.6. We find a large number of 'unsure' objects with very red colours (>3), the reason for which is unclear - it could be, as we concluded earlier, that these objects are background objects, perhaps at high redshifts, and they therefore

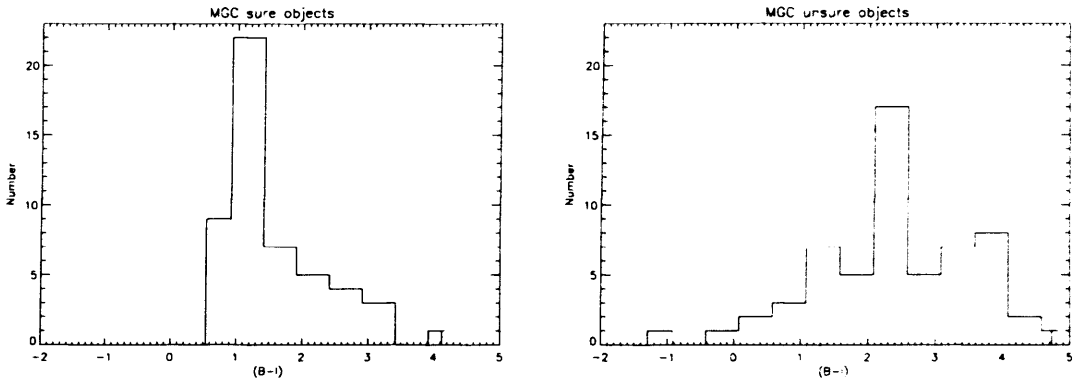

Figure 5.6: Distribution of B-I colours for the 'sure' (left) and 'unsure' (right) objects in the MGS field data.

appear extremely red. The high (B-I) values could also be due to the increased errors on the 'unsure' objects as shown in Fig. 5.7. The objects with larger (B-I) are generally quite faint, and have large errors associated with them.

The mean (B-I) value for the 4 objects within 21 Mpc is 1.15 $\pm$0.33. For the 'sure' objects it is 1.54 $\pm$ 0.79, and for the 'unsure' objects, 2.37 $\pm$ 1.20. There appears to be an increase towards redder mean colours from objects within 21 Mpc to 'sure' to 'unsure' objects. However, within the errors, all three mean (B-I) values ('sure', 'unsure' and objects within 21 Mpc) agree. Fig. 5.7 shows the (B-I) colours for both the 'sure' and 'unsure' objects with respect to each object's apparent magnitude. For the 'sure' objects, the errors in measuring the (B-I) colours increases as the magnitudes get fainter, highlighting the uncertainty of the photometry procedure when probing faint objects. The plot of (B-I) vs. B band apparent magnitude for the 'unsure' objects shows clearly the increased errors in their (B-I) values compared to the 'sure' objects. The errors for these objects are large even at the brighter magnitudes of $\sim$18 because of the clumpy nature of these objects.

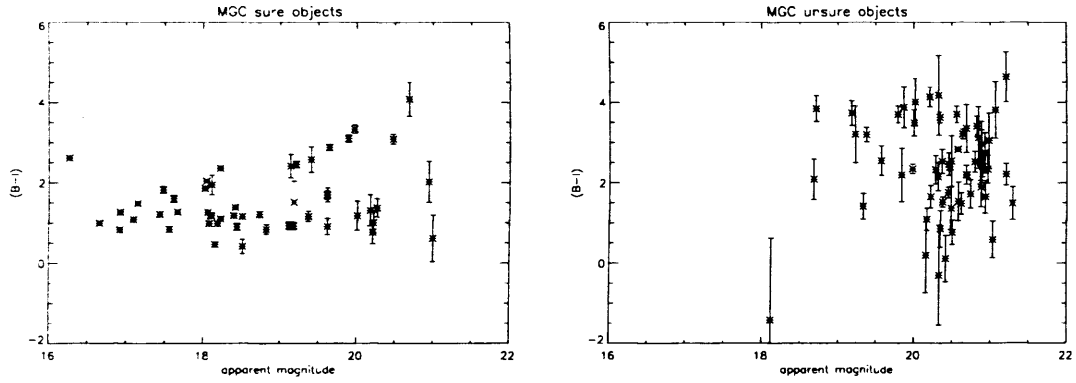

Figure 5.7: Plot of (B-I) colours vs. blue apparent magnitude for the 'sure' (left) and 'unsure' (right) objects in the MGS field data.

5.2 M101

We are interested in comparing the dwarf galaxy populations in different environments down to very faint magnitudes. The field environment gives an indication of what one might expect to see when looking at a random part of the Universe. We described our results for the general field in the previous section. Our main reason for surveying the area around M101 was to look for dwarf galaxy companions of this galaxy, however, using this data we can also carry out an additional survey of the field environment. As for the MGS field data, by using the selection criteria, $4'' \leq \alpha \leq 9''$ and $23 \leq \mu_0 \leq 26$, we can find dwarf galaxies in the area covered by this dataset up to a distance of $\sim$21 Mpc. The results from this M101 data can then be compared with the MGS field result.

As we mentioned above, our primary motivation with observing the area around M101 was to investigate whether this spiral galaxy has a large number of dwarf galaxy companions similar to those around the MW. We would like to know this because the Virgo cluster has a large number of dwarf galaxies, and is currently assembling itself out of LG analogs. Thus it would be interesting to see if these dwarfs are already in place around the giant galaxies out of which Virgo is forming, or if they been produced in the cluster itself. An investigation of the dwarf galaxy population around a giant galaxy will hopefully shed some light on these two possibilities. A lack of dwarfs around M101 would suggest that the dwarf galaxies found in Virgo have been produced by some other mechanism and are not associated with the giant galaxies in the cluster.

As explained in Chapter 4, to investigate the dwarf galaxy population around M101 and detect dwarfs with similar properties to those found in the Virgo cluster, we use the selection criteria of $9'' \leq \alpha \leq 27''$ and $23 \leq \mu_0 \leq 26$. We discuss the results

of this search later in this section. First we will present the results for the field galaxy population around M101, selected with the criteria of $4'' \leq \alpha \leq 9''$ and $23 \leq \mu_0 \leq 26$.

5.2.1 Field objects in the M101 data set

Numbers per sq. degree

Our M101 survey covered 15.3 sq. degrees, and can be seen in Fig.2.10 (Chapter 2). To find objects in the field we used the selection criteria of $4'' \leq \alpha \leq 9''$ and $23 \leq \mu_0 \leq 26$. As with the MGS field data we split our list of objects into 'sure' and 'unsure' detections. The 'sure' objects are those which we are confident to be individual galaxies. The 'unsure' detections are those we could not be sure were true individual galaxies based on their appearance alone. As we discussed in the previous section, we consider the 'unsure' objects to be predominantly background.

In total, we found 62 objects, 51 of which had no previous identification in NED. The 'sure' list contains 45 objects and the 'unsure' list contains 17. The parameters of the 'sure' and 'unsure' detections are given in Tables 5.6 and 5.7 respectively. There are two 'sure' objects (Objects 40 and 41) which we have classified as dE but subsequent SDSS velocities showed that they are background galaxies, and not dE. The morphological classification was done prior to obtaining the velocity information, and even on second inspection of these objects, they appear similar to dE type galaxies, thus they must be LSB background galaxies. In the MGS field data we found a similar object which was classed as spheroidal in morphology but had a high velocity.

Number	RA (J2000)	Dec (J2000)	m	μ_0	scale-length ($''$)	Comment	ID in NED	Velocity (kms^{-1})
0	14 4 20	53 41 6	18.1	23.1	4.0	dIrr	unknown	
1	14 3 27	53 37 53	19.9	25.4	5.0	dIrr	unknown	
2	14 6 50	53 44 30	19.1	25.3	7.0	dIrr	unknown	
3	14 11 20	53 44 51	18.2	23.7	5.0	dIrr	unknown	
4	13 48 1	54 9 43	18.7	23.7	4.0	dIrr	unknown	
5	13 50 19	54 8 17	18.7	23.7	4.0	Sp	2MASX	v_{opt}=38,000
6	14 1 35	54 10 27	19.3	24.3	4.0	dE,N	unknown	
7	14 3 45	53 56 38	18.8	25.5	9.0	dSph	unknown	
8	14 13 9	52 33 54	18.9	23.9	4.0	dSph	unknown	
9	13 52 51	55 47 18	18.0	23.0	4.0	dIrr	unknown	
10	14 2 20	55 39 19	19.2	25.1	6.0	dIrr	unknown	
11	13 53 18	54 13 27	18.1	23.1	4.0	dIrr	MAPS	
12	13 55 7	54 32 33	17.8	23.7	6.0	unsure	unknown	
13	13 57 46	54 18 38	19.2	24.2	4.0	dIrr	unknown	
14	14 6 42	54 14 9	18.8	23.8	4.0	dSph	SDSS galaxy	v_{opt}=34,000
15	14 5 51	54 14 59	18.5	23.5	4.0	dE,N	unknown	
16	14 10 27	54 16 18	18.3	23.8	5.0	dIrr	unknown	
17	14 9 9	54 38 41	18.3	23.3	4.0	unsure	MAPS	
18	14 7 55	54 42 13	17.2	23.1	6.0	dIrr	MAPS	v_{opt}=1800
19	14 14 10	54 46 11	17.3	23.2	6.0	dIrr	MAPS	v_{opt}=93,000
20	14 9 2	54 51 46	18.4	23.9	5.0	dE,N	unknown	
21	14 8 31	54 52 49	18.8	23.8	4.0	dE	unknown	
22	14 10 12	55 22 24	18.5	23.5	4.0	dE	unknown	
23	14 8 34	55 26 50	19.5	24.5	4.0	dSph	unknown	
24	14 9 51	53 25 24	18.4	23.4	4.0	Sp	SDSS galaxy	v_{opt}=44,000
25	14 10 16	53 26 28	18.0	23.5	5.0	Sp	MAPS	
26	14 13 39	53 24 53	18.1	23.1	4.0	Sp	MAPS	v_{opt}=5700
27	14 14 47	53 28 47	18.1	24.0	6.0	Sp	2MASX	v_{opt}=22,500
28	14 14 13	53 16 14	19.5	24.6	4.0	unsure	MAPS	v_{opt}=21,000
29	14 7 19	52 38 13	18.5	23.5	4.0	unsure	unknown	
30	13 54 55	53 10 34	19.2	24.2	4.0	dIrr	unknown	
31	14 14 3	55 49 55	18.1	23.1	4.0	dSph	unknown	
32	13 57 38	51 58 27	17.4	23.2	6.0	dIrr	MCG	
33	13 59 8	52 4 6	19.1	24.6	5.0	dSph	MAPS	v_{opt}=8700
34	14 1 53	51 54 18	20.1	25.1	4.0	dSph	unknown	
35	13 53 13	52 30 54	18.1	23.1	4.0	dE,N	unknown	
36	14 9 50	52 19 55	19.9	24.9	4.0	dIrr	unknown	
37	14 7 18	52 18 6	19.0	24.0	4.0	dIrr	unknown	
38	14 13 5	52 12 52	18.9	23.9	4.0	Sp	unknown	
39	13 46 52	52 35 24	18.1	23.6	5.0	dE	unknown	
40	13 48 5	52 50 23	18.3	23.3	4.0	dE	SDSS galaxy	v_{opt}=58,000
41	13 53 4	52 36 12	18.1	23.1	4.0	dE	SDSS galaxy	v_{opt}=45,000
42	13 52 38	52 40 33	19.4	24.4	4.0	dSph	unknown	
43	13 50 33	52 33 3	20.3	25.3	4.0	dIrr	unknown	
44	14 7 47	54 15 22	20.8	25.8	4.0	dE off-centre	unknown	

Table 5.6: Table of 'sure' detections for the M101 data set

For the 'sure' objects there are ~3 objects per sq. degree; including the 'unsure' objects gives ~4 per sq. degree. This is in excellent agreement with our MGS field result where we found ~2 objects per sq. degree for the 'sure' detections and ~4 per sq. degree for all the detections. There is clearly no excess of galaxies in this region, selected with the above criteria, due to the giant galaxy M101.

Morphologies

The morphologies of the 'sure' objects detected in the M101 and MGS field data are shown in Table. 5.8. The dE classification includes the spheroidal looking objects, and the nucleated dE types; the dIrr classification includes the objects

Number	RA (J2000)	Dec (J2000)	m	μ_0	scale-length ($''$)	Comment	ID in NED
0	14 11 47	54 13 5	19.4	24.4	4.0	clumpy	unknown
1	14 3 3	54 47 12	20.7	25.7	4.0	faint dSph. Good profile	unknown
2	13 55 45	55 8 46	20.9	25.9	4.0	faint clumps. Good profile	unknown
3	13 47 34	52 51 4	20.6	25.7	4.0	faint dSph. Good profile	unknown
4	13 58 46	52 55 32	20.7	25.7	4.0	v. faint dE	unknown
5	14 2 52	52 24 34	18.7	24.2	5.0	clumpy	unknown
6	14 3 60	52 17 12	20.8	25.8	4.0	v. faint clumps	unknown
7	14 7 23	52 29 18	20.3	25.8	5.0	v. faint clumps	unknown
8	14 12 50	52 18 5	20.8	25.8	4.0	v. faint clumps	unknown
0	13 46 26	52 40 26	20.6	25.6	4.0	v. faint clumps	unknown
10	13 46 43	52 33 55	20.4	25.4	4.0	v. faint dIrr	unknown
11	13 53 8	52 36 32	20.8	25.9	4.0	vlsb	unknown
12	13 52 50	52 31 55	20.5	25.5	4.0	vlsb. Good profile	unknown
13	13 52 45	52 37 9	20.4	25.9	5.0	vlsb. Good profile	unknown
14	13 51 45	52 31 24	20.9	25.9	4.0	vlsb. Good profile	unknown
15	13 52 33	52 41 56	21.0	26.0	4.0	vlsb. Good profile	unknown
16	13 55 50	52 31 38	20.4	25.9	5.0	vlsb. Good profile	unknown

Table 5.7: Table of 'unsure' detections for the M101 data set

which do not have any regular shape, whilst the 'Other' classification includes spirals, objects for which the morphology is not clear, and the very LSB objects.

Region	*dE type*	*dIrr*	*Other*
M101	40±9%	38±9%	22±7%
MGS Field	24±7%	33±8%	43±9%

Table 5.8: Percentage morphologies of objects in M101 fields and the MGS field

There are, within the errors, comparable percentages of dE and dIrr type objects in the M101 field region and the MGS field. Since with the MGS and M101 datasets we are looking at two parts of the general field, and found that their number density is the same (~4 per sq. degree), then we would not expect to detect vastly different types of objects. We compare the types of objects detected in the field to the cluster environment at the end of this Chapter.

At the start of this section we explained that with the M101 data we wanted to do two things - first we wanted to find dwarf galaxy companions around M101 which satisfied the criteria of $9'' \leq \alpha \leq 27''$ and $23 \leq \mu_0 \leq 26$. We present the results from this search in Section 5.2.2.

Our second motivation for observing this region was to look at the field population of dwarf galaxies in this region and compare it with our MGS field results.

We have shown above that the number density and types of objects are approximately the same. We would now like to do a comparison with the MW to see how many MW companions would be detected with our field dwarf galaxy selection criteria of $4'' \leq \alpha \leq 9''$ and $23 \leq \mu_0 \leq 26$, if the MW was placed at 6.9 Mpc. As we see below, this gives us an idea of the limits of our selection criteria.

Comparison with the MW

If the MW was placed at the distance of M101, 3 of its companions would satisfy the criteria of $4'' \leq \alpha \leq 9''$ and $23 \leq \mu_0 \leq 26$. Here we assume, as in the previous section, that the maximum distance to which a dwarf galaxy can be considered a companion of MW, is 250kpc. At a distance of 6.9 Mpc, the area covered by a radius of 250kpc is $\sim$ 13.5 sq. degrees. Thus we would expect to detect $\sim$ 0.2 objects per sq. degree around the MW if it were placed at the distance of M101. However, we have shown in both our MGS and M101 field data that with the selection criteria of $4'' \leq \alpha \leq 9''$ and $23 \leq \mu_0 \leq 26$, we would expect to detect $\sim$ 4 objects per sq. degree. Thus for the MW its companion number density would be immersed in the background density. We cannot use the gross properties of the objects being detected to distinguish between field objects within 21 Mpc and companions of M101 similar to those around the MW.

5.2.2 Possible companions of M101

In this section we discuss the results of our search for dwarf galaxy companions around M101 using the selection criteria of $9'' \leq \alpha \leq 27''$ and $23 \leq \mu_0 \leq 26$. Prior to our study, the deepest and most recent survey of the dwarf galaxy population

around M101 was carried out by Bremnes et al. (1999). Reaching an absolute magnitude, M_B,~-13, they found 11 potential companions, 1 of which was classified as dE and the remaining 10 as dIrrs. We discuss whether we would expect to detect the companions studied by Bremnes et al. with our selection criteria later. Bremnes et al's study illustrates the importance of our survey, since with our search we are able to reach even fainter magnitudes, M_B of $\sim$ -8 at the distance of M101.

Over the 15.3 sq. degrees covered in our study of M101, using the selection criteria of $23 \leq \mu_0 \leq 26$ and $9'' \leq \alpha \leq 27''$, we found 1 object - Object 7 from the 'sure' list. The detection algorithm originally picked out another object which satisfied the selection criteria of $23 \leq \mu_0 \leq 26$ and $9'' \leq \alpha \leq 27''$ - Object 44 from the 'sure' list. This object's scale-length was measured to be $21''$ by the detection algorithm. However, this object is situated close ($\sim 1.5'$) to a bright star, and thus its photometry was contaminated by the halo of this star, giving imprecise measurements. Indeed, this object does not appear to be as large as $21''$ as can be seen in Fig. 5.8, especially when compared to Object 7 whose scale-length is $9''$ (Fig. 5.9). Both Figs 5.8 and 5.9 are $43''$ across. We therefore recalculated the parameters of this object using GAIA and found it to be a $4''$ scale-length object. The parameters from GAIA have been used in Table 5.6.

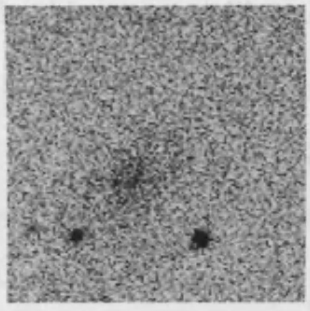

Figure 5.8: Object originally detected as having scale-length, α=21″ (Object 44 from the 'sure' list).

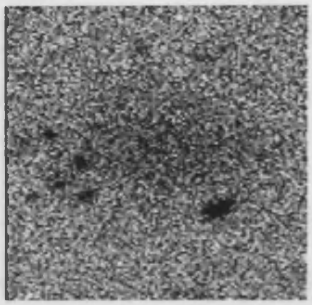

Figure 5.9: Image of the object detected with the criteria $23 \leq \mu_0 \leq 26$ and $9'' \leq \alpha \leq 21''$ in the M101 data. This is Object 7 from the 'sure' list.

So, we were left with only 1 object satisfying the criteria of $23 \leq \mu_0 \leq 26$ and $9'' \leq \alpha \leq 27''$ in our search around M101. From our model (Chapter 4), we would expect ~50% of our objects obeying this selection criteria to lie within 6.9 Mpc. Thus with our single detection there is a 50% chance that it is a dwarf galaxy companion of M101. Ideally we would like to obtain velocity information for this object to determine its distance and verify whether or not it is a companion of M101. However, an optical redshift would be very difficult to obtain since this is a large ($9''$), diffuse object with low surface brightness, μ_0 ~25.5Bμ. It is classified as a dSph, thus it is likely to be gas-poor, and so its HI velocity may also be difficult to obtain. If this object truly is a companion of M101 then, assuming a distance of 6.9 Mpc, its absolute magnitude, M_B,would be ~-10.44 which would make it a newly discovered faint dSph companion of M101.

Comparison with the MW

Since the main aim of our M101 survey was to detect possible companions around M101 we now consider how many of the MW's 11 companions would be detected with our selection criteria of $9'' \leq \alpha \leq 27''$, $23 \leq \mu_0 \leq 26$ if the MW was placed at 6.9 Mpc. Of these 11 companions listed by Mateo (1998), 10 have scale-length

data and absolute magnitudes either from Mateo or HyperLeda[2] from which their central surface brightnesses could be calculated.

For the criteria of $9'' \leq \alpha \leq 27''$, $23 \leq \mu_0 \leq 26$, no MW companions would be detected. The one MW companion which would have a scale-length of $22''$ at 6.9 Mpc (Sextans) would have $\mu_0 > 26 B\mu$, and would therefore be too faint to be selected with our surface brightness criteria. It appears that the MW does not have dwarf galaxy companions which are similar to those which we detect in the Virgo cluster. This is not the case for M101 however; Bremnes et al. (1999) in their study of the dwarf galaxy companions of M101 found 11 definite and possible companions of M101, 3 of which would satisfy the selection criteria of $9'' \leq \alpha \leq 27''$, $23 \leq \mu_0 \leq 26$ and so would be similar to the types of objects we detect in the Virgo cluster. However, 2 of these objects were located just outside the region covered by us (Bremnes et al. covered a wider range in RA and Dec than our fields), and the third object was missed by the detection algorithm as it was positioned right on the edge of the CCD frame.

DGR

The selection criteria of $9'' \leq \alpha \leq 27''$ and $23 \leq \mu_0 \leq 26$ was used when selecting galaxies in the M101 data set to find dwarf galaxy companions of M101 similar to the companions of Virgo cluster galaxies. We found 1 object satisfying this criteria in our data, which gives a minimum DGR of 1:1. Using the same selection criteria for the MW if placed at 6.9 Mpc would give a DGR of zero.

[2] http://leda.univ-lyon1.fr/

Small scale-length possible companions of M101

We discussed previously that with the selection criteria of $4'' \leq \alpha \leq 9''$, $23 \leq \mu_0 \leq 26$, we are unable to distinguish between companions of M101 and field galaxies in the vicinity of M101. However, this does not mean that there *are* no companions in our data - we just cannot differentiate between them and field galaxies without further distance information. Since our primary motivation for surveying the area round M101 was to search for possible dwarf galaxy companions of M101, we can describe the best bet candidates for companions from our 'sure' list of detections based upon the object's parameters.

Given that Bremnes et al's study of the dwarf galaxy population around M101 showed that the majority of dwarfs were late-type in morphology, and had scale-lengths larger than $6''$, we would consider similar objects in our 'sure' list to be best-bet companions of M101 and interesting for further study. These are Objects 2, 3, 10, 12 and 16, and can be seen in Fig. 5.10. Object 32, a dIrr with scale-length of $6''$ was also detected by Bremnes et al. (1999) and was included in our list of detections due to its LSB. We would also consider Objects 20 and 39 as interesting objects for follow-up work since these are both dE-types of scale-length $5''$, thus could be dwarf companions of M101 similar to the dwarf companions found around the MW. Images of these 2 objects can be seen in Fig. 5.11.

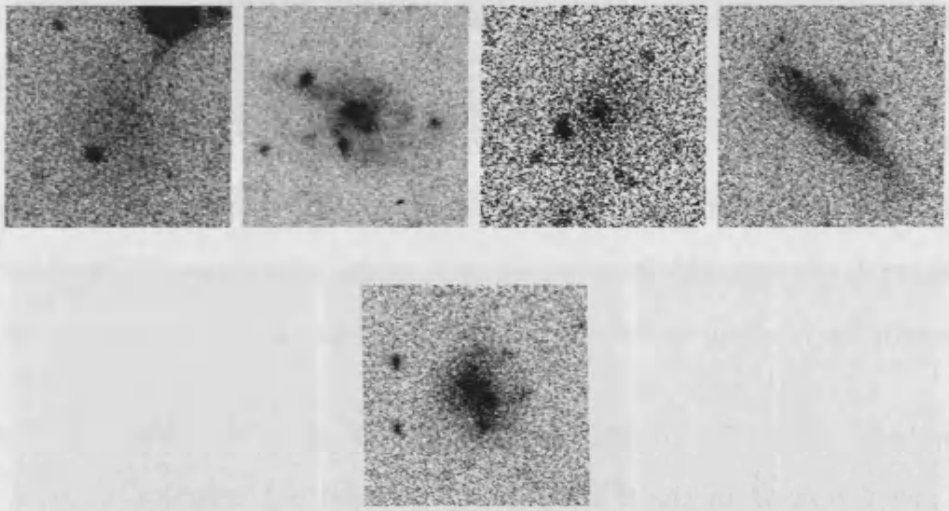

Figure 5.10: Most promising candidates for possible M101 dIrr companions.

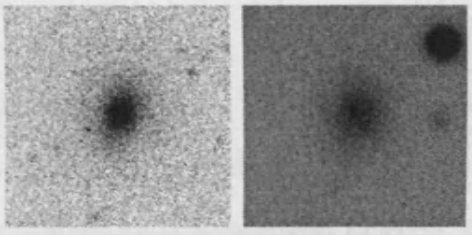

Figure 5.11: Most promising candidates for possible M101 dE companions.

5.3 UMa cluster

Our UMa cluster survey covered a relatively small ~1.68 sq. degrees of the cluster, extending outward from the cluster centre, as shown in Fig. 2.7 (Chapter 2). The fields covered corresponded to a number of fields studied by Trentham et al. (2001) in their larger survey of the cluster. Thus once we had selected possible dwarf galaxies in our fields using the detection algorithm and selection criteria described in Chapter 4, we were able to compare our results with those of Trentham et al. and investigate whether we detected the same objects in our corresponding fields.

Table 5.9 shows the results for our survey of the UMa cluster. In total we found just 6 objects in the 8 fields which satisfied our selection criteria, all of which were classified as 'sure' detections. These can be seen in Fig. 5.12. This corresponds to ~4 objects per sq. degree for the cluster, which is in good agreement with the value obtained for the MGS and M101 data as a whole, but is much less than that obtained for the Virgo cluster (as shown in the next section). The Ursa Major data is perfectly consistent with observations of the general field showing no enhancement of dwarf galaxy numbers.

Index	*RA (J2000)*	*Dec (J2000)*	μ_0	*Scale-length (″)*	*Type*	*Comments*
1	12 04 54	45 07 37	25.30	6.0	Irr	
2	12 04 00	45 24 32	26.19	4.0	Sph	
3	12 06 26	42 26 07	23.15	6.0	Spiral	MAPS galaxy
4	12 19 39	49 20 28	23.78	4.0	Unsure	
5	11 39 28	47 34 13	24.02	5.0	Unsure	PC 1136+4750 z=0.014243
6	11 41 12	47 38 18	24.53	4.0	Sph	

Table 5.9: Table of detections in the Ursa Major cluster

Of the 6 galaxies identified in the UMa data, 2 had identifications in NED (Objects 3 and 5). Object 5 was found to be a background galaxy at a redshift

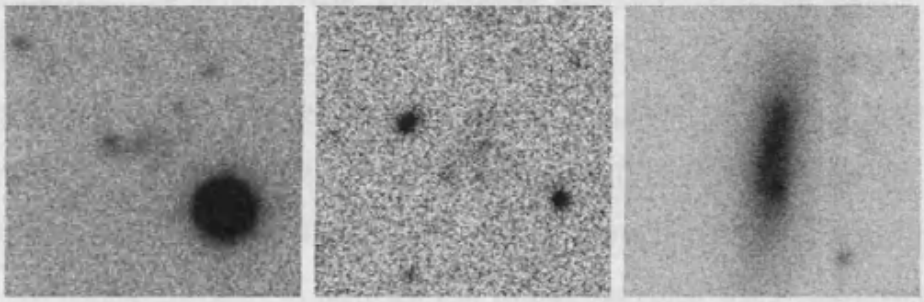

(a) Object 1 - dIrr (b) Object 2 - dSph (c) Object 3 - Sp

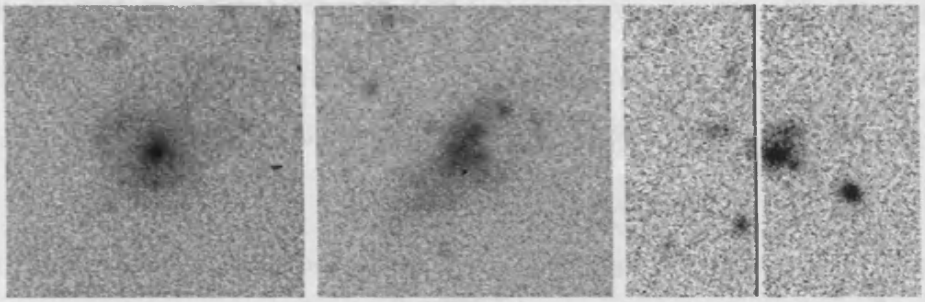

(d) Object 4 - unsure (e) Object 5 - unsure (f) Object 6 - dSph

Figure 5.12: Images and morphology classifications of the objects detected in our survey of the UMa cluster.

of 0.014 (corresponding to $\sim$ 56 Mpc); Object 3 was identified as a MAPS galaxy with no redshift. Of the remaining 4 objects not previously detected, two appeared morphologically similar to the dominant dE population of the Virgo cluster (Objects 2 and 6). Object 1 was considered to be irregular in appearance, whilst for Object 4, the morphology was unclear. There were no bright galaxies in any of the Ursa Major fields so we were not able to calculate a DGR for Ursa Major. So, although Ursa Major shows an enhancement of giant galaxies compared to the general field, it does not seem to have an enhanced dwarf galaxy population.

5.3.1 Comparison with Trentham et al.

As discussed in Chapter 2, Trentham et al. carried out a survey of the UMa cluster using data obtained from the UH8K mosaic camera on the CFHT in 1996 and the CFH12K mosaic camera on the CFHT in 1999, covering a total area of ~18 sq.degrees. Their fields are shown in Fig. 5.13.

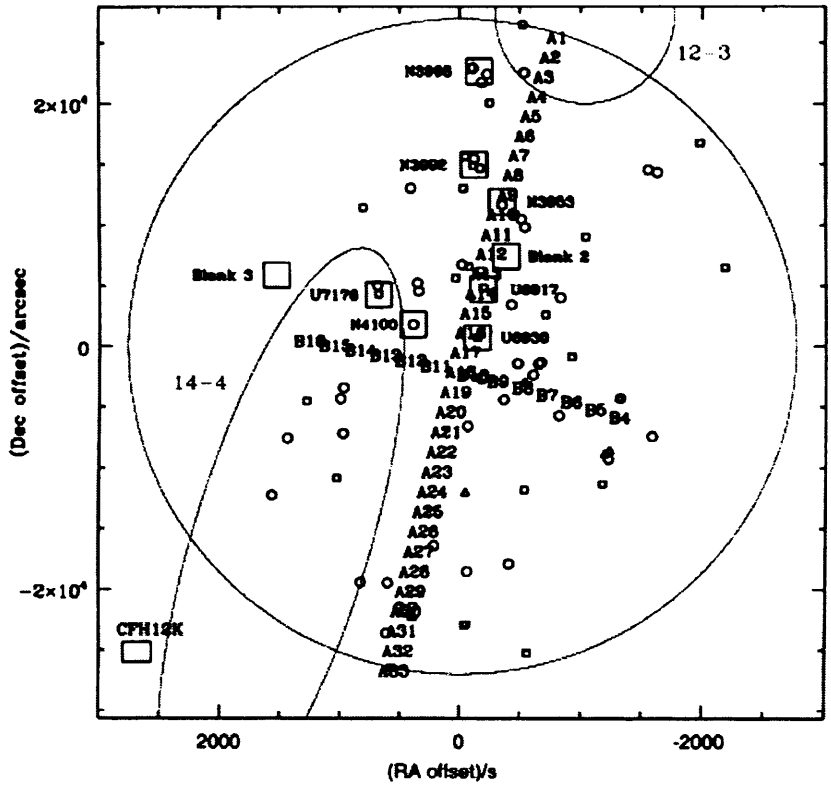

Figure 5.13: Position of Trentham et al's fields in UMa. The large circle shows the extent of the UMa cluster, with the ellipses labelled 12-3 and 14-4 being the neighbouring groups. The large squares in the image represent the fields observed in 1996, whereas the fields observed during the 1999 run are labelled A1-A33 and B4-B16. Also plotted on the diagram as small circles are the positions of known NGC members, small squares represent the known UGC members, and small triangles, other known members of the cluster.

In their UMa study, Trentham et al. considered all galaxies brighter than R~21.5, which, if we assume a typical B-R of 1.5, would give an apparent B

magnitude limit of ~23. Thus Trentham et al's study reaches slightly fainter magnitudes than our UMa survey. As explained in Chapter 2, the selection criteria of their survey is based upon each object satisfying magnitude criteria for the inner (2.2″ - 4.4″) and outer (6″ - 12″) part of the object. They then classify each object as definite (rated '0'), probable (rated '1'), possible (rated '2') and unlikely (rated '3') members of the cluster based upon the magnitude criteria. Using this membership classification criteria, Trentham et al. found a total of 65 dwarf galaxy candidates rated 0-3, giving ~ 4 dwarfs per sq. degree, consistent with our result for this cluster. Our 8 fields corresponded with the positions of 8 of those studied by Trentham et al. thus it was possible to investigate whether our method of selecting dwarf galaxies in the cluster found the same objects as detected by Trentham et al. with their different method. Table 5.10 shows the results for the 8 fields. Each field is discussed separately below.

Field	*Our detections*	*Trentham et al. detections*
UMA20	0	1
UMA25	2	1
UMA31	1	0
UMA18	0	0
UMB13	0	0
UMB16	1	0
UMB08	0	1
UMB05	2	1

Table 5.10: Number of objects found in the fields common to our study of the UMa cluster and those investigated by Trentham et al. (2001).

- **UMA20** - We detected no objects in this field which satisfied our selection criteria. Trentham et al. found 1 object satisfying their selection criteria. Further investigation showed that the position of Trentham et al's object was not covered by our CCD data since our field of view was 0.21 sq. degrees compared with Trentham et al's 0.35 sq. degrees.

- **UMA25** - We found Objects 1 and 2 in this data field. These were not found by Trentham et al., possibly because they did not satisfy their magnitude criteria. However, Trentham et al. also comment that they will miss two types of objects given their selection criteria - the first are extremely LSB disc galaxies with $\mu_0 \geq 27R\mu$. Objects 1 and 2 have $\mu_0 \sim 25.30B\mu$ and $\mu_0 \sim 26.19B\mu$, and if we assume (B-R)=1.5, then we can see that these two objects, although LSB, would still be higher than their surface brightness limit. The second type of object missed by their criteria are faint central surface brightness galaxies ($\geq 20R\mu$) with smooth de Vaucouleurs light profiles as these are mistaken for background ellipticals. Neither object fit this description, thus these 2 objects were likely to have been missed by Trentham et al. because they did not satisfy the magnitude criteria. Trentham et al. found 1 galaxy in this field which we did not include in our list of detections as it had a higher central surface brightness than the limit of our selection criteria.

- **UMA31** - We found Object 3 in this field. This object, also found by Trentham et al. was excluded from their list of detections as it was not detected in HI, and they therefore considered it to be a background galaxy.

- **UMA18** - Neither we nor Trentham et al. found any objects in this field.

- **UMB13** - Neither we nor Trentham et al. found any objects in this field.

- **UMB16** - We found Object 4 in this field. This was not found by Trentham et al. This object has $\mu_0 \sim 23.78B\mu$, thus it cannot have been missed by Trentham et al. because of its surface brightness. However, since Trentham et al. also miss galaxies with smooth de Vaucouleurs light profiles, this could be a plausible reason for them not detecting this object.

- **UMB08** - Trentham et al. found 1 galaxy in this field. Again, these co-

ordinates were not covered by our CCD image thus we found 0 objects in this data field.

- **UMB05** - We found Objects 5 and 6 in this field. Trentham et al,. also found Object 5 and included it in their list of detections, but classified it as a '3' detection; it was probably background but possibly a member. A search in NED gave its redshift as 0.014, thus confirming this objects status as a background galaxy, not part of the UMa cluster.

Although we only surveyed a small area of UMa, our results have enabled us to highlight an important point - even in the overlap of fields looked at in our survey and Trentham's survey we found only one object which we both included in our list of detections. This illustrates how difficult it is to compare different data sets, and how care should be taken when doing so. With individual surveys having different selection criteria and sensitive to different limits, the types of objects detected varies considerably. Thus our survey of different environments using identical instruments, detection and selection methods is extremely useful since we know we will be detecting the same types of objects in each environment, enabling a proper comparison of the dwarf galaxy population in different regions to be made without the need to worry about these differences.

5.4 Virgo cluster

Our Virgo cluster survey consisted of deep CCD images of two perpendicular strips both extending 7° outwards, one from East to West (E-W), the other North to South (N-S). With this data, we are capable of detecting objects down to central surface brightnesses of ~26Bμ and absolute magnitudes, M_B~-10 (for the assumed distance of Virgo of 16 Mpc). These 2 data strips sample different regions of the Virgo cluster, with one lying roughly perpendicular to the supergalactic plane (E-W), and one almost parallel to it (N-S). The results for the E-W strip were presented by Sabatini et al. (2003, 2005). In this section, we present the results for the N-S strip, and compare the results of this strip with those obtained for the E-W strip. The Virgo cluster is not the smooth well ordered cluster that we might like it to be. We described in Chapter 2 the various sub-clumps and clouds from which it is made. Thus we might find quite different numbers and types of galaxies if we look in different parts of the cluster.

Fig. 2.3 (Chapter 2) illustrates the positions of the 2 data strips in the cluster relative to the different sub-clusters and clouds of Virgo. The E-W data strip, as described in Sabatini et al. (2003), covers exclusively subcluster A which may be closer to us than our assumed value of 16 Mpc. At 13 Mpc (Feldmeier et al., 2004) these galaxies would have absolute magnitudes about 0.5 magnitudes fainter than we have assumed. The N-S strip however, overlaps in part with the N and M clouds, as well as subcluster A. If the clouds are twice the distance of the subcluster then any dwarfs associated with them will be 1.5 magnitudes fainter than in the subcluster for the same absolute magnitude. So, do we find differences in the numbers and properties of dwarf galaxies in the two strips that can be associated with the different component parts of the Virgo cluster?

Using the detection algorithm and selection criteria described in the previous chapter, we find a final list of galaxies in the N-S strip to contain 336 objects, 218 of which were previously uncatalogued. In order to compare the results from this strip with the results for the MGS field we have split the detections in a similar way - we define two lists of 'sure' and 'unsure' objects. However, Sabatini et al.'s analysis of the Virgo cluster E-W strip (2003, 2005) did not involve splitting the detections into these two categories. Thus, in order to be consistent with the other data sets which we have studied for this thesis, we went through the objects detected by Sabatini et al. (2003), and classified them as 'sure' or 'unsure' accordingly. We can now make a proper comparison between the objects found in both Virgo data strips and the other environments.

5.4.1 Numbers per sq. degree

In this section we compare the numbers of objects per sq. degree found in the Virgo cluster strips with the numbers found in each environment surveyed in this thesis. This may give some indication of how the environment is affecting the observed galaxy population.

In our N-S strip of the Virgo cluster we found 336 objects, 247 of which we classified as 'sure' detections, and 89 as 'unsure'. This gives ~16 objects per sq. deg for the 'sure' objects and ~ 22 per sq. degree for *all* the objects. Tables A.1 and A.2 in Appendix A give the parameters of the N-S strip 'sure' objects and 'unsure' objects respectively.

We discussed earlier that we considered the 'unsure' objects to be predominantly background (i.e. further than 21 Mpc) objects, and we would therefore

want to exclude them from our Virgo cluster analysis since we are only interested in cluster members. First however we must check that the 'unsure' objects detected in the Virgo data are not members of the cluster.

The 'unsure' objects detected in the Virgo cluster data constitute 6±2 objects per sq. degree which is slightly higher than the number density of field objects designated 'unsure' (~2±1 per sq. degree). We described in Chapter 2 how the Virgo cluster was made up of the main body of the cluster (Subcluster A) with infalling background clouds. Thus this higher number density of 'unsure' objects in the N-S strip is probably due to the presence of these clouds overlapping the data strip. Fig. 5.14 shows a plot of how the number density of 'unsure' objects varies with distance from the cluster centre. The E-W strip objects, plotted with filled circles appear almost constant with distance from cluster centre, which is what would be expected if mainly background objects were being selected, not cluster members, and there was no substructure behind the E-W strip. The N-S strip distribution however is rather more complex with peaks at ~2 and 4-6°. The peak at 2° is due to comparable numbers of objects being detected in this bin as in the other radius bins but over a much smaller area. The peak at ~4-6° is due to the presence of the clouds - as can be seen from Fig. 5.15, this is where the N and M clouds overlap with the N-S strip, thus the presence of the clouds in the 'unsure' objects distribution is evident from this plot.

The analysis of the Virgo cluster data is conducted on the 'sure' objects only as these are the galaxies which we are confident lie in the main part of the Virgo cluster and not objects from the background clouds. A further check that the 'sure' objects are composed mainly of cluster galaxies is given in the next section where we consider how their number density varies with distance from the cluster centre.

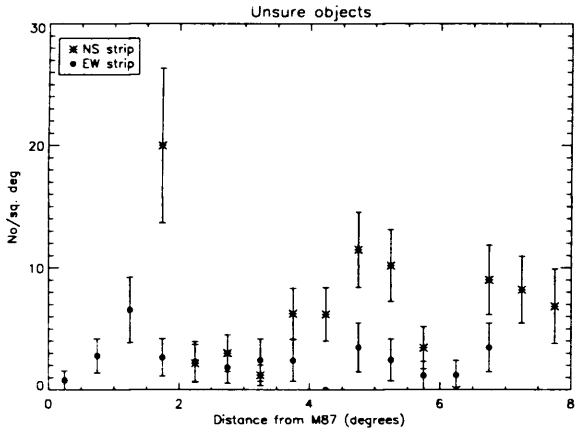

Figure 5.14: Surface number density of 'unsure' objects with increasing distance from cluster centre

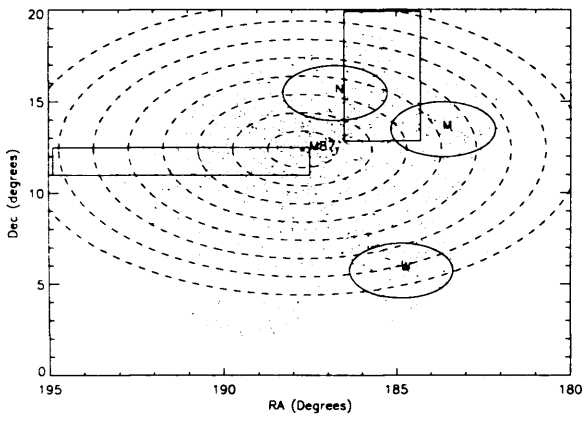

Figure 5.15: This figure illustrates the position of the data strips in the Virgo cluster, together with all VCC galaxies (dots). Also plotted are circles of radii from 1 to 8 ° from the cluster centre (defined as M87).

In the E-W strip of the Virgo cluster, Sabatini et al. (2003) found 223 objects, 191 of which we classified as 'sure' and 32 'unsure'. This gives $\sim$15 objects per sq. degree for the 'sure' objects and $\sim$17 per sq. degree for all the objects. Thus within the simple Poisson counting errors, there are comparable numbers of dwarf galaxies per unit area in the two Virgo strips. The 'unsure' E-W strip objects constitute $\sim 2 \pm 1$ objects per sq. degree which is consistent with the general field 'unsure' object number density.

If we now consider the other environments surveyed in this thesis, it is clear that there are many more objects per sq. degree in the Virgo cluster compared to the general field and the lower density UMa cluster (both $\sim$ 4 per sq. degree). There appears to be a strong relation between the number density of dwarf galaxies and the environmental density - this suggests that either something is preventing the formation of dwarf galaxies in the lower density field and UMa cluster, or dwarf galaxies are being created in the higher density Virgo cluster.

We can investigate the environmental effects on dwarf galaxy formation and evolution by looking at their parameters such as colours, their possible association with bright galaxies and the distribution of dwarf galaxy types with position in the cluster. However, before we do this we must check that the objects whose properties we will be investigating, actually *are* predominantly cluster members. This can be done by looking at how their number density varies with distance from the cluster centre, and is discussed in the next section.

5.4.2 Number density profile

The number density profile is a final check that the objects we have selected in the Virgo cluster data are mainly cluster members. Although our selection criteria was designed to maximise cluster detections and minimise background contamination, it was chosen following a simulation of a cluster at the distance of Virgo with a *uniform* background Universe as described in Chapter 4. In reality however, Virgo is an irregular cluster currently assembling itself out of various sub-clusters and clouds. As we discussed in Chapter 2, the main body of the cluster is at approximately 16 Mpc, but there are also background clouds at twice this distance, and these may contaminate the objects chosen with our selection criteria. From our survey of the general field with the MGS data we concluded that the number density of objects when surveying a random piece of sky, should be $\sim$ 4 objects per sq. degree. Any additional objects which we may detect towards Virgo will therefore be due to the cluster itself and any structures behind it. We concluded from the MGS data that the 'unsure' objects were mainly background objects (beyond 21 Mpc), so we would not want to include these in our Virgo cluster analysis. We have plotted the number density profile of the 'sure' objects for the 2 Virgo data strips in Fig. 5.16 as a check that we are predominantly selecting cluster members.

The plot begins at a distance of $\sim$ 1° from M87, as the N-S data strip is offset slightly to the NW of M87. On this Fig. we have plotted the data points for the N-S strip (* symbol), a least squares fit of an exponential-plus-constant function for the N-S strip 'sure' objects (solid line), where the constant represents the background, and the least squares fit of an exponential-plus-constant for the E-W strip 'sure' objects (dashed line). We discuss the fits in more detail below.

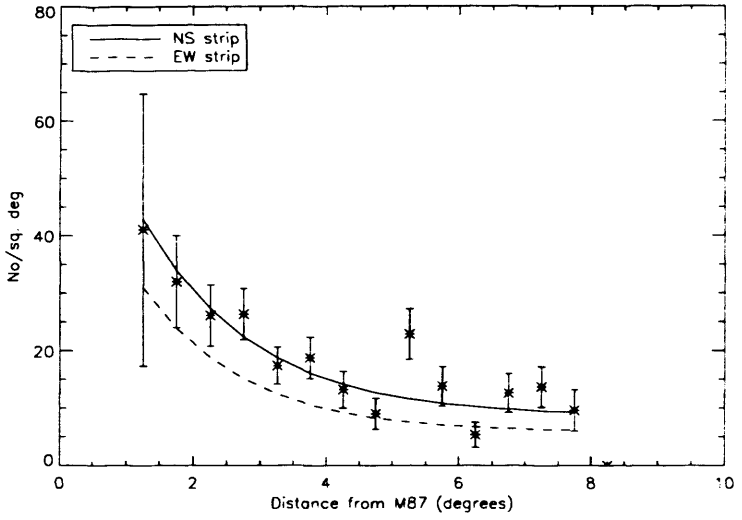

Figure 5.16: Surface number density of 'sure' objects with increasing distance from cluster centre for the N-S strip (solid line) and E-W strip (dashed line), taken from Sabatini et al. (2003). The data points are for the N-S strip.

N-S Strip

The N-S strip data is best fitted by an exponential function with scale-length of $1.6° \pm 0.7°$ and background constant of $\sim 9 \pm 2$ galaxies per sq. degree. The scale-length is consistent with the cluster core radius of 1.5° as found by Binggeli et al. (1987), but the background value is slightly higher than we would expect if the cluster edge had been reached. We showed earlier in the Chapter that for the general field we would expect to detect ~2 'sure' objects per sq. degree. So, in the direction of the N-S strip, the additional number density of objects due to the cluster, is $\sim 7 \pm 2$ per sq. degree. However, this value at the edge of the strip is still higher than the field value that we would expect to detect if we had reached the end of the Virgo cluster with this data strip. The most obvious explanation for this is that we have not reached the edge of the cluster and it actually extends further than our data-strip covers. This is plausible since the N-S strip lies along the supergalactic plane so the cluster edge is not so well defined in this direction.

There is however another possibility for the higher background density of objects in the N-S strip. If we assume that the cluster edge *has* been reached, it could be that the 'sure' detections which we assume to be predominantly cluster members, contain some objects from the background clouds which lie in the projected region of our data strip. As we discussed earlier, the simulations carried out to choose the best selection criteria for selecting Virgo cluster members was for a cluster at the distance of Virgo, but with a *uniform* background Universe. Here we have a data-strip which covers not only the main body of the Virgo cluster, but also part of the 2 background clouds. So although we hope to minimise the detection of objects from these clouds both with our selection criteria and by excluding the 'unsure' objects, it is a real possibility that we may still be picking up some objects from these clouds. The number density profile indicates that to some extent, this is true - if we were picking similar numbers of cluster members and background objects we would expect to see a flat distribution with increasing distance from the cluster centre. In reality we see a nicely decreasing profile. However, looking at the data points for the N-S strip, there appears to be a peak in the number density of objects at $\sim 5°$. We can see from Fig. 5.15 that the N and M clouds overlap with the N-S strip between 2-5° from the cluster centre so the peak seen in the N-S strip could be due to contamination from the clouds. If this is true, then this would explain why there appears to be an excess of galaxies at the end of the strip compared to the field density of objects. Although we discuss it in more detail later, we can see that the ratio of dE to dIrrs with respect to distance from the cluster centre (Fig. 5.17) substantiates this theory of contamination from the background clouds. In the E-W strip where there are no clouds there is a clear morphology-density relation. For the N-S strip, however, such a relation does not exist. We need not be too worried about this contamination since the general shape of the number density profile supports the view that our 'sure' objects are

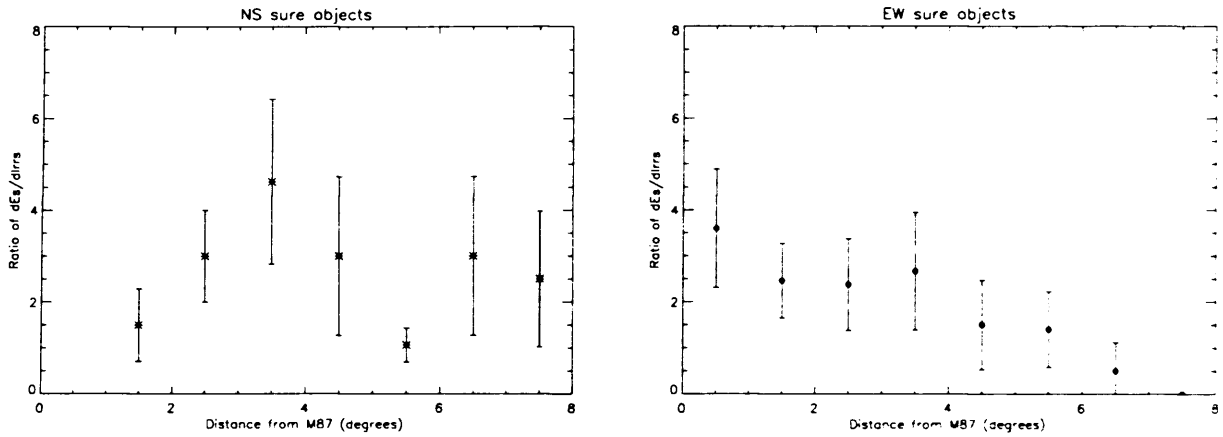

Figure 5.17: Ratio of dEs to dIrrs with increasing distance from cluster centre for the 'sure' objects in both the N-S (left) and E-W (right) strips

mainly cluster galaxies, and the influence of the background clouds is minimal.

E-W Strip

The E-W strip is best fitted by an exponential function with scale-length of 1.5 °±0.2°, consistent with both the N-S strip and the cluster core radius, and a background value of $\sim 6 \pm 1$ galaxies per sq. degree. As explained earlier, the field number density of 'sure' objects was ~2 per sq. degree, so any excess in the Virgo strips must be due to the cluster. So, the additional number density of objects due to the cluster in the E-W region, is ~4±1 object per sq. degree. Within the errors, this is consistent with the general field number density of 'sure' objects. We can therefore assume that with the E-W data strip, the cluster edge has been reached.

5.4.3 Ratio of dEs to dIrrs

It has been shown previously that dEs are more likely to be found in the centres of galaxy clusters whilst dIrrs are more prevalent in the outskirts of clusters (e.g. Fornax - Drinkwater et al. 2001, Virgo - Binggeli et al. 1987, Sabatini et al., 2003). This dwarf morphology-density relation is similar to that found for giant galaxies (Dressler, 1980). Such a relation could be an important indication of where the dEs, found in such large numbers in the cluster, come from. We discussed in Chapter 1 that they could either be the primordial population predicted by CDM, or they could have formed by some other mechanism in the cluster. One such mechanism, described in detail in Chapter 1 is that of infalling dIrrs being morphologically transformed into the dEs found in clusters. Evidence of a morphology-density relation would therefore support this theory.

Fig. 5.17 shows a plot of the ratio of dEs to dIrrs, taken from the 'sure' lists, with increasing distance from the cluster centre for both the N-S (left) and E-W (right) data strips. In the E-W strip we see a regular smooth decline in the ratio with distance from M87. This evidence supports our conclusion in the previous section that with this data-strip, the cluster edge is reached. However, the ratio of dE to dIrr for the N-S strip is very different - there is no clear decline in the outer regions and within the errors, the ratio is approximately constant at $\sim$3. There does however appear to be a peak around 3°, corresponding to the positions of the background N and M clouds. This suggests our data is indeed contaminated by objects from the N and M clouds.

5.4.4 Galaxy colours

We saw with our earlier comparison of the numbers of objects per sq. degree in Virgo with the lower density UMa cluster and field, that there are many more dwarf galaxies in Virgo. The question that we would like to answer is, why? Are the large numbers of dwarfs detected by us in Virgo the predicted population from CDM theory or have they formed more recently in the cluster environment? To distinguish between the two possibilities we need to try and understand the nature of the galaxies in our sample. Our two Virgo datastrips cover very different parts of the cluster. The N-S strip overlaps two background clouds and the E-W strip samples only the main body of the cluster. Thus a comparison of the colours of the objects detected in the 2 strips may give us a clue as to their evolution and the effect of environment on their evolution.

B-I colours were calculated for the dEs and dIrrs in the 'sure' lists for the N-S and E-W data strips using the aperture photometry procedure described in Chapter 3. Errors in the colours using this procedure were typically ± 0.2 magnitudes, although they were slightly higher for the faint objects. A summary of the mean (B-I) colours for the different galaxy types in each strip is shown in Table 5.11. The mean colours for each object type in both strips are the same. There is no difference in colour between dEs and dIrrs or between objects in each strip. This suggests that within the Virgo cluster, any environmental effects work across the whole of the cluster and are not stronger or weaker at any one position within the cluster. This is also indicated by Fig 5.18 where we have plotted the (B-I) colours against increasing distance from the cluster centre for the 'sure' objects in both the N-S strip (left) and E-W strip (right). There does not appear to be any relation between colour and position in the cluster - the (B-I) range appears fairly

constant.

There does however appear to be a greater scatter in the N-S strip B-I colours compared to those in the E-W strip. We commented earlier that there is some contamination of the N-S Strip by the background clouds, as seen in the number density profile, and plot of the ratio of dEs to dIrrs. Thus the greater scatter in Fig. 5.18 could be another indication that the objects in the N-S strip are contaminated by fainter objects in the background clouds.

Data Strip	*Type*	*Mean (B-I)*	*Std dev.*
N-S	Sure dE	1.8	0.44
E-W	Sure dE	1.8	0.31
N-S	Sure dIrr	1.8	1.15
E-W	Sure dIrr	1.8	0.64
N-S	All Sure	1.8	0.72
E-W	All Sure	1.8	0.44

Table 5.11: Mean colours of objects in the N-S and E-W data strips

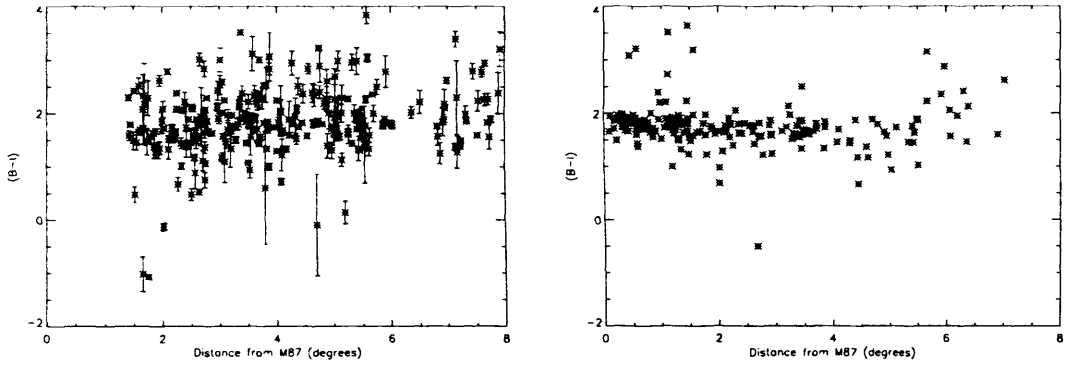

Figure 5.18: (B-I) colours with increasing distance from the cluster centre for the N-S strip (left) and E-W strip (right).

On average, the Virgo cluster objects, are redder than the mean (B-I) colours of the 4 MGS field objects detected within 21 Mpc. Their mean (B-I) was 1.2±0.3. Although within the Virgo cluster itself there is no difference in the stellar popu-

lations of galaxies at different positions in the cluster, environment *does* have an effect on the stellar populations of the galaxies with galaxies becoming redder in denser environments (as also found by Sabatini et al. 2005).

5.4.5 DGR

We mentioned at the start of this Chapter that the Virgo cluster is currently forming out of LG and small group analogues. A comparison of the DGRs of such groups with the Virgo cluster DGR will therefore give an indication of whether some dwarfs may have been created in the cluster environment.

As stated earlier in the chapter, we define the DGR as the number of dwarfs with -10$\geq M_B \geq$-14, divided by the number of galaxies with $M_B \leq$-19. The absolute magnitudes of the dwarfs in Virgo are derived by assuming a distance for all the dwarf galaxies of 16 Mpc (Jerjen et al., 2004). A point to note here is that we have an uncertainty in the distances of the dwarfs since we cannot be sure whether they are in the main part of the cluster (Subcluster A), or in the background clouds. For the giant galaxies at the back edge of the clouds, if we set a velocity criterion of v<2000kms^{-1} (Binggeli et al. 1987), and assume that the dwarfs and giants are in the same substructure, hopefully this will not affect our results too much. The data for the giant galaxies is taken from LEDA.

We calculated the DGR for the N-S and E-W strips using only the 'sure' detections and found a DGR of 22±7 for the N-S strip and 14±4 for the E-W strip. Thus, within the errors, there is no difference between the DGRs of the N-S and E-W strips.

We showed previously that the DGR of the field is far less than that obtained

for the Virgo cluster, at a value of no greater than 6. The issue now is where did the excess number of dwarfs come from in Virgo to increase the DGR by a factor of ~3? Were they created in the cluster environment? This is discussed further in Chapter 7 in relation to the predicted DGRs from CDM theory. In our final section presenting our Virgo cluster results we look at whether the dwarf galaxies detected in Virgo are associated with the giants or whether there is evidence of a cluster population of dwarf galaxies. The latter would suggest that some process in the cluster environment is forming these galaxies and they are not the primordial population predicted by CDM.

5.4.6 Association with bright galaxies

The positions of each 'sure' object detected in the Virgo N-S strip are plotted with crosses in Fig. 5.19. Also plotted are the positions of the giant galaxies in the strip; their tidal radii are shown by the ellipses. We take the tidal radius of the giant to be ~150 kpc (Sabatini et al. 2003), and assume that this is the maximum distance from the giant galaxy that a companion dwarf can be bound.

The giant galaxies in the N-S data strip consist of 3 ellipticals, 5 spirals and 3 lenticulars. We investigated whether there was a preference for the detected 'sure' objects to be associated with a certain giant galaxy type; the results are given in Table 5.12.

Approximately 60% of the 'sure' objects are at a projected distance less than or equal to the tidal radius of the giants. This is however, the *maximum* percentage of objects which could be associated with the giant galaxies, since these are only projected distances for the objects. This leaves a minimum of 40% of detections

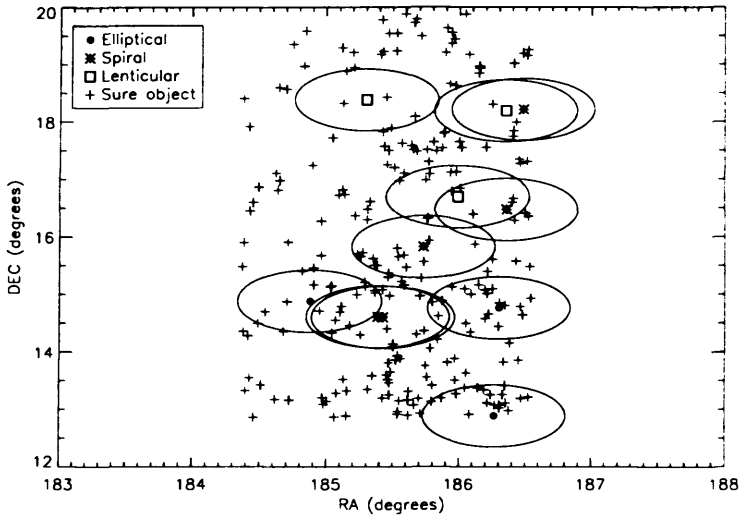

Figure 5.19: Positions of giant galaxies in relation to 'sure' detections (crosses) in the N-S strip. The ellipses indicate a radius of 150kpc - the approximate tidal radius of the giants in Virgo.

Giant galaxy type	*N° of objects within 150kpc radius*	*% objects within 150kpc radius*	*N° of objects per giant*
Elliptical	55	22	~18±4
Spiral	71	29	~14±4
Lenticular	22	9	~7±3

Table 5.12: The association of detected 'sure' objects with giant galaxies

which are not companions of the brighter galaxies - they are a 'cluster' population. The same percentage of unbound dwarfs was found by Sabatini et al. (2003) for the E-W strip. It seems clear that a significant fraction of the Virgo cluster dwarfs have been created in the cluster environment. The mechanisms for this are discussed in Chapter 7.

5.5 Summary

In this Chapter we have presented the results from our optical searches for LSB dwarf galaxies in 4 different environments of the Universe. The results for each region are summarised in Table 5.13 and are discussed in more detail in Chapter 7.

Region	*No/sq. deg*	*Mean DGR*	*Mean (B-I)*	*% dE*	*% dIrr*	*% Other*
MGS field	2; 2; 4	6 (max)	1.2 ± 0.3	24%	33%	43%
M101 ($9'' \leq \alpha \leq 27''$)	~0.1	1	-	100%	-	-
M101 ($4'' \leq \alpha \leq 9''$)	3; 1; 4	-	-	40%	38%	22%
UMa	~4	-	-	33%	17%	50%
Virgo N-S Strip	16; 6; 22	22 ± 7	1.8 ± 0.7	54%	22%	24%
Virgo E-W Strip	15; 2; 17	14 ± 4	1.8 ± 0.4	62%	26%	12%

Table 5.13: Summary of optical results from surveys of the MGS field, M101 region, UMa cluster and Virgo cluster. The numbers of objects per sq. degree are given as 'sure'; 'unsure'; 'all'. The remaining columns are for the 'sure' objects only, with the exception of the MGS field mean (B-I) value which is that for the 4 objects within 21 Mpc.

We have defined the background counts for our data fields by analysing the MGS field data. We assume that the background objects are those which we classified as 'unsure' detections. Their number density in the field is ~2 per sq. deg.

The mean (B-I) colour of the 4 objects found in the field within 21 Mpc is bluer than those of the 2 cluster data strips, suggesting that star formation is more recent in these objects than in Virgo. Further evidence to support this is presented in the next chapter with the presentation of the HI content of field and cluster dwarfs. From a comparison of the types of objects found in the field and Virgo, it appears that the cluster environment is predominantly populated with dE galaxies, whereas in the field, dIrr galaxies dominate.

One possible companion of M101 was found using the selection criteria adjusted for objects at the distance of M101. If the MW were placed at the distance of M101 however, we would not expect to detect any companions with our selection criteria.

It is evident from the numbers of objects per sq. degree in each environment that there are many more dwarf galaxies in the Virgo cluster compared to the other environments of the Universe. The UMa cluster, general field and area around M101 have comparable numbers of dwarfs per sq. deg. The Virgo Cluster also has a higher number of dwarfs in relation to giant galaxies compared to the other regions. This is interesting since as explained in Chapter 2, the Virgo cluster is supposedly assembling itself out of discrete units like the MW and M101 which have DGR values much lower than the cluster itself. The question of where these 'extra' dwarf galaxies come from is discussed in Chapter 7.

Chapter 6

Results - HI

In the previous chapter we described the results from our optical search for LSB dwarf galaxies in 4 different environments. In this chapter we present our HI results for 2 of these environments - the MGS field and the UMa cluster. We have pointed HI observations of 58 objects from our MGS field data - 33 from the 'sure' list of optical detections and 25 from the 'unsure' list. There were two main objectives for investigating the HI properties of the optical detections from the field. First, as we described in the previous Chapter, we had optical velocities for a small number of the field objects and wished to determine distances to the remaining objects. For a proper comparison of field dwarf galaxies with Virgo cluster dwarf galaxies we had to restrict our analysis to field objects within 21 Mpc. Thus HI velocities would enable us to verify which field objects could be excluded from our comparison. Our second motivation in observing the MGS field objects at 21cm was to investigate how the environment affects the gas content of the objects in the field compared to the cluster. Pointed HI observations of dwarf galaxies in the Virgo cluster have already been taken using Arecibo by Sabatini et al. (2005). These galaxies were

detected using the same selection criteria on data obtained in an identical way (instrument, exposure time etc) as for our MGS field data. Thus, by comparing the results of the HI observations in these 2 contrasting regions, we can see how the environment may play a part in the evolution of these galaxies.

Our UMa cluster HI data consisted of an 8° × 8° HIJASS data cube covering a region which overlaps our optical data fields. However, we would not expect to detect the optically detected galaxies in our HI survey. The HI detection limit for the UMa data was $M_{HI} \geq 2 \times 10^8 M_\odot$, thus for an object to be detected in both surveys it would be an extraordinary object with $M_{HI}/L_B > 138$ for the faintest dwarf (M_B=-10). With this data therefore we looked for HI detections with no optical counterparts (dark galaxies). We described in Chapter 1 the apparent discrepancy between predicted numbers of low mass DM haloes in low density environments compared with observations of dwarf galaxies. A possible explanation for this discrepancy is that the low mass DM haloes exist but SF has been suppressed in them, so the haloes themselves are not visible as dwarf galaxies. A search at 21 cm should uncover these objects if they exist and if they contain sufficient gas to be detected within the limits of the survey. With the UMa data we can also investigate the environmental effects of the cluster environment on the gas content of galaxies by comparing the HI properties of galaxies in UMa to those in the higher density Virgo cluster. A comparison of the results from our HI survey to those from Davies et al.'s (2001) blind HI survey of the Virgo cluster may help us to understand why, in our optical search, we find many more dwarf galaxies in the Virgo cluster compared to the less dense UMa cluster.

6.1 MGS

In the previous Chapter we presented the results from our optical search for LSB dwarf galaxies in 30 sq. deg of the MGS field. In total, 110 objects were found, 51 of which were classified as 'sure' objects, and 59 as 'unsure'. During observing runs in May 2003 and January 2004, we obtained pointed HI observations using the Arecibo 305m radio telescope of 58 of these objects; 33 from the 'sure' list and 25 from the 'unsure' list. The HI parameters of this sample are given in Tables 5.1 and 5.2 of Chapter 5. In the comments column, 'NO' refers to those objects not observed at 21cm; those observed but not detected at 21cm are labelled 'ND'. For a 4σ detection with velocity width of 50kms^{-1}, we would expect to detect objects with $M_{HI} \geq 2.83 \times 10^4 d^2 M_{\odot}$ where d is the distance to the object in Mpc.

6.1.1 HI detection efficiency

Of the 33 objects observed from the 'sure' list, 16 (48%) were detected at 21cm. From the 'unsure' list, 2 of the 25 (8%) objects observed were detected at 21 cm, and one of these was only a marginal detection which needs further observations. We described in the previous Chapter that we consider the 'unsure' detections to be predominantly background objects and not nearby dIrrs - the lack of HI detections from the 'unsure' list of objects supports this. We would expect most nearby dIrrs to be gas-rich and therefore detectable in HI. A detection efficiency of 8% however shows that this is not the case for the 'unsure' objects - they are more likely to be background groups of objects than nearby dIrrs.

The detection efficiency for the MGS field 'sure' objects was much higher than that of the Virgo cluster survey (Sabatini et al. 2005). In their HI study

of the Virgo cluster dwarf galaxies, Sabatini et al. looked at 103 of their optical detections, 89 from the 'sure' list and 14 from the 'unsure' list. They detected 5 objects in total, all from the 'sure' list. This gives a HI detection efficiency of ~6%. Thus the objects in the field are generally much more gas-rich than those in the Virgo cluster. This could be due to two reasons - it could be that SF is enhanced in the cluster environment compared to the field or that Virgo cluster galaxies are subject to tidal stripping in the cluster. Enhanced SF in cluster galaxies could result from tidal interactions which are prevalent in the cluster environment but far less common in the field. So more of the HI gas would be converted to stars, making Virgo cluster galaxies gas-poor. Tidal stripping in the cluster environment via encounters with other galaxies and the cluster potential itself, could remove HI gas from Virgo cluster galaxies. If this is the case then we would expect to detect more HI in field objects since in lower density environments, such encounters with other galaxies are rare. We discuss this further in the following Chapter.

6.1.2 Field Objects within 21 Mpc

In order to compare similar galaxies in both the field and the Virgo cluster, we must restrict our field object analysis to those within 21Mpc. Of the 16 'sure' objects detected at 21cm, only 4 were found to lie within this distance. The remaining 12 were further away (assuming purely Hubble flow, ignoring peculiar motions and using H_0=75kms^{-1}Mpc^{-1}, a velocity of ~1575kms^{-1}, corresponds to a distance of ~21 Mpc). These objects must therefore be background gas-rich LSB galaxies. Our simulation of a background Universe, described in Chapter 4, predicted that 45% of the objects detected with our selection criteria, should lie within 21 Mpc. So, ~23 of our 'sure' detections should lie within this distance. If we consider

the 18 objects from the 'sure' list which we did not observe at 21cm to lie within 21Mpc, and include the 4 whose HI velocities confirm they lie within 21 Mpc, then our model predictions and our observations are consistent.

Although, as discussed in the previous Chapter, we consider the 'unsure' MGS field objects to be largely background groups of objects, there was one marginal HI detection from this list (Object 48 from Table 6.2) which placed the object within 21Mpc. However, this needs additional HI observations before the validity of this detection can be confirmed.

We describe the objects detected within 21Mpc in more detail below and give an estimate of their HI mass to light ratios, M_{HI}/L_B. This parameter tells us about the relative efficiency of converting the galaxy's neutral gas into stars. A large M_{HI}/L_B value implies that either the galaxy is very young and has not had time to convert its gas into stars, or that the SF process itself is very inefficient for some reason, perhaps due to the galaxy's environment. Here we assume that a typical gas-rich dwarf galaxy ($M_{HI}\sim10^{8.5}M_\odot$ and M_B=-16) will have M_{HI}/L_B of $\sim$1. The L_B value was calculated using the equation,

$$L_B/L_\odot = 2.512^{(M_\odot - M_B)} \tag{6.1}$$

where $M_\odot$=5.4 (Banks et al. 1999).

The 4 objects from the 'sure' list within 21 Mpc are shown in Fig. 6.1 with their corresponding spectra.

- **Objects 12 and 13** - these two objects from the 'sure' list are separate optical sources but fall within the same Arecibo beam. We assume by their close association on the sky and their appearance, that they are both at the

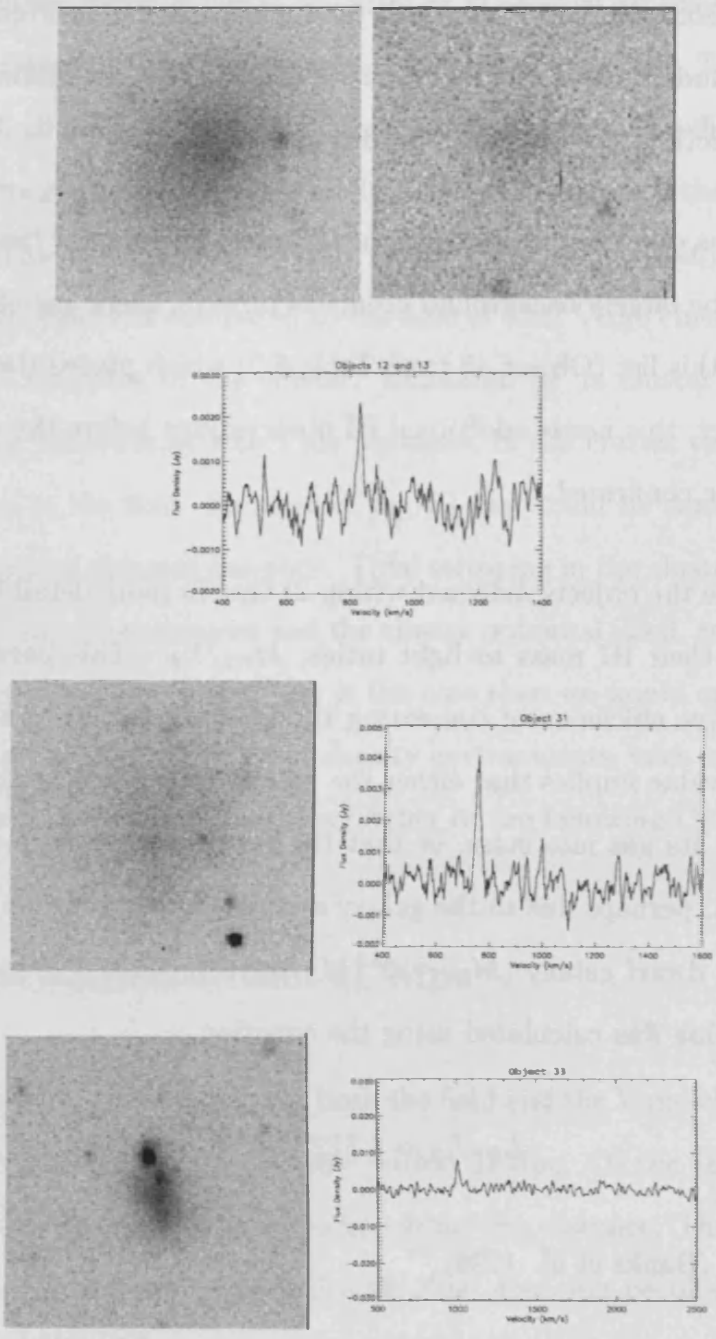

Figure 6.1: The four objects and their spectra from the MGS detected within 21 Mpc. From top to bottom, they are Objects 12, 13, 31, 33.

distance indicated by the 21cm velocity of 835 kms^{-1}. Object 12 also has an optical redshift coincident with the HI detection. We assume that the HI

detected in the Arecibo beam is associated predominantly with the brighter object (12). It has the appearance of a dwarf spheroidal galaxy and a very small HI mass that is only detected because of its narrow (V_{50}~25kms^{-1}) velocity width. With a HI mass of ~$1.6\times10^6 M_\odot$ and $M_B = -13.3$, compared to a typical gas-rich dwarf galaxy, it has a very low $M_{HI}/L_B = 0.05$. It also has the bluest colour of all the 4 objects detected within 21 Mpc, with (B-I)=0.83±0.05, so it appears that recent SF has been very efficient at converting the galaxy's neutral gas into stars. Object 13 is a somewhat fainter dSph with $M_B = -10.0$. Since both these objects are classified as dSphs but have an HI detection, this makes them interesting objects as generally, dSph type galaxies are considered to be gas-poor. As noted in the previous chapter, these two objects are most certainly associated with the giant galaxy, NGC 3521. There is the possibility, therefore, that the HI gas detected at the position of these 2 dwarfs could be due to this giant galaxy. The extent of the giant galaxy's HI radius is assumed to be 2.4 times that of the optical radius (Davies et al. 2001), which is ~12′. The dwarfs however are situated ~18′ from NGC 3521, so it is unlikely that the HI detection is from NGC 3521. HI mapping of this giant galaxy would be required to distinguish between them. This giant galaxy may be responsible for enhancing recent SF in these 2 dwarf galaxies via tidal interactions, resulting in their blue colour and their relatively low HI mass.

- **Object 31** - this is another dSph galaxy with a HI detection. It has a low M_{HI}~$2\times10^6 M_\odot$. It has $M_B = -12.4$ and $M_{HI}/L_B = 0.15$ and its small amount of atomic hydrogen is detected at v=754kms^{-1} because of the small velocity width (V_{50}~24 kms^{-1}). From the 4 objects detected within 21 Mpc, this galaxy had the reddest (B-I) colour of 1.6±0.09.

- **Object 33** - this object has much more of an irregular appearance than the other 3 objects detected in HI within 21Mpc, and, as might be expected for a dIrr, has a higher HI gas content. With a $M_{HI}\sim 1\times10^7 M_\odot$, and $M_B = -12.4$, it has a $M_{HI}/L_B = 0.8$, which is typically what you would expect for a gas-rich dwarf galaxy. It has a velocity width, $V_{50}\sim$98kms^{-1} and has a recessional velocity, v$\sim$1018 kms^{-1}.

In addition to these 4 'sure' objects detected in HI, there was also one object from Table 5.2 (Object 48), which was considered to be a marginal HI detection with a 4σ peak at v_{HI} = 940 km s^{-1}. Its measured velocity width was 28kms^{-1}, and had a calculated $M_{HI}\sim 2\times10^6 M_\odot$. This object is shown in Fig. 6.2, with its HI spectra. Further HI observations are needed to verify this as a HI detection.

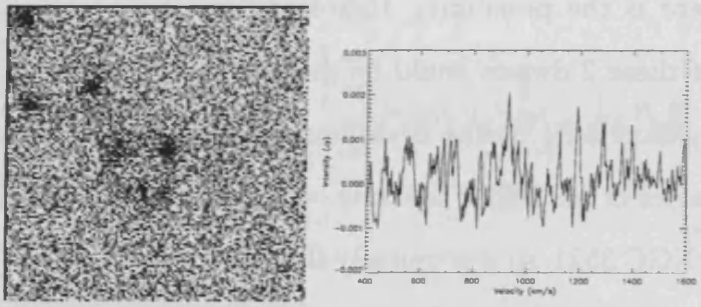

Figure 6.2: Image and HI spectra for the marginal HI detection from the 'unsure' list (Object 48).

6.1.3 Field Objects beyond 21 Mpc

We detected 14 objects at 21cm in the MGS field data which lie beyond 21Mpc and are nearly all dwarf galaxies ($M_B\geq$-16), with the exception of 2 which have $M_B\sim$-17. This suggests they are all gas-rich LSB galaxies since they were detected in both our optical survey and with our pointed HI observations. The majority of

the objects also have large M_{HI}/L_B, implying that these galaxies are either very young or they have been inefficient at converting their gas into stars. The mean M_{HI}/L_B value for these objects is 2.61±1.34, which is much higher than that of the 4 objects within 21 Mpc, which was 0.33±0.41, and higher than the typical value for a gas-rich dwarf galaxy. However, this is not too surprising since we would not expect to detect objects with low masses of HI at large distances as they would fall below our detection limit.

Below we describe the HI and optical properties of each galaxy detected in HI beyond 21 Mpc. The B band image of each object is shown in Fig. 6.3 with its corresponding HI spectra.

- **Object 4** This galaxy has a morphology which cannot be clearly identified from the B band image, and was therefore classified as a 'sure' detection with an unclear morphology. It was detected in HI at 7323kms^{-1}. With a HI mass of $\sim$7.9×10$^8 M_\odot$ and M_B=-15.55, this dwarf galaxy has M_{HI}/L_B=3.31, which is higher than that of a typical gas-rich dwarf galaxy, suggesting that SF has been inefficient in this galaxy.

- **Object 6** This dwarf galaxy has an irregular appearance on the B band image, with a diffuse cloud enveloping several central bright regions. It was detected at 5642kms^{-1} and has M_{HI}=5.0×10$^8 M_\odot$. With an absolute magnitude, M_B of -15.33, this galaxy has a high M_{HI}/L_B of 2.67.

- **Object 10** This dwarf galaxy is classed as having an irregular morphology. The B band images shows a bright central region with a diffuse extended tail. With a HI detection at 1772kms^{-1}, it lies just beyond 21 Mpc. It has M_{HI}=1.3×10$^8 M_\odot$ and M_B=-13.67, giving it a large mass to light ratio, M_{HI}/L_B=2.97.

- **Object 19** This galaxy appears to have two central bright regions with possible faint spiral arms extending from each. This galaxy was detected at 11,901kms^{-1} so is the furthest LSB galaxy detected by our HI observations. With a M_B=-17.20 and M_{HI}=3.2×10$^9 M_\odot$, again it has a large M_{HI}/L_B of 2.87.

- **Object 21** This galaxy appears on the B band image to be an irregularly shaped diffuse cloud. It was detected at 7791kms^{-1} and has M_B=-15.88. With a M_{HI} of 1.3×10$^9 M_\odot$, it has one of the highest M_{HI}/L_B values of all our galaxies detected at 21cm, with M_{HI}/L_B=3.86, suggesting that star formation has been extremely inefficient in this diffuse object.

- **Object 26** This object, also classified as a dIrr appears to have a number of HII regions with a faint diffuse cloud extending outwards from the galaxy. It was detected at 6224kms^{-1} and has M_B=-15.50. With a M_{HI} of 4.0×10$^8 M_\odot$, it has M_{HI}/L_B=1.74.

- **Object 27** This spiral galaxy was detected at 7509kms^{-1} and is the brightest object in our HI sample beyond 21 Mpc, with a M_B=-17.60. It is also one of the higher SB objects with μ_0~23.7 Bμ. Its M_{HI} is 1×10$^9 M_\odot$, giving a relatively low M_{HI}/L_B of 0.63.

- **Object 28** This diffuse dwarf irregular galaxy was detected just beyond 21 Mpc at a velocity, v ~2062kms^{-1}. It has a relatively high SB of μ_0~23.4 Bμ and has M_B=-15.50. With a M_{HI} of 4.0×10$^8 M_\odot$, it has M_{HI}/L_B of 1.74. This galaxy was also identified in NED as an irregular galaxy, KDG 118, with an optical velocity of 4642kms^{-1}.

- **Object 34** This dwarf galaxy was the faintest HI detection from our 'sure' list beyond 21Mpc, with a central surface brightness, μ_0~26.0 Bμ and M_B=-

11.47. It is not clear from the B band image what the morphology of this galaxy is, hence its classification as 'unclear'. This galaxy was detected at 2340kms^{-1} and has a M_{HI}=7.9×10$^6 M_\odot$. Its calculated M_{HI}/L_B is not much higher than that of a typical gas-rich dwarf, with a value of 1.42.

- **Object 42** This LSB (μ_0~25.5 Bμ) dIrr galaxy appears on the B band image to be a rather narrow and elongated object. It was detected at 3728kms^{-1} and has M_B=-12.98. With a M_{HI} of 1.3×10$^8 M_\odot$, this galaxy has the largest mass to light ratio of this sample, with M_{HI}/L_B=5.58. This galaxy also has the reddest (B-I) colour of all the objects observed in HI beyond 21 Mpc, with a value of 3.1±0.1. Since this galaxy is obviously gas-rich, it must still be forming stars, thus its red colour cannot be attributed solely to a primarily old stellar population. The other factor to consider is the metallicity of the galaxy, but NIR colours are needed to comment further on this.

- **Object 43** This dwarf galaxy was classified as having an unsure morphology as it is not clear from the B band image whether it is spheroidal or irregular. It has a bright spheroidal centre, but there also appears to be a very faint, diffuse tail extending from the lower part of the galaxy. This object was detected at 7335kms^{-1} and has M_B=-15.75. With a M_{HI} of 6.3×10$^8 M_\odot$, this galaxy has M_{HI}/L_B=2.18.

- **Object 47** This dwarf galaxy was classified as a spheroidal as the B band image shows a diffuse spheroidal object with a bright region offset from the centre. Detected at a velocity of 1610kms^{-1}, it is only just beyond our distance limit of 21Mpc. Identified in NED as an APMUKS spheroidal galaxy, its optical velocity of 1574kms^{-1} actually places it just inside 21 Mpc. With a M_B of -13.56 and M_{HI} of 2.5×10$^7 M_\odot$, it has a low mass to light ratio, M_{HI}/L_B, of 0.65.

- **Object 51** This irregular galaxy appears to have a diffuse cloud surrounding an extended bright central region. It was detected at 1859kms^{-1} and has M_B=-14.37. With a M_{HI} of 2.5×10$^8 M_\odot$ it has M_{HI}/L_B=3.10, which was among the largest HI mass to light ratios calculated for the objects detected in HI beyond 21 Mpc.

- **Object 41 ('unsure' list)** This clumpy looking object was detected in HI at 5127kms^{-1} and has M_B=-14.16. Of all the objects detected at 21cm, this has the lowest surface brightness, with μ_0~26.3 Bμ. With a M_{HI} of 2.5×10$^8 M_\odot$ it has a high HI mass to light ratio of M_{HI}/L_B=3.75, indicating that the conversion of gas into stars in this object, has been very inefficient. As an 'unsure' detection this object would have been considered as a background group of objects based on the optical data alone. However, its HI detection has shown it to be a relatively nearby dIrr galaxy.

6.1.4 Non-detections

From the 58 MGS objects observed at 21cm, 18 were detected giving an overall HI detection efficiency of 31%. Our detection limit for the MGS objects was $M_{HI} \geq 2.83\times10^4 d^2 M_\odot$ thus, the non-detection of HI in 40 of the observed objects implies either that they contain masses of HI less than this limit, or that they are background objects at velocities greater than the upper velocity range of our data.

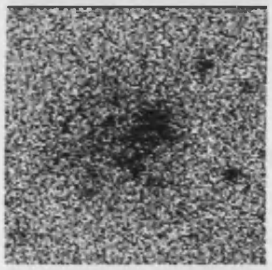

(a) Object 4 - unclear

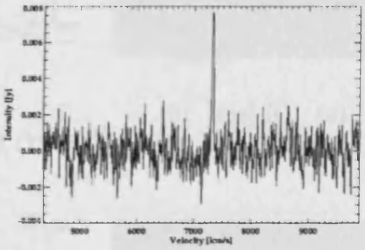

(b) Object 4 v=7323kms^{-1}

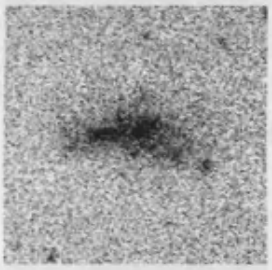

(c) Object 6 - Irr

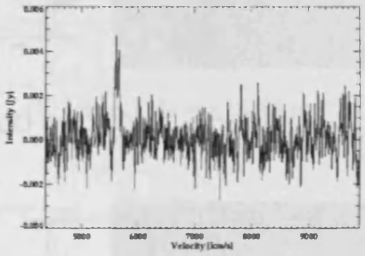

(d) Object 6 v=5642kms^{-1}

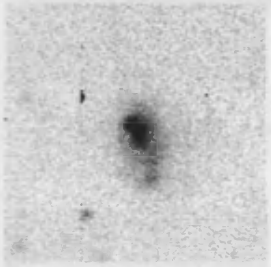

(e) Object 10 - Irr

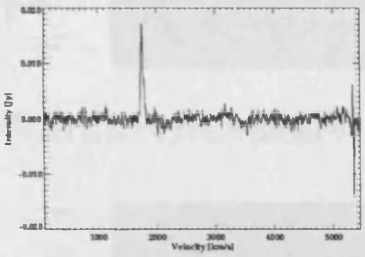

(f) Object 10 v=1772kms^{-1}

Figure 6.3: The 14 objects detected beyond 21 Mpc in the MGS with their corresponding HI spectra.

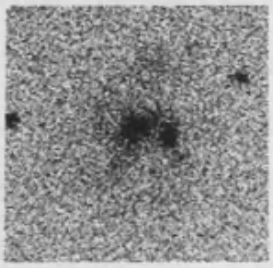

(a) Object 19 - Spiral

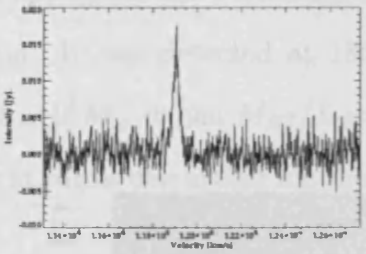

(b) Object 19 v=11,901kms^{-1}

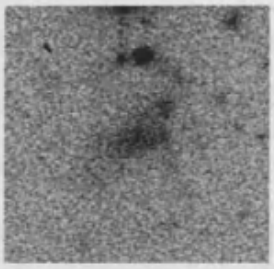

(c) Object 21 - Irr

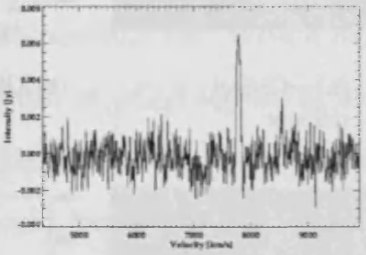

(d) Object 21 v=7791kms^{-1}

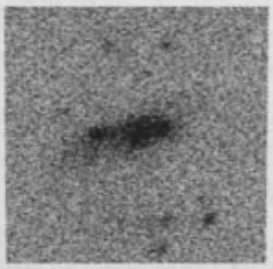

(e) Object 26 - Irr

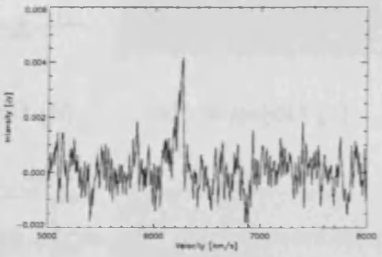

(f) Object 26 v=6224kms^{-1}

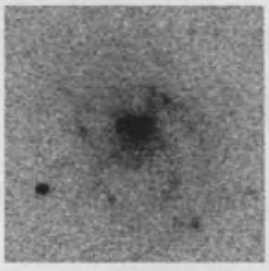

(g) Object 27 - Spiral

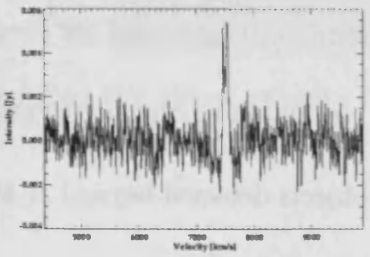

(h) Object 27 v=7509kms^{-1}

Figure 6.3: continued from previous page....

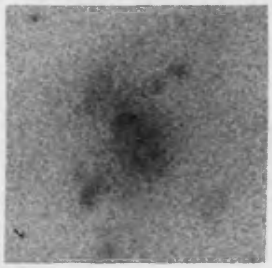

(i) Object 28 - Irr

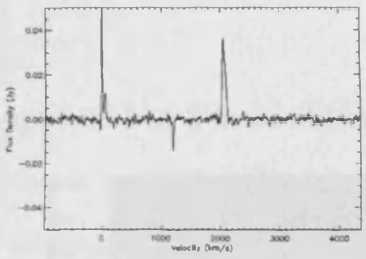

(j) Object 28 v=2062kms^{-1}

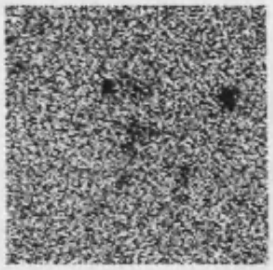

(k) Object 34 - unclear

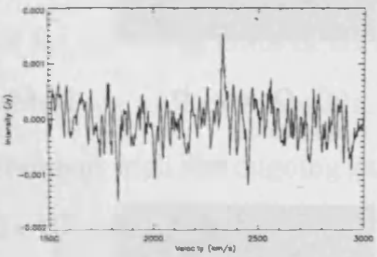

(l) Object 34 v=2340kms^{-1}

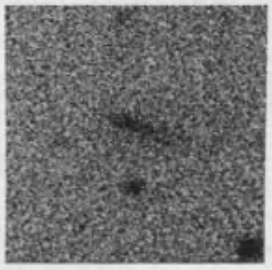

(m) Object 42 - Irr

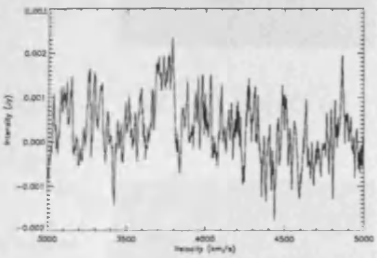

(n) Object 42 v=3728kms^{-1}

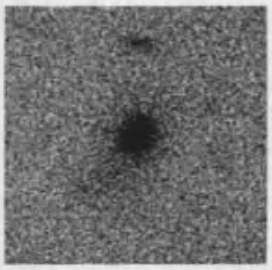

(o) Object 43 - unsure

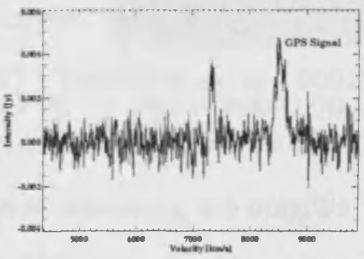

(p) Object 43 v=7335kms^{-1}

Figure 6.3: continued from previous page....

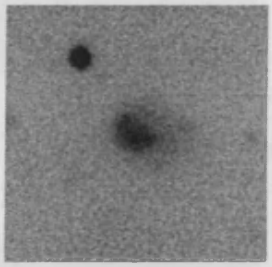

(q) Object 47 - Spheroidal

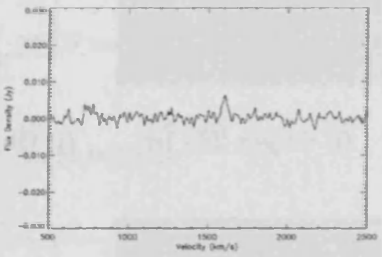

(r) Object 47 v=1610kms^{-1}

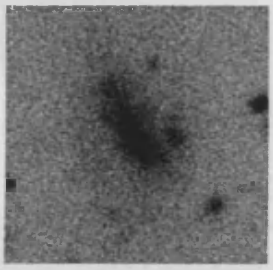

(s) Object 51 - Irr

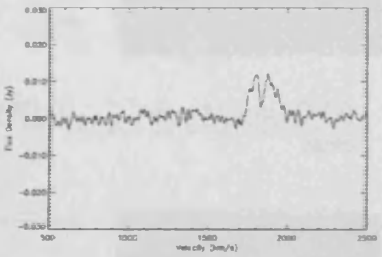

(t) Object 51 v=1859kms^{-1}

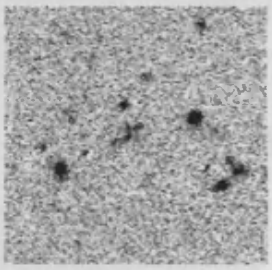

(u) Object 41 'unsure' detection

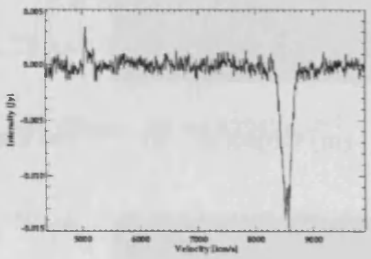

(v) Object 41 v=5127kms^{-1}

Figure 6.3: continued from previous page....

6.2 UMa cluster

As explained at the start of this Chapter, we had 2 main objectives for our UMa HI data cube. The first was to carry out a search for HI objects with no optical counterparts, as these could be the 'missing' low mass DM haloes predicted by CDM. We present our results from our blind HI survey of the UMa data cube in the following section. Our HI mass limit for detecting galaxies in UMa was $M_{HI} \geq 2 \times 10^8 M_\odot$. The second objective for surveying UMa in HI was to investigate the issue of the effect of the environment on galaxy evolution. Since the UMa cluster is a relatively low density environment with few ongoing galaxy interactions, it would be interesting to compare the HI properties of galaxies in this cluster to those detected in the Virgo cluster where there is vigorous galaxy interaction. Thus in Section 6.2.5 we compare our UMa HI results with the results of a similar HI survey carried out by Davies et al. (2001) in the Virgo cluster.

6.2.1 HI detections in UMa

Initially we inspected the HI data cube by eye to find possible dark galaxies in the velocity range of the UMa cluster. We used the velocity range defined by Tully et al. (1996), of $628 < V_{helio} < 1138$ kms^{-1} to define the extent of the cluster, centered upon ($11^h59^m28.3^s$;49°05′18″) (Trentham et al., 2001). An automated galaxy finder, *Polyfind*, was then applied to the data. Finally, the cube was also checked by eye by a second person, thus ensuring all possible HI sources in the above velocity range, with $M_{HI} \geq 2 \times 10^8 M_\odot$ were found.

In total, we found 32 detections of HI in the UMa cluster. Of these, 13 were detected by eye alone and 19 by both eye and with *Polyfind*. We discuss the objects

missed by *Polyfind* later. The independent by eye search found 31 detections with no additional objects which had been missed either in the first search by eye or by the *Polyfind* algorithm.

The HI properties of all 32 objects detected in UMa are given in Table 6.1, and their HI spectra are shown in Fig. 6.5. Objects 1-19 are those which were detected in both the by eye search and by the *Polyfind* routine. Objects 20-32 are those which were found by eye but missed by *Polyfind*. The HI parameters of each object are given in Columns 4-10 of Table 6.1; the properties of their probable optical counterpart, as given in NED, are given in columns 11-14. Since our first aim with this data-set was to search for dark galaxies, we searched NED in order to see if the objects detected in HI had optical counterparts. All 32 detections were found to have optical counterparts within 6′ and 100kms^{-1} in velocity, thus we found no candidates for dark galaxies in the UMa cluster. The detections consisted of two Im classified galaxies, 3 Sm type galaxies (morphologically classified by de Vaucouleurs (1991) as between spiral and irregular type galaxies) and 27 spiral galaxies.

Although we found no dark galaxy candidates in our blind HI search of the UMa cluster, we should not be too surprised at this result since our detection limit for this survey was quite high, at $M_{HI} \geq 2 \times 10^8 M_{\odot}$. A deeper search of UMa is needed to probe lower masses if we wish to unearth any possible galaxies which may be associated with the low mass DM haloes predicted by CDM theory.

Below we discuss the galaxies that we *did* detect at 21cm in UMa, as well as those galaxies which we might have expected to detect in our HI data, but with our by eye and *Polyfind* searches, we failed to find. Following this, in Section 6.2.5, we compare the properties of our HI detected galaxies in UMa with those detected

in a similar survey of the denser Virgo cluster.

HI mass to light ratios

A typical spiral galaxy, similar to the Milky Way (M_B~-20), containing ~$10^{10} M_\odot$ of HI (Zwaan et al. 1997), would have a M_{HI}/L_B ~0.7. The mean value of M_{HI}/L_B for our UMa galaxies is 0.7±0.9, which agrees well with this estimate, thus we are detecting MW type galaxies in our HI survey. There are however, exceptions. One of the detected galaxies, classified as an irregular galaxy (Object 7), also has M_B~-14.9, making it a dIrr in the UMa cluster. We stated earlier that a typical gas-rich dwarf galaxy has M_{HI}/L_B ~1, but this object has a M_{HI}/L_B ~ 4.3, making it either a very young object or very inefficient at forming stars. Since dwarf galaxies are considered to be the building blocks of giant galaxies in the hierarchical structure formation scenario, we assume that this galaxy is not younger than the other giant galaxies detected within the cluster. It is however located in a low density cluster and it will therefore not have been subject to many interactions. Perhaps SF was not triggered in this object until more recently so it has not had time to convert a large fraction of its HI gas into stars, resulting in its large M_{HI}/L_B.

Spatial distribution of gas-rich galaxies

The positions of each galaxy detected in the HI data cube are plotted in Fig. 6.4 (* symbols). The labelled UGC galaxies, plotted with diamonds, are those which were not detected at 21cm and are discussed in the next section. Also plotted in Fig. 6.4 is the extent of the data cube (rectangular region) and the extent of the cluster, as outlined by the ellipse.

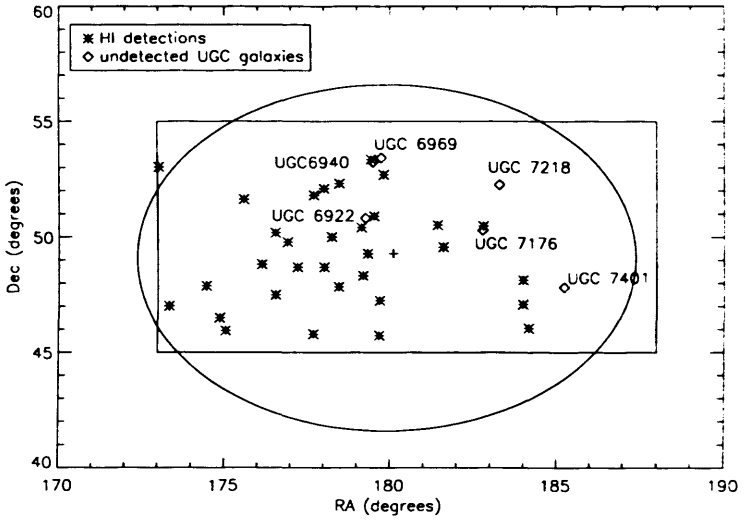

Figure 6.4: Positions of HI detections marked as stars, in the HI data cube region (shown as rectangle). Also plotted as an ellipse is the area covered by the UMa cluster (as defined earlier), and the positions of the UGC galaxies which were not detected in HI. These are discussed in the text.

ID	RA	*DEC*	S_{int}	S_{peak}	*rms*	*Vel*	W_{50}	W_{20}	M_{HI}	*Probable optical*	*Opt. posn.*	*Opt. vel. offset*	M_B	M_{HI}/L_B
	(J2000)	(J2000)	(Jy kms^{-1})	(mJy)	(mJy)	(kms^{-1})	(kms^{-1})	(kms^{-1})	$M_\odot$	*association*	*offset (')*	(kms^{-1})		$M_\odot/L_\odot$
1	12:11:02.10	50:28:27.41	98.230	382	11.1	766.230			7.67×10^9	NGC 4157	0.7	+7.77	-20.72[2]	0.27
2	12:06:12.12	49:33:58.80	40.726	172	14.2	1075.242	371.396	391.298	3.18×10^9	NGC 4100	1.2	-1.242	-20.51[2]	0.14
3	12:05:30.73	50:31:12.77	102.310	359	8.7	752.870	335.944	366.223	7.98×10^9	NGC 4088	1.3	+4.13	-20.95[2]	0.23
4	11:59:04.86	52:42:00.02	31.831	237	13.5	1084.102	174.233	191.778	2.48×10^9	UGC 06983	0.7	-2.102	-18.58 [2]	0.63
5	11:57:55.69	50:54:12.37	9.222	169	10.9	925.873	53.227	72.097	7.197×10^8	UGC 06956	4.8	-8.873	-15.98[3]	2.0
6	11:58:38.13	47:14:54.32	33.831	149	9.3	890.719	259.648	278.178	2.64×10^9	NGC 4010	0.8	+5.251	-19.30[2]	0.35
7	11:58:37.93	45:43:55.85	7.272	157	15.3	1136.183	41.359	64.667	5.68×10^8	UGCA259	2.7	+17.817	-14.89[3]	4.34
8	11:57:09.15	49:16:46.60	43.608	400	15.1	777.526			3.4×10^9	UGC 06930	1.4	?	-18.86[2]	0.67
9	11:56:35.48	48:19:32.99	13.228	148	8.8	952.616	90.010	206.004	1×10^9	NGC 3985	1.2	-4.616	-17.92[3]	0.47
10	11:53:44.10	52:18:54.44	39.813	169	9.3	1033.650	402.473	425.244	3.11×10^9	NGC 3953	1.0	+18.35	-21.05[2]	0.08
11	11:53:40.14	47:51:14.40	38.951	197	8.4	799.242	253.656	291.394	3.04×10^9	NGC 3949	0.4	+0.758	-20.22[2]	0.17
12	11:51:55.92	48:42:17.79	5.965	93	7.4	975.444	65.114	101.313	4.66×10^8	NGC 3928	1.9	+12.556	-17.71[3]	0.27
13	11:48:42.88	48:41:43.58	80.012	337	9.2	965.515	259.996	302.285	6.24×10^9	NGC 3893	1.2	+1.485	-20.55[2]	0.26
14	11:44:24.98	48:49:20.31	13.782	186	9.9	898.018	86.148	106.348	1.08×10^9	UGC 06713	0.8	+0.982	-16.12[3]	2.66
15	11:40:05.51	45:56:29.04	23.258	588	12.0	847.226	39.490	56.861	1.82×10^9	UGC 06628	0.2	+1.774	-17.81[3]	0.95
16	11:39:21.67	46:30:09.00	28.148	328	14.3	724.316	87.481	127.345	2.20×10^9	NGC 3782	0.7	+14.684	-17.83[3]	1.12
17	11:37:43.88	47:53:17.25	49.188	302	7.8	742.342	220.427	260.092	3.84×10^9	NGC 3769/ Arp280 G Pair NGC 3769A	0.3 / 0.6/ 1.3	-5.342/ +5.658/ +18.658	-19.32[2] - -16.64	- - -
18	11:32:05.90	53:02:00.66	132.741	403	23.7	996.911	465.592	484.278	1.04×10^{10}	NGC 3718	4.8	-3.911	-20.06 [3]	0.68
19	11:33:17.50	47:00:56.14	79.764	436	19.0	853.461	258.358	283.752	6.22×10^9	NGC 3726	1.0	+12.539	-20.76[2]	0.21
20	12:16:34.18	46:02:29.82	4.533	68	15.1	752.821	132.318	170.755	3.54×10^8	UGC07301	2.7	-40.821	-16.25[3]	0.77
21	12:15:48.53	47:04:43.98	29.747	116	14.5	1034.676	383.079	409.346	2.32×10^9	NGC 4217	0.9	-7.676	-20.33 [2]	0.12
22	11:57:33.77	53:21:22.12	66.880	283	10.4	1057.036	455.370	478.414	5.26×10^9	M109	1.2	-10.786	-20.31[3]	0.27
23	11:56:23.68	50:24:35.65	21.789	163	9.3	916.198	182.179	204.172	1.7×10^9	UGC 06917	1.4	-5.198	-18.63[2]	0.41
24	11:52:49.74	50:00:14.24	5.691	94	9.1	990.769	77.735	104.393	4.44×10^8	UGC 06849	2.6	+4.231	-16.19 [3]	1.03
25	11:51:53.87	52:05:47.50	15.381	137	13.0	1011.045	136.008	156.798	1.22×10^9	UGC 06840	2.1	+34.955	-16.61 [3]	1.91
26	11:50:41.94	51:48:31.09	20.315	133	9.9	941.018	273.343	286.929	1.59×10^9	NGC3917	1.1	+23.982	-19.65 [2]	0.15
27	11:50:41.65	45:47:23.05	10.704	113	12.4	794.536	137.269	155.216	8.35×10^8	UGC 06818	1.3	+13.464	-17.30 [3]	0.69
28	11:47:30.72	49:46:49.12	3.062	58	10.3	932.564	84.362	94.349	2.39×10^8	UGC 06773	5.1	-8.564	-16.78 [3]	0.32
29	11:46:02.69	50:10:51.34	5.518	70	13.3	751.399	83.235	175.050	4.31×10^8	NGC 3870	1.5	+4.601	-17.28 [3]	0.36
30	11:46:03.61	47:29:46.25	19.367	103	9.1	885.605	340.650	365.972	1.51×10^9	NGC 3877	0.7	+9.395	-20.60 [2]	0.06
31	11:42:15.00	51:37:25.73	8.510	62	11.7	995.406	179.773	310.012	6.64×10^8	UGC 06667	2.3	-22.406	-17.83[2]	0.34
32	12:15:49.47	48:08:14.87	6.048	69	13.0	713.886	130.297	155.332	4.72×10^8	NGC 4218	0.6	+16.114	-17.45 [3]	0.34

Table 6.1: Table of objects detected by both eye and *polyfind* (Objects 1-19) in the UMa HI data cube and by eye only (Objects 20-32)

[2] M_B values taken from Verheijen et al. 2001

[3] M_B values taken from Tully et al. 1996

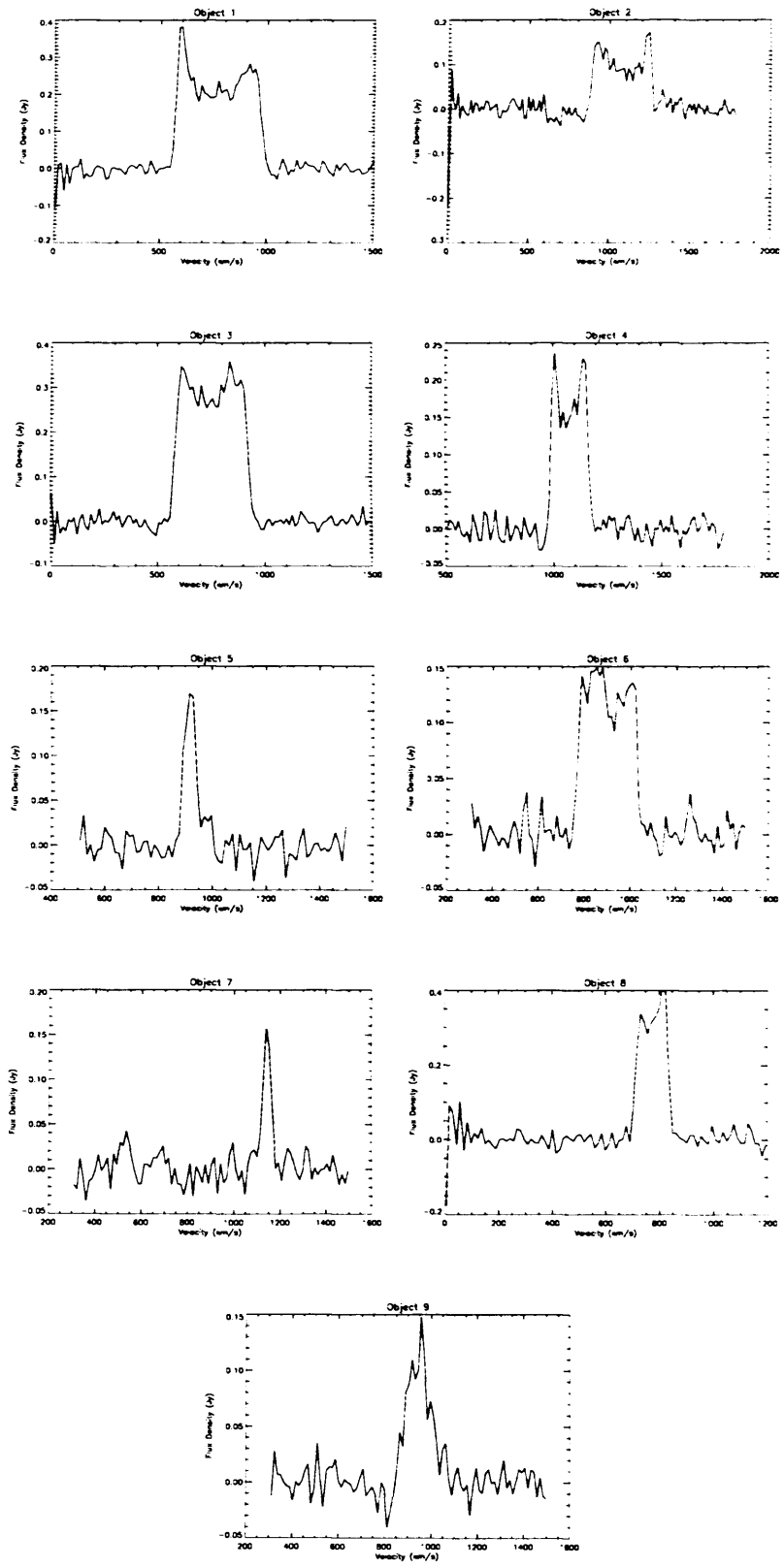

Figure 6.5: Spectra of detections found both by eye and by *polyfind*.

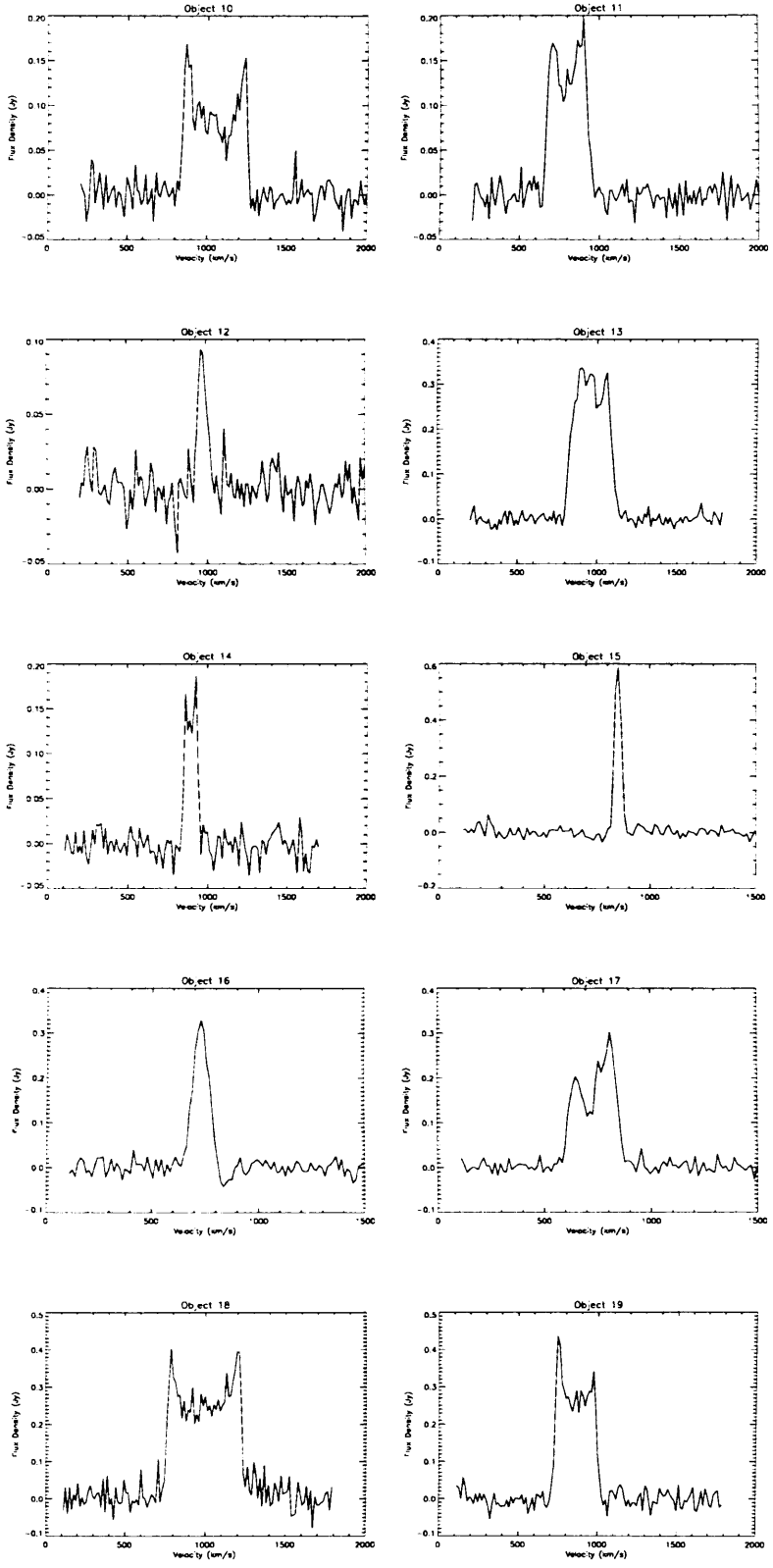

Figure 6.5: continued...

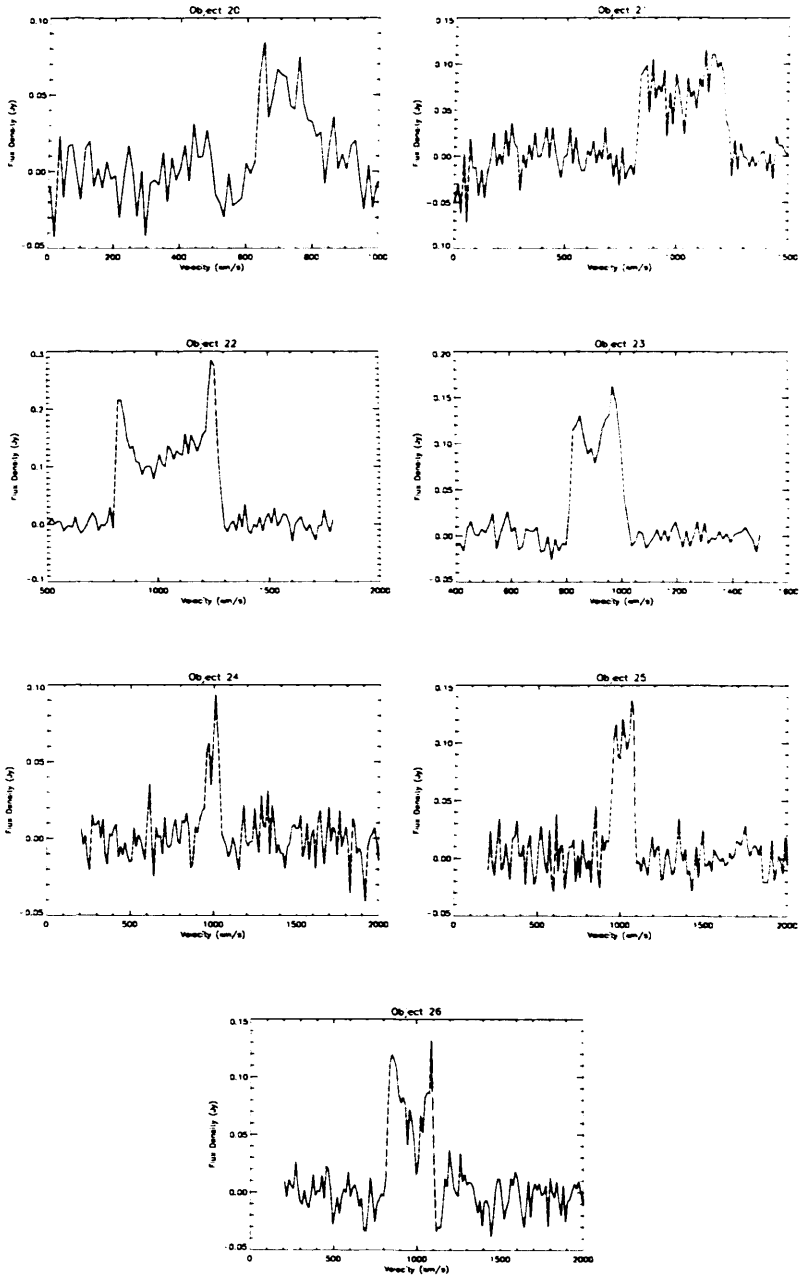

Figure 6.5: continued...

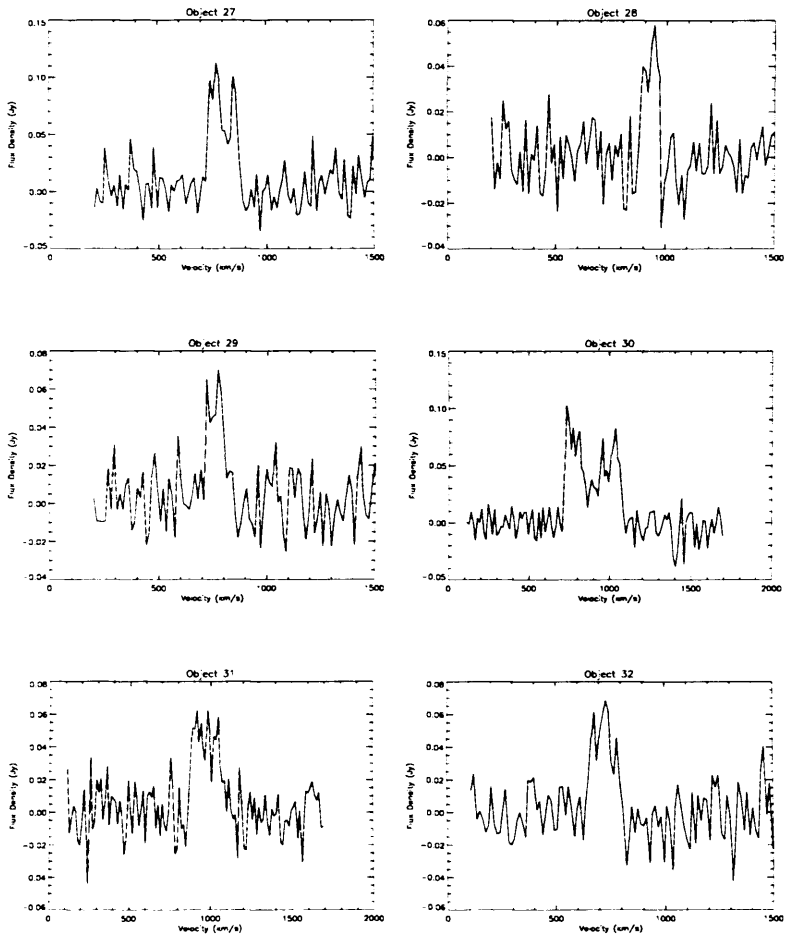

Figure 6.5: continued...

6.2.2 Undetected galaxies in the UMa HI survey

As can be seen in Fig. 6.4, there were 6 UGC galaxies in the area covered by the HI data cube, all late-types, which we might expect to have detectable amounts of HI gas. These galaxies were missed in both our search by eye, and by the *Polyfind* routine when searching for HI detections in UMa. The first 3 galaxies (UGCs 6922, 7218 and 7401) were missed due to their faintness or invisibility on the data cube. We carried out a second search of the cube around the positions and velocities of these objects, but this did still not convincingly show that the detections were real. These 3 galaxies, although late-types, must have HI masses below our detection limit of $M_{HI} \geq 2 \times 10^8 M_{\odot}$.

The remaining 3 galaxies missed in our HI search (UGCs 6940, 6969 and 7176) were positioned very close in RA, Dec and velocity to other brighter galaxies which *were* detected in the 'by eye' search. A second inspection of the data cube at these galaxy positions did not reveal the obvious detection of a galaxy - they appeared to overlap with the brighter galaxies, thus they were missed in the 'by eye' search method. As explained in Chapter 4, the *Polyfind* procedure detects peaks which are greater than 4σ of the measured noise in each channel and then fits a series of Gaussian templates to the peak, picking the best fitting template as a possible detection if its correlation coefficient is >0.75. This procedure however includes multiple detections of single objects - these are then analysed by a second program, *Polypurge*. This routine chooses the best-fitting template for the multiple detections for peaks $>4.5\sigma$. Thus for the 3 galaxies which are positioned very close to brighter galaxies, it is likely that *Polypurge* took them as multiple detections of one object, and chose the object with the best fitting template as the single detection. Further investigation of the objects which were removed by the *Polypurge* proce-

dure verified that this was the case. It is clear that the automated procedure has some problems in detecting all possible objects in a data cube. This is discussed further in the next section.

6.2.3 Objects missed by *Polyfind*

Apart from the 6 UGC galaxies not detected either in the by eye search or by the *Polyfind* routine, there were 13 HI detections found by eye which were missed by *Polyfind*. This would be a rather worrying result if we had relied solely on searching UMa with this automated procedure. However, we also carried out 2 searches by eye on the data, so it seems reasonable to assume that the majority of HI sources in our region of UMa with $M_{HI}>2\times10^8 M_{\odot}$, have been detected in our survey. The main advantage of using an automated selection algorithm such as *Polyfind* is that searching data cubes by eye is extremely labour intensive, and an automated procedure is much quicker. In order for *Polyfind* to be used as an effective single search tool in future HI surveys, its detection methods must be improved so that HI sources are not missed. This was not part of this thesis work, but it would be advantageous for future work on *Polyfind* to find out *why* the algorithm missed these particular objects in UMa.

The *Polyfind* algorithm detects all peaks over 4.5σ with velocity widths, $V_{50}>25 kms^{-1}$ and correlation coefficients greater than 0.75. The objects missed by *Polyfind* all had velocity widths greater than $25 kms^{-1}$ and peak signals $>4.5\sigma$. These 13 objects must therefore have been missed due to their correlation coefficients being below the limit of 0.75. This would occur if *Polyfind* could not successfully fit a Gaussian template to the peaks. Obviously, further work to improve the Gaussian fitting routine in *Polyfind* and the *Polypurge* routine needs to be carried out if they

are to be used as efficient detection algorithms in future HI searches.

6.2.4 Comparison with optical data

In our optical survey of the UMa cluster we found 6 objects in the search area of 1.68 sq. degrees. One of the objects corresponds to an object in NED with an optical redshift of 0.014, so it is actually a background object projected onto the UMa cluster area. None of the objects found in the optical search corresponds to those found in the HI search. We have already explained that since our HI detection limit was quite high, such an object would have M_{HI}/L_B of $\sim$138 to be detected in both surveys so we should not be surprised that none of the dwarfs detected in the optical survey were found in the HI survey. A deeper HI survey in UMa reaching lower HI masses must be undertaken before we exclude the possibility of the existence of these objects.

6.2.5 Comparison with Virgo

In this section we wish to compare the HI properties of the UMa cluster with those of the Virgo cluster. Such a comparison will help us to understand the nature of the galaxies in these two environments and see how the environment may affect their evolution. We would expect in a cluster as densely populated as Virgo, that many galaxy-galaxy interactions are taking place. This, combined with the presence of a hot, X-ray emitting intra-cluster gas could strip the gas from cluster galaxies. Investigating such processes in clusters may in turn explain why, in our optical search for LSB dwarf galaxies in these 2 regions, we find many more dwarfs per sq. degree in Virgo than in the UMa cluster.

Davies et al. (2004) carried out a 21cm HI survey of the Virgo cluster covering $8°\times4°$ using the multi-beam receiver on the Lovell 76m telescope at Jodrell Bank. With integration times per pointing of 3500s, this survey was $\sim$9 times deeper than that of the standard HIJASS survey from which our UMa HI data was obtained, and had an rms noise of $\sim$4mJy beam^{-1} compared to $\sim$13mJy beam^{-1}. By restricting our analysis of Virgo to those galaxies with $M_{HI}>2\times10^8 M_\odot$ we can make direct comparisons with our UMa results.

Davies et al. found 31 objects with $M_{HI}>10^7 M_\odot$ for a 4.5σ peak detection and 50kms^{-1} width galaxy. Of these, 19 have $M_{HI}>2\times10^8 M_\odot$. We compare the HI mass to light ratios and column densities of these 19 Virgo cluster galaxies with the 32 HI detections in UMa. Our comparison of the HI mass distribution in the two clusters however includes all 31 Virgo cluster galaxies detected by Davies et al., and all 32 UMa HI detections. This will enable us to compare the depths of the two surveys and comment on how a dense cluster such as Virgo, may affect the gas in its member galaxies.

HI mass to light ratios

As we have said previously, the HI mass to light ratio gives information on how efficient the conversion of gas into stars is in a galaxy, or in cluster environments, how efficient gas stripping mechanisms are. Galaxies suffer ram pressure stripping as they move through a hot ICM. X-ray observations have shown that such a hot gas exists in the Virgo cluster (Bohringer et al. 1994), whereas in the UMa cluster, there is no such hot intra-cluster gas. Thus lower M_{HI}/L_B values for Virgo cluster galaxies when compared with UMa cluster galaxies could indicate either more efficient SF in Virgo cluster galaxies, increased gas stripping of galaxies in Virgo,

or a combination of the two.

The distribution of M_{HI}/L_B values for the Virgo and UMa cluster galaxies is shown in Fig. 6.6. The Virgo objects are plotted with a dashed line, the UMa objects with a solid line. The two distributions are similar for both clusters although there is one galaxy in UMa which has a relatively high M_{HI}/L_B of ~4.3. This is Object 7 from Table 6.4, and as discussed earlier, is a gas-rich dwarf irregular galaxy. It may have such a large M_{HI}/L_B due to lack of interactions in the low density UMa cluster, resulting in an inefficient rate of SF. The similarity of the M_{HI}/L_B distributions for the remaining galaxies in the 2 clusters indicates that we cannot tell by this parameter alone whether the environment affects galaxies more in the dense Virgo cluster, or in the lower density UMa cluster.

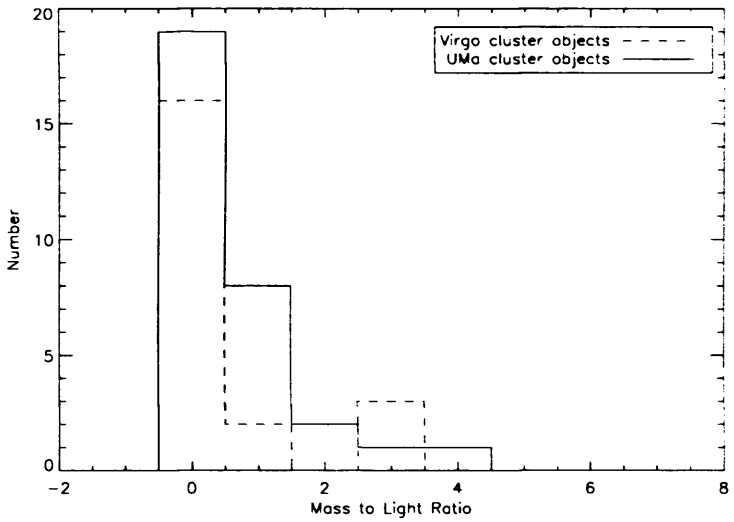

Figure 6.6: Comparison of $M_{HI}/L_B$for UMa and Virgo cluster objects.

HI column densities

For both the Virgo and UMa objects, the HI column densities were calculated using the formulae:

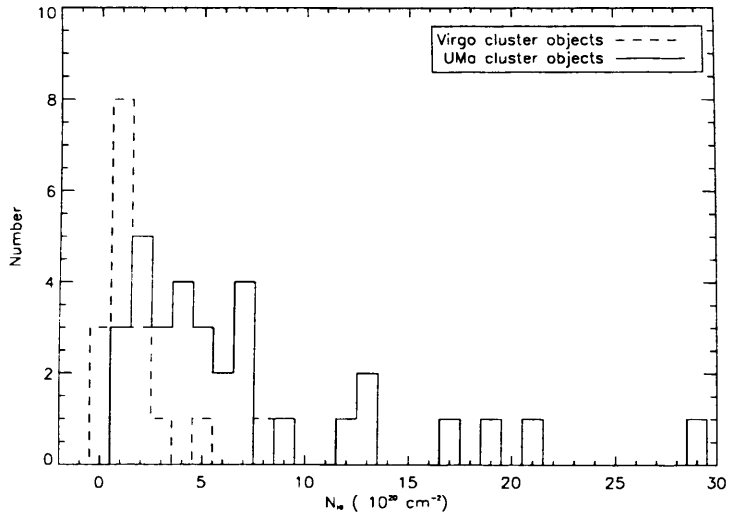

Figure 6.7: Comparison of HI column densities for UMa and Virgo cluster objects.

$$N_{HI} = 10^{20.1} \frac{M_{HI}}{\pi {R_{HI}}^2} cm^{-2} \tag{6.2}$$

where N_{HI} is the HI column density of the galaxy, M_{HI} is the galaxy's HI mass and, following Davies et al. (2001),

$$R_{HI} = 2.4 R_{25} \tag{6.3}$$

where R_{HI} is the HI radius, and R_{25} is the radius of the galaxy at the 25 mag per sq. arcsec B-band isophote.

We plot the two clusters' HI column density distributions in Fig. 6.7, the Virgo cluster objects with a dashed line and the UMa cluster objects with a solid line. It is clear from this plot that the galaxies detected in the Virgo cluster have on average, lower HI column densities than those galaxies detected in the UMa cluster where they appear more spread. Shaye (2004) found a minimum HI column density

limit above which SF can occur, to be $\sim$(3-10)$\times 10^{20}$cm^{-2}. All except one of the Virgo cluster galaxies have N_{HI} lower than this limit. The UMa cluster galaxies however have fewer galaxies which have HI column densities below the critical value for SF. We might therefore expect the UMa galaxies to have consumed more of their gas in the SF process than the galaxies in Virgo. Their M_{HI}/L_B distributions however (Fig. 6.6) show no such evidence for increased gas consumption in the UMa galaxies compared to Virgo. Clearly the global HI column density of galaxies is only one factor which determines how SF progresses in individual galaxies.

HI mass distribution

The HI mass distribution of galaxies can be one method of measuring how a galaxy's evolution is being influenced by its environment. A comparison of HI mass functions for all 31 objects detected in the Virgo cluster with 31 objects in the UMa HI cluster survey is shown in Fig. 6.8. The Virgo HI data, taken from Davies et al. (2004), is plotted with a dashed line. The UMa cluster data is plotted with the solid line. It is clear that in order to conduct a thorough comparison of the Virgo cluster with UMa, an extension of the UMa survey depth to lower mass limits is needed. At present, with the limited data we have, we cannot compare the HI mass functions of the two clusters. However, since we are interested in how the environment affects galaxy evolution, by looking at the Virgo cluster HI mass function alone, we can comment on the influence of the Virgo cluster on the HI content of its member galaxies.

There appears to be a turnover in the HI mass function for the Virgo cluster data for HI masses below $\sim 10^{8.5} M_{\odot}$. Davies et al. comment that this may be due to incompleteness at the lower masses, which can hopefully be overcome

with the advent of more sensitive HI surveys such as the Arecibo Galaxy Environment Survey (AGES , Auld et al. in prep). However, if this turnover is a real phenomenon in the Virgo cluster HI mass function, then this indicates a distinct lack of HI gas in low mass galaxies. Either the efficiency of converting HI gas into stars is more effective in low mass galaxies in Virgo, or these low mass galaxies can be stripped of their gas more easily than higher mass galaxies. We discuss such stripping mechanisms in the Virgo cluster in more detail in the next Chapter.

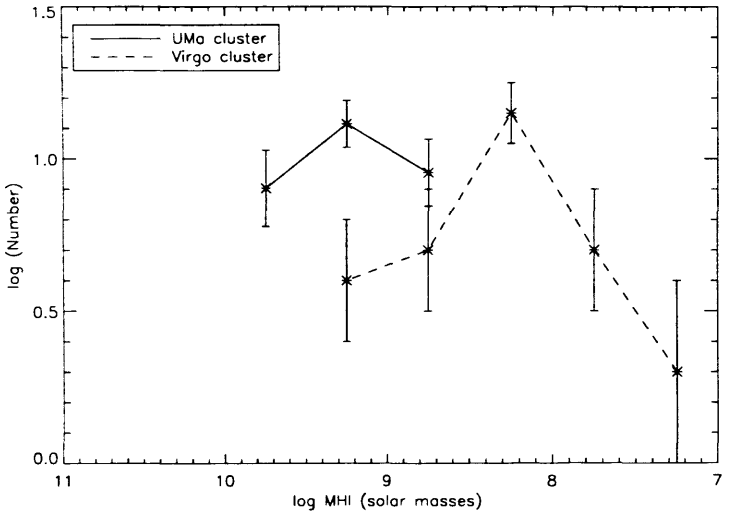

Figure 6.8: Comparison of HI mass functions for the UMa and Virgo clusters.

6.3 Summary

We made pointed HI observations of 58 objects taken from our list of detections in our optical search for LSB dwarf galaxies in the field. Of these objects, 18 were detected at 21cm, giving an overall detection efficiency of 31%. This is much higher than the HI detection efficiency for the Virgo cluster, of 5% (Sabatini et al. 2005). This suggests the galaxies detected optically in the field are generally more gas-rich than those detected in the cluster environment. This could be due to increased

galaxy interactions in the cluster environment which would either enhance the SF in the cluster galaxies, or strip the HI gas from them. Both scenarios would result in a lower HI gas content in cluster galaxies. Since such interactions are rare in the field environment, we would expect the field galaxies to contain more HI gas than their cluster counterparts.

We explained in Chapter 4 that for a proper comparison of field and Virgo cluster objects we must restrict our field object analysis to those within 21 Mpc. From the objects detected in HI, 4 were within this distance. The remaining 14 were found to be background gas-rich LSB galaxies, which were included in our optical search for dwarf galaxies as they also have low surface brightnesses which satisfied our selection criteria.

With a minimum HI mass detection limit, $M_{HI} \geq 2 \times 10^8 M_\odot$ for UMa, we found 32 objects in an area covering $8° \times 8°$ of the cluster using both a manual search by eye and an automated galaxy finder. We found no candidates for dark galaxies in this cluster, since all the HI detections had optical counterparts, identified in NED. The HI detected galaxies have a mean M_{HI}/L_B value which agrees well with what is expected for a typical gas-rich spiral galaxy ($M_{HI}/L_B \sim 0.7$). There was however one HI detection of a dwarf galaxy in UMa which had a large M_{HI}/L_B of ~ 4.3. A typical gas-rich dwarf galaxy has $M_{HI}/L_B \sim 1$, thus SF in this particular galaxy must be extremely inefficient. This could be attributed to being a member of a less dense cluster.

Chapter 7

Discussion and Conclusions

In this chapter we present a summary and discussion of the results from our investigation of LSB dwarf galaxies in different environments. As discussed in Chapter 1, the hierarchical clustering theory of structure formation in the Universe predicts the existence of large numbers of small mass objects in all regions of the Universe today, and if star formation occurs in these objects then they should be visible as dwarf galaxies. However, as we have shown in this thesis, observations have failed to find the large numbers of dwarfs in the lower density regions, whereas in higher density environments such as the Virgo cluster, they have been discovered in numbers similar to those predicted by CDM. There are two possibilities for these results:

- CDM is incorrect and the dwarf galaxies observed in clusters are not the predicted primordial population. In some way, dwarf galaxy numbers are enhanced in clusters.
- CDM is correct but the formation of dwarf galaxies in the lower density

environments is suppressed by any number of feedback processes compared to high density environments.

Our data sampled environments of increasing density in the Universe - the general field, region around M101, the lower density UMa cluster and the higher density Virgo cluster. By using identical data-sets in our surveys and probing fainter magnitudes than previous surveys, we have been able to extend our knowledge of LSB dwarf galaxy populations to include the extremely faint objects with $M_B \sim$-10. With additional HI and colour information as presented in Chapters 5 and 6, we can now investigate the possible formation scenarios of the dwarf galaxies we detected. First we summarise the main results of our investigation:

MGS field

- There are very few dwarf galaxies per sq. degree in the field ($\sim 2 \pm 1$) compared to the Virgo cluster.
- Pointed HI observations gave a HI detection efficiency of $\sim$ 31%, which is much higher than that of the Virgo cluster (5%). Thus field objects are more gas-rich than those found in the cluster.
- The mean (B-I) colour of objects in the MGS field data within 21 Mpc is bluer than the values found for the 2 data strips in the Virgo cluster.
- A large number of gas-rich background dwarf galaxies were found with our pointed HI observations.
- The HI detection associated with Objects 12 and 13 has the smallest mass value in the sample. These objects are the bluest objects of the 4 within 21 Mpc and are most certainly associated with a giant galaxy, NGC 3521. The

tidal effect of this nearby giant galaxy could be triggering star formation in these 2 objects.

M101

- There are comparable numbers of dwarfs per sq. degree (~3±2) in the field around M101 as in the MGS field data.
- One possible companion of M101 was found using the selection criteria adjusted for objects at the distance of M101. If the MW were placed at the distance of M101 however, we would not expect to detect any companions with our selection criteria.
- The number density of objects detected in the field is higher than the number density of MW companions if it were placed at 6.9 Mpc (~0.2 sq. degrees). Thus we are unable to distinguish between companions of nearby galaxies and field galaxies with our current selection criteria.

Ursa Major cluster

- There are comparable numbers of dwarf galaxies per sq. degree in this cluster (~4±2) compared to the general field. There is no evidence of an enhanced cluster dwarf galaxy population.
- A blind HI search of UMa resulted in the detection of 32 objects, all of which had been previously catalogued. We found no HI objects without an optical counterpart.
- A deeper HI survey of UMa is needed to allow us to probe the low mass end of the UMa cluster mass function for a proper comparison with the Virgo

cluster.

Virgo cluster

- There are a large number of LSB dwarf galaxies in the Virgo cluster (~16-22/sq. deg) in both the area extending East-West which samples the main body of the cluster, and the North-South area which also samples two background clouds which are assumed to be falling into the Virgo cluster from behind. Thus, the Virgo cluster seems to be assembling itself out of subclusters and clouds that are already rich in dwarf galaxies compared to the environment of the general field.
- Within the errors, the (B-I) colours of the objects in the 2 data-strips are similar. There is no evidence for any systematic difference in dwarf galaxy (B-I) colour between dwarf galaxies in different parts of the cluster, although there are larger errors on the N-S strip colours due to a larger fraction of faint galaxies.
- The HI detection efficiency for the E-W strip objects is much less than that for the MGS field objects (5% compared to 31%).

Comparison of DGRs

A comparison of the DGRs for each environments is given in Table 7.1. Also given for comparison is the DGR from integrating the 2dF LF of Norberg et al. (2002) between $-10 \geq M_B \geq -14$ and $-19 \geq M_B \geq -24$ for varying faint-end slopes. For α ~-1.2 we find a DGR of 18:1. For steeper LFs, consistent with CDM simulations ($\alpha = -1.6$ to -2.0, but keeping M_B^* constant) we have DGRs in the range, 367:1

to 8371:1 (note that this is for galaxies of all surface brightnesses), and as can be seen in the Table, none of the environments match such high DGRs. For the MW, if placed at a similar distance to the Virgo cluster, we have DGR $\approx 2:1$. For the general field we have a DGR of 6:1. For the Virgo cluster we found mean DGRs of 22±7 for the N-S strip and 14±4 for the E-W strip. The possible reasons why the ratios of low mass to high mass objects in different environments are so different are discussed in the following section.

Survey/simulation	*DGR*
MGS field	6:1 (max)
M101	1:1
MW	2:1
Virgo cluster N-S strip	22:1
Virgo cluster E-W strip	14:1
LF ($\alpha = -0.6$)	0.24:1
LF ($\alpha = -0.8$)	1:1
LF ($\alpha = -1.0$)	4:1
LF ($\alpha = -1.2$)	18:1
LF ($\alpha = -1.4$)	80:1
LF ($\alpha = -1.6$)	367:1
LF ($\alpha = -1.8$)	1735:1
LF ($\alpha = -2.0$)	8371:1

Table 7.1: DGRs for the surveys and simulations

7.1 Environmental differences

Lemson & Kauffmann (1999) investigated the influence of environment on DM haloes using N-body simulations and found that the MF is 'skewed towards high-mass objects in overdense regions of the Universe and towards low-mass objects in underdense regions'. Thus from these results, one would expect to find a lower DGR in the Virgo cluster, and higher DGR in the general field. This is the complete opposite to what we find in our optical surveys of these regions. Our results for the

MGS field gave a maximum possible DGR of 6:1 whereas for the Virgo cluster we found a DGR of ~22:1. Kauffmann et al's (1993) results for the field as discussed in Chapter 1 also overpredicted the numbers of low mass DM haloes compared to observations. This, they conclude, is due to many of the haloes remaining dark and therefore undetectable. This possibility is discussed later. First we look at whether the theoretical predictions for environments similar to those looked at in our optical searches also have large dwarf galaxy populations.

In Chapter 1 we discussed the N-body simulations conducted by Moore et al. (1999) which investigated the substructure of galactic and cluster sized DM haloes. The simulation results showed that the distribution of masses around these two haloes were extremely similar, and both contained a large amount of substructure. Given that objects of masses $\sim 10^{11} M_{\odot}$ should collapse and form from 1σ fluctuations at z~2, the galactic DM halo presented by Moore et al. at z~0, should be an accurate representation of what the DM distribution of a galaxy would look like now.

We can therefore compare the results of Moore et al's galactic DM halo with our results for the observed number of companions around M101. From the simulations, one would expect to find a large number of dwarf companions surrounding M101 if we assume that light traces the dark matter distribution. However, with our deep CCD imaging of the region around M101, only 1 possible companion of M101 was found. Bremnes et al. (1999), in their deep study of the M101 dwarf galaxy population, found only 11 companions. Around a similar galaxy, our Milky Way, there are only 11 known companions (Mateo 1998). Clearly, either the simulations using the currently favoured CDM model are incorrect, or the DM substructure does exist but the individual DM haloes themselves do not contain enough stars to light them up and reveal them as dwarf galaxies. The mecha-

nisms which may cause this star formation suppression are discussed later in this Chapter.

The UMa cluster is populated by mainly late-type galaxies and has no concentration towards a central core. This cluster is likely to be relatively young cluster which is still forming out of systems similar to M101. If this is the case then, following Moore et al's simulations, we might expect to find a large number of dwarf galaxies in this cluster. However, from our observations of M101 we would not expect to detect a significant dwarf galaxy population in UMa since, according to the results of our M101 survey, constituent parts themselves do not contain a large population. This is exactly the result which we obtain - UMa has a comparable number density of objects to M101 and the general field of $\sim 4\pm2$ per sq. degree.

The Virgo cluster of galaxies is a completely different environment to the others studied in this thesis. Moore et al. (1999) predicted large amounts of substructure for a DM halo similar in size to Virgo, and this is what we find with our optical data - there is a large population of dwarf galaxies in the cluster. We know from X-ray studies (Binggeli et al. 1993; Bohringer et al. 1994) that the Virgo cluster is assembling itself out of discrete units. Thus either these units already have large populations of dwarf galaxies associated with them or there must be something going on in the Virgo cluster which creates dwarf galaxies. Observations of regions such as M101 (this thesis) and the MW (Mateo, 1998) would suggest that the Virgo cluster cannot have assembled out of LG type units *without* some additional physical mechanism being involved which would increase the numbers of dwarfs in the cluster. We discuss the possible mechanisms in the next section.

7.1.1 Creation of dwarf galaxies

Harassment

Moore et al. (1999) suggested 'galaxy harassment' as a solution to the excess dwarf galaxy population in the Virgo cluster. In this scenario, infalling LSB disk galaxies are 'harassed' by giant cluster galaxies and morphologically transformed into dEs. However, Sabatini et al. (2005) calculated that if the dwarf galaxies found in the cluster originally came from a population of larger field galaxies then they should have tidal radii of the order $\sim$ 7kpc. The dwarf galaxies in our sample have scale-lengths between 4″ and 9″, which, at the distance of Virgo correspond to physical scale-sizes of 0.25kpc to 0.75kpc. Moore et al. (1998) give the smallest radius of a harassed galaxy to be $\sim$1.67kpc, which is larger than the sizes of objects which we are detecting in Virgo. So, although galaxy harassment may be a viable method of forming larger scale-size faint galaxies in the Virgo cluster, it does not explain the large dwarf galaxy population with smaller scale-lengths found in our optical search.

Another prediction of the harassment scenario is that stars torn out from the harassed galaxies will lie along narrow streams which follow the orbital path of the galaxy. Davies et al. (2005) carried out a search for these tidal arcs around 38 dE galaxies found in our survey of the N-S strip of the Virgo cluster. The tidal streams are predicted to have surface brightness values of $\sim$27.5 Bμ, thus the dE data was smoothed to increase its surface brightness limit from 26 Bμ to $\sim$28 Bμ. A Haar smoothing method was then applied to the data to extract any tidal features centered upon the dEs. From this search, Davies et al. found no evidence for tidal streams which could be associated with the sample of dEs from our Virgo cluster

survey. One obvious reason for this is because the streams are fainter than our limit of 28 Bμ. If this is the case, then they will not be detectable with our current data. The second possibility for the non-detection of these streams is that they do not exist. This is highly unlikely however since other studies have produced evidence which confirm the existence of these streams. Feldmeier et al. (1998) found evidence of Intra-cluster planetary nebulae (IPN) in Virgo and Ferguson et al.(1998) detected intra-cluster stars in deep blank field Virgo images. Both these types of objects are predicted outcomes of the harassment scenario, thus their observation in the Virgo cluster lends credence to this mechanism of dwarf formation.

Tidal interactions

As described in Chapter 1, tidal interactions between galaxies in galaxy clusters result in gas and stars being pulled out from the interacting galaxies into giant streams, along which clumps of gas and stars form. Over time the stream fades, and the clump is classified as a tidal dwarf galaxy (TDG). Hunsberger et al. (1996) investigated the formation of these dwarf galaxies in a study of 42 compact Hickson groups. Down to $M_R$$\sim$-14, they found 47 candidate TDGs, all with diameters in the range 1-6h_{75}^{-1} kpc. Although larger than our sample of dwarf galaxies in Virgo, Hunsberger et al's study nonetheless illustrates the possibility that a number of dwarf galaxies in clusters could have formed in the tidal tails of giant galaxies. However, one problem with this theory is that simulations of TDGs predict that only 1-2 form with each interaction if the galaxy cluster collapses at a high redshift. So their results should be interpreted as a prediction of how many TDGs would be expected to survive for $\sim 10^{10}$ yrs in the cluster environment. Evolution of the cluster could result in merging of the TDGs or falling back onto their parent galaxy.

We can calculate how many TDG producing interactions there could be in Virgo by considering a simple rate equation.

The number of interactions (N) which may produce a TDG in a cluster depends upon four parameters - the number density of galaxies (ρ), their interaction cross section (σ), their velocity (v) and the age of the cluster (T). Thus,

$$N \sim \rho \sigma v T \tag{7.1}$$

If we assume, as do Okazaki & Taniguchi, that only interactions between disk galaxies (S0 and spirals) produce TDGs, then from Tully & Shaya (1994) we can calculate, ρ, the number density of galaxies in the cluster. The interaction cross section of the galaxies is assumed to be their virial radius - this, together with the mean velocity of these galaxy types are also obtained from Tully & Shaya. We find that there could be 13 interactions per Gyr, given the above information. So, if we assume that each interaction makes, at most, 2 TDGs, this means that we would expect 26 TDGs to be formed every Gyr. Given that a galaxy cluster the size of Virgo ($\sim 10^{14} M_{\odot}$) should be forming from a 1σ fluctuation at present, it seems extremely unlikely that TDGs make up a large fraction of the cluster dwarf population, and certainly not large enough to account for the hundreds of dwarf galaxies which we find in Virgo today.

Morphological transformation

Another explanation for the large number of predominantly dE galaxies which we find in the Virgo cluster is the possibility that infalling dIrrs have been transformed

into dEs. The morphology-density relation of Dressler (1980) extends to dwarf galaxies, where dEs are found in the centre of clusters, and dIrrs reside towards the outskirts. This was found by Sabatini et al. (2003) for the E-W strip, but not by us however in the N-S strip due to contamination of this strip by the background clouds. It has been postulated (van Zee et al. 2004) that as the dIrrs fall into the cluster, they have their gas stripped by ram pressure stripping and become the objects which we classify as dEs. However, the importance of ram pressure stripping on the evolution of cluster dwarf galaxies in Virgo was investigated by Sabatini et al.(2005) who found that only those dwarfs within the cluster core ($\sim$0.5Mpc or 1.5°) would be affected by this process. For the E-W strip, they conclude that the dwarfs they detect within the projected cluster core would be severely tidally disrupted if they were actually located in the core, thus they must be outside the core region, and therefore will not be subject to ram pressure stripping. The majority (99%) of the galaxies detected in our N-S Virgo cluster strip are outside the projected core region due to the offset of this strip from the cluster centre. Thus the effect of ram pressure stripping on these galaxies must be negligible. Sabatini et al. suggest that enhanced star formation triggered by interactions with the cluster and galaxy potentials, accelerates the evolution of the infalling dIrrs from the clouds so that they resemble the dEs which we see in Virgo today.

Ideally we would like to find the ages of the stellar populations in the cluster dwarf galaxies to ascertain whether they are indeed the primordial population as predicted by CDM, or, if they have young stellar populations, have they formed more recently due to the processes described above. Given the complexities of modelling stellar populations (changes in the initial mass function, metallicity of the gas and star formation history) it is extremely difficult to learn very much from

the two broad band colours we have from our optical data. Ideally we would like to observe individual stars and construct stellar colour magnitude diagrams as has been done for Local Group galaxies (Mateo, 1998, Grebel, 1997) and other nearby galaxies (Pritzl et al., 2003, Grossi, 2005), but this is currently not possible at the distance of the Virgo cluster. What we can do with our available data is compare the galaxy colours with those of other stellar systems to see if this gives us a clue as to their possible formation scenario in the cluster.

7.1.2 Cluster galaxy colours

Sabatini et al. (2005) discussed the (B-I) colours of the galaxies detected in the E-W strip and, as explained in Chapter 5, they concluded that there was no systematic change in colour with absolute magnitude (unlike that for giant elliptical galaxies), that there was no systematic change in colour with projected distance from the cluster centre and that there is no significant difference between the colours of the galaxies classified as dE and dIrr. As shown in Chapter 5, these conclusions are confirmed for the N-S strip.

Below we will compare our Virgo cluster dwarf galaxy (B-I) colours to those of other stellar systems. Given the errors on our individual colours (typically 0.2 mag, but can be much larger for some of the faint objects) and the scatter in the colours of objects of a given type, taken from other papers, we do not believe that the exact filter system used is crucial to this analysis (if it was we would not be able to make any comparisons). We have used Cousins/Johnson filters calibrated against Landolt standards. The other work described below almost invariably uses Landolt standards, but they are often less clear about the exact B and I filters used.

As a first comparison, our mean colours of galaxies classified as dE compare very well with those recently published by van Zee et al., (2004), though their sample galaxies are all brighter than $M_B = -15.5$. They have high quality accurate photometry for 16 dE galaxies 13 of which have (B-I) colours with a mean of 1.9±0.1. This compares to our mean value for dEs of (B-I)=1.8±0.4 and so the two are consistent with each other.

Giant elliptical galaxies are generally redder than the colours given above for dE galaxies. For a sample of 26 elliptical galaxies with (B-I) colours Michard, (2000) find a mean value of 2.1±0.1. They also give a value of (B-I)=2.1 for the central Virgo cluster galaxy M87. This is redder than both its Globular Cluster (GC) systems (see below) and its dE cluster companions. Giant ellipticals are red because they are both old and metal rich. GCs are bluer generally because they are old, but metal poor. So, our cluster dE galaxies must therefore be either relatively metal poor or younger or some combination of the two compared to the giant ellipticals. Given a hierarchical formation process where dwarf sized objects merge to form larger galaxies, the dE galaxies should not be younger than the giant ellipticals. If they were older and metal rich like the giants then they should be redder. If they are older and metal poor then they could be bluer and so the hierarchical picture is viable as long as the dE galaxies are sufficiently metal poor to account for their blue colours.

The simplest stellar systems to compare with our dwarf galaxies are globular clusters (GCs). Couture et al. (1990) derived (B-I) colours for the GC population of M87, the brightest of which overlap with the faintest dwarf galaxies in our sample. If we assume that each globular cluster arises from a single star formation burst then their star formation history is easy to model. If we also assume (as do Couture et al.) that they are all approximately the same age, then their colours

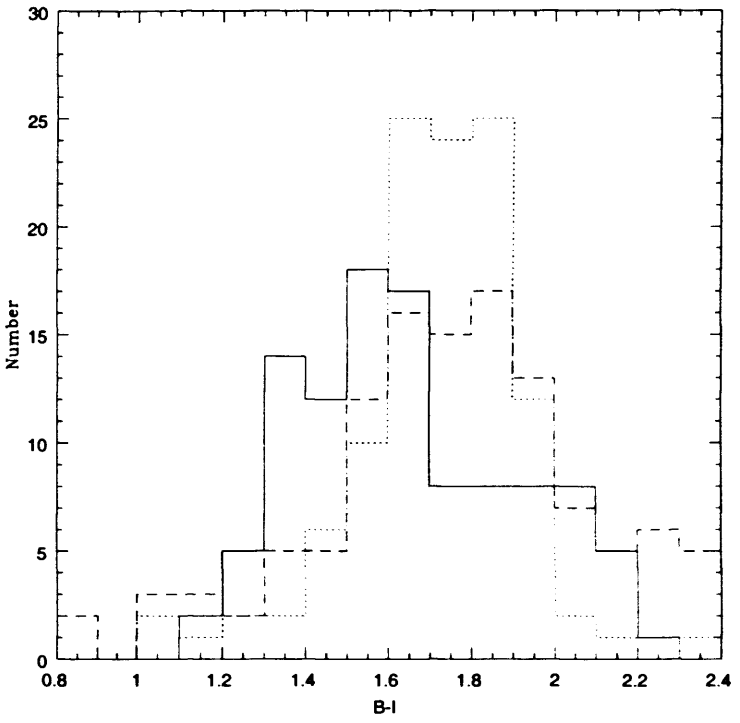

Figure 7.1: (B-I) colours for galaxies in the N-S (short dash), E-W strip (long dash) and M87 globular clusters (solid line).

are merely a reflection of their metallicities. In Fig. 7.1 we show a histogram of the (B-I) colours of the M87 GCs compared to our data from the two Virgo strips. The similarity of the colour distribution for the two strips is apparent, along with that of the M87 GCs. The mean values of (B-I) for the 'sure' objects in the two strips are 1.8±0.7 (N-S) and 1.8±0.4 (E-W) compared to 1.65 ± 0.25 for the GCs. Using the Couture et al. calibration from (B-I) to metallicity gives a mean value of [Fe/H]=-0.93 for our dwarfs which is a fairly reasonable tenth of the solar value. From their (B-I) colours alone there is no reason to suspect that the star formation history of these Virgo cluster dwarf galaxies is any different to that of the GCs of M87.

However, there are two problems with this simple interpretation. Firstly, there

are multiple pathways to these (B-I) colours for galaxies that have different ages, star formation histories and metallicities. It is known that the Local Group dwarf galaxies have more complex star formation histories than GCs (Grebel et al., 2003). Secondly, the formation mechanism of these two stellar systems should, according to hierarchical theory, be quite different. Elliptical galaxy GCs are thought to form as either the result of previous mergers or as part of the monolithic collapse that formed the galaxy (depending on your view of elliptical galaxy formation, Forbes et al.1998). Dwarf galaxies are supposedly the seeds of giant galaxy formation while the GCs are the fruits. The possibility of a link between dwarf galaxies and GCs is something that does require further investigation, particularly in the light of the continued debate over objects like ωCen which may have a dual personality as both an ex-dwarf galaxy and a GC (Freeman 1993, Ideta & Makino, 2004).

For the central elliptical galaxy of the Fornax cluster (NGC1399) Forbes et al. found that it has a bi-modal distribution of GC colours. The central regions have a red (metal rich) population with (B-I) approx 2.1 while the outer regions have a blue population (metal poor) with (B-I) approx 1.7. A mean value of (B-I)=1.7$\pm$0.3 is just what Karick et al. (2003) find for the dE population of the Fornax cluster thus suggesting once more that there may be a link between dwarf galaxies and GCs. This mean value of the Fornax dE galaxy population is also perfectly consistent with the colours of our Virgo dE galaxies. We can compare the Karick et al. (2003) dE data for the Fornax cluster with our data for the Virgo cluster. Similar data sets (range of absolute magnitudes) can be compared by limiting the Karick et al. data to those galaxies fainter than $m_B > 17.5$ (31 galaxies). In Fig. 7.2 we have plotted the (B-I) distribution for this subset of the Fornax data along with our Virgo data. Again, as for the GCs, the distribution of colours is very similar to that of the Virgo galaxies. There are also some very blue

(B-I<1.0) galaxies classified as dE and two quite red (B-I≈1.7) galaxies classified as dI (there are only two dI galaxies in this subset of the data).

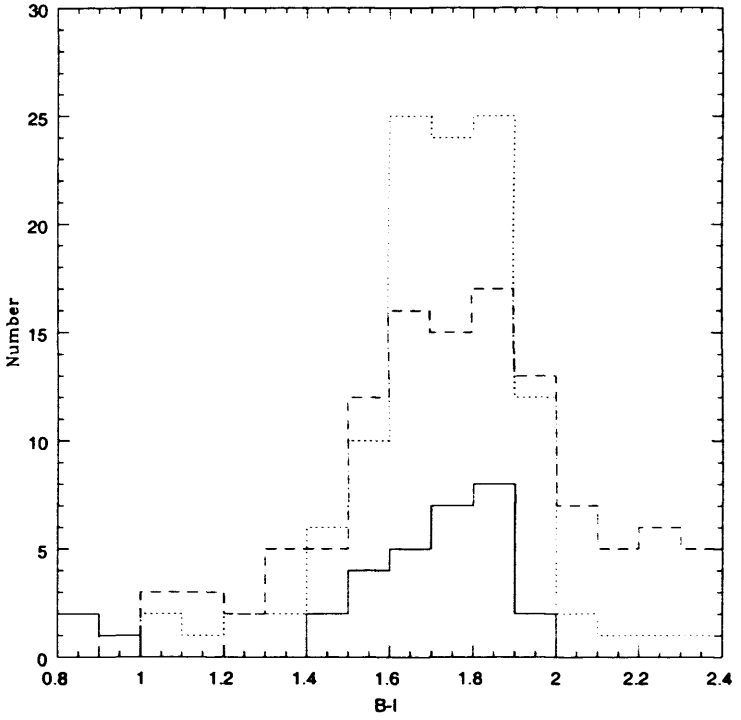

Figure 7.2: (B-I) colours for dE galaxies in the N-S (short dash), E-W strip (long dash) and Fornax cluster (solid line).

Heller and Brosch (2001) presented (B-I) colours for a sample of 28 Virgo cluster dIrr galaxies. Again these galaxies are brighter than the galaxies in our sample ($M_B < -15$). The mean (B-I) colour of their sample is 1.3±0.4 compared to our dIrr sample which has a mean of (B-I)=1.8±0.8. Although systematically bluer than our dIrr population, the scatter is large and there are some surprisingly red galaxies in their sample, for example (B-I)=2.1. Their sample also includes (as does ours) some extremely blue galaxies, e.g. (B-I)=0.52. For our sample the scatter in colour is much larger at fainter magnitudes, possibly because we have underestimated the errors, but an alternative is that we have a sample of galaxies that are still progressing through their star formation cycle. For galaxies

like this star formation may occur in a series of bursts. What we see are galaxies at various stages in this star formation process either just starting a burst of star formation, a long way from a new burst or some stage in between. Such a model of star formation bursts has been proposed by Gerola et al. 1980 (Stochastic Self-Propagating Star Formation or SSPSF). In this model it is the feedback from star formation that eventually leads to further delayed star formation in other parts of the galaxy - not a complete removal of the interstellar medium. Bursts of star formation at intervals of order 10^8 years can lead to variations in colour consistent with those observed (Davies and Phillipps, 1988, Evans et al.1990).

7.1.3 Suppression of dwarf galaxies

We have described the possible mechanisms which could create dwarf galaxies in the Virgo cluster region to produce the large population which we found in our optical survey of the cluster. We now need to discuss why we detect very few dwarf galaxies in the general field, the region around M101 and the low density UMa cluster, when CDM theory predicts large numbers here. The mechanisms commonly used to explain this discrepancy were introduced in Chapter 1; here we discuss them further in relation to our results.

SN winds and pressure confinement

The most common mechanism invoked when attempting to suppress the formation of dwarf galaxies, is that of gas expulsion via SN winds. This was first suggested by Dekel & Silk (1986). In this scenario the first generation of SN inject energy into the halo gas, giving it enough energy to escape the halo and thereby preventing

further star formation, rendering the halo invisible. In order to make this effect environmentally dependent, pressure confinement must be added. Once the SN winds blow out the gas in the halo, depending on the environment, the gas will either be lost to the IGM or it will be pressure confined due to the external pressure, and eventually fall back onto the galaxy, allowing further episodes of SF to occur. As discussed in Chapter 1, Babul & Rees (1992) calculated the density needed in each environment to either allow the gas to escape, or to push it back into the galaxy's halo. At the centre of high density regions, such as the Virgo cluster core, one would expect the gas to be confined to the galaxy halo due to the high external pressure of the ICM, resulting in either very close or one prolonged star-burst. This, suggests Babul & Rees, would explain nucleated dwarf galaxies in cluster centres. For the remaining dwarfs outside the cluster core but still experiencing a high external pressure in the cluster, the gas would fall back onto the galaxy on a longer time-scale resulting in many bursts of star formation. In the low density environments such as UMa and the field, there would be little external pressure being exerted on the expelled gas, thus all the gas would be lost from the galaxy. However, a problem with this theory and our results is that Babul & Rees predict that a consequence of pressure confinement in the cluster environment would be that the mean colours of the dEs should depend on distance to the cluster core - those further out would have bluer colours as they will experience star formation later than those in the central part of the cluster. In our N-S and E-W Virgo cluster data strips, as explained in Chapter 5, we found no evidence for a change in (B-I) colour with distance from the cluster centre, implying that the process of pressure confinement does not apply to the galaxies in our strips. To investigate this further, we used the ICM temperatures from X-ray surveys of the Virgo cluster to estimate the pressure that the ICM would exert on galaxies within the cluster, and compared the results to those limits given by Babul & Rees (1992). Unfortunately, current

X-ray data is only available for the core of the Virgo cluster (i.e. a region of $\sim 2^\circ$ from M87), thus we were unable to look at whether pressure confinement would work outside this region. In addition we cannot estimate a model for how the temperature of the X-ray gas depends upon cluster radius since this is still a matter of debate - Irwin & Bregman(2000) looked at BeppoSax data for a sample of 11 clusters within the redshift range, z=0.03 - 0.2 and found that the temperature profile of the IC gas was approximately flat. This, they say, agrees with the study of White (2000). However, it contrasts with the results of Markevitch's (1998) study using ASCA data of 30 clusters within a redshift range 0.04 to 0.09. In their study, Markevitch et al. found a significant decrease in temperature of the IC gas with radius. More recently, Arnaud (2005) in their review of X-ray observations of galaxy clusters, comments that still *'no consensus has been reached yet on the exact shape of the (temperature) profiles'*. Thus with no knowledge of how the temperature of IC gas varies with cluster radius in Virgo, our investigation on the role of pressure confinement in the Virgo cluster is limited to the core region surrounding M87.

Shibata et al. (2001) studied the temperature of the ICM in Virgo using ASCA data covering a region of 19 sq. deg. The region covered by their survey is shown in Fig. 7.3 in relation to our N-S and E-W Virgo data strips, and the clouds and subclusters of Virgo. The 60 fields studied by Shibata et al. are shown as the smaller circles centered upon M87 and extending mainly North-South. They cover approximately 2° of the E-W strip and extend to $\sim 3^\circ$ from M87, covering a small corner of the N-S strip. We therefore consider the effect of pressure confinement due to the IC gas in these small regions of the two data strips. Shibata et al. found only a small variation in the temperature of the IC gas with position in the cluster. Their results are shown in Fig. 7.4 - the top left figure is a 2D temperature map

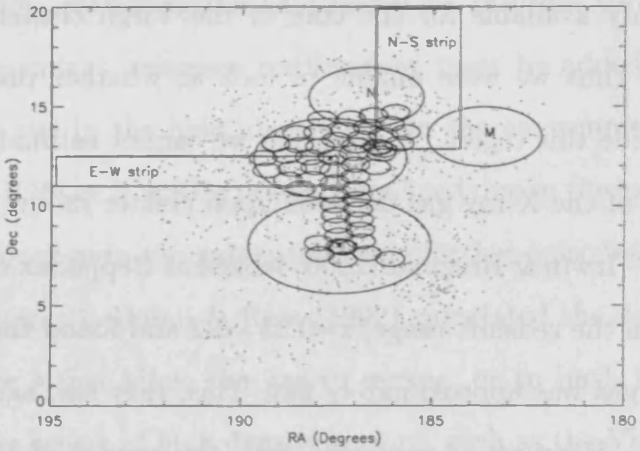

Figure 7.3: Region of Virgo cluster covered by ASCA X-ray survey of Shibata et al. (2001) (small circles) in relation to the N-S and E-W data strips. Also plotted are the Virgo clouds and subclusters (large ellipses), and the positions of the VCC galaxies (dots).

of the Virgo cluster, with the black circle representing M87, the inverted triangle representing M86, and the triangle, M49. The temperature scale goes from blue to yellow/white with increasing temperature. The temperature distribution with respect to distance from M87 in the North-South direction of the ASCA fields is plotted in the top right of Fig. 7.4. The lower left figure illustrates the temperature distribution in the E-W direction. So, around M87 the mean temperature, T, was found to be ~2.5keV. Northward of M87 they found T~2 keV, and southward, in Subcluster B, they found T~1.5 keV.

Using Boltzmann's constant, the X-ray temperature of the gas can be converted to temperature in Kelvins, and using n~4×10^{-2}cm^{-3} (Vollmer et al. 2001), we can find nT for these regions in Virgo to be compared with the values given by Babul & Rees.

- An X-ray temperature of 2.5 keV corresponds to a gas temperature, T~ 26×10^{6}K, giving nT~1.2×10^{6}cm^{-3}K.

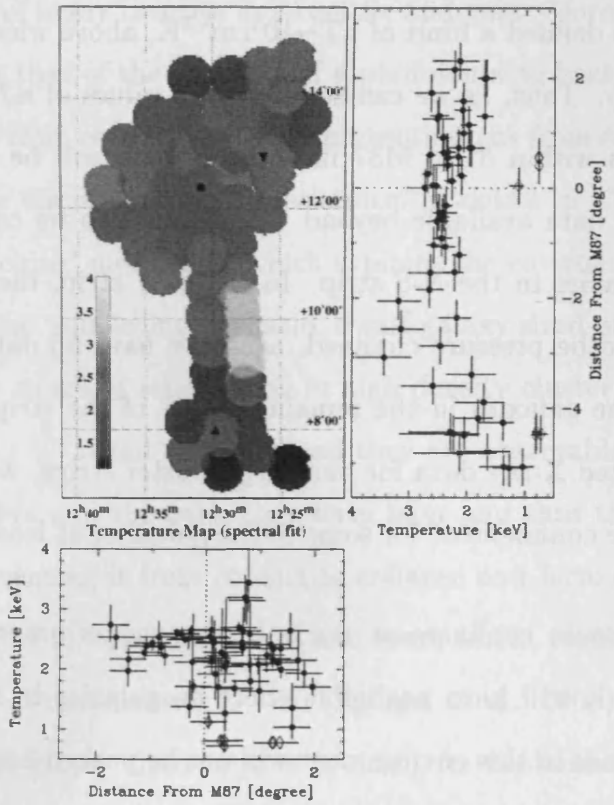

Figure 7.4: X-ray temperature distribution of Virgo cluster (Shibata et al. 2001). The top left figure shows the 2D temperature distribution. Here, the black circle represents M87, the triangle, M49 and the inverted triangle, M86. The temperature distribution with respect to M87 in the N-S and E-W direction are shown in the top right and bottom left plots respectively.

- An X-ray temperature of 2.0 keV corresponds to a gas temperature, T$\sim$ 23×10^6K, giving $nT\sim0.9\times10^6$cm^{-3}K
- An X-ray temperature of 1.5 keV corresponds to a gas temperature, T$\sim$ 17×10^6K, giving $nT\sim0.7\times10^6$cm^{-3}K

Babul & Rees defined a limit of nT$\sim10^5$cm^{-3}K, above which gas will be confined to the galaxy. Thus, as we can see from the values of nT calculated above, the dwarf galaxies within 3° of M87 in the N-S strip will be pressure confined. There is no X-ray data available beyond this distance so we cannot comment on the remaining galaxies in the N-S strip. In the E-W strip, those galaxies within 2° of M87 will also be pressure confined, again we have no data to calculate the confinement for the galaxies in the remaining part of the strip. Thus, although we have only limited X-ray data for our Virgo cluster strips, we can see that the process of pressure confinement for some of the galaxies, at least, is a possibility.

Although pressure confinement works in the cluster environment, Babul & Rees predict that it will have negligible effect on galaxies in the field, thus gas expelled by SN winds in this environment will not be pushed back onto the galaxy. Mac-Low & Ferrara (1999) investigated whether SN winds could blow out the gas completely from dwarf galaxies with masses in the range 10^6-$10^9 M_\odot$. They showed gas was only lost via SN winds in haloes $<10^6 M_\odot$, and this was only a few percent of the total mass of the galaxy. In all other cases, the SN explosions only resulted in blowing holes in the gas. Thus gas expulsion via SN winds cannot be the main mechanism which would explain why we see only small numbers of dwarf galaxies in low density environments.

Photoionization

Kauffmann et al. (1993) concluded that there may be many DM haloes present in low density environments but that they are not observable as they have not been lit up by star formation. *Why* this should be the case for some DM haloes and not others is the topic of many theories in structure and galaxy formation simulations. One such theory is that of the presence of a photoionizing background preventing the gas in the halo from cooling, therefore preventing gas from collapsing and stars from forming. We discussed such a mechanism in detail in Chapter 1, together with Tully's 'squelching' mechanism which explains the environmental dependence of this theory. In the 'squelching' scenario, dwarf galaxy sized objects are assumed to form before the epoch of reionization in high density cluster sized regions such as Virgo, thus their SF is not inhibited and they are observable. In lower density regions such as UMa and the field, they form later and thus the UV background heats the gas, preventing it from cooling to collapse and form stars. However, in their model, Tully et al. used z_{reion} of 6 and more recent results of WMAP have pushed the epoch of reionization to $\sim$20 (Spergel et al. 2003), a time when the formation of dwarf galaxy sized objects is rare. As explained earlier, these low mass objects are more commonly formed at redshifts $\sim$6, thus Tully's model needs adjusting with respect to the WMAP result and is probably not viable at all.

Although Tully et al's squelching scenario has problems explaining the environmental dependence of dwarf galaxy populations, the effect of photoionization on low mass DM haloes may well play a part in the formation of galaxies in the idea known as 'downsizing' (Cowie, 1996). This scenario, born out of observational evidence that larger galaxies have older stellar populations than lower mass ones is apparently contrary to hierarchical theory of structure formation which says that

low mass objects form first, and larger ones later. However, if photoionization is considered in the hierarchical formation scenario, then this apparent contradiction can be explained. Kepner et al. (1999) investigated the epoch of galaxy formation in low mass haloes in the presence of a background UV field. For haloes with circular velocities in the range 15-70kms^{-1}, they used sem-analytic models to look at haloes which formed after z$\sim$5 from 1σ perturbations. Their Fig. 1 (shown here as Fig. 7.5) illustrates the relation between the halo's circular velocities and redshift of virialization, showing, as expected, that smaller objects form first and larger ones, later.

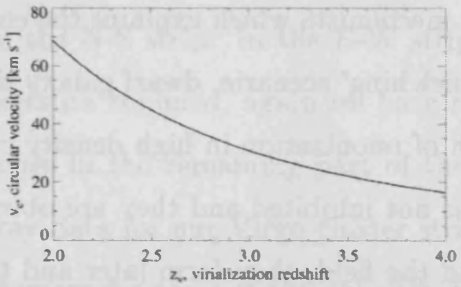

Figure 7.5: Relation between halo circular velocity and redshift of virialization taken from Kepner et al. (1999).

Kepner et al. proposed three stages for the gas in the DM haloes - firstly the gas is ionised by the UV radiation. As the flux of this radiation decreases, the gas slowly condenses toward the centre of the halo and becomes neutral. This increases the optical depth of the gas, thus preventing the ionising photons from reaching the gas at the centre of the halo, thereby allowing it to cool. For star formation to occur, the gas must cool further - this is done via H_2 cooling once molecular hydrogen is formed in the halo. This is the third stage for the gas and occurs once the UV background has decreased sufficiently in intensity. In their models, Kepner et al. looked at the effects of varying intensity UV fields on haloes with masses in the range $3\times10^8 M_\odot$-$5\times10^{10} M_\odot$, corresponding to gas masses in the

range $3\times10^5 M_\odot$-$5\times10^9 M_\odot$. The results of one of their models are shown in Fig. 7.6. With a background flux decreasing in amplitude, this plot shows the formation

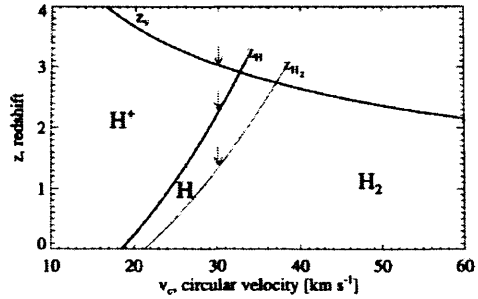

Figure 7.6: Plot showing redshifts of collapse, H formation and H_2 formation in relation to halo circular velocity (Kepner et al. 1999). For a halo with v_{circ}~30kms^{-1}, the redshifts for each process are shown by the arrows.

of a galaxy with circular velocity, 30kms^{-1} from a 1σ perturbation. At z~3, the perturbation collapses but the gas inside is ionised by the external UV flux until z~2.5. At z~1.5, H_2 can form, allowing the gas to begin cooling. Galaxies with larger circular velocities can begin cooling their gas at earlier redshifts, thus SF in larger objects occurs prior to SF in smaller-sized objects. This delay in forming low mass objects due to the UV background is a good explanation for the 'downsizing' scenario.

The recent discovery of an extremely low luminosity and low surface brightness dSph companion to the MW (Willman et al. 2005) has highlighted the possibility that the predicted population of low mass haloes in CDM may actually exist. Kleyna (2005) et al. comment that this new dSph, which has a M/L of over 500M$_\odot/L_\odot$ and absolute magnitude, M_V~-6.75, *'may represent the best candidate for a "missing" CDM halo'*. They conclude that there must be more dark and massive dwarfs hiding in the region around the MW. It is therefore extremely important that searches for such objects are carried out if we are to properly check the consistency of observations with CDM predictions.

If photoionization does result in there being many low mass DM haloes in the Universe which have not been able to form stars to make them visible as dwarf galaxies, then gravitational lensing could be used as a probe of substructure. This is an ideal tool to use since light is deflected gravitationally by matter, whether it is light or dark, thus if there were small dark haloes present in the Universe, they could be detected by this means. Such studies have been carried out (Metcalf & Zhao, 2002, Bradac et al. 2002) and preliminary results show evidence for the presence of substructure. Dalal & Kochanek (2002) studied seven four-image lens systems, six of which had flux anomalies which they commented could be due to the effects of substructure. They also rule out the possibilities of other effects causing the flux anomalies in a further study of their data (Kochanek & Dalal, 2003), concluding that '*low mass haloes remain the best explanation of the phenomenon*'. However, if these low mass DM haloes do exist in the numbers predicted by CDM, then as they fall through the disk of their parent galaxy, they should heat the disk and cause it to thicken (Tóth & Ostriker, 1992, Moore et al, 1999b). This is contrary to some observations of old thin disk systems or galaxies with no thick disk components, although it is now being argued that the amount of heating and thickening has been overestimated (Font et al., 2001, Velázquez & White, 1999). This is clearly a matter for further investigation.

At the start of this discussion, we gave two possibilities for our observed dwarf galaxy numbers in each environment surveyed. We have discussed the various mechanisms which may account for the vastly different numbers of dwarfs found in Virgo compared to the field and Ursa Major, and now we refer back to the two possibilities and summarise the evidence for and against each one.

The first possibility was that CDM is incorrect and the dwarf galaxies found in the Virgo cluster are not all the predicted primordial population - some have been

formed in the cluster environment. Our first evidence in support of this is that there appears to be a cluster population of dwarf galaxies which are not associated with giant galaxies in the cluster. Further evidence comes from our comparison of the mean (B-I) colours of the cluster dE galaxies and the giant ellipticals. The dE galaxies are bluer than the giants, which may imply that they are younger. However, this is only true if the dEs are metal rich - if they are sufficiently metal poor then this would account for their bluer colours. Clearly more information is needed on the metallicities of these dwarfs before a conclusion can be drawn regarding this. Another indication that some dwarf galaxies may have formed in the cluster environment is evidence of interactions between galaxies via their HI properties. Sabatini et al. (2005) made pointed HI observations of their dwarf galaxies in the E-W strip, but had only a 5% detection efficiency. This implies that either the dwarfs in Virgo have been stripped of their gas in the cluster environment or they have had their star formation enhanced in the cluster, probably by interactions. It is possible that in such interactions a population of infalling dwarfs can be morphologically transformed from dIrrs into dEs in the cluster environment. However, this would result in a morphology-density relation where dEs would be found mainly at the centre of the cluster and dIrrs predominantly at the outskirts. There was evidence of such a relation in the E-W strip, but no such fall in dEs from cluster centre to cluster edge in the N-S strip. This was however, due to the contamination of the N-S strip from the background N and M clouds. Another problem with the formation of dwarfs in the cluster environment is that, as we discussed earlier in this Chapter, the dwarf galaxies detected by our survey of Virgo are too small to have been formed by the harassment scenario where infalling LSB disk galaxies are transformed into dEs via tidal interactions. There have also not been a high enough number of tidal interactions in the cluster to form the correct amount of TDGs to explain the high number of dwarf galaxies in Virgo. Finally,

we found no change in mean (B-I) colour of the objects with position in the cluster. This may imply that the galaxies all have the same formation scenario. Thus, given all this evidence it seems unlikely that a large population of dwarf galaxies have been formed within the cluster environment.

The second possibility that we gave at the start of this Chapter was that CDM was in fact correct, but that dwarf galaxy formation has been suppressed in the lower density environments. Our first piece of evidence for this argument is the lack of dwarf galaxies that we found in the field and UMa compared to both the Virgo cluster and predictions of CDM. If we assume that CDM is correct, then some process must be going on in the low density environments which prevents or suppresses the formation of stars in the low mass haloes, preventing us from detecting the dwarf galaxies. We had a higher HI detection efficiency for the field objects than the Virgo cluster objects, thus the field objects must have more HI gas. This means that SF cannot have been enhanced in these galaxies, or they would be HI-poor, thus it is a possibility that there are many DM haloes in the low density environments which have not had their star formation turned on yet. However, our search for such dark objects in the UMa cluster came up with no such candidates - all the galaxies detected in HI had optical counterparts. This is not too surprising however since the mass limit of our HI UMa survey was quite high at $\sim 2 \times 10^8 M_{\odot}$. Our lack of detections of dark galaxies does not mean that there are no dark objects in the Universe - Minchin et al. (2005) recently discovered an excellent candidate for a massive dark galaxy in the Virgo cluster. Willman et al. (2005) have also recently detected a new, very faint MW dSph companion with an inferred central mass-to-light ratio of $\sim 500 M_{\odot}/L_{\odot}$ (Kleyna et al. 2005), which is also considered possibly to be one of the 'missing' low mass haloes predicted by CDM. Another piece of evidence to support the existence of DM haloes with

little or no star formation are the results of gravitational lensing studies which have detected substructure (Dalal & Kochanek, 2002; Kochanek & Dalal, 2003) in 4 lensing systems. Given these new detections of a dark galaxy, and a new faint companion of the MW, it seems plausible and highly likely that we have not detected all possible low mass haloes predicted by CDM. However, as can be seen from Table 7.1, even given the possibility that there are these objects yet to be detected in the Universe, the observations would still fall short of the numbers predicted by CDM. We discussed earlier the mechanisms which could create dwarf galaxies in the Virgo environment. Harassment would not create the types of galaxies which we detect in our surveys. Tidal interactions would create ~26 per Gyr, which would result in an increase in the Virgo DGR to ~46:1 (assuming they are all associated with the giant galaxies). Thus there would still be a discrepancy between the observed DGR and the predicted CDM value of 80:1 (assuming α=-1.4). Recent discoveries of faint galaxies in the LG raises the possibility that there are fainter dwarf galaxies in Virgo which we cannot detect at present. It is only with further searches however that we will be able to see if such objects exist, and if so, if they exist in numbers high enough for the discrepancy between CDM and observations to be reconciled.

Appendix A

NS strip Virgo cluster objects

Number	*RA* (*J2000*)	*Dec* (*J2000*)	*m*	μ_0	*scale-length* ($''$)	*Comment*
0	12 19 20	18 58 15	19.3	24.8	5.0	unknown, dIrr
1	12 19 0	19 21 22	18.1	23.1	4.0	unknown, dIrr/sp?
2	12 20 48	19 12 47	18.3	23.8	5.0	unknown, dIrr/sp?
3	12 20 28	19 17 36	17.7	23.2	5.0	unknown, dIrr/sp?
4	12 19 23	19 35 14	17.7	23.6	6.0	TH230, dE
5	12 22 50	12 55 38	20.7	25.7	4.0	unknown, dIrr
6	12 22 12	13 8 52	19.4	24.4	4.0	unknown, dSph
7	12 22 28	13 9 47	19.4	24.9	5.0	vcc0556, dE
8	12 22 10	12 57 45	19.2	24.7	5.0	unknown, dIrr
9	12 22 9	12 55 1	20.2	25.3	4.0	unknown, dIrr
10	12 22 28	12 53 57	18.7	23.7	4.0	unknown, dSph
11	12 23 11	13 8 3	20.9	25.9	4.0	unknown, vlsb
12	12 22 47	13 11 22	20.9	25.9	4.0	unknown, vlsb
13	12 22 39	13 4 19	18.2	23.3	4.0	unknown, Sp
14	12 25 31	12 58 38	18.9	25.7	9.0	vcc0804, dE,N
15	12 25 13	13 1 32	17.4	24.2	9.0	vcc0779, dE,N
16	12 24 19	12 54 46	18.5	24.4	6.0	vcc0719, dE
17	12 26 6	13 12 53	19.3	24.3	4.0	unknown, dE
18	12 25 25	13 6 37	20.3	26.1	6.0	unknown, dIrr
19	12 25 5	13 4 33	19.9	25.4	5.0	unknown, dSph
20	12 25 14	13 4 20	20.7	25.7	4.0	unknown, dIrr
21	12 24 52	13 6 40	16.7	23.5	9.0	vcc0753, dE,N
22	12 23 55	13 16 18	20.3	25.8	5.0	unknown, dIrr
23	12 23 29	13 11 41	20.2	25.2	4.0	unknown, dIrr
24	12 21 54	13 27 42	20.7	25.7	4.0	unknown, dIrr
25	12 22 29	13 18 57	18.5	24.0	5.0	vcc0557, dE
26	12 23 53	13 30 24	19.2	24.7	5.0	TH328, dE,N
27	12 23 12	13 25 8	18.7	24.9	7.0	vcc0624, dE,N
28	12 23 2	13 33 33	19.3	24.8	5.0	vcc0605, dE,N
29	12 25 53	13 11 33	19.3	24.3	4.0	vcc0850

Continued on next page

Number	RA (J2000)	Dec (J2000)	m	μ_0	scale-length (″)	Comment
30	12 25 19	13 15 23	18.4	24.6	7.0	vcc0789, dE
31	12 24 46	13 20 26	17.8	23.7	6.0	TH215, dIrr
32	12 24 58	13 15 15	20.9	25.9	4.0	unknown, vlsb
33	12 24 11	13 22 27	18.2	25.0	9.0	vcc0704, dE
34	12 24 34	13 22 25	19.2	25.4	7.0	TH337, dIrr/dE
35	12 25 23	13 24 46	20.8	25.8	4.0	unknown, vlsb
36	12 24 13	13 37 57	18.1	24.4	7.0	vcc0708, dE
37	12 25 48	13 51 16	18.2	24.9	9.0	vcc0845, dE
38	12 25 21	13 49 10	19.1	25.4	7.0	TH313, dIrr
39	12 22 1	14 8 9	18.6	24.9	7.0	vcc0519, dE,N
40	12 22 1	14 5 19	20.6	25.6	4.0	unknown, dIrr
41	12 22 9	13 55 50	18.0	23.5	5.0	unknown, dIrr/sp/dE
42	12 23 21	14 12 54	20.3	25.3	4.0	unknown, dIrr
43	12 23 8	14 3 37	20.4	25.4	4.0	unknown, dE
44	12 22 57	14 21 48	19.9	25.8	6.0	unknown, dE,N
45	12 22 43	14 18 10	19.7	25.9	7.0	TH418, dIrr
46	12 21 50	14 23 60	20.3	25.3	4.0	unknown, dSph
47	12 24 13	14 29 38	18.7	24.5	6.0	TH293, dIrr
48	12 24 21	14 20 31	19.0	24.0	4.0	unknown, Sp
49	12 25 11	14 26 29	17.7	24.4	9.0	vcc0777, dE
50	12 23 23	14 37 26	19.1	24.1	4.0	unknown, dE,N
51	12 23 29	14 53 23	18.7	24.2	5.0	vcc0643, dE
52	12 25 55	14 38 29	19.0	25.2	7.0	IBM88, dIrr/dE
53	12 24 53	14 39 19	18.0	23.9	6.0	vcc0757, dE
54	12 24 48	14 34 36	17.0	23.7	9.0	vcc0748, dE
55	12 25 51	14 47 16	20.3	25.3	4.0	unknown, dSph
56	12 25 23	14 48 13	17.2	23.4	7.0	vcc0795, dE,N
57	12 25 13	14 50 51	18.3	25.0	9.0	vcc0780, dE
58	12 23 11	14 51 45	17.1	23.9	9.0	vcc0625, dE
59	12 22 49	14 57 57	20.2	25.2	4.0	unknown, dIrr
60	12 22 16	15 13 6	19.4	24.9	5.0	unknown, dSph
61	12 22 21	15 9 36	19.0	24.5	5.0	vcc0547, dE
62	12 23 47	15 7 32	17.1	23.9	9.0	vcc0668, dE
63	12 26 10	14 55 45	17.1	23.9	9.0	vcc0878, dE
64	12 24 51	15 0 39	19.0	24.5	5.0	vcc0754, dE
65	12 24 35	15 9 51	18.8	25.0	7.0	IBM88, dE,N
66	12 24 10	15 5 40	20.2	25.7	5.0	unknown, dIrr
67	12 24 22	15 0 1	18.0	23.1	4.0	unknown, Sp
68	12 25 0	15 5 38	19.5	24.5	4.0	unknown, dSph
69	12 24 47	15 4 26	18.0	23.0	4.0	unknown, dIrr
70	12 22 51	15 16 31	17.2	23.9	9.0	vcc0594, dE
71	12 22 24	15 28 16	17.1	23.9	9.0	vcc0554, dE,N
72	12 21 52	15 22 9	18.5	23.5	4.0	unknown, dE
73	12 21 52	15 17 48	19.9	24.9	4.0	unknown, dE
74	12 22 56	15 33 35	18.9	24.8	6.0	vcc0600, dE
75	12 26 8	15 28 54	18.9	24.8	6.0	TH348, dIrr/dE
76	12 24 51	15 23 41	19.7	25.2	5.0	TH389, dIrr/dE
77	12 22 8	15 47 57	16.4	23.2	9.0	vcc0530, dIrr
78	12 22 20	15 40 47	19.4	24.9	5.0	TH372, dIrr/dE
79	12 22 10	15 39 11	18.9	25.7	9.0	TH318
80	12 22 6	13 51 22	18.9	23.9	4.0	2MASX, Sp
81	12 21 53	13 48 32	20.5	25.5	4.0	unknown, dSph
82	12 22 15	13 53 2	19.6	24.6	4.0	unknown, dSph

Continued on next page

Number	*RA* (J2000)	*Dec* (J2000)	*m*	μ_0	*scale-length* ($''$)	*Comment*
83	12 21 57	13 39 4	20.8	25.8	4.0	unknown, dIrr
84	12 21 49	13 35 49	20.9	25.9	4.0	unknown, vlsb
85	12 23 53	13 52 57	17.2	24.0	9.0	vcc0674, dE,N
86	12 23 39	13 49 4	19.1	24.5	5.0	TH325, dIrr
87	12 22 59	13 45 25	19.3	24.7	5.0	vcc0603, dE
88	12 25 43	15 34 30	18.8	24.3	5.0	vcc0829, dE
89	12 25 0	15 36 16	17.2	23.9	9.0	vcc0761, dE
90	12 24 29	15 52 8	20.4	25.4	4.0	unknown, dIrr
91	12 23 5	15 55 55	17.5	24.3	9.0	TH199, dE
92	12 23 46	16 47 27	17.0	23.8	9.0	vcc0666
93	12 25 38	16 39 53	17.5	24.3	9.0	vcc0818
94	12 25 36	16 35 46	17.6	24.4	9.0	vcc0813, dE,N
95	12 24 2	16 50 22	17.8	23.6	6.0	unknown, int
96	12 25 32	14 9 10	17.1	23.9	9.0	vcc0808, dE,N
97	12 23 3	16 19 42	19.6	25.4	6.0	vcc0610, dE
98	12 23 2	16 18 38	20.2	25.3	4.0	unknown, dSph
99	12 26 5	16 21 18	18.2	24.9	9.0	unknown, int
100	12 25 40	16 16 54	19.1	25.9	9.0	TH110, vlsb
101	12 24 24	16 23 15	18.3	25.1	9.0	vcc0726, dE,N
102	12 25 60	16 24 14	19.1	24.6	5.0	unknown, dIrr/dE
103	12 24 2	16 50 22	17.2	23.1	6.0	unknown
104	12 21 49	18 25 46	17.6	24.4	9.0	vcc0505, dE,N
105	12 22 60	16 58 59	17.7	23.5	6.0	TH228, dE
106	12 22 3	17 12 4	18.5	24.7	7.0	vcc0521, dE
107	12 22 20	17 6 28	20.6	25.6	4.0	unknown, dIrr
108	12 22 12	16 58 28	19.1	25.0	6.0	vcc0536, dE
109	12 23 44	17 6 49	20.7	25.7	4.0	unknown, dIrr
110	12 23 55	17 7 45	20.8	25.8	4.0	unknown, dIrr
111	12 23 6	17 5 26	20.2	25.7	5.0	TH416, dIrr/dE
112	12 23 4	17 18 14	20.0	25.1	4.0	unknown, dSph
113	12 21 52	17 29 57	19.8	25.3	5.0	TH266, vlsb
114	12 21 50	17 14 58	18.8	23.8	4.0	unknown
115	12 23 29	17 32 26	17.6	23.8	7.0	vcc0644, dE
116	12 23 18	17 29 20	19.6	25.4	6.0	unknown, dSph
117	12 23 1	17 30 45	20.3	25.3	4.0	unknown, dIrr
118	12 22 43	17 29 2	19.7	24.7	4.0	unknown, dE
119	12 22 37	17 31 0	19.8	24.8	4.0	unknown, dSph
120	12 25 48	17 20 50	19.0	24.0	4.0	unknown, dIrr
121	12 26 2	17 18 25	20.0	25.0	4.0	unknown, dIrr
122	12 25 50	17 16 16	19.7	25.1	5.0	unknown, dIrr
123	12 24 4	17 32 58	17.1	23.0	6.0	vcc0696
124	12 24 48	17 33 12	20.1	25.1	4.0	unknown, dIrr
125	12 23 13	17 38 42	19.3	24.3	4.0	unknown, dIrr
126	12 22 34	17 35 9	20.0	25.0	4.0	unknown, dIrr
127	12 21 42	17 49 41	18.2	24.4	7.0	vcc0495, dE
128	12 22 16	17 37 33	19.8	25.3	5.0	unknown, dE
129	12 21 44	17 34 14	19.3	24.3	4.0	unknown, dIrr
130	12 23 33	17 49 16	18.3	25.1	9.0	vcc0647, dE
131	12 23 32	17 47 41	16.6	23.4	9.0	vcc0646, dE
132	12 23 60	17 39 6	17.9	23.4	5.0	vcc0689
133	12 25 38	17 50 38	18.7	24.6	6.0	TH379, dE
134	12 25 37	17 44 40	19.2	26.0	9.0	unknown, vlsb
135	12 21 57	17 53 32	17.0	23.7	9.0	vcc0515, dE

Continued on next page

Number	RA (J2000)	Dec (J2000)	m	μ_0	scale-length ('')	Comment
136	12 22 39	18 5 22	18.7	25.5	9.0	TH382, dIrr/dE
137	12 25 43	17 59 26	18.7	23.7	4.0	vcc0830, dE
138	12 24 59	18 18 12	18.6	23.6	4.0	unknown, dE
139	12 23 43	18 39 43	16.5	23.3	9.0	vcc0663, dE
140	12 23 53	18 37 57	16.9	23.1	7.0	vcc0677, dE
141	12 24 35	18 50 56	19.9	25.4	5.0	unknown, dSph
142	12 25 39	19 1 24	19.6	24.6	4.0	RadioS
143	12 24 36	18 58 13	20.3	25.3	4.0	unknown, dIrr
144	12 24 37	18 56 15	18.1	24.9	9.0	TH229, dE
145	12 24 18	19 10 40	19.5	25.0	5.0	unknown, dIrr
146	12 25 55	19 11 50	18.3	25.0	9.0	TH304, dIrr/dE
147	12 26 3	19 9 18	19.8	24.8	4.0	unknown, dIrr
148	12 23 46	19 21 53	20.4	25.4	4.0	unknown, vlsb
149	12 23 35	19 12 30	18.9	23.9	4.0	unknown, dSph
150	12 21 53	19 32 39	19.6	24.6	4.0	unknown, dSph
151	12 22 7	19 32 41	20.3	25.3	4.0	unknown, dE
152	12 21 42	19 13 44	19.6	24.6	4.0	unknown, dE
153	12 22 7	19 14 17	20.3	25.3	4.0	unknown, vlsb
154	12 23 46	19 33 33	20.3	25.3	4.0	unknown, vlsb
155	12 23 51	19 26 43	18.9	23.9	4.0	2MASX
156	12 22 51	19 29 48	19.9	24.9	4.0	unknown, dE
157	12 26 5	19 15 32	18.0	23.1	4.0	unknown, dSph
158	12 23 37	19 37 54	20.3	25.4	4.0	unknown, vlsb
159	12 21 41	19 46 52	20.2	25.2	4.0	unknown, dSph
160	12 22 42	19 47 41	18.9	23.9	4.0	unknown, dSph
161	12 22 38	19 43 51	20.0	25.0	4.0	unknown, dE
162	12 22 22	19 53 5	19.4	24.5	4.0	unknown, dIrr
163	12 24 11	19 52 38	20.0	25.0	4.0	unknown, dIrr
164	12 17 49	12 51 33	20.7	25.7	4.0	unknown, dSph
165	12 18 53	13 9 29	20.7	25.7	4.0	unknown, vlsb
166	12 18 27	13 10 15	19.7	25.2	5.0	unknown, dSph
167	12 20 36	12 53 6	18.6	24.5	6.0	vcc0426, dE,N
168	12 19 53	13 11 55	18.4	23.9	5.0	unknown, dSph
169	12 20 0	13 8 20	19.9	24.9	4.0	unknown, dSph
170	12 19 55	13 5 17	20.2	25.2	4.0	unknown, dSph
171	12 20 15	12 51 56	18.0	23.8	6.0	vcc0401, dE
172	12 21 42	13 11 39	19.4	24.4	4.0	unknown, dSph
173	12 17 42	13 32 55	19.9	25.8	6.0	unknown, dSph
174	12 18 2	13 25 13	19.0	24.0	4.0	unknown, dSph
175	12 17 35	13 19 37	20.8	25.8	4.0	unknown, dSph
176	12 21 54	13 15 2	19.8	24.8	4.0	TH392, dIrr
177	12 21 15	13 20 48	16.9	23.6	9.0	vcc0461, dE
178	12 20 37	13 19 13	20.4	25.9	5.0	unknown, vlsb
179	12 20 18	13 16 47	20.2	25.2	4.0	unknown, dSph
180	12 21 52	13 30 59	18.3	23.3	4.0	unknown, dIrr/dE
181	12 21 54	13 27 42	20.7	25.7	4.0	unknown, dIrr
182	12 20 31	13 31 9	17.5	24.3	9.0	vcc0421, dE
183	12 21 49	13 35 50	21.1	26.1	4.0	unknown, vlsb
184	12 21 23	13 35 0	20.4	25.9	5.0	unknown, dSph
185	12 18 42	14 20 57	19.5	25.0	5.0	unknown, dIrr
186	12 17 57	14 29 30	21.1	26.1	4.0	unknown, vlsb
187	12 17 31	14 21 21	17.8	24.5	9.0	vcc240, dE,N
188	12 17 39	14 16 39	17.8	24.6	9.0	vcc245, dE,N

Continued on next page

Number	*RA* (J2000)	*Dec* (J2000)	*m*	μ_0	*scale-length* ($''$)	*Comment*
189	12 21 1	14 17 34	19.6	24.6	4.0	unknown, dE
190	12 20 16	14 32 49	19.7	24.8	4.0	unknown, dE
191	12 20 10	14 19 47	18.1	23.1	4.0	unknown, dE
192	12 20 42	14 27 19	18.9	23.9	4.0	unknown, dE,N
193	12 18 10	14 41 46	16.3	23.1	9.0	vcc273, dE
194	12 18 49	14 52 7	18.2	23.2	4.0	unknown
195	12 20 24	14 41 29	17.2	23.9	9.0	vcc414, dE
196	12 19 48	14 42 24	17.9	24.7	9.0	vcc0372, dE,N
197	12 20 27	14 47 8	17.3	24.0	9.0	vcc0418, dE
198	12 17 29	15 28 33	20.2	26.1	6.0	unknown, vlsb
199	12 19 37	15 27 18	18.6	25.4	9.0	vcc360, dE
200	12 19 16	15 23 47	17.2	24.0	9.0	vcc335, dE
201	12 21 52	15 17 47	20.0	25.0	4.0	unknown, dSph
202	12 21 27	15 30 11	18.9	23.9	4.0	vcc0478, dE
203	12 21 31	15 29 58	18.6	25.4	9.0	vcc0481, dE
204	12 21 54	14 58 20	19.2	25.1	6.0	unknown, dIrr/dE
205	12 21 28	15 1 18	17.6	24.4	9.0	vcc0477, dIrr
206	12 20 55	14 59 25	17.6	24.3	9.0	vcc0444, dE
207	12 19 37	15 9 42	16.6	23.4	9.0	vcc0361, dE
208	12 20 7	15 7 16	20.2	25.7	5.0	unknown, dIrr
209	12 20 9	15 8 34	19.0	24.0	4.0	unknown, dIrr/dE
210	12 21 42	15 4 34	17.1	23.4	7.0	vcc0494, dE
211	12 21 27	15 3 49	20.3	25.3	4.0	unknown, dE
212	12 21 9	15 12 34	20.3	25.3	4.0	unknown, dIrr
213	12 21 10	15 7 57	17.8	23.3	5.0	unknown, dSph
214	12 21 24	15 37 16	18.0	24.3	7.0	vcc0472
215	12 21 1	15 39 17	20.1	25.1	4.0	unknown, dIrr
216	12 20 56	15 41 50	20.8	25.8	4.0	unknown, dE
217	12 19 51	15 40 19	18.0	24.8	9.0	vcc0378, dE
218	12 21 6	15 43 14	17.6	24.4	9.0	vcc0454, dE
219	12 18 51	15 54 20	19.7	25.9	7.0	TH374, vlsb
220	12 17 32	15 53 47	20.5	26.0	5.0	unknown, dIrr
221	12 17 44	16 26 47	19.2	25.1	6.0	unknown, dIrr
222	12 21 13	16 17 38	19.4	24.4	4.0	TH332, dIrr
223	12 20 52	16 21 50	19.0	25.8	9.0	TH180, vlsb
224	12 19 51	16 16 8	18.6	24.5	6.0	TH289, dIrr/dE
225	12 21 15	16 28 34	18.3	23.3	4.0	MAPS, Sp
226	12 17 59	16 51 35	20.3	25.3	4.0	unknown, dE
227	12 17 49	16 35 47	19.2	24.7	5.0	TH347, dIrr
228	12 18 33	16 48 29	20.3	25.8	5.0	unknown, dIrr
229	12 21 19	16 36 34	17.6	23.1	5.0	vcc0469, dE
230	12 20 30	16 48 58	20.0	26.3	7.0	unknown, vlsb
231	12 20 33	16 43 55	20.8	25.9	4.0	vcc433, dIrr/dE
232	12 20 23	16 43 18	20.6	26.1	5.0	unknown, vlsb
233	12 18 37	16 58 28	17.2	23.1	6.0	MAPS
234	12 18 30	17 6 12	18.1	23.1	4.0	unknown, dIrr
235	12 19 35	17 14 24	20.1	25.6	5.0	TH439, dIrr
236	12 20 11	17 43 6	17.9	24.7	9.0	TH244, dE,N
237	12 21 42	17 49 41	19.1	24.6	5.0	vcc0495, dE
238	12 17 42	17 55 3	20.3	25.3	4.0	unknown, dIrr
239	12 17 32	18 24 19	17.7	24.5	9.0	TH207, dE
240	12 20 30	18 19 15	17.5	24.3	9.0	vcc0422, dE
241	12 18 48	18 34 13	20.3	25.3	4.0	unknown, dE

Continued on next page

Number	*RA* (J2000)	*Dec* (J2000)	*m*	μ_0	*scale-length* ($''$)	*Comment*
242	12 18 35	18 35 49	19.9	26.1	7.0	TH420, dIrr/dE
243	12 20 50	18 56 47	19.8	24.8	4.0	unknown, dSph
244	12 20 35	18 53 3	18.8	24.7	6.0	TH305, dE
245	12 21 38	19 10 48	19.9	25.8	6.0	unknown, dIrr
246	12 20 48	19 12 47	18.7	23.7	4.0	unknown, dSph

Table A.1: Table of 'sure' detections for the Virgo NS strip

Number	RA (J2000)	Dec (J2000)	m	μ_0	scale-length ($'$)	Comment
0	12 21 36	18 37 18	20.3	25.8	5.0	unknown, dIrr
1	12 21 45	18 31 33	21.2	26.2	4.0	unknown, vlsb
2	12 20 30	18 41 54	21.0	26.0	4.0	unknown, dIrr
3	12 19 16	18 59 51	21.2	26.2	4.0	unknown, vlsb
4	12 17 40	19 11 25	20.7	26.2	5.0	unknown, dIrr
5	12 19 4	19 3 45	20.8	25.8	4.0	unknown, dE
6	12 19 37	19 48 22	20.4	26.6	7.0	unknown, vlsb
7	12 19 59	19 51 54	20.8	26.3	5.0	unknown, vlsb
8	12 19 24	19 43 55	20.2	25.7	5.0	unknown, dIrr
9	12 23 46	12 55 31	21.1	26.1	4.0	unknown, vlsb
10	12 21 48	12 59 56	20.3	25.3	4.0	unknown, dIrr
11	12 25 23	13 16 3	20.5	26.3	6.0	unknown, vlsb
12	12 25 24	13 32 37	19.9	25.8	6.0	unknown, dIrr
13	12 25 22	13 32 42	19.8	26.0	7.0	unknown, dIrr
14	12 25 27	13 32 30	20.9	25.9	4.0	unknown, vlsb
15	12 25 20	13 26 7	21.1	26.1	4.0	unknown, vlsb
16	12 25 29	13 24 54	21.0	26.0	4.0	unknown, vlsb
17	12 24 54	13 23 30	21.2	26.2	4.0	unknown, vlsb
18	12 24 60	13 36 32	20.5	26.3	6.0	unknown, vlsb
19	12 24 37	13 36 44	21.1	26.2	4.0	unknown, vlsb
20	12 25 24	14 23 29	21.0	26.0	4.0	unknown, vlsb
21	12 24 47	14 58 26	21.1	26.1	4.0	unknown, vlsb
22	12 25 20	15 5 45	20.9	25.9	4.0	unknown, vlsb
23	12 25 7	15 9 56	20.9	26.4	5.0	unknown, vlsb
24	12 24 24	15 42 15	20.8	26.3	5.0	unknown, unsure
25	12 26 9	16 53 15	19.9	26.1	7.0	unknown, vlsb
26	12 23 57	17 1 32	21.0	26.0	4.0	unknown, vlsb
27	12 23 15	16 55 52	20.5	26.0	5.0	unknown, vlsb
28	12 22 53	16 52 45	20.9	25.9	4.0	unknown, vlsb
29	12 22 56	17 10 11	20.6	26.1	5.0	unknown, vlsb
30	12 21 51	17 31 35	19.6	25.8	7.0	unknown, vlsb
31	12 21 54	17 23 9	19.9	25.4	5.0	unknown, dIrr
32	12 23 2	17 29 42	20.6	25.6	4.0	unknown, dSph
33	12 23 6	17 23 43	20.1	25.1	4.0	unknown, dIrr
34	12 22 49	17 31 37	20.1	25.6	5.0	unknown, dIrr
35	12 22 27	17 28 39	20.4	25.4	4.0	unknown, dIrr
36	12 26 3	17 20 18	19.5	25.7	7.0	unknown, vlsb
37	12 25 41	17 12 25	19.7	25.6	6.0	unknown, unsure
38	12 25 42	17 26 44	20.2	25.7	5.0	unknown, vlsb
39	12 24 48	17 24 38	19.2	25.9	9.0	unknown, dIrr
40	12 23 50	17 37 17	20.3	25.3	4.0	unknown, vlsb
41	12 22 17	17 46 1	19.9	25.4	5.0	unknown, vlsb
42	12 24 14	17 33 18	20.5	25.5	4.0	unknown, vlsb
43	12 23 55	17 52 40	20.5	25.5	4.0	unknown, vlsb
44	12 23 54	19 6 18	20.1	25.1	4.0	unknown, dIrr
45	12 25 12	18 57 13	20.0	25.9	6.0	unknown, vlsb
46	12 23 57	19 10 6	20.6	25.6	4.0	unknown, vlsb
47	12 25 5	19 7 46	20.1	25.6	5.0	unknown, vlsb
48	12 24 41	19 7 57	20.3	25.8	5.0	unknown, vlsb
49	12 23 22	19 12 17	19.5	25.3	6.0	TH187, vlsb
50	12 22 43	19 29 18	19.9	25.8	6.0	unknown, vlsb
51	12 24 47	19 25 17	20.3	25.8	5.0	unknown, vlsb
52	12 22 45	19 36 46	20.4	25.4	4.0	unknown, vlsb
53	12 23 2	19 53 27	20.7	25.7	4.0	unknown, vlsb
54	12 24 45	19 34 4	20.3	25.3	4.0	unknown, vlsb
55	12 23 51	19 44 9	20.5	25.5	4.0	unknown, vlsb
56	12 21 57	13 39 5	20.8	25.8	4.0	unknown, dIrr
57	12 21 9	13 35 22	19.1	25.8	9.0	unknown, dSph
58	12 20 2	13 33 44	20.4	26.3	6.0	unknown, dIrr
59	12 18 37	14 21 57	20.0	25.0	4.0	unknown, dIrr
60	12 19 6	15 7 11	20.4	25.4	4.0	unknown, dIrr
61	12 18 50	15 23 16	21.2	26.2	4.0	unknown, vlsb
62	12 21 1	15 17 25	20.3	26.2	6.0	unknown, vlsb
63	12 18 47	15 38 52	21.0	26.0	4.0	unknown, vlsb
64	12 17 26	15 52 24	20.9	26.0	4.0	unknown, vlsb
65	12 20 31	14 54 35	20.8	26.2	5.0	unknown, vlsb
66	12 19 36	15 8 45	21.0	26.1	4.0	unknown, vlsb
67	12 19 37	15 4 8	20.7	26.2	5.0	unknown, vlsb
68	12 21 27	15 9 20	21.1	26.1	4.0	unknown, vlsb
69	12 20 53	15 5 9	20.6	26.1	5.0	unknown, vlsb
70	12 21 52	15 51 58	21.0	26.5	5.0	unknown, vlsb
71	12 21 20	15 45 13	20.9	26.4	5.0	unknown, vlsb
72	12 20 42	15 50 7	20.6	26.5	6.0	unknown, vlsb
73	12 20 36	15 52 16	20.8	26.3	5.0	unknown, vlsb
74	12 18 25	15 57 14	20.6	26.1	5.0	unknown, dIrr
75	12 17 56	16 11 40	20.4	25.4	4.0	unknown, dIrr
76	12 17 58	16 9 19	21.1	26.1	4.0	unknown, vlsb
77	12 17 51	16 5 1	20.4	25.8	5.0	unknown, dIrr
78	12 18 38	16 13 33	20.8	25.8	4.0	unknown, vlsb
79	12 18 33	16 2 51	20.7	26.2	5.0	unknown, vlsb
80	12 20 40	15 57 46	21.2	26.2	4.0	unknown, vlsb
81	12 19 43	16 11 60	20.8	26.3	5.0	unknown, vlsb
82	12 20 51	16 9 26	20.8	25.8	4.0	unknown, dIrr
83	12 21 43	16 30 8	20.7	25.7	4.0	unknown, dIrr
84	12 20 44	16 51 45	20.8	25.8	4.0	unknown, dIrr
85	12 18 17	17 28 34	21.2	26.2	4.0	unknown, vlsb
86	12 18 13	18 38 18	21.2	26.3	4.0	unknown, vlsb
87	12 18 10	18 36 8	21.2	26.2	4.0	unknown, vlsb
88	12 20 14	19 5 25	20.9	25.9	4.0	unknown, dIrr

Table A.2: Table of 'unsure' detections for the Virgo NS strip

Bibliography

Abell G. O., 1960, PASP, 72, 459

Babul A., Rees M. J., 1992, MNRAS, 255, 346

Banks G. D. et al., 1999, ApJ, 524, 612

Barnes D. G. et al., 2001, MNRAS, 322, 486

Bender R., Paquet A., Nieto J.-L., 1991, A&A, 246, 349

Bertin E., Arnouts S., 1996, A&AS, 117, 393

Binggeli B., Sandage A., Tammann G. A., 1985, AJ, 90, 1681

Binggeli B., Tammann G. A., Sandage A., 1987, AJ, 94, 251

Binggeli B., Popescu C. C., Tammann G. A., 1993, A&AS, 98, 275

Binggeli B., 1999, Lecture Notes in Physics, Berlin Springer Verlag, 530, 9

Blanton M. R. et al., 2001, AJ, 121, 2358

Bohringer H., Briel U. G., Schwarz R. A., Voges W., Hartner G., Trumper J., 1994, Nature, 368, 828

Bradač M., Schneider P., Steinmetz M., Lombardi M., King L. J., Porcas R., 2002, A&A, 388, 373

Bremnes T., Binggeli B., Prugniel P., 1999, A&AS, 137, 337

Conselice C. J., Gallagher J. S., Wyse R. F. G., 2001, ApJ, 559, 791

Couture J., Harris W. E., Allwright J. W. B., 1990, ApJS, 73, 671

Cowie L. L., Songaila A., Hu E. M., Cohen J. G., 1996, AJ, 112, 839

Dalal N., Kochanek C. S., 2002, ApJ, 572, 25

Davies J. I., Phillipps S., 1988, MNRAS, 233, 553

Davies J. I., de Blok W. J. G., Smith R. M., Kambas A., Sabatini S., Linder S. M., Salehi-Reyhani S. A., 2001, MNRAS, 328, 1151

Davies J. et al., 2004, MNRAS, 349, 922

Davies J. I., Roberts S., Sabatini S., 2005, MNRAS, 356, 794

de Vaucouleurs G., de Vaucouleurs A., 1964, Reference catalogue of bright galaxies. University of Texas Monographs in Astronomy, Austin: University of Texas Press, —c1964

de Vaucouleurs G., 1961, ApJS, 6, 213

Deady J. H., Boyce P. J., Phillipps S., Drinkwater M. J., Karick A., Jones J. B., Gregg M. D., Smith R. M., 2002, MNRAS, 336, 851

Dekel A., Silk J., 1986, ApJ, 303, 39

Dressler A., 1980, ApJ, 236, 351

Drinkwater M. J., Gregg M. D., Holman B. A., Brown M. J. I., 2001, MNRAS, 326, 1076

Driver S., De Propris R., 2003, Ap&SS, 285, 175

Driver S. P., Liske J., Cross N. J. G., De Propris R., Allen P. D., 2005, MNRAS, 360, 81

Driver S. P., 1999, ApJ, 526, L69

Efstathiou G., 1992, MNRAS, 256, 43P

Evans R., Davies J. I., Phillipps S., 1990, MNRAS, 245, 164

Feldmeier J., Ciardullo R., Jacoby G. H., 1998, Bulletin of the American Astronomical Society, 30, 1304

Feldmeier J. J., Ciardullo R., Jacoby G. H., Durrell P. R., 2004, ApJ, 615, 196

Ferguson H. C., Binggeli B., 1994, A&A Rev., 6, 67

Ferguson H. C., Tanvir N. R., von Hippel T., 1998, Nature, 391, 461

Font A. S., Navarro J. F., Stadel J., Quinn T., 2001, ApJ, 563, L1

Forbes D. A., Grillmair C. J., Williger G. M., Elson R. A. W., Brodie J. P., 1998, MNRAS, 293, 325

Freeman K. C., 1993, in ASP Conf. Ser. 48: The Globular Cluster-Galaxy Connection. p. 608

Ftaclas C., Struble M. F., Fanelli M. N., 1984, ApJ, 282, 19

Garcia A. M., 1993, A&AS, 100, 47

Gerola H., Seiden P. E., Schulman L. S., 1980, ApJ, 242, 517

Gooch R., 1996, in ASP Conf. Ser. 101: Astronomical Data Analysis Software and Systems V. p. 80

Grebel E. K., Gallagher J. S., Harbeck D., 2003, AJ, 125, 1926

Grebel E. K., 1997, Reviews of Modern Astronomy, 10, 29

Grossi M., Disney M. J., Minchin R. F., Pritzl B. J., Knezek P. M., Saha A., Gallagher J. S., Freeman K. C., 2004, in ASP Conf. Ser. 327: Satellites and Tidal Streams. p. 324

Heller A. B., Brosch N., 2001, MNRAS, 327, 80

Holmberg E., 1950, Meddelanden fran Lunds Astronomiska Observatorium Serie II, 128, 1

Hubble E., 1936, ApJ, 84, 158

Hubble E., 1936, ApJ, 84, 270

Hubble E., 1936, ApJ, 84, 517

Hunsberger S. D., Charlton J. C., Zaritsky D., 1996, ApJ, 462, 50

Ideta M., Makino J., 2004, ApJ, 616, L107

Irwin J. A., Bregman J. N., 2000, ApJ, 538, 543

Jensen J. B., Tonry J. L., Luppino G. A., 1999, ApJ, 510, 71

Jerjen H., Binggeli B., Barazza F. D., 2004, AJ, 127, 771

Jerjen H., Tully B., Trentham N., 2004b, Publications of the Astronomical Society

of Australia, 21, 356

Karachentsev I. D., Karachentseva V. E., Richter G. M., Vennik J. A., 1995, A&A, 296, 643

Karachentsev I., 1996, A&A, 305, 33

Karick A. M., Drinkwater M. J., Gregg M. D., 2003, MNRAS, 344, 188

Kauffmann G., White S. D. M., Guiderdoni B., 1993, MNRAS, 264, 201

Kepner J. V., Babul A., Spergel D. N., 1997, ApJ, 487, 61

Kiang T., 1961, MNRAS, 122, 263

Kleyna J. T., Wilkinson M. I., Evans N. W., Gilmore G., 2005

Klypin A., Kravtsov A. V., Valenzuela O., Prada F., 1999, ApJ, 522, 82

Kochanek C. S., Dalal N., 2003, in AIP Conf. Proc. 666: The Emergence of Cosmic Structure. p. 103

Kravtsov A. V., Gnedin O. Y., Klypin A. A., 2004, ApJ, 609, 482

Lang R. H. et al., 2003, MNRAS, 342, 738

Lemson G., Kauffmann G., 1999, MNRAS, 302, 111

Liske J., Lemon D. J., Driver S. P., Cross N. J. G., Couch W. J., 2003, MNRAS, 344, 307

Mac Low M., Ferrara A., 1999, ApJ, 513, 142

Markevitch M., Forman W. R., Sarazin C. L., Vikhlinin A., 1998, ApJ, 503, 77

Mateo M. L., 1998, ARA&A, 36, 435

Mayer L., Governato F., Colpi M., Moore B., Quinn T., Wadsley J., Stadel J., Lake G., 2001, ApJ, 559, 754

Metcalf R. B., Zhao H., 2002, ApJ, 567, L5

Michard R., 2000, A&A, 360, 85

Milne M. L., Pritchet C. J., 2002, Bulletin of the American Astronomical Society, 34, 1169

Minchin R. et al., 2005, ApJ, 622, L21

Miralda-Escudé J., 2003, Science, 300, 1904

Mobasher B. et al., 2003, ApJ, 587, 605

Moore B., Frenk C. S., White S. D. M., 1993, MNRAS, 261, 827

Moore B., Ghigna S., Governato F., Lake G., Quinn T., Stadel J., Tozzi P., 1999, ApJ, 524, L19

Moore B., Lake G., Quinn T., Stadel J., 1999, MNRAS, 304, 465

Norberg P. et al., 2002, MNRAS, 336, 907

Oemler A. J., 1974, ApJ, 194, 1

Okazaki T., Taniguchi Y., 2000, ApJ, 543, 149

Phillipps S., Parker Q. A., Schwartzenberg J. M., Jones J. B., 1998, ApJ, 493, L59+

Pritchet C. J., van den Bergh S., 1999, AJ, 118, 883

Pritzl B. J. et al., 2003, ApJ, 596, L47

Reaves G., 1956, AJ, 61, 69

Roberts S. et al., 2004, MNRAS, 352, 478

Sabatini S., Scaramella R., Testa V., Andreon S., Longo G., Djorgovski G., de Carvalho R. R., 2000, Memorie della Societa Astronomica Italiana, 71, 1091

Sabatini S., Davies J., Scaramella R., Smith R., Baes M., Linder S. M., Roberts S., Testa V., 2003, MNRAS, 341, 981

Sabatini S., Davies J., van Driel W., Baes M., Roberts S., Smith R., Linder S., O'Neil K., 2005, MNRAS, 357, 819

Sandage A., Tammann G. A., 1974, ApJ, 194, 223

Sandage A., Binggeli B., Tammann G. A., 1985, AJ, 90, 1759

Schaye J., 2004, ApJ, 609, 667

Schechter P., 1976, ApJ, 203, 297

Shibata R., Matsushita K., Yamasaki N. Y., Ohashi T., Ishida M., Kikuchi K., Böhringer H., Matsumoto H., 2001, ApJ, 549, 228

Spergel D. N. et al., 2003, ApJS, 148, 175

Stil J. M., Israel F. P., 2002, A&A, 389, 29

Susa H., Umemura M., 2004, ApJ, 600, 1

Thoul A. A., Weinberg D. H., 1996, ApJ, 465, 608

Toth G., Ostriker J. P., 1992, ApJ, 389, 5

Trentham N., Hodgkin S., 2002, MNRAS, 333, 423

Trentham N., Tully R. B., 2002, MNRAS, 335, 712

Trentham N., Tully R. B., Verheijen M. A. W., 2001, MNRAS, 325, 385

Trentham N., 1997, MNRAS, 286, 133

Tully R. B., Shaya E. J., 1984, ApJ, 281, 31

Tully R. B., Verheijen M. A. W., Pierce M. J., Huang J., Wainscoat R. J., 1996, AJ, 112, 2471

Tully R. B., Somerville R. S., Trentham N., Verheijen M. A. W., 2002, ApJ, 569, 573

Tully R. B., 1988, Nearby galaxies catalog. Cambridge and New York, Cambridge University Press, 1988, 221 p.

van Zee L., Haynes M. P., Salzer J. J., 1997, AJ, 114, 2497

van Zee L., Barton E. J., Skillman E. D., 2004, AJ, 128, 2797

van Zee L., Skillman E. D., Haynes M. P., 2004, AJ, 128, 121

Velazquez H., White S. D. M., 1999, MNRAS, 304, 254

Verheijen M. A. W., Sancisi R., 2001, A&A, 370, 765

Verheijen M. A. W., Trentham N., Tully R. B., Zwaan M. A., 2000, in ASP Conf. Ser. 218: Mapping the Hidden Universe: The Universe behind the Milky Way - The Universe in HI. p. 263

Vollmer B., Cayatte V., Balkowski C., Duschl W. J., 2001, ApJ, 561, 708

White D. A., 2000, MNRAS, 312, 663

Willman B. et al., 2005, ApJ, 626, L85

Yasuda N., Fukugita M., Okamura S., 1997, ApJS, 108, 417

Zwaan M. A., Verheijen M. A. W., Briggs F. H., 1999, Publications of the Astronomical Society of Australia, 16, 100

Zwaan M. A. et al., 2003, AJ, 125, 2842

Zwicky F., 1957, Morphological astronomy. Berlin: Springer, 1957

Zwicky F., 1964, ApJ, 140, 1626